

NASA CONTRACTOR REPORT

NASA CR-66098

NASA CR-66098

GPO PRICE \$ _____

CFSTI PRICE (S) \$ _____

MAIL PRICE (D) 3.75

MAIL PRICE (MF) 1.25

FREE _____

N66 31852

(ACCESSION NUMBER)	(THRU)
<u>202</u>	<u>1</u>
(PAGES)	(CODE)
<u>CR-66098</u>	<u>30</u>
(NASA CR OR TMX OR AD NUMBER)	(CATEGORY)

FEASIBILITY STUDY FOR LUNAR WORM

by F. A. Dobson and D. G. Fulton

Prepared under Contract No. NAS 1-5709 by

AERONUTRONIC
DIVISION OF PHILCO CORPORATION
A SUBSIDIARY OF *Ford Motor Company*
FORD ROAD, NEWPORT BEACH, CALIFORNIA

for

NATIONAL AERONAUTICS AND SPACE ADMINISTRATION - WASHINGTON, D.C. - MAY 1966

FEASIBILITY STUDY FOR LUNAR WORM
PLANETARY ROVING VEHICLE CONCEPT

By F. A. Dobson and D. G. Fulton

Distribution of this report is provided in the interest of information exchange. Responsibility for the contents resides in the author or organization that prepared it.

Prepared under Contract No. NAS 1-5709 by

AERONUTRONIC

DIVISION OF PHILCO CORPORATION

A SUBSIDIARY OF *Ford Motor Company,*

FORD ROAD NEWPORT BEACH, CALIFORNIA

for

NATIONAL AERONAUTICS AND SPACE ADMINISTRATION

PHILCO CORPORATION

A SUBSIDIARY OF *Ford Motor Company*

AERONUTRONIC DIVISION

FORD ROAD NEWPORT BEACH, CALIFORNIA

July 27, 1966

RSC-6720

National Aeronautics and Space Administration
Langley Research Center
Langley Station
Hampton, Virginia

Attention: Mr. H. J. Pelton
Mail Stop 126

Subject: Contract NAS1-5709
Final Report

Gentlemen:

In accordance with the reporting requirements contained in the subject contract, enclosed are fifteen (15) copies of the Final Technical Report entitled "Feasibility Study of Lunar Worm Roving Planetary Vehicle Concept - NAS CR# 66098".

For your information, distribution has been made in accordance with the list provided in your letter of June 15, 1966.

Very truly yours,



W. L. Davenport
Contract Administrator
Re-entry and Space System Programs

WLD:sem

CONTENTS

	Page
SUMMARY	1
INTRODUCTION	3
SYMBOLS	4
MOBILITY ANALYSIS	9
Lunar Soil Model	10
Extension-Contraction Type of Vehicle	12
Soil Considerations	12
Extension-Contraction Vehicle Performance	21
Rib-Walking Type of Vehicles	28
Rib-Walking	28
Double-Acting Bellows	31
Considerations for Design Applications	32
Traveling Wave Vehicle	33
Hard Surface Performance.	33
Soft Surface Performance	37
Considerations for Design Applications	42
BELLOWS ANALYSIS	43
Corrugated Bellows	43
Bellows Analysis	43
Design Conditions.	45
Design Charts	49
Considerations for Design Applications	58
Membrane Bellows	58
Spring Force	59
Shear Transfer to the Ground.	69
Consideration for Design Applications	72
DESIGN STUDIES	73
Scope	73
Steering and Control	74
Lunar Shelter	77
Large Lunar Shelter	77
Small Lunar Shelter	87
Solar-Mechanical Energy Transfer System for Extension- Contraction Vehicle	95
Design Evaluation.	98
Small Unmanned Vehicle	98
Possible Configurations.	98
Bellows Design	100
Design Evaluation.	111
Manned Extended-Range Roving Vehicle	113
Configuration Requirements	113
Design Evaluation.	117

CONTENTS (Continued)

	Page
OVERALL EVALUATION	118
Comparison with Other Vehicles	118
Vehicle Types	118
Vehicle Parameters	118
Mission Suitability	122
Mission Requirements	122
Ability to Fulfill Mission Requirements	125
Versatility versus Complexity	128
CONCLUDING SECTION.	129
Concluding Remarks	129
Recommendations for Future Work	130
APPENDIX A - UNITS AND CONVERSION FACTORS	131
APPENDIX B - THE ENGINEERING LUNAR MODEL SURFACE (ELMS)	133
APPENDIX C - MOBILITY OF EXTENSION-CONTRACTION TYPE OF VEHICLE	135
Analysis of Case I	136
Analysis of Case II	138
Analysis of Case III (ELMS Model)	140
Results	142
APPENDIX D - MATHEMATICAL MODEL OF WAVE MOTIONS	143
APPENDIX E - MOBILITY OF A TRAVELING WAVE IN SOFT SOIL WITH NO HYSTERESIS	148
Introduction.	148
Analysis - Entire Wave Below Soil Surface	148
Part of Wave Above Soil Surface.	158
Results	161
APPENDIX F - CORRUGATED BELLOWS METHODS.	162
Design Charts	162
Calculation of Bellows Parameters for Large Lunar Shelter	174
References	178

ILLUSTRATIONS

Figure		Page
1	Soil Friction Coefficient Versus Soil Displacement	10
2	Footprint Pressure Versus Penetration	12
3	Possible Cleat Configurations	13
4	Geometry of Planing Surface	15
5	Dimensionless Planing Parameter.	17
6	Planing Surfaces on a Vehicle Bottom	18
7	Lightly Loaded and Heavily Loaded Planing Vehicles	19
8	Experimental Friction Coefficient in Sand	20
9	Work to Expand a Vehicle Fixed At One End	22
10	Equivalent Drag-To-Weight Ratio of Extension-Contraction Vehicles	24
11	Vehicle on a Slope	25
12	Effect of Slope on Equivalent Drag.	27
13	Rib-Walking Motion	29
14	Equivalent Drag-To-Weight Ratio of a Rib-Walking Vehicle On the Moon	30
15	Rib-Walking Velocity Limitation Imposed By Jumping	31
16	Double-Acting Bellows	32
17	Snake Swimming.	34
18	Traveling Wave Model.	34
19	Traveling Wave Made Up of Cranks	35
20	Motion of a Rigid Traveling Wave Device On a Hard Surface.	35

ILLUSTRATIONS (Continued)

Figure		Page
21	Equivalent Drag-To-Weight Ratio of a Traveling Wave Vehicle On a Hard Surface On the Moon	36
22	Maximum Penetration Depth of a Traveling Wave.	38
23	Traveling Wave Velocity Ratio	39
24	Equivalent Drag-To-Weight Ratio	40
25	Maximum Slope Capability	41
26	Bellows Operating Range	46
27	Bellows Travel (Schematic)	46
28	Bellows Section	47
29	Loading Condition	48
30	Maximum Vehicle Strain Referred to Maximum Extended Length	51
31	d/b For the Vehicle Which Will Just Contain the Internal Pressure	52
32	Minimum Vehicle Empty Mass	53
33	Minimum Empty Vehicle Footprint Pressure	54
34	Material Thickness Required to Achieve Minimum - Weight Design	55
35	Vehicle Mass to Volume Ratio	56
36	Planing Criterion For Bellows Design	57
37	Bellows Configuration	58
38	Bellows Geometry	59
39	Comparison of Spring Force Expressions	62
40	Bellows Geometry Relationship.	64

ILLUSTRATIONS (Continued)

Figure		Page
41	Bellows Axial Membrane Load	65
42	Bellows Spring Rate	66
43	Geometry of Bellows Bending	67
44	Geometry of Convolution	69
45	Shear Stiffness of One Convolution.	71
46	Centipede Bridging	74
47	Boa Model	75
48	Boa Steering Mechanism	75
49	Boa Model Turning	76
50	Boa Bridging	77
51	Large Lunar Shelter	78
52	Large Lunar Shelter and Alternate Corner Configurations .	80
53	Stress Condition of Bellows	81
54	Bellows and Feet in Extended Position	82
55	Feet and Bellows in Closed Position	83
56	Moving Shelter Travel Per Cycle	85
57	Power to Move Large Lunar Shelter 0.1 mph	88
58	Small Lunar Shelter Layout	89
59	Small Lunar Shelter	90
60	Travel Per Cycle	91
61	Power Required	93
62	Surface Temperature of Smooth Cylinder With Gold and Silicate Surfaces	96

ILLUSTRATIONS (Continued)

Figure		Page
63	Estimated Performance of Extension-Contraction Bellows Vehicle Utilizing Solar-Mechanical Energy Transfer System	97
64	Double-Acting Bellows Concepts	99
65	Circular Bellows With Feet	101
66	Cycles to Failure Versus Maximum Reversed Bending Stress For CRES 321 Bellows	102
67	Dimensions of Unmanned Vehicle	104
68	Bellows Buckling Modes	105
69	Critical Conditions for Strain	105
70	Cable Displacement	106
71	Bellows Convolution Shape	108
72	Maximum Deflection Per Convolution Versus Bellows Depth	109
73	Axial Spring Rate Per Convolution Versus Bellows Depth	110
74	Bellows Depth Versus Mass Per Convolution	112
75	Lunar Supply Vehicle	114
76	Lunar Supply Vehicle Preliminary Sketch	115
77	Vehicle Systems for Comparison	119
78	Vehicle Obstacle Clearance Capability	120
79	Vehicle Footprint Pressures	123
80	Vehicle Obstacle Climbing Capability	124
81	Equivalent Drag-to-Weight Ratio of Present Systems	126
82	Equivalent Drag-to-Weight Ratio of Worm-Type Vehicles	127

ILLUSTRATIONS (Continued)

Figure		Page
C-1	Case I τ/σ Constant	137
C-2	Case II τ/σ Proportional to Displacement	139
C-3	Case III Elms Model - Vehicle Fixed At One End	141
D-1	Vehicle Configuration	143
D-2	Coordinate System	144
D-3	Displacements	145
E-1	Traveling Wave Made Up of Cranks	148
E-2	Continuous Wave Surface	149
E-3	Traveling Wave Point of Zero Velocity	152
E-4	Frictional Forces on a Wave	157
E-5	Partially Submerged Wave	158
F-1	Payload to Gross Weight Ratio for Stainless Steel Bellows.	163
F-2	Useful Load to Gross Weight Ratio for Fiberglass Bellows	164
F-3	Vehicle Footprint Pressure	166
F-4	Vehicle Footprint Pressure for Small d/b	166
F-5	Minimum Allowable Design Pressure.	168
F-6	Bellows Force at Maximum Deflection	170
F-7	Vehicle Empty Mass	171



ARTIST'S CONCEPTION OF LUNAR WORM

FEASIBILITY STUDY FOR LUNAR WORM
PLANETARY ROVING VEHICLE CONCEPT

By. F. A. Dobson and D. G. Fulton
Aeronutronic, Division of Philco Corporation

SUMMARY

A feasibility study has been carried out of various concepts of using a bellows to provide cross country mobility, particularly on the moon. Effort was directed primarily toward analytical treatment of bellows mobility and of bellows structure including both corrugated and membrane bellows, and applying the results to several brief design studies of typical missions. All concepts studied can have all moving parts internally located in a protected, pressurized environment and can be considerably foreshortened during delivery.

The concept wherein the bottom surface of the vehicle moves in the form of a traveling wave similar to the motion used by snakes and centipedes appears to be potentially the most versatile.* As compared with current cross country vehicles, it is capable of moderate to high speeds over rough terrain with a smoother ride and less vehicle bounce, good maneuverability, good propulsive efficiency, better ability to climb obstacles and to bridge crevices. It can be designed with a very low footprint pressure for use over a wide variety of surfaces including even fluid-like soils through which it is capable of swimming.

The double-acting bellows concept, which is a variation of rib-walking, where adjacent ribs contacting the surface are 180° out of phase, appears quite suitable for unmanned vehicles with regard to simplicity, ease of deployment, weight and power requirements but the ride tends to be rough and ability to clear obstacles is somewhat limited. A version of this concept can be designed which is within the present state-of-the-art of metal bellows technology.

The extension-contraction bellows concept, wherein the vehicle alternately shortens and lengthens and propulsion is derived from asymmetry built into the lower surface, is the simplest concept considered but also requires the most power because of friction in sliding over the terrain. It is restricted in footprint loading and maneuverability but is uniquely suited for incorporation of a novel solar-mechanical energy transfer system which holds some promise as a lightweight, inexpensive means for supplying mechanical energy for propulsion.

*The mechanization of the traveling wave motion is the subject of a prior, independent, Aeronutronic invention disclosure dated February 5, 1965, entitled "Peristaltic Track."

The study also includes fundamental analytical treatment of a stepped surface planing over soil, of wave motions which might be used by a variety of vehicles and of the structure of membrane bellows. A lunar soil model suitable for short stroke and cyclic motion studies was developed.

INTRODUCTION

An important part of the overall program for lunar exploration is transportation over the surface of the moon. The characteristics of this surface are still largely unknown and are the subject of widely differing predictions. It is agreed, however, that in certain respects (such as reduced gravity, extreme vacuum, severe temperature extremes, and various hazards such as radiation and meteorites), the environment will differ greatly from that on earth. For these reasons, lunar vehicles undoubtedly will have to possess new and unusual features. These will be in addition to the basic off-road capability which is necessary in traversing unprepared surfaces. A variety of concepts for providing this mobility have been considered, some of which depart substantially from conventional wheeled and tracked vehicles such as walkers, walking-beam wheels, elastic wheels, and jumpers (pogo type).

The purpose of this study is to investigate the possibility of satisfying the special requirements for lunar vehicles by use of new concepts based on sealed expandable bellows. A bellows offers significant advantages including no external moving parts in the harsh lunar environment, low footprint pressure desirable for surfaces of unknown texture or bearing strength, ability to bridge crevices, convenience for packaging, and possibility of increasing effective wall thickness for emergency protection from radiation during solar flares. Because of the similarity between an elongated bellows and various types of worms or caterpillars, it is logical to investigate the use of worm-like motions of the bellows for propulsion. For this reason, this concept is named the "Lunar Worm." The major task of the study is to determine the feasibility of a bellows for providing vehicle mobility on the lunar surface with secondary tasks to explore in a preliminary manner its use for several possible mission applications, to provide a gross comparison between the performance of bellows vehicles and other type vehicles and to point out the direction of further effort.

Mobility analyses were made for extension-contraction type bellows vehicles, for rib-walking type bellows vehicles, and for traveling wave type bellows vehicles. Structural analyses were made for preformed bellows and inflatable membrane bellows including the development of an analytical technique for the latter. Design studies were made for movable lunar shelters, a small unmanned vehicle having limited range and a manned roving vehicle having extended range. Overall evaluation was made from considerations of mobility, structural limitations, and propulsive energy.

Information on the present state-of-the-art in convoluted metal bellows design was furnished by Solar Division of International Harvester Corporation, under subcontract to Aeronutronic. The design study of the Small Unmanned Vehicle is based upon designs proposed by Solar.

SYMBOLS

A	Amplitude of a wave; length of the cranks of a traveling-wave device
a_c	Contracted length of a vehicle segment
a_e	Extended length of a vehicle segment
B	Location of the point on a wave surface that is fixed with respect to the ground
b	Width of vehicle; width of track; for bellows design, the effective vehicle width or the distance between points where bending moment changes sign
C	Constant of proportionality for ELMS model
c	Coefficient of soil cohesion
D	Drag force; external drag; diameter
D_e	Equivalent drag
D_e/W	Equivalent drag-to-weight ratio
d	Bellows depth
E	Modulus of elasticity; location of the intersection of a wave surface with the ground surface
e	δ/L vehicle strain; with an exponent - the Napierian base
F	Allowable stress; allowable fatigue stress
f	Frequency; internal stress
G	Modulus of rigidity
g	Acceleration due to local gravity
g_e	Acceleration due to Earth's gravity
H	Tractive force
h	Vehicle height
I	Moment of inertia
J	$(l^2 \gamma_s)/m_p$ dimensionless planing parameter

j	Soil displacement from its initial location
K_c	Modulus of soil deformation due to cohesion
K_ϕ	Modulus of soil deformation due to friction
K_1	Soil parameter reflecting degree of soil compactness
K_2	Soil parameter reflecting the fundamental character of the soil shear curve
k_a	Effective coefficient of friction of the aft-moving portion of an extension-contraction vehicle
k_f	Effective coefficient of friction of the forward-moving portion of an extension-contraction vehicle
L_c	Closed (stored) length of a bellows vehicle
L	Vehicle length; of an extension-contraction vehicle - the minimum length during an operating cycle
L_s	Length of stroke of an extension-contraction vehicle
l	Effective length in the direction of motion of a planing surface
M	Mass; total vehicle mass
M_b	Bending moment
M_e	Empty vehicle mass
M_u	Mass of useful load
m_p	Loading on a planing surface per unit of width normal to the direction of motion
N	Number of bellows convolutions in a vehicle
N_s	Number of segments of a segmented vehicle
n	Number of segments of a vehicle which are extended; exponent, dimensionless factor reflecting stratification of the soil
P	Force; force exerted on the end of the vehicle
P_s	Bellows spring force
P_f	Frictional force
P_t	Power required to move a wave surface on a moving vehicle; power required to propel a vehicle

p	Point on an extension-contraction vehicle which is instantaneously at rest with respect to the ground; vehicle footprint pressure
p_e	Footprint pressure of empty vehicle
p_p	Vehicle planform loading
p_{al}	Maximum allowable planform loading for a vehicle to plane according to the planing theory
p_i	Internal pressure in a vehicle
q	Running load in a member per unit of length (width)
R	Ratio of vehicle length per foot (planing surface) to the effective length of the foot in the direction of motion
R_s	Spring rate
r	Radius (of vehicle); hoop radius; horizontal resistance to motion along the shear plane
S	Area; footprint area
S_p	Planform area
s	Distance traveled
T	Period, time per cycle
t	Time; bellows material thickness
t_e	Effective thickness
V	Volume; vehicle enclosed volume
v	Vehicle (average) forward velocity
v_t	Tangential velocity of a wave surface with respect to the vehicle
v_w	Wave velocity relative to the ground
W	Weight in the local gravity; total vehicle weight
w	Weight of one segment of a segmented vehicle
X	Location of a point on a wave surface
X_o	Distance between the node of the transverse wave and the corresponding node of the longitudinal wave

x	Longitude coordinate of a wave
x, y, z	Generalized orthogonal coordinate
y	Distance from the neutral axis to the extreme fiber (in calculating bending stress)
z	Depth of penetration of the soil surface
α	Angle of attack of a planing surface with respect to the vehicle
β	Slope of a wave surface
γ	Specific mass of structural material
γ_s	Specific mass of the soil
δ	Bellows extension per disc
Δ	Incremental value
η	Efficiency
θ	Slope angle
λ	Wavelength
μ	Friction coefficient
μ_s	Soil friction coefficient; $\tan \varphi$
μ_a	Coefficient of friction of the aft-moving portion of an extension-contraction vehicle
μ_f	Coefficient of friction of the forward-moving portion of an extension-contraction vehicle
ν	Poisson's ratio
ξ	Particle displacement
π	3.14
ρ	Local radius of curvature
σ	Normal soil pressure
τ	Soil shear stress

- ϕ Angle of friction between soil grains
- ψ Phase angle between adjacent cranks of a traveling wave vehicle
- ω Angular velocity

MOBILITY ANALYSIS

In this section, generalized expressions are developed for velocity and power requirements of various configurations as a function of soil characteristics. Although a number of simplifying assumptions are made, the results are considered accurate enough for use in carrying out gross comparisons between different systems.

The statement of work for this study required the use of the NASA Engineering Lunar Model Surface (ELMS). It subsequently developed that ELMS had been developed for wheeled or tracked vehicle analyses but was not adequate for the present study which required analysis involving cyclic motion of the vehicle contacting the surface. In addition, certain of the ELMS relations were dimensionally inconsistent for analytical studies of this nature. Therefore, it became necessary to develop soil models which were both appropriate and realistic for the present study.

To obtain a clear picture of the mobility mechanism, the bottom surface of the vehicle which actually contacts the soil is treated as a thrust-producing mechanism. All sources of drag, such as bulldozing, sliding friction along the sides of the vehicle, climbing angle, and drag due to some object or vehicle being towed, are lumped together as "external drag." The ratio of external drag to total vehicle weight is treated as an equivalent climbing slope, which is considered to be the independent variable in most of the charts which follow. Since the traction is obtained by friction with the soil, the equivalent climbing slope can never be greater than the average vehicle-to-soil friction coefficient. The velocities are handled in nondimensional form.

The power required for propulsion under various conditions is given by an "equivalent drag-to-weight ratio," which is equal to the propulsive power divided by the vehicle weight and the average velocity. This ratio is called "specific power" by some authors. For a propulsive system with no losses, the equivalent drag-to-weight ratio would be equal to the equivalent slope. In an actual case, the equivalent drag-to-weight will always be greater than the equivalent slope and will become infinite when the vehicle stalls. When the equivalent slope becomes negative (that is, on a down grade) the equivalent drag-to-weight becomes quite small, and in some cases may become negative indicating that power may be recovered from the propulsion system.

The mobility studies are divided into three major sections, the first of which is concerned with the Extension-Contraction motion, the second with the Rib-Walking motion and the third with Traveling Wave motion, which is a generalization of rib walking.

LUNAR SOIL MODEL

For quantitative comparisons of different mobility systems, it is necessary to set up a soil model. Since the NASA Engineering Lunar Model Surface (ELMS), as mentioned previously, was found to have shortcomings, two other models were introduced. In this section the three models will be discussed briefly. A more detailed description of the ELMS will be found in Appendix B.

In an analysis of vehicle mobility, the soil characteristics of greatest importance is the friction coefficient between the vehicle traction surface and the soil. This friction coefficient, μ , is equal to τ/σ , the ratio of shear stress to normal stress at the interface between the soil and the vehicle. The value of τ/σ specified in the ELMS is shown as a function of soil slippage, or horizontal displacement in curve III, Figure 1.

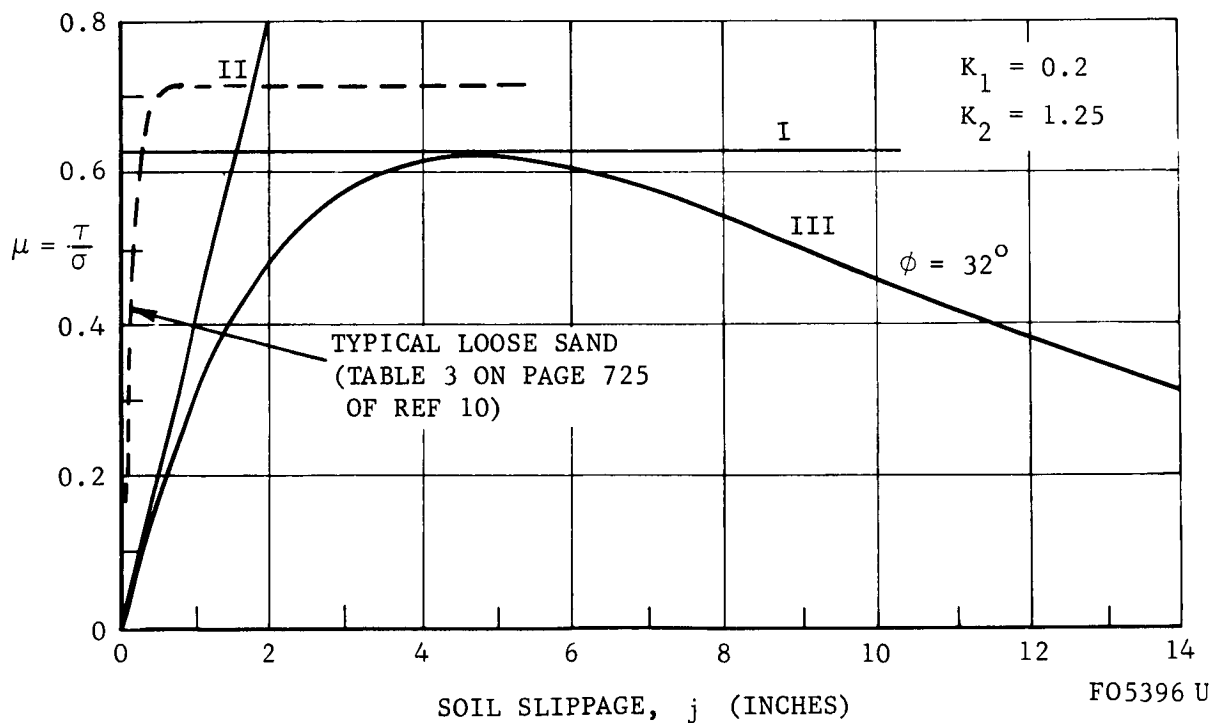


FIGURE 1. SOIL FRICTION COEFFICIENT VERSUS SOIL DISPLACEMENT

The difficulties inherent in the ELMS are illustrated in Figure 1. In the first place the choice of independent variable is not appropriate. To make the relation correct dimensionally, the slip, which is measured in inches, would have to be divided by some other length -- presumably the length of the test section originally used to obtain the empirical relation. Since no information is available on this point curve III on Figure 1 cannot be used for general analytical work. The second difficulty with the ELMS is that the friction coefficient τ/σ approaches zero for very small or very large displacements. When an attempt is made to use curve III in a graphical analysis of reciprocating motion, it is found that for very short or very long strokes the drag

disappears, which is not considered reasonable. The third difficulty in using the ELMS, particularly for reciprocating motions is that the friction coefficient is not defined for negative slippage. Some type of hysteresis must be present; but the form of the hysteresis loop cannot be deduced from the data given.

In the hope of obtaining an analytical solution for the extension-contraction motion, Soil Model II has been considered. This model is represented on Figure 1 by the straight line II through the origin, with the same slope as the initial slope of line III. Although this model is considerably simpler to manipulate than the original model, it also gives unrealistic results, and is not considered satisfactory.

Since any reciprocating device disturbs the soil and can be considered to operate in something resembling loose sand after the first stroke, a third soil model has been developed based on the observed behavior of loose sand (ref. 10). These data presented in Figure 1 indicate that the friction coefficient increases very rapidly with slippage up to a constant value which is independent of further displacement. This behavior suggests that the most logical soil model would simply employ a constant friction coefficient, which is represented by line I in Figure 1. This soil model allows the desired performance relations to be obtained in simple closed-form expressions, and has been used in all subsequent work.

A soil characteristic second only in importance to friction coefficient is soil hardness or the footprint pressure developed as penetration normal to the surface of the soil is increased. The range of soil hardnesses specified in the ELMS is shown in Figure 2. All three soil models use this relation, which shows that the soils being considered develop footprint pressures approximately proportional to penetration depth. The proportionality constant, however, varies by more than two orders of magnitude for different soils.

Figure 2 defines footprint pressure while penetration is increasing or held constant, but not while decreasing. This is a disadvantage, but not a serious one for the present study. The distinguishing characteristic of bellows-type vehicles is their low footprint pressure, which will be shown later (Fig. 79) is not expected to exceed 30 pounds per square foot or about two-tenths of a pound per square inch on the moon. Inspection of Figure 2 shows that except in the case of the "extreme soil" the resulting penetration depth will be negligible and can be ignored completely. For the extreme soil, where the penetration may be appreciable, the angle of internal friction is expected to be quite low -- that is the soil behaves more like a liquid than a solid. Since a pressure which varies directly with depth is equivalent to a buoyant force, the footprint pressure for deep penetrations will be considered as a function of penetration depth only regardless of direction of motion.

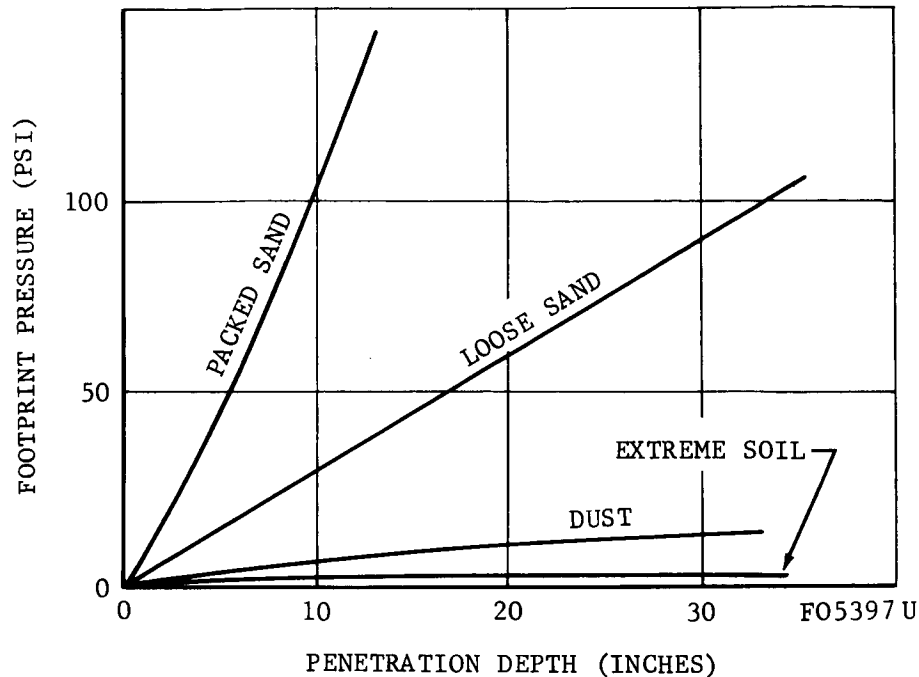


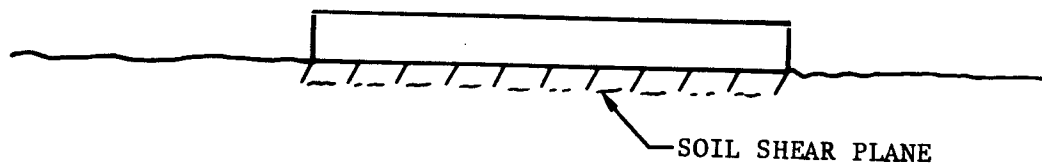
FIGURE 2. FOOTPRINT PRESSURE VERSUS PENETRATION

EXTENSION-CONTRACTION TYPE OF VEHICLE

The extension-contraction type of vehicle is a bellows vehicle that is provided with a means of alternately increasing and decreasing its length, and derives its propulsion from this motion. The propulsion comes from a difference in friction coefficient of the advancing and the retreating portion of the vehicle which is obtained by some sort of asymmetry in the construction of its lower surface. The primary reason for considering such a concept is the possibility of achieving a low footprint pressure device with a very simple mechanization, and with no exposed moving parts. The means of achieving the fore and aft differential in friction coefficient is discussed under Soil Considerations.

Soil Considerations

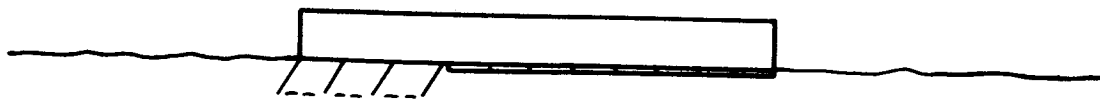
Producing the friction coefficient differential. - The most obvious way of attempting to cause the fore and aft differential in friction coefficient required for extension-contraction propulsion is to put cleats which slant in an aft direction on the bottom surface of the vehicle as in Figure 3(a). If the vehicle has a typical planform loading the result is likely to be as illustrated; both forward and aft moving cleats are fully imbedded in the soil. In a frictional material, this will result in the soil shearing along a plane at the lower edge of the cleats, and the resulting friction will be independent of the direction of motion or the inclination of the cleats. If, however, the cleats are built at a



(a)



(b)



(c)

F05398 U

FIGURE 3. POSSIBLE CLEAT CONFIGURATIONS

shallow angle, and the vehicle is lightly loaded, the situation depicted in Figure 3(b) occurs. In this case, the forward-moving cleats ride on top of the soil and a friction coefficient differential is produced. This phenomenon will be referred to as planing, and the "cleats" will be referred to as planing surfaces. The conditions for which planing will occur are discussed below, and it is shown that the primary requisite is a low vehicle planform loading. The disadvantage of this concept is its lack of versatility. It appears that a design can be conceived for almost any type of soil, but a given design will work in only a narrow range of soils.

Another alternative is to hinge the cleats as in Figure 3(c). If the surface of the folded cleat is a normal rough surface, the friction coefficient of the forward-moving portion will be the tangent of the sand friction angle. Bekker³ indicates that the cleats on the aft moving portion may increase the friction by about 20 percent. For lightly loaded configurations, the weight of sand carried between the extended cleats is significant and the cleat augmentation may be greater than 20 percent. There is a possibility that the exposed surface of the folded cleats may be coated with a low-friction material such as tetrafluorethylene. Tests of this material on sand made by the contractor showed a friction coefficient of about 0.25. The folding cleats, shown in Figure 3, have the disadvantage of requiring exposed moving parts which is contrary to one of the primary advantages of the worm concept.

Although a limited amount of analysis in this section will utilize the tractive effort as given by the ELMS model, most of the results are based upon a friction coefficient which is independent of the soil displacement as discussed in the section on Lunar Soil. The preceding discussion applies in either case where, in considering the ELMS model, the term "friction coefficient" refers to the magnitude of $\tan \varphi$.

Theory of planing. - Using the Coulomb Earth Pressure theory as given by Jumikis,⁴ the geometry of a planing surface is shown in Figure 4. The surface is considered two-dimensional, with an angle of attack, α , and is moving to the right. The internal friction angle of the sand is φ , and the friction angle of the sand against the surface is φ_1 . The surface is supporting a running load of m_p pounds mass per unit width (normal to the paper). It is desired to find the length, l , which will be in contact with the soil, and the horizontal force which will be required to move the planing surface.

It is assumed that the triangular section of soil ABC moves with the planing surface. Shearing takes place along the plane AC, but the soil is just at the point of shearing on the plane AB.

If the soil has a mass of m_s pounds per unit width, the total weight being moved is $(m_p + m_s)g/(g_e)$ per unit width, and the resistance is $r = (m_p + m_s)g/(g_e) \tan \varphi$ pounds per unit width. The effective friction coefficient therefore becomes:

$$\mu_e = \frac{g_e r}{g m_p} = \left(1 + \frac{m_s}{m_p} \right) \tan \varphi = \tan (\varphi_1 + \alpha) \quad (1)$$

J is the dimensionless planing parameter which relates the critical load on the planing surface to the soil density and the geometry of the planing surface. Since the critical load varies inversely with J, it is desirable to have the value of J as small as possible. To facilitate the use of Equation (4) in the design, the value of the dimensionless ratio $J = l^2 \gamma_s / m_p$ is plotted as a function of the angle of attack α , and the friction angles ϕ and ϕ_1 in Figure 5.

The curves of Figure 5 show that, if the planing surface is rough enough to force shearing to take place in the soil ($\phi_1 = \phi$), the value of J can never be less than about 4. However if the planing surface is very smooth or has a low-friction coating ($\phi_1 < \phi$), the value of J can be considerably decreased, allowing higher loadings to be used.

If the lower surface of a vehicle has a number of planing surfaces arranged in tandem, certain geometric constraints must be met for the planing analysis to be valid. The arrangement shown in Figure 6 is the maximum length of planing surface that can be effective on a vehicle surface. The problem is assumed to be two-dimensional. Increasing the length of the cleats will not increase the soil contact area because one cleat will shade the one behind to a degree determined by the soil friction angle, ϕ . The relationship between vehicle surface area and maximum cleat length is

$$l_v = l \cos \alpha + l \frac{\sin \alpha}{\tan \phi} \quad (5)$$

$$R = \frac{\Delta l_v}{l} = \cos \alpha \left(1 + \frac{\tan \alpha}{\tan \phi} \right) \quad (6)$$

The ratio, R, approaches 1.0 for small angle of attack, α , but is never less than 1.0.

The loading on the planing surfaces may now be referred to the planform loading of the vehicle. The vehicle planform loading, p_p is defined as the total vehicle weight (in the local gravity) divided by the projected area of the vehicle bottom surface. Considering only the weight supported by one cleat,

$$p_p = \frac{M}{S} \cdot \frac{g}{g_e} = \frac{m_p}{l_v} \cdot \frac{g}{g_e} \quad (7)$$

where small letters refer to quantities per unit of vehicle width. From Equation (4) the allowable loading on the planing surface is

$$m_p = \frac{l^2 \gamma_s}{J} \text{ lbm}$$

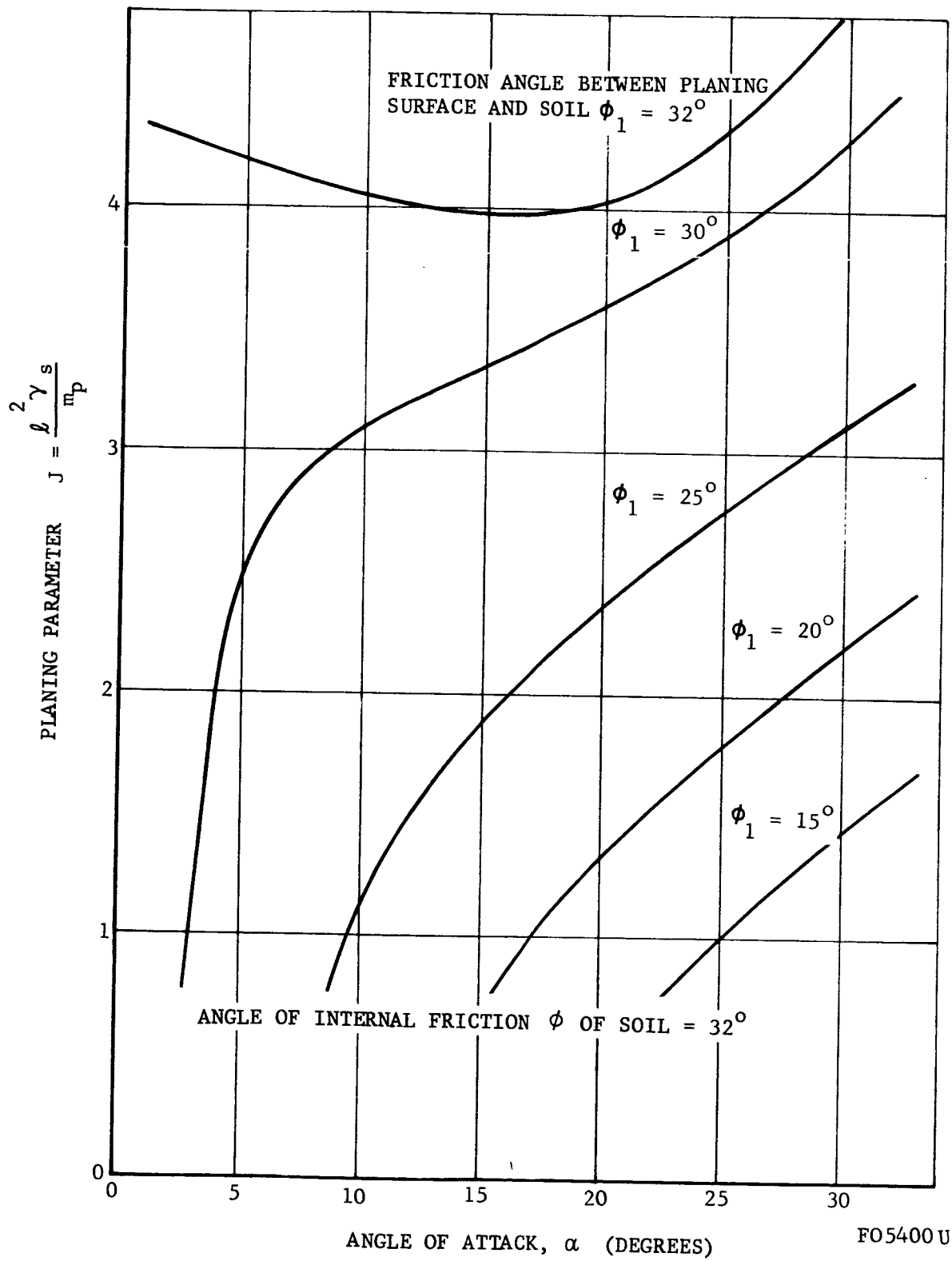


FIGURE 5. DIMENSIONLESS PLANING PARAMETER

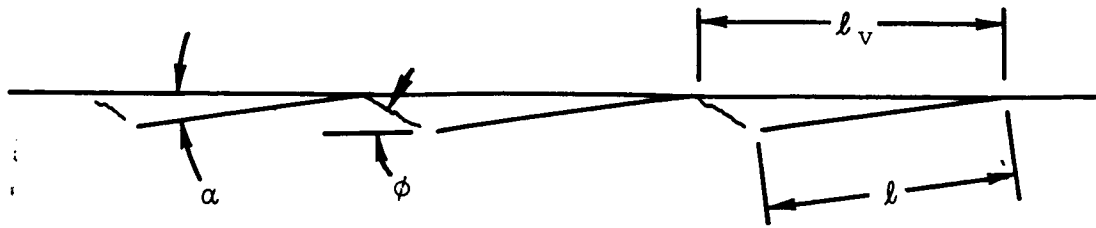


FIGURE 6. PLANING SURFACES ON A VEHICLE BOTTOM

per unit of vehicle width. The corresponding pressure acting on the planing surface is

$$p = \frac{m_p}{l} \cdot \frac{g}{g_e} = \frac{l \gamma_s}{J} \cdot \frac{g}{g_e} \quad (8)$$

This amount of vehicle loading will result in a vehicle planform loading of

$$P_{al} = p_p \cdot \frac{l}{l_v} = \frac{l \gamma_s}{RJ} \cdot \frac{g}{g_e} \quad (9)$$

which is the maximum allowable vehicle planform loading if the planing analysis is to be valid.

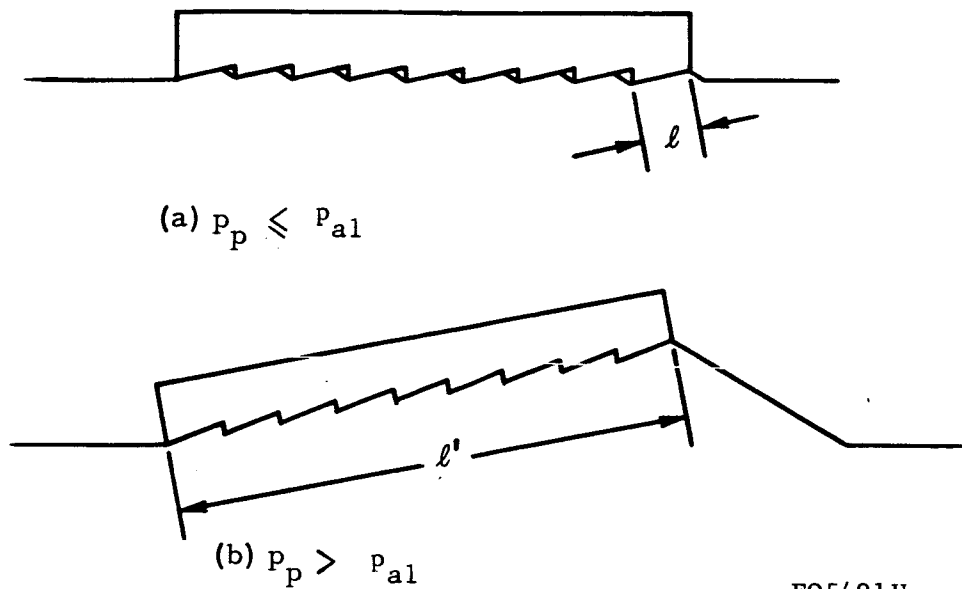
To obtain a useful expression for allowable footprint pressure, take $\alpha = 6$ degrees, $\gamma_s = 50 \text{ lbm/ft}^3 = 0.029 \text{ lbm/in.}^3$, $\phi_1 = \phi = 32$ degrees, $g_e/g = 6$. From Figure 5, $J = 4.07$.

$$R = \cos 6^\circ \left(1 + \frac{\tan 6^\circ}{\tan 32^\circ} \right) = 1.16$$

Then the maximum allowable vehicle footprint pressure is

$$P_{al} = \frac{(0.029)}{(1.16)(4.07)(6)} l = \frac{l}{1000} \text{ psi} \quad l \sim \text{in.}$$

Presumably, if a vehicle is built with a greater footprint pressure than this, it will either dig into the soil, or will assume a positive angle of attack and a mound of sand will be built up under the vehicle as shown in Figure 7. The situation depicted is a rigid object being towed through the sand. As the



F05401U

FIGURE 7. LIGHTLY LOADED AND HEAVILY LOADED PLANING VEHICLES

loading is increased above p_{al} , the vehicle assumes an angle of attack and a new planing situation develops with the entire bottom of the vehicle acting as a planing surface. The new allowable loading is based on the vehicle length, l , rather than the step length, l .

$$p_{al} = \frac{l' \gamma_s}{RJ} \cdot \frac{g}{g_e} \quad (10)$$

Therefore, as the loading of a vehicle is increased above p_{al} , a pile of sand can be expected to begin to build up in front of the vehicle.

Experimental data. - The experimental data shown in Figure 8 provides a rough verification of this simplified planing theory and indicates the consequence of exceeding the loading given by Equation (10). This test was conducted in dry sand with a density of approximately 100 lb/ft³, and a friction angle of 30 degrees. The model had a rough wood surface, and the geometry is shown in Figure 8.

The allowable loading for planing was calculated by using $J = 4.0$ as given by Figure 5. The differential in friction coefficient between the forward and aft directions disappears rapidly as p_{al} is exceeded, and is nearly nonexistent at a loading of twice the allowable loading. Therefore, it may be concluded that although the expression for allowable loading, given by Equation (9), may not be entirely accurate, it is nevertheless a reasonable criterion for the loading of an extension-contraction vehicle.

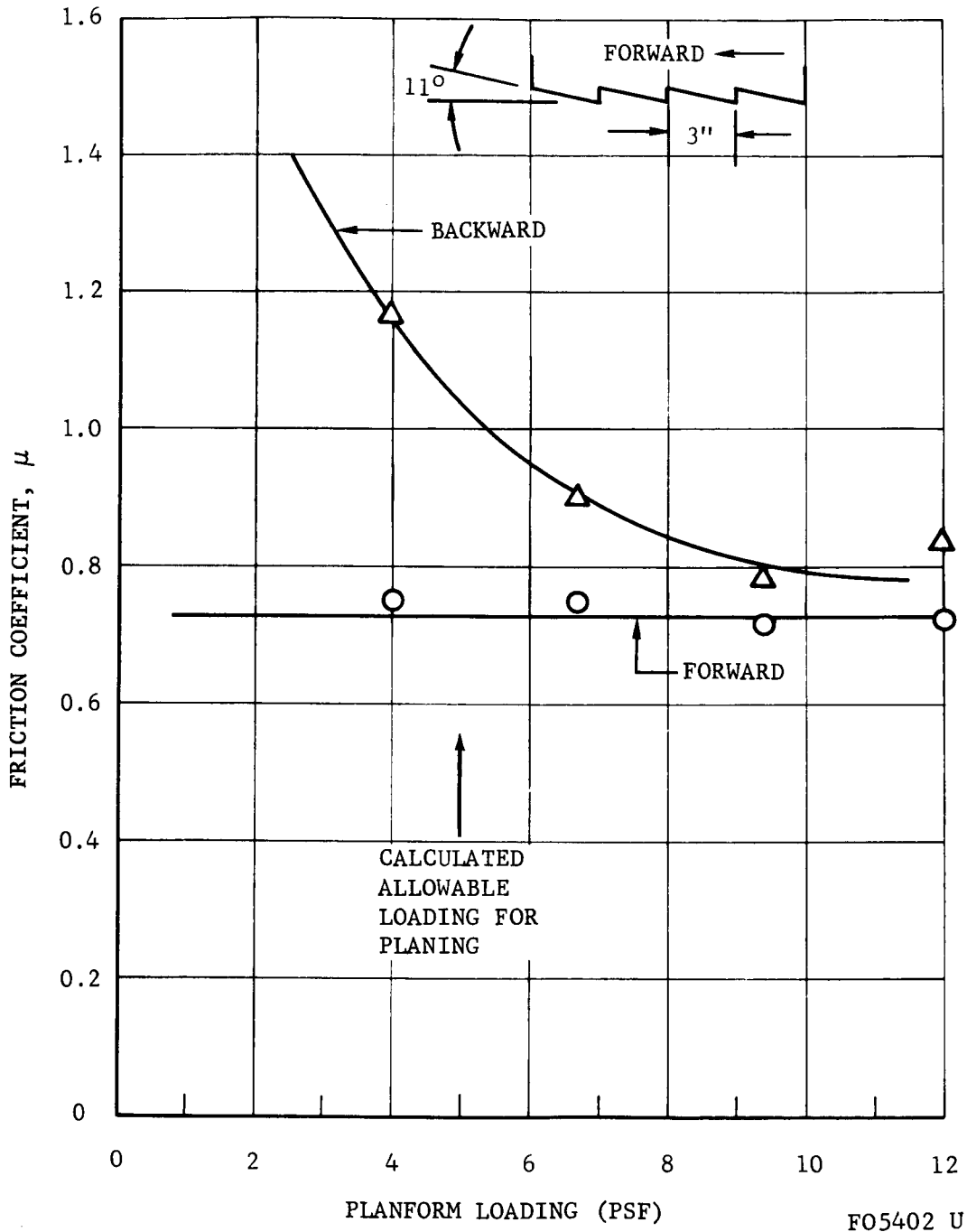


FIGURE 8. EXPERIMENTAL FRICTION COEFFICIENT IN SAND

Extension-Contraction Vehicle Performance

The analysis of the mobility of the extension-contraction vehicles was made by equating the tractive forces for each end of the vehicle, i. e., thrust equal to drag. No dynamic forces were considered. The detailed analysis is given in Appendix C. The primary parameter used for comparing the propulsive efficiency of vehicles is equivalent drag-to-weight ratio. This equivalent drag is not necessarily identifiable as an actual drag on the vehicle, but it is the drag which would consume the same power as the vehicle when applied at the average vehicle velocity. The equivalent drag-to-weight ratio may be given as

$$\frac{D_e}{W} = \frac{\text{power}}{W \times \text{velocity}}$$

or

$$\frac{D_e}{W} = \frac{\text{work}}{W \times \text{distance}}$$

Three assumed soil characteristics were analyzed:

Case I. τ/σ constant - this is the classical friction coefficient where frictional force is proportional to normal force. This model is considered a good representation of loose sand if the vehicle stroke is large compared to the cleat size.

Case II. τ/σ proportional to soil displacement, j . This form is the first order approximation to the Engineering Lunar Model Surface (ELMS) for small soil displacement.

Case III. $\tau/\sigma = C (e^{-0.1 j} - e^{-0.4 j})$ - Engineering Lunar Model Surface (ELMS). From Appendix B, the nominal value of C for a smooth surface is 1.32.

The comparison of these three soil models was made by making the constant friction coefficient for Case I equal to the peak value of τ/σ for the ELMS model; and the constant of proportionality for Case II, that which matches the slope of the ELMS model at the origin. In each case, the nominal multiplying constant for the aft-direction was taken as 1.2 times that for the forward direction, following the reasoning given on page 14.

The reason for studying Case II is that it gives information about the ELMS model since it is the first order approximation to the ELMS model for a small stroke. A complete solution to Case III was not obtained.

Power requirements for the three soil models. - The work required to extend a vehicle segment which has one end fixed to the ground is shown in Figure 9. This is obtained by integration of force times distance over the vehicle surface at any instant, and then integration over the stroke length as shown in Appendix C. Case II and Case III are parabolic with zero slope at the origin, and as expected, are equivalent for small stroke lengths. The friction coefficient assumed for Case I is equal to peak value of τ/σ for the ELMS model.

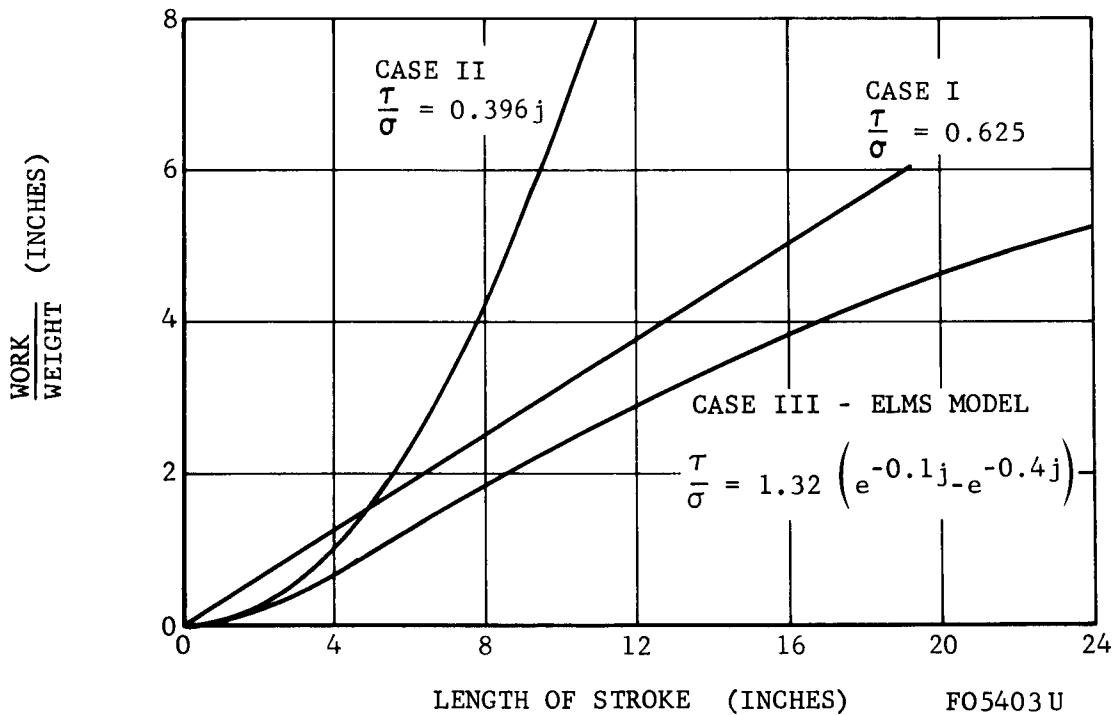


FIGURE 9. WORK TO EXPAND A VEHICLE FIXED AT ONE END

For Case I and Case II, the instantaneous stationary point, p , of a vehicle which is free to move remains fixed on the vehicle and on the ground during any half cycle of extension-contraction. The location of the point p is found by equating the forward force to the aft force on the vehicle. The motion of the vehicle midpoint (referred to here as the cg) is proportional to the distance from the point p to the cg . The work for the portion of the

vehicle on each side of the stationary point may be found as for Figure 9.
The equivalent drag-to-weight ratio is found by

$$\frac{D_e}{W} = \frac{\text{Work}}{W \times s}$$

The assumption is made that each succeeding expansion or contraction is just like the first; that is, the soil displacement, j , is taken as starting from zero at the point at which the motion reverses direction.

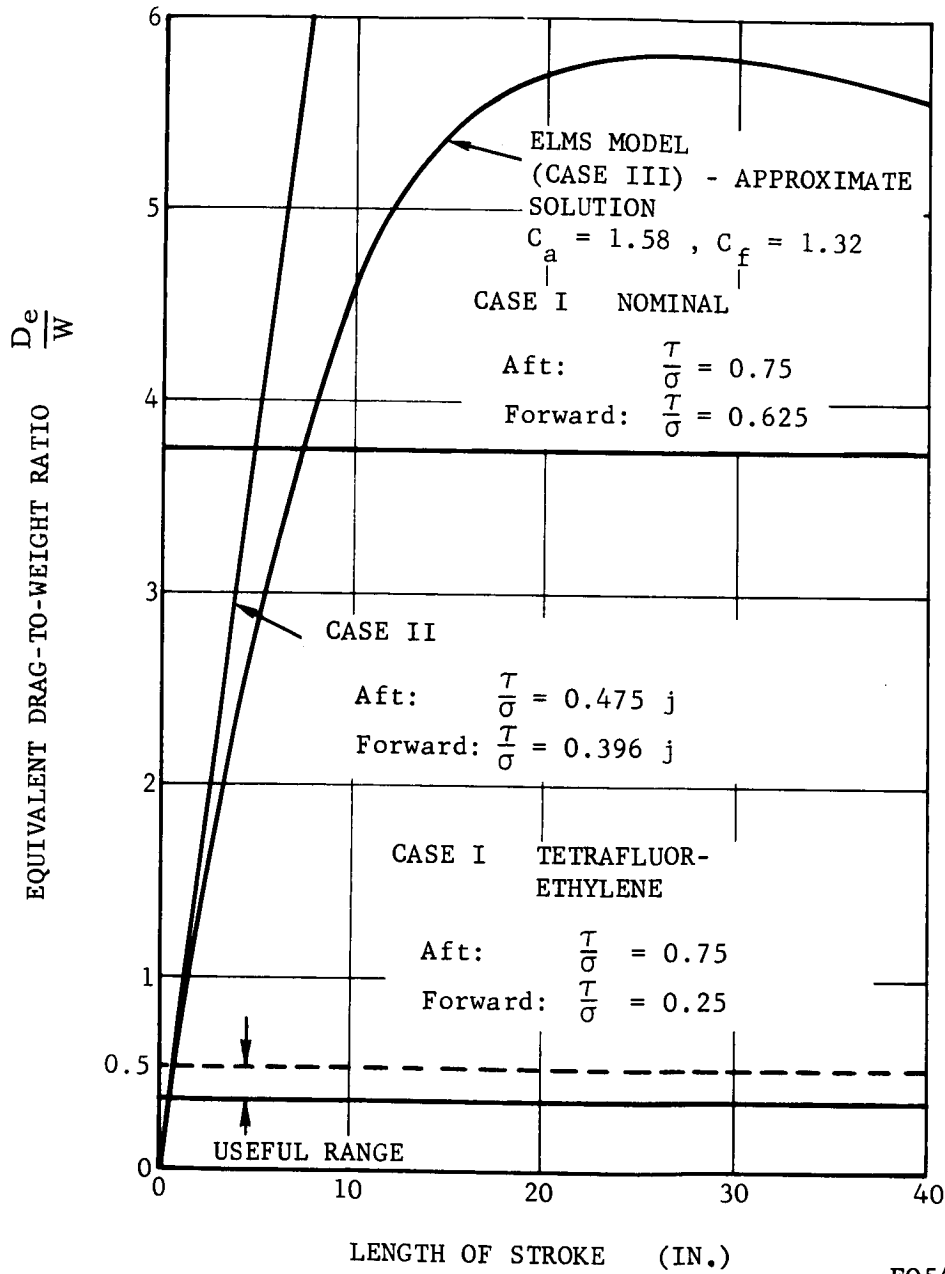
The result given in Appendix C is shown in Figure 10. The worst assumed condition for Case I is a friction coefficient equal to maximum τ/σ for the nominal ELMS model for the forward-moving portion, and 20 percent greater than this for the aft-moving portion. The best assumed condition is for tetrafluorethylene on the forward-moving portion.

For Case III the stationary point p does not remain at a fixed point on the ground, but moves from its initial location. Then, since the soil shear stress is a function of the past history of the soil motion, the horizontal force is a complex function of the stroke and the location of the stationary point has not been solved. It appears that a rigorous solution requires a step-by-step numerical integration of the process. The initial location of the stationary point, however, is given as in Case II, and indications are that it does not depart greatly from this location up to stroke lengths of about 10 inches. Therefore, an approximate solution can be obtained by assuming that the stationary point remains fixed throughout a stroke (half cycle). This is the result shown on Figure 10, and is accurate for small stroke lengths. It can be shown numerically that the initial motion of the stationary point is toward the rear of the vehicle (for an expansion stroke) and the vehicle will move further than predicted by the approximation. Therefore, at least the initial departure of the actual D_e/W from the approximation shown in Figure 10 will be on the downside, i. e., the actual efficiency will be better than predicted.

Figure 10 shows that the drag-to-weight ratio using the ELMS model (Case III) may be made arbitrarily small by using either a very small or a very large stroke length. This occurs because the friction coefficient given by the ELMS model approaches zero for either small or large soil displacements. This causes serious doubts as to the validity or completeness of the soil model, at least when applied to the present situation.

As discussed in the section on Lunar Soil, the results for Case I should be representative of the performance of the vehicle in loose sand, if the vehicle stroke is large. All further analysis and comparisons will be based upon this model.

For conventional vehicles, the equivalent drag-to-weight ratio varies from a few percent (wheeled vehicle on smooth surface) to about 1.0 for off-road operation in poor soil. For this study it will be assumed that the useful range of drag-to-weight ratios is below 0.5. It should be noted that the installed power in any vehicle must be several times the propulsive power for operation on level ground to allow for acceleration, climb, transmission losses and



F05404 U

FIGURE 10. EQUIVALENT DRAG-TO-WEIGHT RATIO OF EXTENSION-CONTRACTION VEHICLES

operation at less than full throttle. The general level of the drag-to-weight ratios shown on Figure 10 indicates that, at best, this type of device will be marginally acceptable, and that if the concept is to be successful, all available means should be used to minimize power consumption.

Slope capability. - A vehicle on a slope, θ , is shown in Figure 11. A constant friction coefficient, μ , as in Case I is assumed, and the subscripts f and a refer to the portion of the vehicle forward and aft of the stationary point.

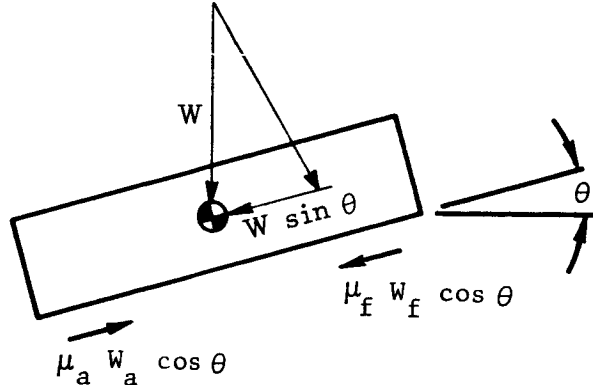


FIGURE 11. VEHICLE ON A SLOPE

The equilibrium of forces parallel to the slope is

$$\mu_a W_a = \mu_f W_f + W \tan \theta \quad (11)$$

where,

$$W = W_a + W_f$$

Substituting

$$W_a = \frac{L_a}{L} W \quad \text{and} \quad W_f = \frac{L_f}{L} W$$

This reduces to

$$\frac{L_a}{L} (\mu_a - \tan \theta) = \frac{L_f}{L} (\mu_f + \tan \theta)$$

or,

$$L_a k_a = L_f k_f \quad (12)$$

where,

$$k_a = \mu_a - \tan \theta \quad \text{and} \quad k_f = \mu_f + \tan \theta \quad (13)$$

Equation (12) is identical to the expression given in Appendix C defining the relationship between L_a and L_f . Other expressions from Appendix C can be shown to apply on a slope if the k_a and k_f , as given by Equation (13), are used. The resulting equivalent drag-to-weight ratio is

$$\frac{D_e}{W} = \frac{k_a k_f}{k_a - k_f} \quad (14)$$

This is shown in Figure 12 for several assumed values of friction coefficient. The maximum slope a vehicle can climb is given by

$$\begin{aligned} k_a &= k_f \\ \mu_a - \tan \theta &= \mu_f + \tan \theta \\ (\tan \theta)_{\max} &= 1/2 (\mu_a - \mu_f) \end{aligned} \quad (15)$$

This expression defines the asymptotes of the curves of Figure 12 since the equivalent drag-to-weight ratio approaches infinity at the maximum slope capability. This, of course, means that the forward travel goes to zero and the power required remains finite.

From Appendix C, the force which must be exerted on the end of the vehicle to extend it against the frictional force is

$$P = 1/2 W \frac{k_a k_f}{k_a + k_f} = 1/2 W \frac{(\mu_a - \tan \theta) (\mu_f + \tan \theta)}{\mu_a + \mu_f} \quad (16)$$

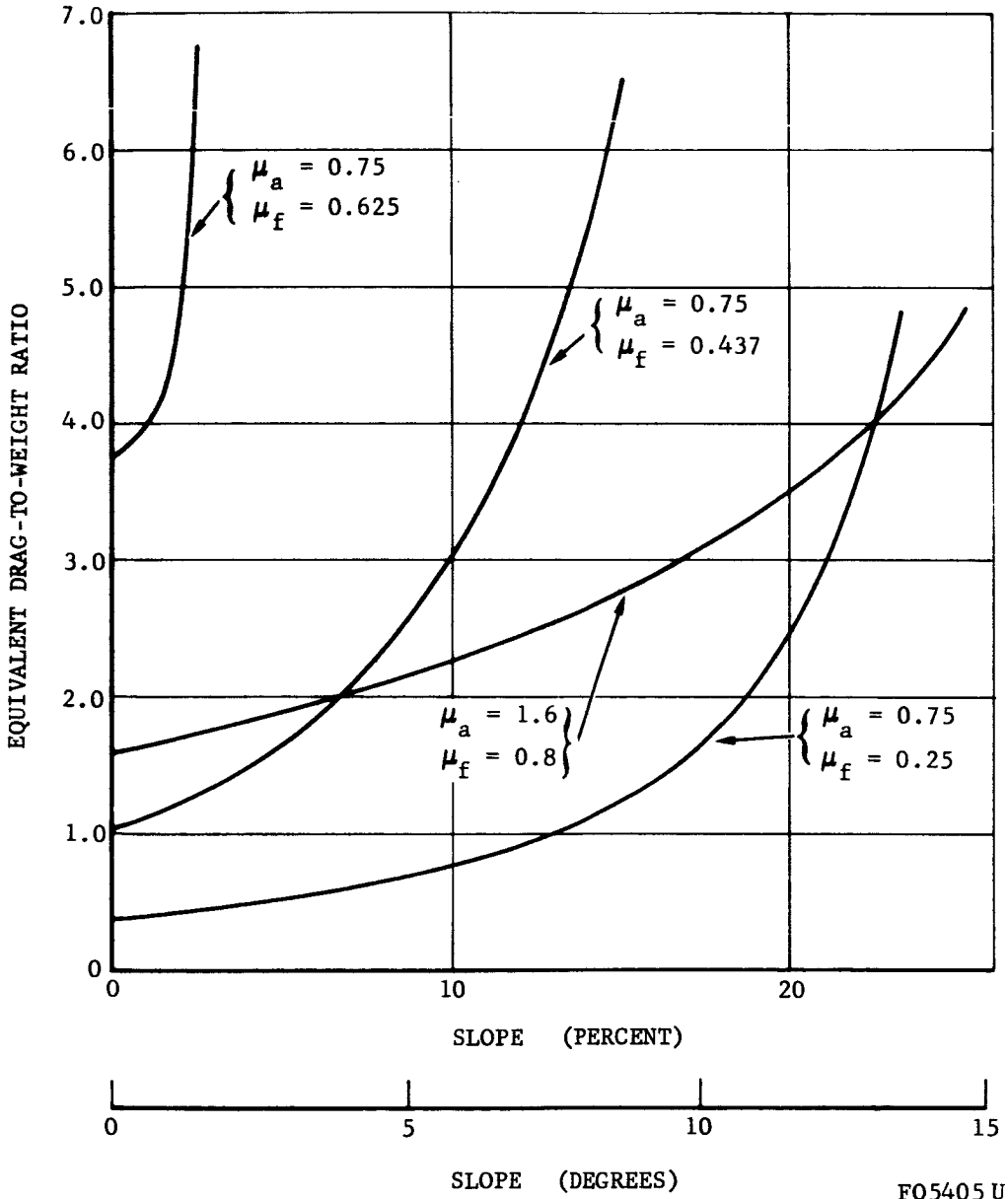
Setting the derivative of this with respect to $\tan \theta$ equal to zero gives

$$\tan \theta = 1/2 (\mu_a - \mu_f) \quad (17)$$

which happens to be the maximum slope the vehicle can climb. Putting this into Equation (16) gives the maximum value of the extension force:

$$P_{\max} = \frac{W}{8} (\mu_a + \mu_f) \quad (18)$$

Incremental extension. - In the preceding discussion, and in Appendix C, a vehicle with uniform strain throughout its length at all times has been assumed. The vehicle has been assumed to be constrained to this type of motion by some sort of internal mechanism, if necessary. A more realistic case might be a simple bellows with a spring force which is small compared with the friction force. In this case, each bellows convolution must have a restraining member to keep it from extending beyond its intended length. Also, in a vacuum, some device, such as a spring, must be provided to contract the vehicle. Now, if an extension stroke is begun with application of



FO5405 U

FIGURE 12. EFFECT OF SLOPE ON EQUIVALENT DRAG

opposed forces on each end of the vehicle, the bellows segments will pop out to their extended length, one at a time, as the magnitude of the force is increased. It may be shown that the distance traveled and the work required per stroke are the same for this case as for the uniform-strain case treated previously. The magnitude of the force required is not the same, however. For the uniform extension case, the extension force is a constant value of

$$P = 1/2 W \frac{k_a k_f}{k_a + k_f} \quad (19)$$

throughout the stroke. For the incremental extension case, the extension (or contraction) force varies linearly from zero at the beginning of the stroke to twice the value given by Equation (19) at the end of the stroke. Because of the linear variation, the work required is the same for either case.

CONSIDERATION FOR DESIGN APPLICATION

The principal problem relating to the extension-contraction mode of operation is the design of a bellows lower surface which will achieve an adequate differential in shear between aft moving and the forward moving portions. The general level of drag-to-weight ratios tend to be high and all means should be used to minimize power required. One such means is the use of a low friction type coating such as tetrafluorethylene on the bellows lower surface during the forward stroke operation. A variable geometry profile such as a hinged or flexible cleat offers promise as it tends to retract during the forward stroke. A fixed geometry type bellows can be designed to plane and not bulldoze for any given soil but is not versatile for a range of soils. Footprint loading should be kept low. Configurations utilizing this mode of operation are restricted to forward motion only because of the ratchet-type operation inherent in the concept.

RIB-WALKING TYPE OF VEHICLES

The rib-walking concept consists of a circular motion of the vehicle ribs in which each rib or bellows convolution is 180 degrees out of phase with the adjacent one. This motion is analyzed below. In addition, two modifications to this motion are proposed in the following sections. The double-acting bellows is a rib-walking device with only three feet, and the traveling-wave has multiple moving ribs with less than 180 degrees phase angle between adjacent ribs. A mathematical model is given in Appendix D which may be used to describe any of these motions.

Rib-walking

If a rib-walking vehicle is operating on hard ground, and has no spring suspension, the motion of its center of gravity is as shown in Figure 13.

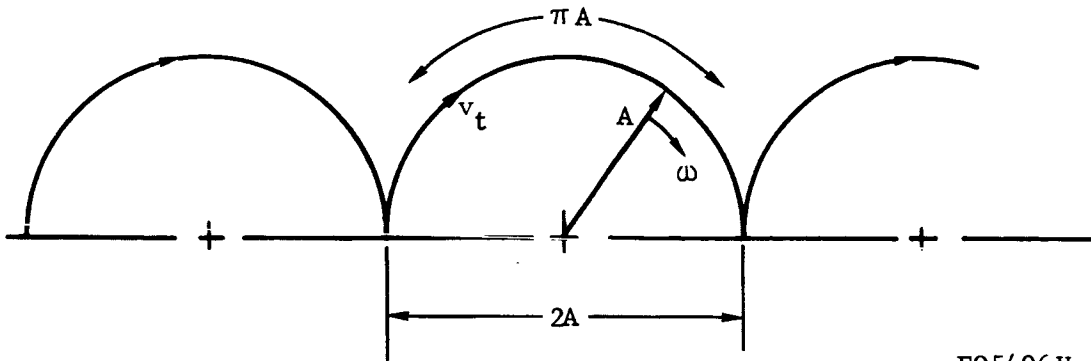


FIGURE 13. RIB-WALKING MOTION

Each arc is the path described by one (e. g., odd-numbered) set of ribs. At the tangent point of the arcs, that set of ribs leaves the ground, and the adjacent (e. g., even-numbered) set takes over.

It is assumed that the change in height shown in Figure 13 is accomplished without the expenditure of power, but that the kinetic energy of the system is lost each time the load is transferred to a new set of ribs. The tangential velocity is

$$v_t = A \omega \quad (19)$$

but the average horizontal velocity of the vehicle is

$$v = \frac{2}{\pi} v_t \quad (20)$$

The work required for each circular arc of Figure 13 is the kinetic energy lost at one impact

$$\text{Work} = \frac{1}{2} \frac{W}{g} v_t^2 = \frac{1}{2} \frac{W}{g} \left(\frac{\pi}{2} v \right)^2 \quad (21)$$

The equivalent drag-to-weight ratio is then

$$\frac{D_e}{W} = \frac{\text{Work}}{W_s} = \frac{\frac{1}{2} \frac{W}{g} \left(\frac{\pi}{2} v \right)^2}{W \cdot 2A}$$

$$\frac{D_e}{W} = \frac{\pi^2}{16g} \cdot \frac{v^2}{A} \quad (22)$$

This result is shown in Figure 14. The efficiency, then, improves with increasing radius of motion, A.

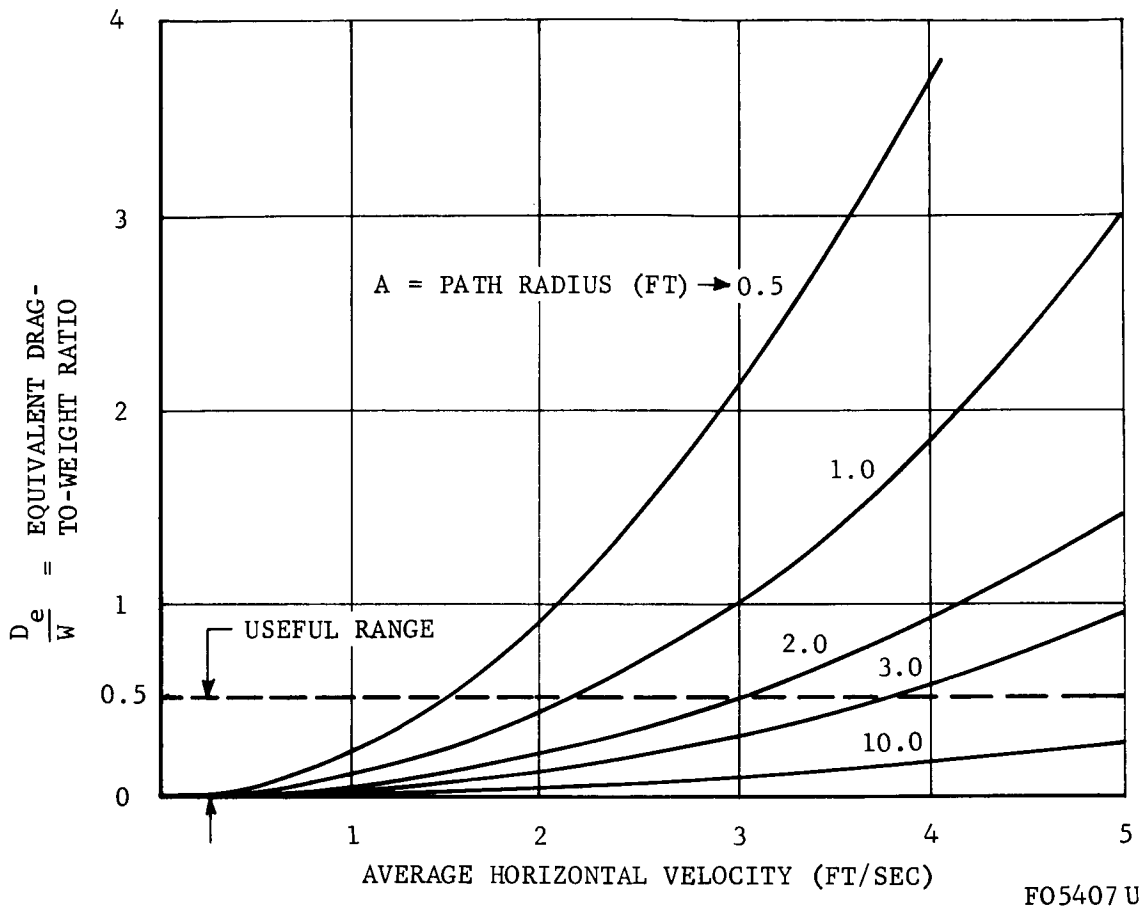


FIGURE 14. EQUIVALENT DRAG-TO-WEIGHT RATIO OF A RIB-WALKING VEHICLE ON THE MOON

A practical consideration of this motion is the roughness of the ride. The motion shown in Figure 13 involves a change in both vertical and horizontal velocity from zero to a maximum during each cycle. An additional consideration is that the vehicle will begin to jump at the velocity at which centrifugal force exceeds the vehicle weight and the analytical expressions will no longer apply. This velocity is given by

$$W = \frac{W}{g} \cdot \frac{v_t^2 \text{ jump}}{A}$$

$$v_{\text{jump}} = \sqrt{\frac{2}{\pi} g A} \quad (23)$$

and is plotted in Figure 15. Both Figures 14 and 15 indicate that this motion is limited to low speeds and that a large radius is desired.

The effectiveness of the rib-walking motion may be improved if a non-circular path is used for the travel of the feet. However, this considerably complicates the mechanism and also reduces the clearance for the forward moving feet.

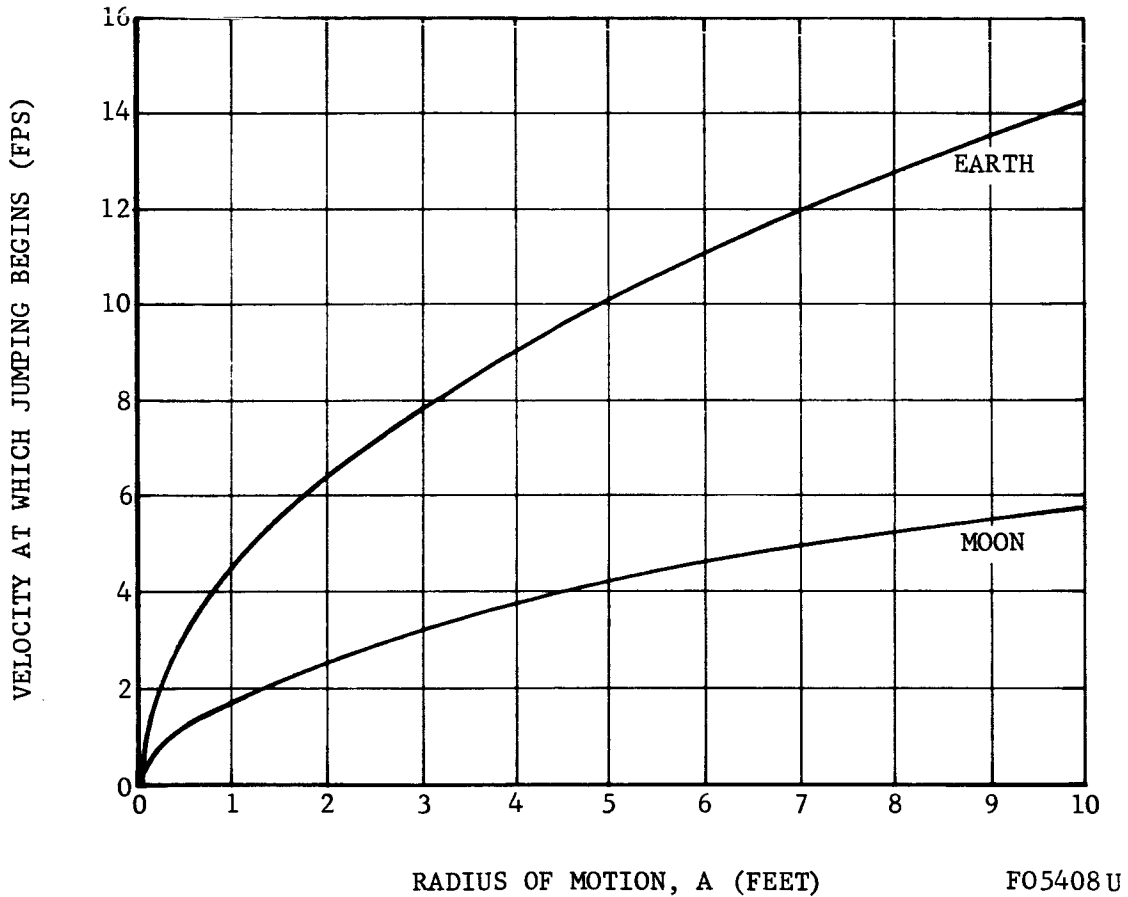
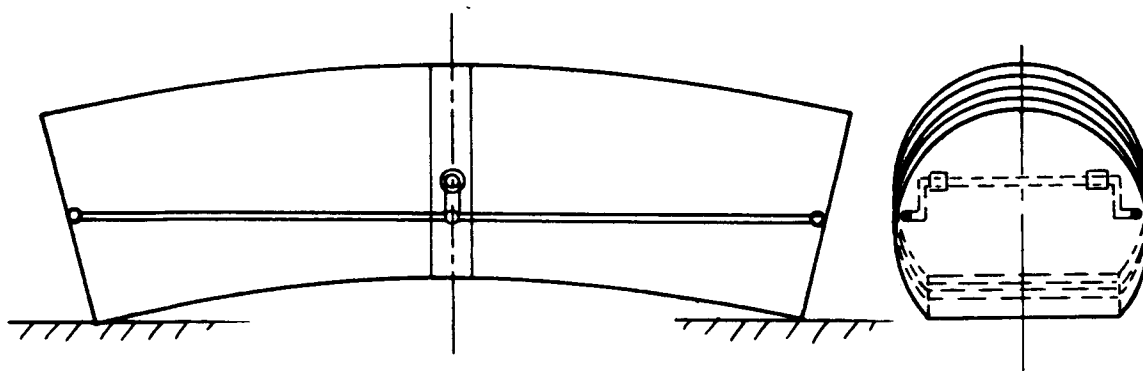


FIGURE 15. RIB-WALKING VELOCITY LIMITATION IMPOSED BY JUMPING

Double-acting Bellows

The analysis of rib walking showed that performance improves with increasing radius of motion, and is independent of the number of ribs. This, then, led to the simplification shown in Figure 16, which is a mechanization which approximately simulates rib walking with only three ribs. This device is called a double-acting bellows, and consists simply of a crank at the center of the vehicle which moves a member that is attached to the two ends. The two ends move in phase with each other, and the center moves 180 degrees out of

phase with them. In the position shown in Figure 16, the center is moving forward, and the ends are approximately stationary. After a rotation of 180 degrees, the vehicle will be curved concave upward, and the ends will be moving forward.



F05409 U

FIGURE 16. DOUBLE-ACTING BELLOWS

The exact form of this motion depends upon actual construction details, such as the bellows stiffness and the type of member used to attach the crank to the ends.

In soft soil, the forward-moving portion of the vehicle will not be lifted completely clear of the ground, and will be slid along to a degree dependent on the degree of vehicle curvature and the hardness of the soil. In this respect it is related to an extension-contraction vehicle that partially lifts its forward-moving part. The mobility of this device has not been analyzed, but it is felt that its performance falls somewhere within the spectrum of the vehicles that have been analyzed.

Considerations for Design Applications

The rib-walking motion where adjacent ribs are 180 degrees out of phase has relatively low drag-to-weight ratios at very low forward velocities but not at modest velocities except where the path radius of the walking motion is large (which in turn increases the roughness of the ride due to high vertical displacements). The double-acting bellows concept offers a simplified approach for improving the performance of a bellows-type vehicle by achieving a large effective radius without a correspondingly high vertical displacement.

TRAVELING WAVE VEHICLE*

For many years Aeronutronic has conducted studies of improved concepts for off-road vehicles based on analyses of mobility in nature. One of the first things learned in a study of animals is that most of them - in particular the ones which move close to the ground - tend to be long and slender. The extreme examples of the slenderizing trend are the snakes and various species of worms. These animals take advantage of their elongated form to spread their weight over a large area, and the resultant low ground pressure allows them to move over very soft ground.

The methods of propulsion used by worm-like creatures vary considerably, but can be grouped generally into two classes. One class, represented by animals such as the earthworm, the measuring worm, and the leech, utilize an intermittent motion in which one part of the body and then another is moved forward. The other class, which includes the snakes, centipedes, millipedes, and most caterpillars use one portion of the body after another for propulsion, but the body as a whole travels forward with a smooth, continuous motion.

Further study of the second class of animals just mentioned reveals that the propulsive movements in every case take the form of waves of motion which pass along the body, with several complete wavelengths over the body length. It is interesting to observe that in some animals these waves progress from head to tail and in some from tail to head. Only those animals in which the waves move from head to tail have the power of swimming, either through a fluid or between obstacles, with a snake-like motion. The effect of this traveling wave motion can be seen clearly when a snake is swimming on the surface of water as shown in Figure 17.

One animal chosen for study by Aeronutronic was the centipede. Analysis of the centipede showed that its feet move in a manner which forms a wave pattern moving from head to tail, and that in doing this, they move approximately in circles with nearly constant angular velocity and phase relationship. This observation prompted the construction of the mechanical model shown in Figure 18. This traveling wave model is made up of a series of cranks, rotating synchronously, with a 15 degree phase difference between cranks. This device can be used to simulate waves that either move aft as on a centipede, or forward as on a millipede, and has been very helpful in analyzing the possible motions. This previous work has been adapted to this study.

Hard Surface Performance

One way of reducing the losses of the rib-walking device on a hard surface is to make the phase angle between adjacent ribs less than 180 degrees. The resulting motion for a phase angle of 45 degrees is shown in Figure 19, and is called a traveling wave.

*See footnote on Page 1.



FIGURE 17. SNAKE SWIMMING

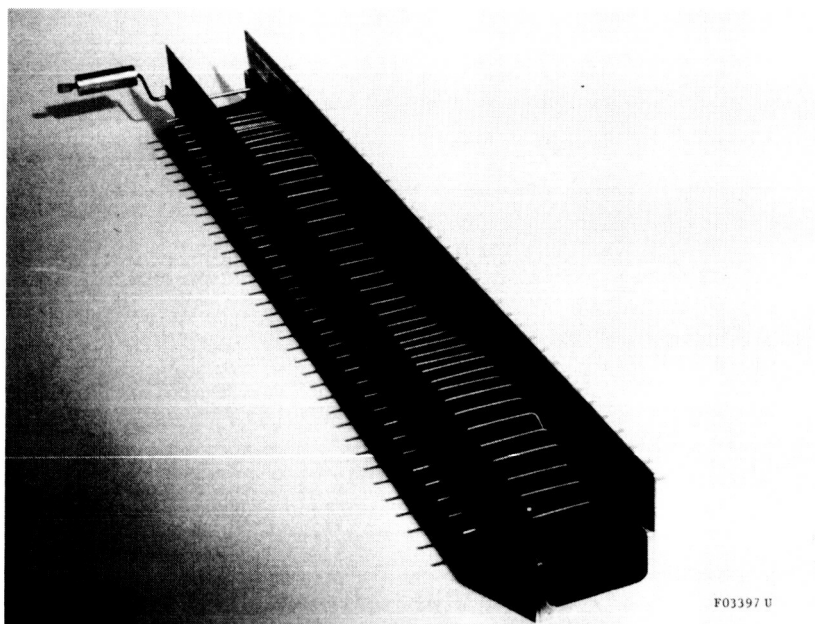
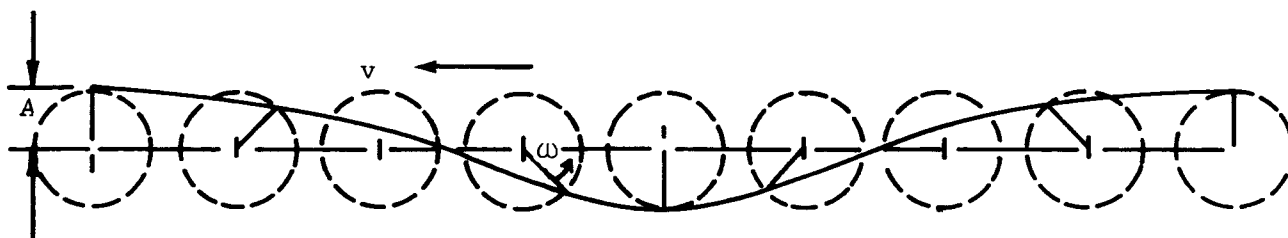


FIGURE 18. TRAVELING WAVE MODEL



F05412 U

FIGURE 19. TRAVELING WAVE MADE UP OF CRANKS

The energy loss of this device on a hard surface may be seen from examination of its motion as shown in Figure 20. The phase angle between adjacent cranks is ψ . There is no discontinuity in the horizontal velocity at the point of transfer of the load from one crank to the next and only the kinetic energy due to the vertical component of velocity is assumed to be lost.

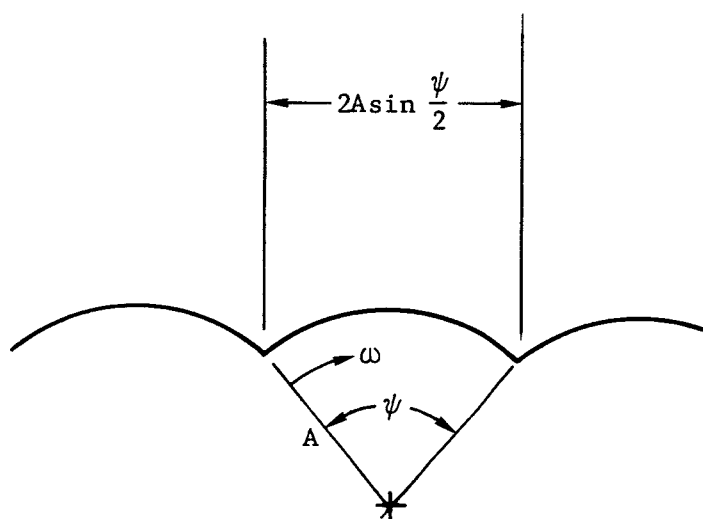


FIGURE 20. MOTION OF A RIGID TRAVELING-WAVE DEVICE ON A HARD SURFACE

The work required per arc of travel is kinetic energy lost at one transfer,

$$\text{Work} = \frac{1}{2} \frac{W}{g} (A \omega \sin \frac{\psi}{2})^2 \quad (24)$$

The average horizontal velocity is

$$v = A \omega \frac{2 \sin \frac{\psi}{2}}{\psi} \quad (25)$$

and the distance traveled on each crank is

$$s = 2 A \sin \frac{\psi}{2} \quad (26)$$

Therefore, the equivalent drag-to-weight ratio is

$$\frac{D_e}{W} = \frac{\text{Work}}{W s} = \frac{1}{2g} \frac{(A \omega)^2 \sin^2 \frac{\psi}{2}}{2A \sin \frac{\psi}{2}}$$

$$\frac{D_e}{W} = \frac{1}{16 A g} \frac{\psi^2}{\sin \frac{\psi}{2}} v^2 \quad (27)$$

For $\psi = 180$ degrees, this reduces to Equation (22), which was given for a rib-walking vehicle. It is shown in Figure 21 for moon gravity and a crank radius of one foot.

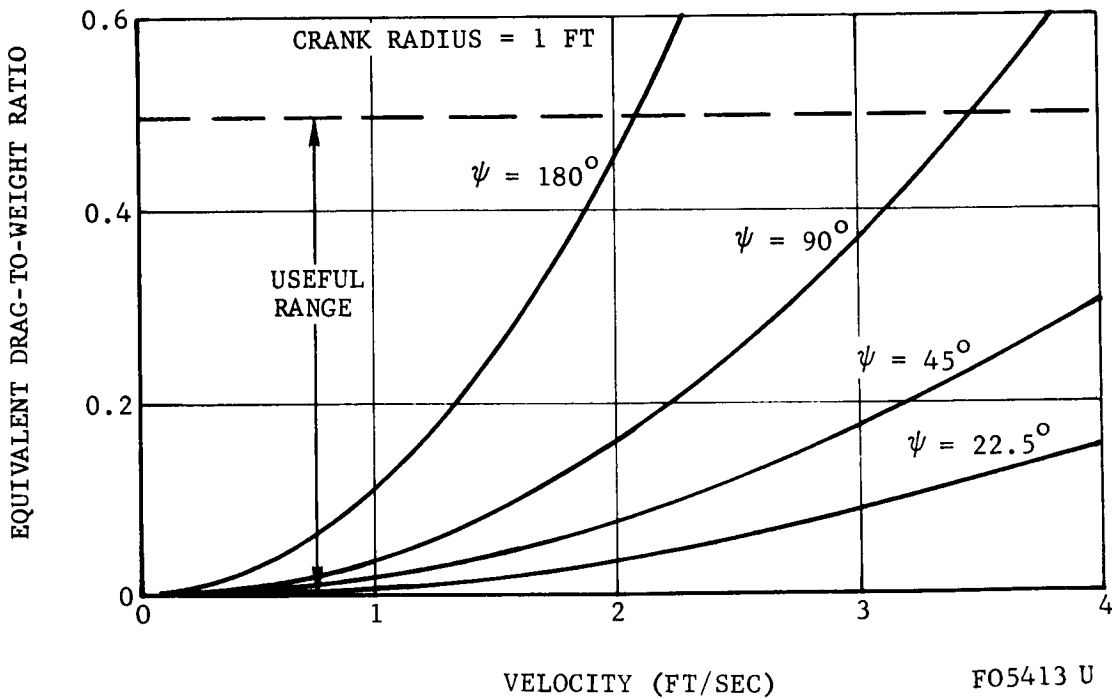


FIGURE 21. EQUIVALENT DRAG-TO-WEIGHT RATIO OF A TRAVELING WAVE VEHICLE ON A HARD SURFACE ON THE MOON

The additional cranks in the wavelength are seen to greatly reduce the power losses as well as smooth the ride. Theoretically, this vehicle will begin to jump at the same velocity as the rib-walking device as shown in Figure 15. However, for a large number of cranks (ψ small), the amplitude of the vertical motion becomes small, and small deflections of the vehicle and soil will serve to reduce the tendency to jump and to further smooth the ride.

Soft Surface Performance

It is seen that a wave as shown in Figure 19 moves toward the rear of the vehicle as the vehicle moves forward. It is possible to make the wave move in the same direction as the vehicle motion (at least on a hard surface) by turning the device in Figure 19 upside down. It is felt, for most applications, that it is advantageous for the wave to move aft, since this minimizes the wave velocity with respect to the ground and thereby reduces the vehicle sensitivity to ground surface irregularities. Furthermore, in very soft soil, or even in a liquid, the vehicle is propelled by the swimming action of the rearward-moving wave. An analysis of this type of vehicle has been made for certain soil characteristics, and the results of this are given below. The details of this analysis are given in Appendix E.

The analysis is based on the concept of Figure 19, but many cranks are assumed, giving a continuous, smooth surface, and the radius is assumed small compared to the wavelength, resulting in a sinusoidal wave shape. Therefore, kinetic energy losses of the type shown in Figure 21 need not be considered.

The coefficient of friction between the soil and the wave surface is assumed to be a constant, μ , which is independent of soil displacement. The normal force on the wave surface is assumed to be directly proportional to the depth below the original soil surface, regardless of the direction of the motion of the wave surface. The results of the analysis, based on these assumptions, are given in Figures 22 to 25. The results are normalized by the friction coefficient, μ , where possible, so that the results may be applied for any friction coefficient. All forces not acting directly on the wave surface are lumped as "external drag," and may be actual drag forces or the component of the gravity force when on a slope, or a combination of these.

Figure 22 shows the depth to which a wave will sink into the soil as a combined function of the planform loading, amplitude and soil pressure gradient, $K\phi$. The performance in the following figures is given as a function of this penetration parameter, z_m/A . The vehicle velocity ratio is shown in Figure 23. This is the ratio of the vehicle velocity under the given conditions to the theoretical velocity on a hard surface. For reference, note that $z_m/A = 2$ corresponds to a wave surface with its top just even with the soil surface. The equivalent drag-to-weight ratio is shown in Figure 24. The fact that D_e/W is negative in some regions is due to the vehicle's ability to recover energy on a down-slope. Figure 25 shows the maximum slope capability of the vehicle. It is of interest to note that a vehicle that is sunk into the soil to the midpoint of the wave (where $z_m = A$) can climb a slope equal to the friction coefficient.

A = WAVE AMPLITUDE
 K_{ϕ} = SOIL PRESSURE GRADIENT
 z_m = MAXIMUM PENETRATION DEPTH

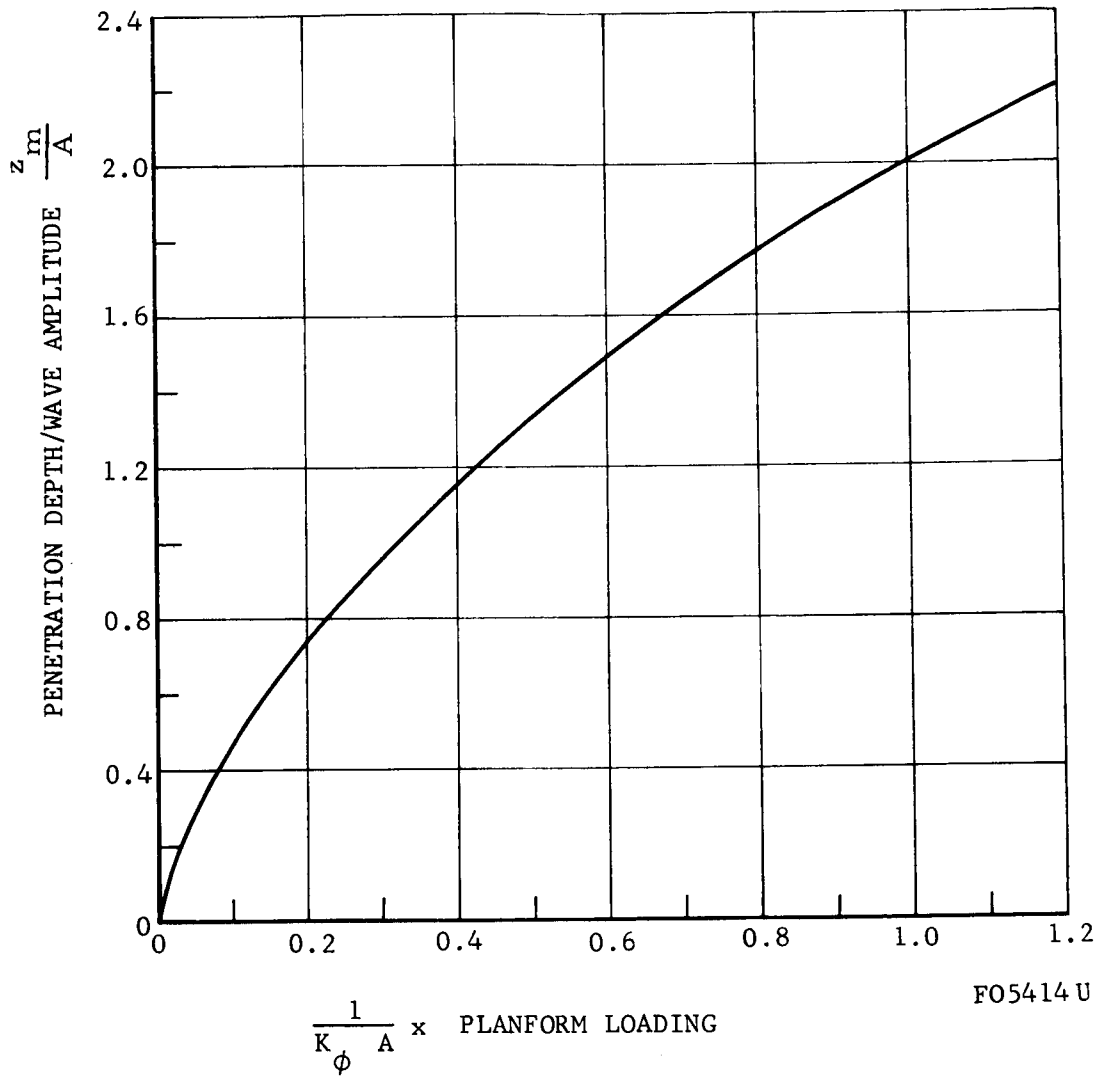


FIGURE 22. MAXIMUM PENETRATION DEPTH OF A TRAVELING WAVE

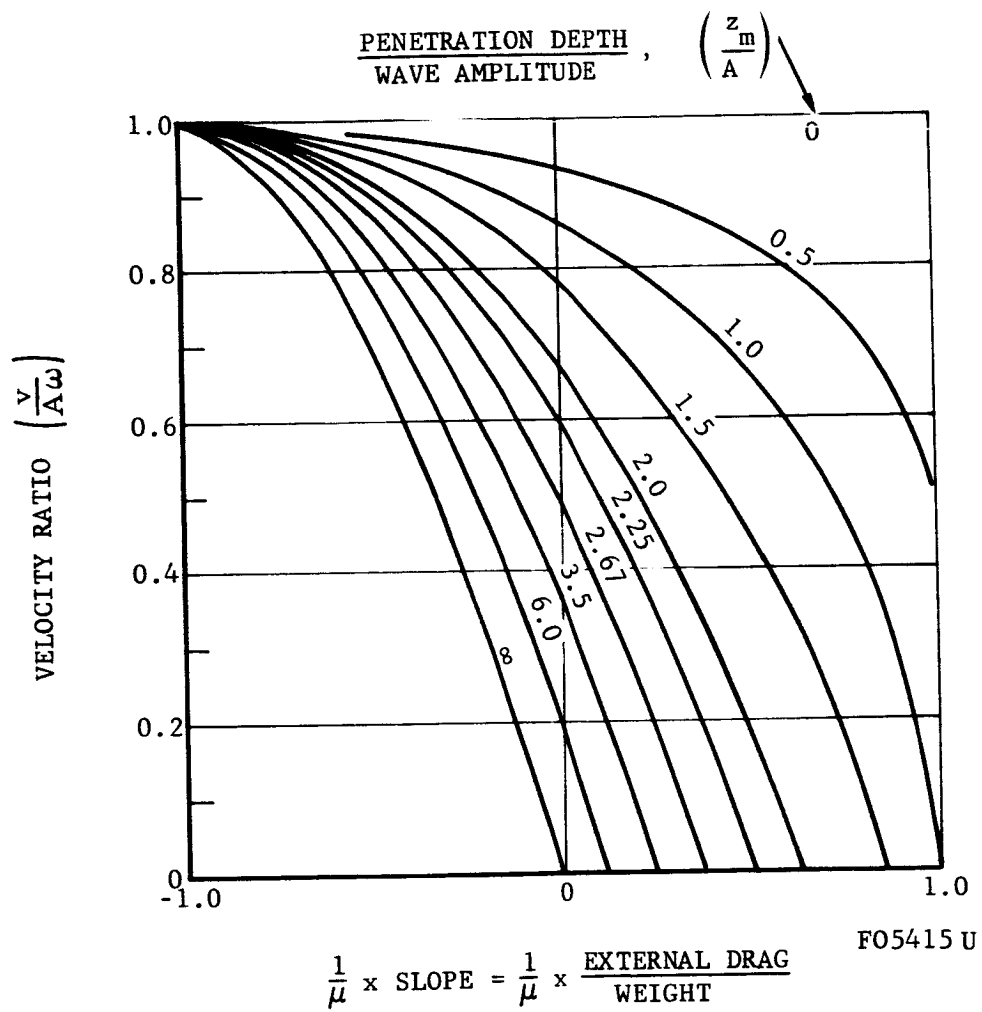
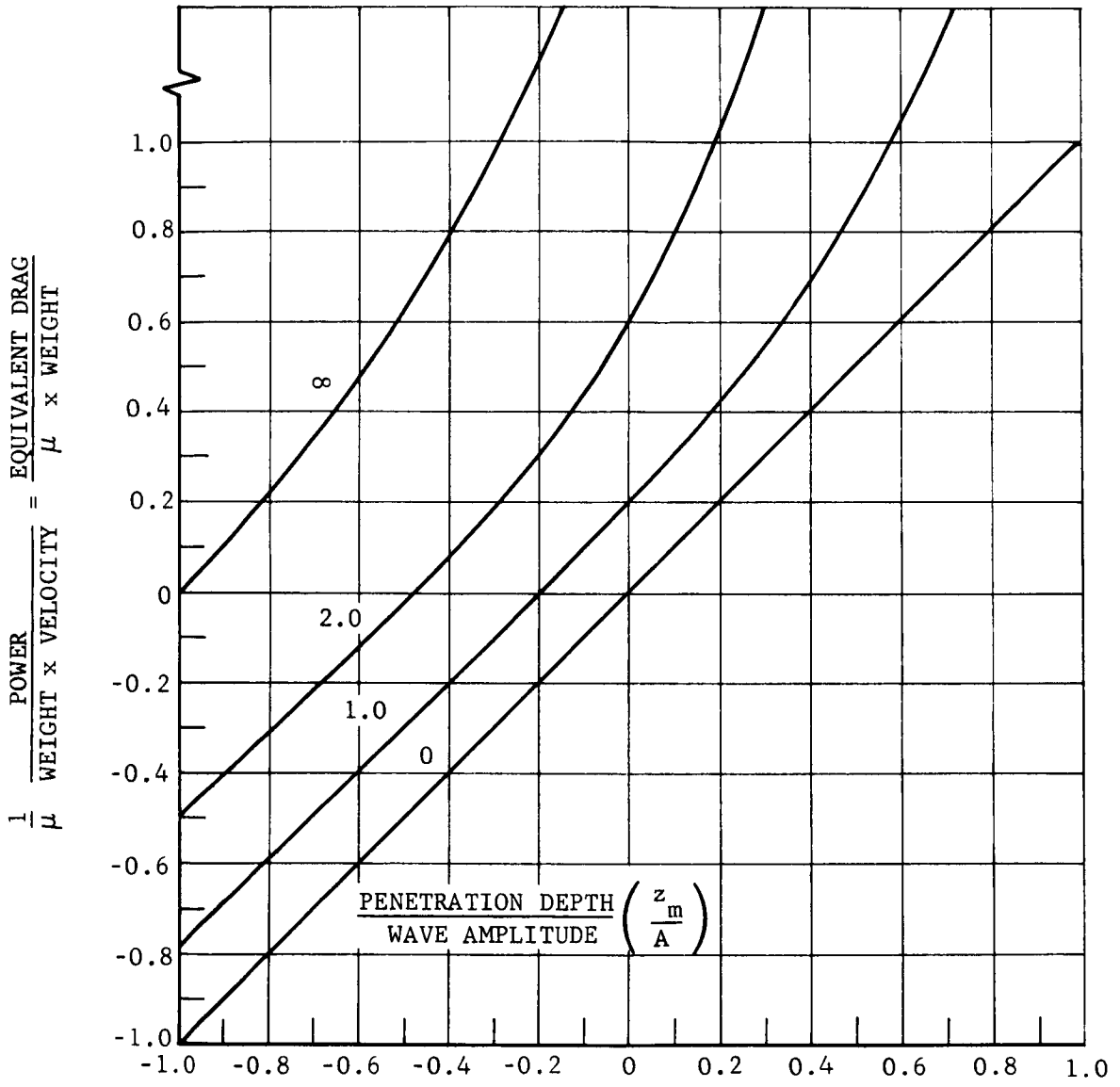


FIGURE 23. TRAVELING-WAVE VELOCITY RATIO



F05416 U

$$\frac{1}{\mu} \times \frac{\text{EXTERNAL DRAG}}{\text{WEIGHT}} = \frac{1}{\mu} \times \text{SLOPE}$$

FIGURE 24. EQUIVALENT DRAG-TO-WEIGHT RATIO

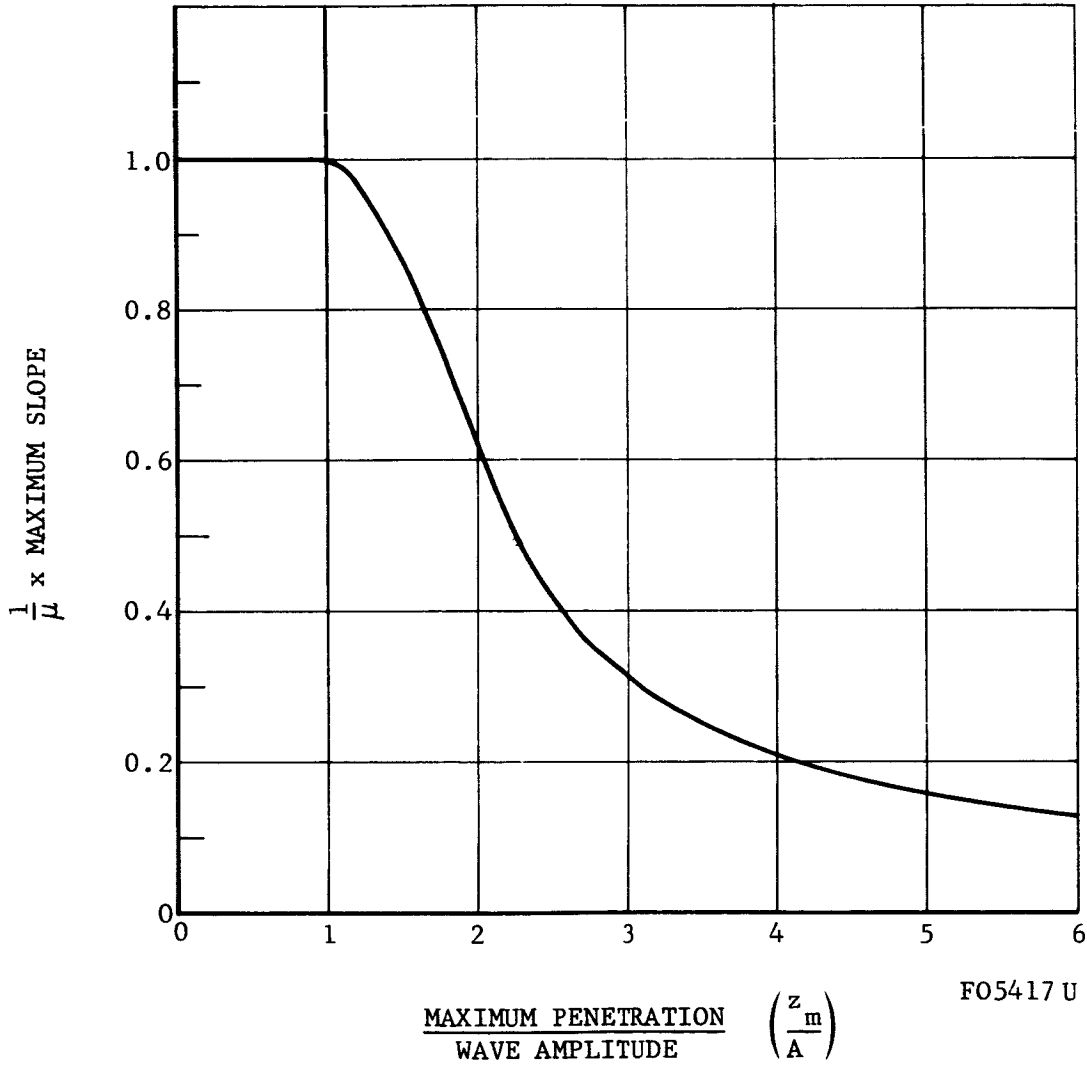


FIGURE 25. MAXIMUM SLOPE CAPABILITY

Considerations for Design Applications

The traveling wave motion can provide relatively low drag-to-weight ratios at all forward velocities. This ratio decreases significantly with decrease in phase angle between adjacent bellows segment particularly for high forward velocities. Decrease in phase angle also smooths the ride. It is advantageous to have the traveling wave move aft since this not only reduces the vehicle sensitivity to ground surface irregularities but also provides locomotion over and through very low-strength surface materials even when completely submerged although at a decrease in propulsive efficiency.

BELLOWS ANALYSIS

Two major classes of bellows are of interest in this study. In one class, which will be referred to as corrugated bellows, the loads are taken by bending stresses in the bellows skin. In the other class, which will be referred to as membrane bellows, the skin is thin and flexible, but reinforced by fibers or rings. In the latter class, most of the loads are taken by the membrane stresses which are produced by the internal pressure. In the following paragraphs some of the design equations for the two classes of bellows are summarized.

CORRUGATED BELLOWS

Corrugated bellows are made either from annular discs welded together along their inner and outer edges, or are formed by one of several methods from tubular blanks. The former process allows close spacing of the convolutions and, therefore, a low spring rate. However, the resulting bellows is not well adapted to high pressure usage. The latter process produces a smoothly-curved convolution shape which avoids stress concentrations. This shape is close to a shape which can take pressure stresses in tension rather than in bending. The bellows can adjust itself to high pressures by small changes in contour. It is, therefore, standard practice to ignore the pressure stresses in formed bellows of standard proportions.

In the case of welded bellows, the shape is such that the pressure stresses are not significantly relieved by small deformations, and these stresses should be added to the stresses caused by deflection to obtain the total stress.

Bellows Analysis

Except for the difference noted and the changes in material properties caused by welding, the welded and formed bellows can be treated by the same methods. In this study the two-dimensional equations proposed by Den Hartog based on a suggestion by Timoschenko, will be used. These equations are developed and compared with test results in Reference 5. Although the equations apply exactly only to small extensions of flat-plate bellows whose depth is small compared to the bellows radius, they give good results on any bellows whose walls do not slope more than about 15 degrees and where the bellows depth is less than 15 percent of the bellows radius. This range covers all the applications of interest in this study.

The following relations are for circular bellows of mean diameter D , convolution depth d , and material thickness t . They apply to one convolution of a formed bellows or to a pair of discs in a welded bellows.

Stress due to a deflection δ per convolution, with modulus of elasticity E:

$$f_e = \frac{3 E t \delta}{2 d^3} \quad (28)$$

Stress due to internal pressure p_i is:

$$f_b = \frac{d^2 p_i}{2 t^2} \quad (29)$$

The spring rate is:

$$\frac{P_s}{\delta} = \frac{\pi E D t^3}{2 d^3} \quad (30)$$

For a complete bellows of N convolutions, the spring rate will be:

$$R_s = \frac{P_s}{N\delta} = \frac{\pi E D t^3}{2 N d^3} \quad (31)$$

and the bending stiffness is:

$$\frac{M}{\theta} = \frac{R_s D^2}{8} = \frac{\pi E D^3 t^3}{16 N d^3} \quad (32)$$

A bellows of length L, whose ends are restrained against rotation and translation will buckle laterally at a critical internal pressure:

$$P_{\text{buckle}} = \frac{2 \pi R_s}{L} \quad (33)$$

In the case of a pressurized welded bellows, when it is desired to obtain the maximum deflection without allowing the total stress ($|f_e| + |f_b|$) to exceed an allowable value, F, the optimum geometry is given by:

$$\frac{d}{t} = \sqrt{\frac{F}{p_i}} \quad (34)$$

For a bellows so designed, the maximum deflection per convolution is:

$$\delta_{\max} = \frac{F^2 t}{3 p_i E} \quad (35)$$

At this extension, the stress due to deflection, Equation (28), equals the stress due to pressure, Equation (29), and the total spring load in the bellows is

$$P = \frac{\pi D d}{6} p_i \quad (36)$$

That is, the spring load is equal to that caused by the pressure acting over 1/6 of the bellows depth. In most cases this is negligible.

Design Conditions

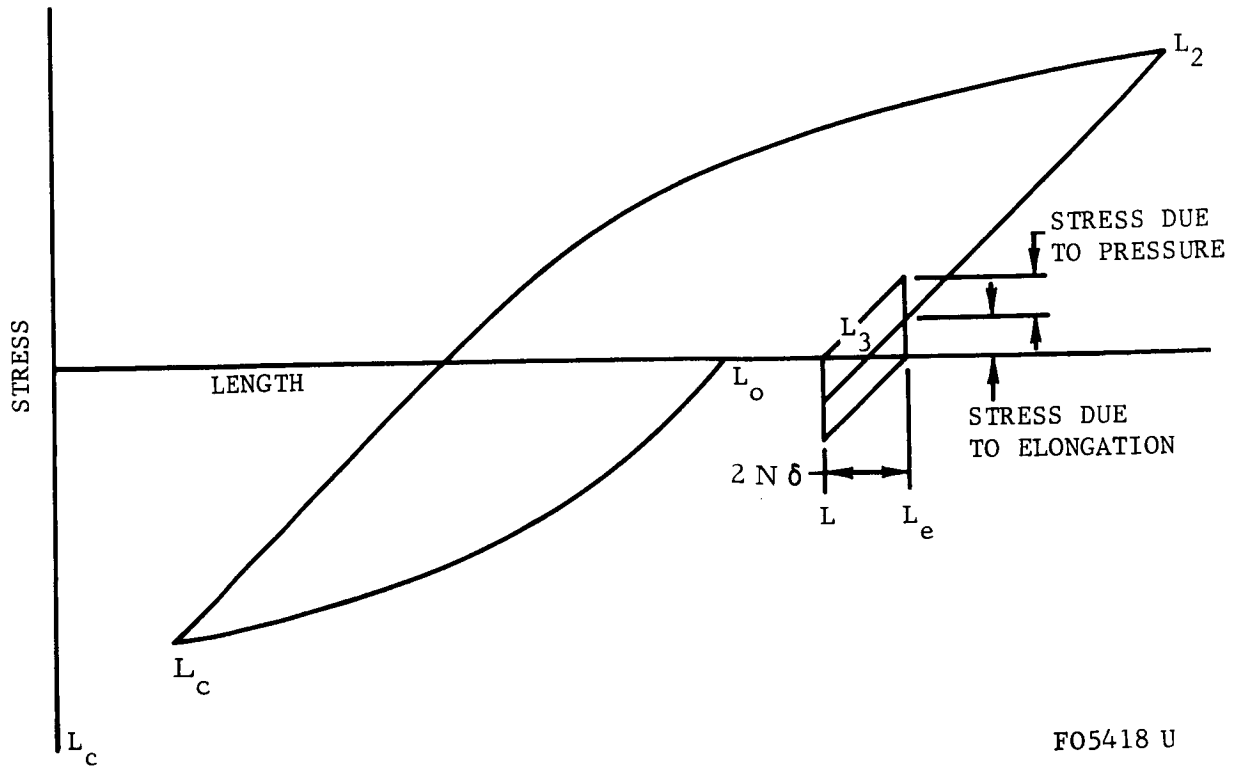
The conditions under which a bellows would actually be used in a vehicle are described in the following paragraphs.

The bellows will be made up originally to some length L_0 and then compressed to a shorter length L_C for shipment. On arrival it will be expanded to some new length L_2 and will then operate about a point L_3 with a stroke not exceeding δN from Equation (35). Only during this last phase will the full internal pressure be present, and since for optimum design the stress caused by pressure equals that due to elongation, the latter will be limited to half the fatigue limit or about 12,500 psi. This is based upon the assumptions that (1) the pressure stress is considered, and is added to the deflection stress, and (2) the internal pressure increases and decreases simultaneously with bellows extension and contraction so that the same fatigue limit applies to both pressure stress and deflection stress. Both of these assumptions are approximately valid for an extension-contraction vehicle made of welded metal bellows. The operating points discussed are shown plotted approximately to scale on a stress strain diagram for stainless steel in Figure 33

Since the operating point L_3 in Figure 26 can be set at will, it will be located for the purpose of this study so that the maximum operating length ($L_3 + \delta N$) will fall within the linear operating range of the bellows, that is that the elongation per convolution be not greater than 50 percent of the ring depth. This range of travel is shown schematically in Figure 27.

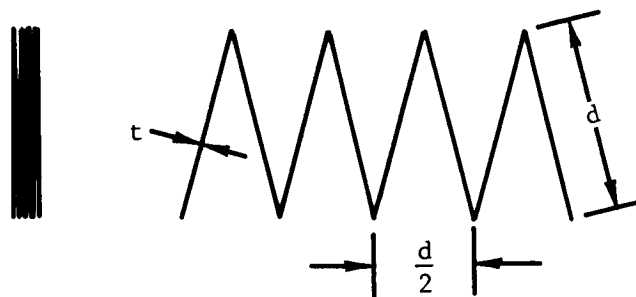
The closed length is equal to $2Nt$, where N is the number of convolutions, and for optimum design, from Equation (34).

$$t = d \sqrt{\frac{p_i}{F}}$$



F05418 U

FIGURE 26. BELLOWS OPERATING RANGE



F05411 U

FIGURE 27. BELLOWS TRAVEL (SCHEMATIC)

Therefore, the closed length is given by

$$L_c = 2Nd \sqrt{\frac{P_i}{F}} \quad (37)$$

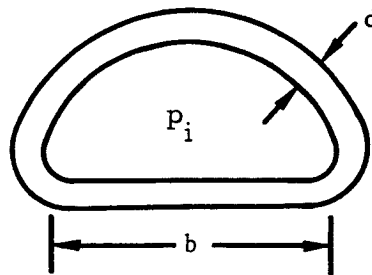
and the maximum extended length by

$$L_e = 2Nd \left[\sqrt{\frac{P_i}{F}} + \frac{1}{4} \right] \quad (38)$$

The effective thickness at maximum extended length is

$$t_e = d \frac{L_c}{L_e} = \frac{d Nd \sqrt{\frac{P_i}{F}}}{Nd \left[\sqrt{\frac{P_i}{F}} + \frac{1}{4} \right]} = \frac{d}{1 + \frac{1}{4} \sqrt{\frac{F}{P_i}}} \quad (39)$$

The most probable shape for the bellows section is a flattened oval as shown in Figure 28. This provides maximum surface contact, and is reasonably stable against overturning. For the purpose of this study it will be assumed that the section shape is such that the circumference is equal to 3 times the flat width b .



F05410 U

FIGURE 28. BELLOWS SECTION

For the shape shown in Figure 28, the most severe design condition is probably as indicated in Figure 29, where the section is supported at A and B and the horizontal span is subjected to bending from internal pressure, payload, and its own weight.

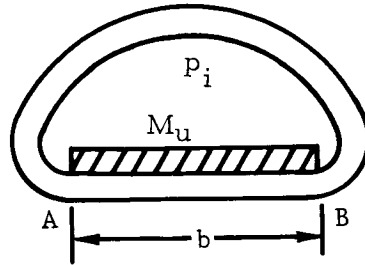


FIGURE 29. LOADING CONDITION

To simplify the analysis it will be assumed that inflection points occur at A and B. Then, if conditions are uniform along the bellows and the useful load per unit length is called M_u , the running load across the span AB per unit length is:

$$r = p_i + \left(\frac{M_u}{b} + t_e \cdot \gamma \right) \frac{g}{g_e} \text{ lb/in.} \quad (40)$$

when p_i is in psi, M_u is in pounds mass per inch along bellows axis, t_e is in inches, γ is in pounds mass per cubic inch, and g/g_e is ratio of local gravity to standard earth gravity ($g/g_e = 1/6$ on moon).

If the tension in member AB is neglected, the maximum bending moment at the center would be:

$$M_{b_{\max}} = r \frac{b^2}{8} \quad (41)$$

and this is equal to the maximum resisting moment of a unit length of the bellows, which is:

$$M_b = F \frac{I}{y} = \frac{d^2}{12} t_e \quad (42)$$

Equating (41) and (42), and using the value of r from Equation (40) gives:

$$\left[p_i + \left(\frac{M_u}{b} + t_e \gamma \right) \frac{g}{g_e} \right] \frac{b^2}{8} = F \frac{t_e d}{6} \quad (43)$$

where t_e is given by Equation (39).

Solving for useful load, M_u ,

$$\frac{M_u}{b} = \frac{g_e}{g} \left(\frac{4}{3} \frac{t_e dF}{b^2} - p_i \right) - t_e \gamma \quad (44)$$

The empty weight is:

$$M_e = 3 b t_e \gamma \quad (45)$$

The useful load to gross weight ratio may be given as:

$$\frac{\text{Useful load}}{\text{Gross weight}} = \frac{\frac{M_u}{b}}{\frac{M_u}{b} + \frac{M_e}{b}} \quad (46)$$

Substituting Equations (44) and (45) into this, using Equation (39) for t_e , and multiplying through by

$$\left(1 + \frac{1}{4} \sqrt{\frac{F}{p_i}} \right),$$

this may be written as:

$$\frac{\text{Useful load}}{\text{Gross weight}} = \frac{f\left(\frac{d}{b}\right) - \gamma b}{f\left(\frac{d}{b}\right) + 2\gamma b} \quad (47)$$

where:

$$f(x) \triangleq \frac{g_e}{g} \left[\frac{4}{3} F x - \frac{p_i}{x} \left(1 + \frac{1}{4} \sqrt{\frac{F}{p_i}} \right) \right] \quad (48)$$

Design Charts

In order to define the design limitations and the effect of parameter variations, design charts have been prepared. These charts apply specifically to welded metal bellows, where pressure stresses are considered, and are based upon the equations presented previously. The stresses caused by pressure and deflection are assumed to vary together so that the same allowable fatigue limit applies to both.

The derivation of the relations used for the charts and additional charts are given in Appendix F. Unless otherwise noted, the charts are based on stainless steel with a fatigue limit of 25,000 psi, and a mass density of 0.283 lbm/in.³

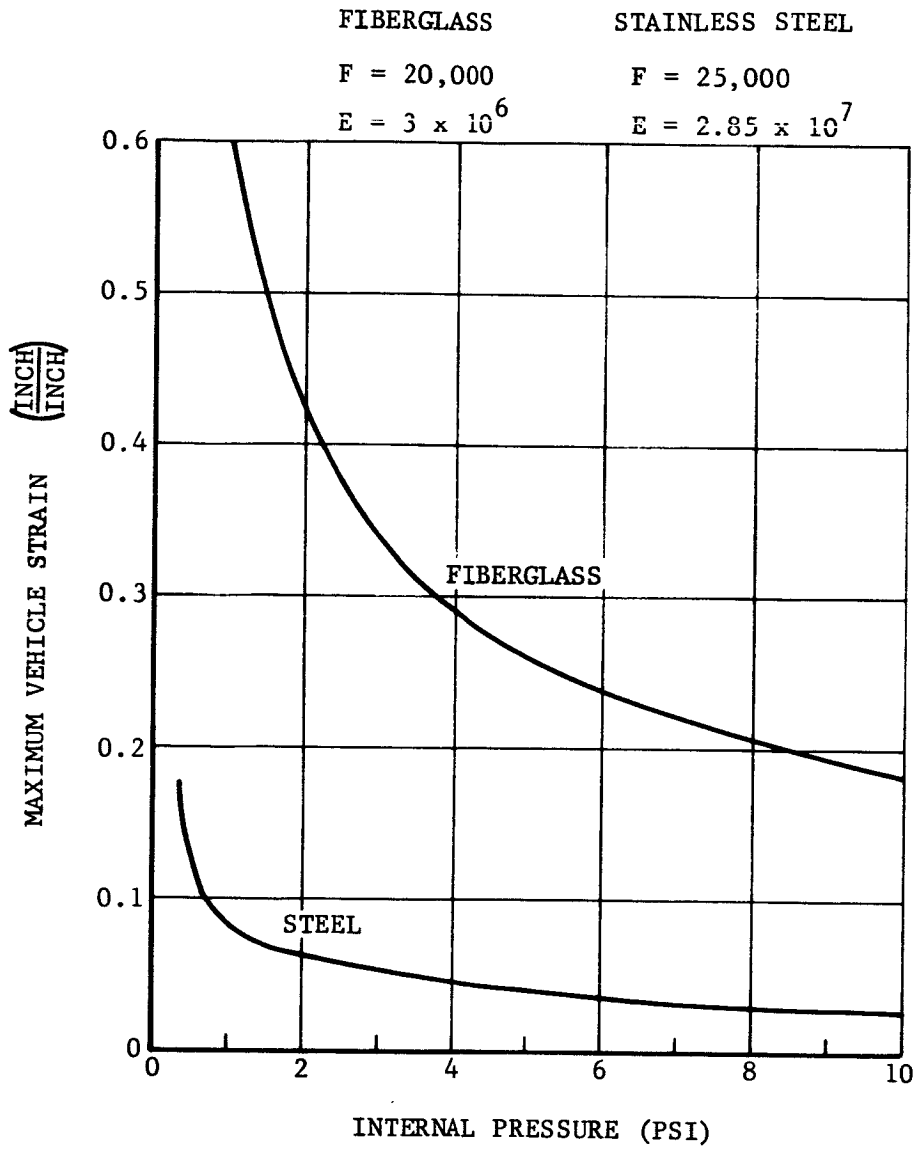
Figure 30 shows the allowable elongation of vehicles made of stainless steel compared with fiberglass. Assumed material properties are shown. The allowable elongation is the property most effected by the difference in these materials. The parameters on the remainder of the charts are shown for stainless steel, but would not be much different if they were shown for fiberglass.

Figure 31 defines a design condition which is useful in determining the limiting factors of lightweight design. The bellows depth-to-width ratio given here is for the vehicle which will structurally just contain the internal pressure; that is, it will withstand the bending stress in the bottom beam caused by internal pressure load, but not that caused by useful load weight or by its own weight. This condition is given by the solution of Equation (43) for $\gamma = M_u = 0$. It is clear that (under the design assumption that have been made) this vehicle will not quite work, even with no useful load. It can be shown, however, that only a small increase in d/b over the limiting case will allow the vehicle to structurally carry its own weight, and that a further fairly small increase will allow the vehicle to carry a very substantial payload. Figure 31 shows that a 60 percent useful load may be carried by a 400 inch wide vehicle with only slightly larger d/b than for the limiting case. The limiting condition is useful in being quite close to a useful design and the charts which follow are based upon this condition.

Figures 32, 33, and 34 give the empty mass, the footprint pressure, and the material thickness of the limiting design condition. The value given for each of these parameters is the limiting value, and the values for a useful design are slightly higher.

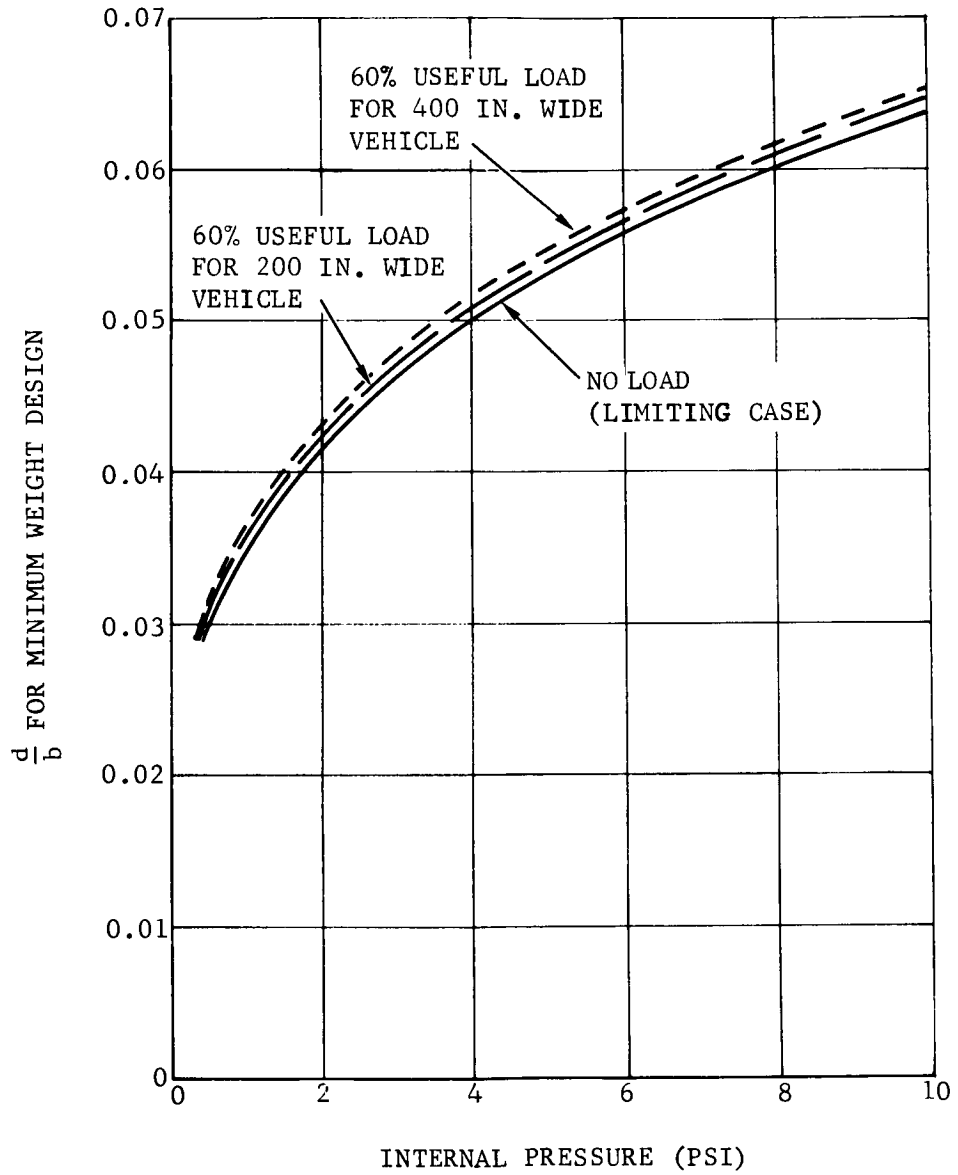
Figure 35 gives the ratio of empty mass to enclosed volume, which is a measure of the structural efficiency. The values for a cylinder and a sphere, shown here for reference, are much smaller than for the bellows devices. This is because the cylinder and sphere take the loads in tension, which is much more efficient than the bending mode in which the bellows operate. This comparison gives some idea of the penalty which is being paid for the mobility in the shelter designs.

Figure 36 is based upon the planing criteria discussed in the mobility section. The components of the planing parameter on the abscissa are bellows material density, γ ; soil density, γ_s ; R , the geometry factor from Equation (6), and J , given in Figure 5. The resultant pressure given is the maximum internal pressure to which a bellows vehicle can be designed if it is to meet the planing criterion.



F05419 U

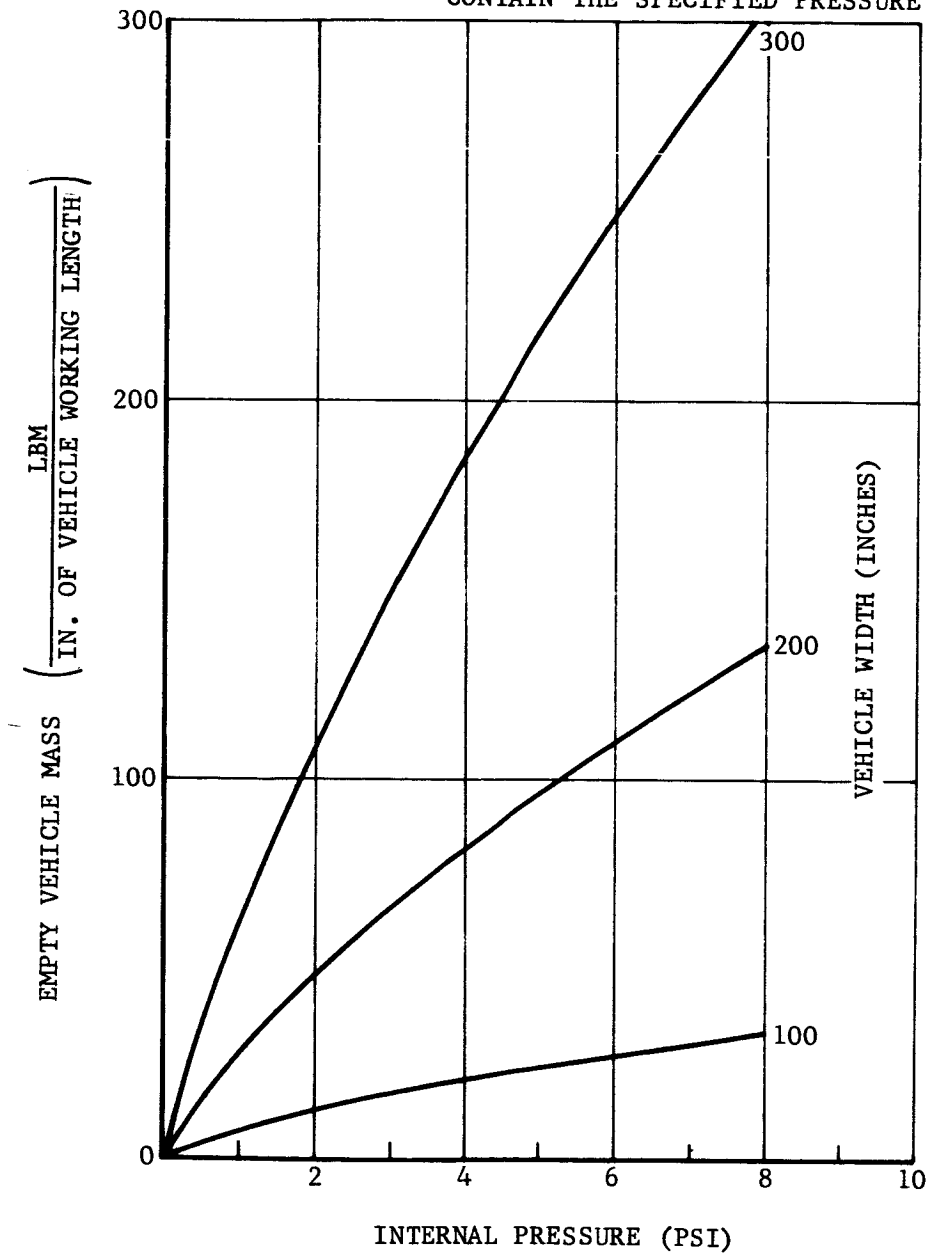
FIGURE 30. MAXIMUM VEHICLE STRAIN REFERRED TO MAXIMUM EXTENDED LENGTH



F05420 U

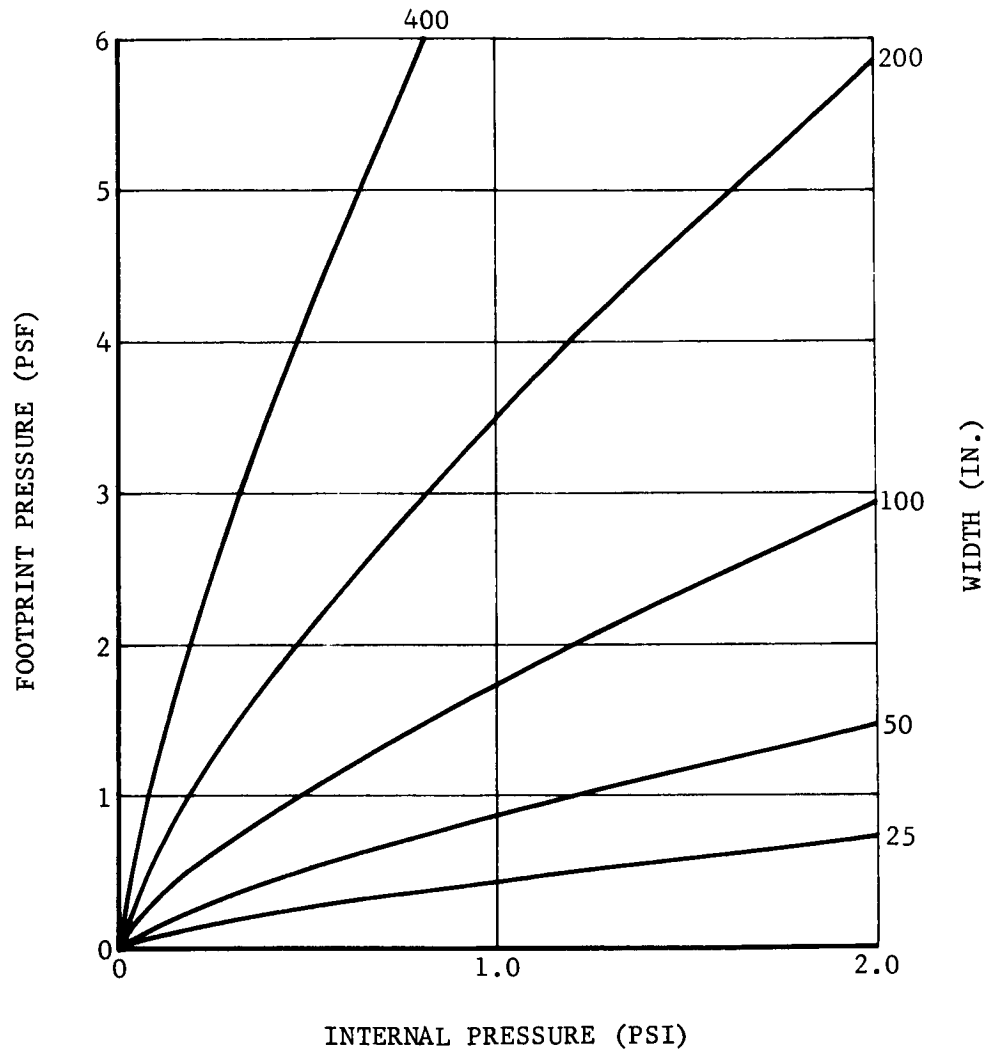
FIGURE 31. $\frac{d}{b}$ FOR THE VEHICLE WHICH WILL JUST CONTAIN THE INTERNAL PRESSURE

VEHICLE DESIGNED TO JUST
CONTAIN THE SPECIFIED PRESSURE



FO5421 U

FIGURE 32. MINIMUM VEHICLE EMPTY MASS



F05422 U

FIGURE 33. MINIMUM EMPTY VEHICLE FOOTPRINT PRESSURE

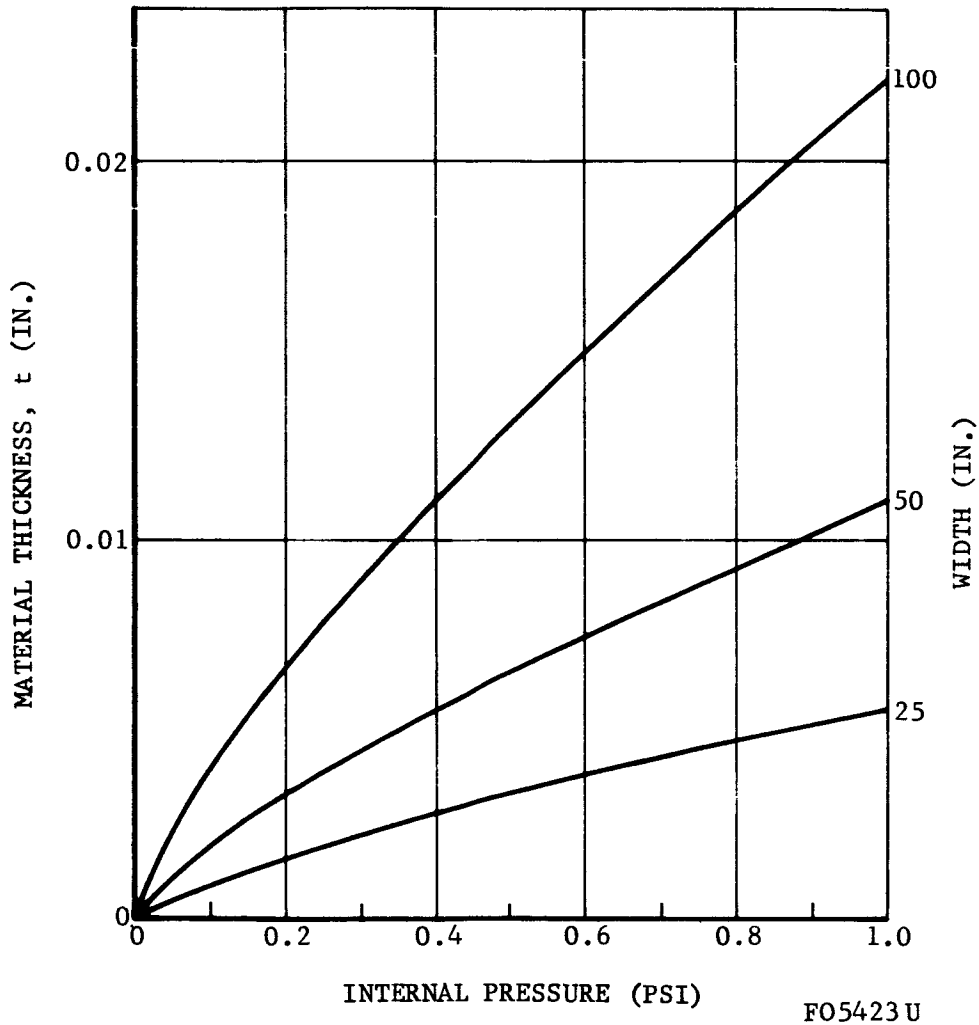
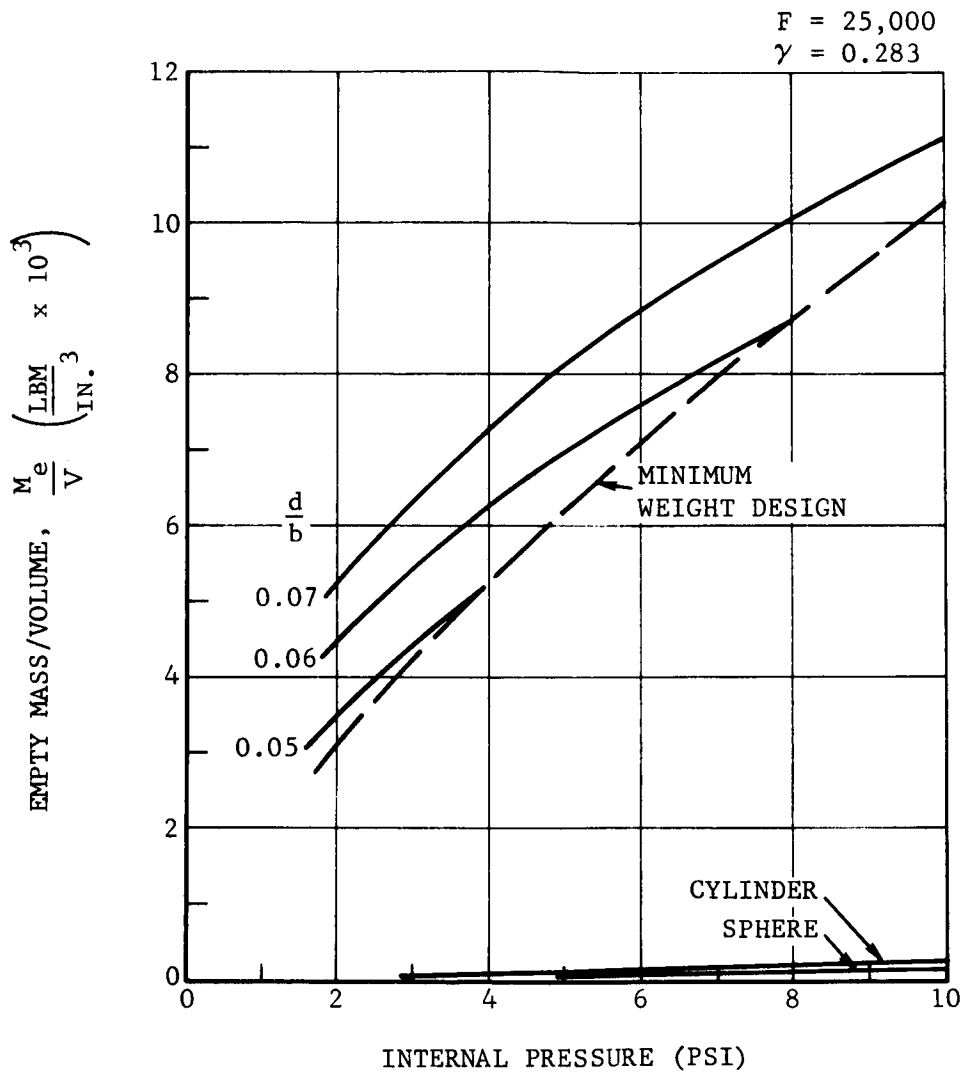


FIGURE 34. MATERIAL THICKNESS REQUIRED TO ACHIEVE MINIMUM - WEIGHT DESIGN



FO5424 U

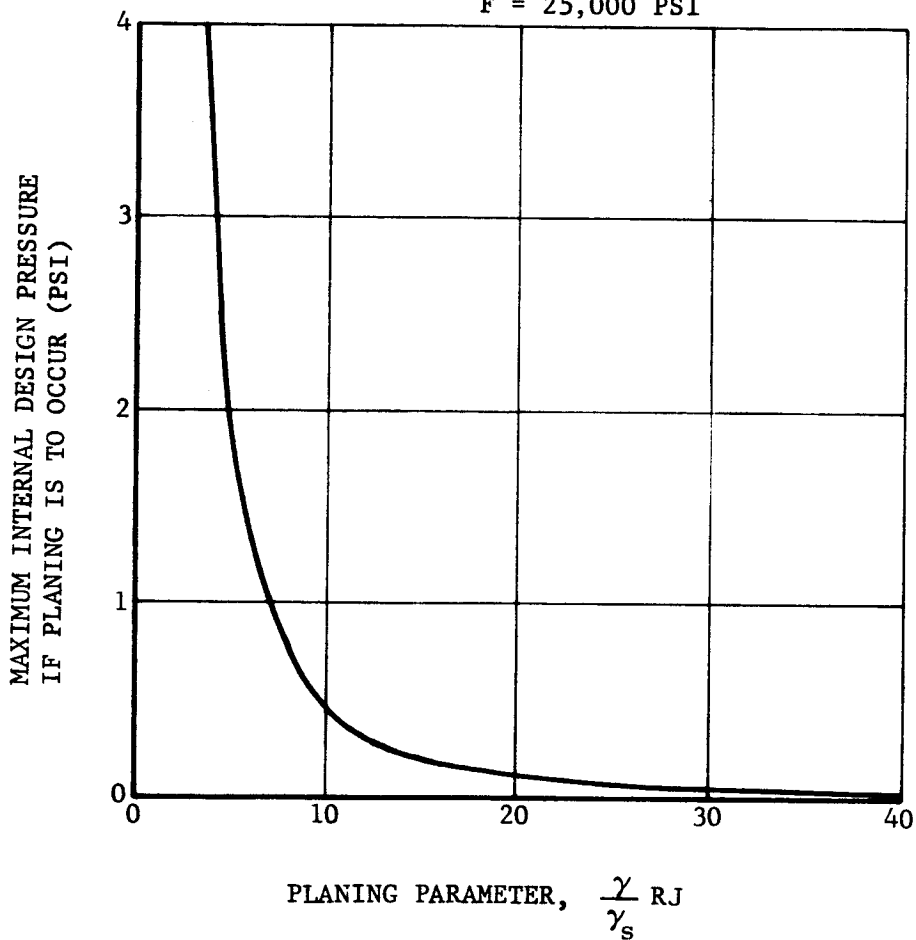
FIGURE 35. VEHICLE MASS TO VOLUME RATIO

CONDITIONS:

NO USEFUL LOAD WHILE MOVING
EACH BELLOWS CORRUGATION

HAS A FOOT

F = 25,000 PSI



F05425 U

FIGURE 36. PLANING CRITERION FOR BELLOWS DESIGN

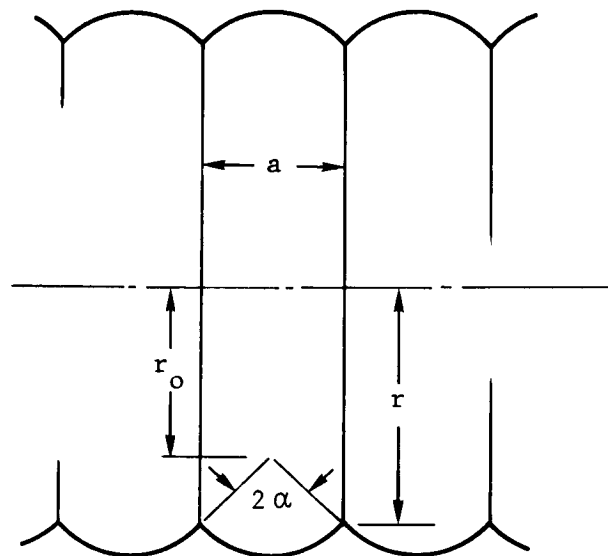
Considerations for Design Applications

In the design of corrugated bellows where loads are taken by bending stress in the skin, the pressure differential is a key factor in establishing geometry, skin gauge and structural weight, because of the local stresses introduced and requirements to prevent buckling. This is particularly important when the cross section of the bellows is noncircular. For a non-circular shape, the structural weight required to carry sizable payloads is very little more than that required for the empty structure. For convoluted bellows, the generally high stresses at the outer edge of the convolutions make difficult the attachment of any type foot or flexible cleat.

MEMBRANE BELLOWS

The membrane bellows refers to membrane-type bellows reinforced by rings or fibers. The membrane and the reinforcements are assumed to have negligible bending stiffnesses.

A longitudinal section of such a bellows is shown in Figure 37. It is made up of a number of rings with radius r and spaced a distance a apart. Between the rings is stretched a membrane which, because of the internal pressure, bulges out to approximately circular convolutions as shown.



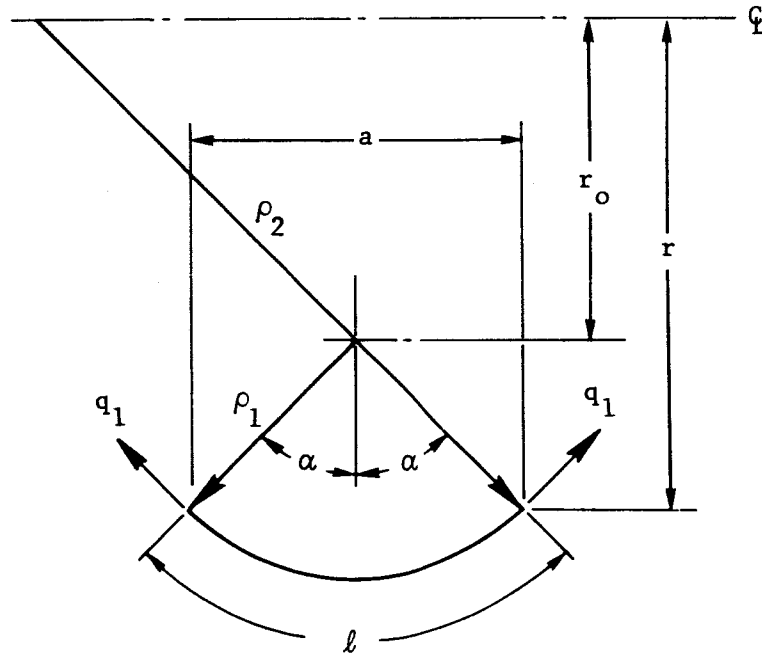
F05426 U

FIGURE 37. BELLOWS CONFIGURATION

If there is no external force acting on the bellows, it will extend to some length at which the internal forces are in equilibrium. To hold the bellows at any other length requires a force which depends on the internal pressure, geometry, and material properties. This spring force can be estimated as shown in the following paragraphs.

Spring Force

An enlarged section of the membrane is shown in Figure 38. The meridional section is assumed to be circular, with a radius ρ_1 . The other principal radius at the attachment point to the ring is ρ_2 .



F05427 U

FIGURE 38. BELLOWS GEOMETRY

The meridional tension force per unit width is q_1 lb/in., and the corresponding circumferential force q_2 . From membrane theory we have:

$$\frac{q_1}{\rho_1} + \frac{q_2}{\rho_2} = p_i \quad (49)$$

The radial deflection of the membrane at the ring attachment is given by:

$$\delta = \frac{r}{Et} (q_2 - \nu q_1) \quad (50)$$

where E is the elastic modulus, t is the thickness, and ν is Poisson's ratio for the membrane.

For most cases of practical interest, the ring will be designed so that its elongation is quite small compared to its radius. If this is the case, Equation (50) can be simplified by putting $\delta = 0$, giving:

$$q_2 = \nu q_1 \quad (51)$$

From geometry

$$\rho_1 = (r - r_0) \sec \alpha \quad (52)$$

and

$$\rho_2 = r \sec \alpha \quad (53)$$

Substituting Equations (51), (52), and (53) into (49) gives:

$$\frac{q_1}{(r - r_0) \sec \alpha} + \frac{\nu q_1}{r \sec \alpha} = p$$

or

$$q_1 = \frac{p r (r - r_0) \sec \alpha}{r + \nu (r - r_0)} \quad (54)$$

The net longitudinal force at the ring section is the difference between the longitudinal pressure force and the longitudinal component of membrane tension acting around the ring,

$$P = p_i \pi r^2 - 2 \pi r q_1 \cos \alpha.$$

or

$$\frac{P}{p_i \pi r^2} = 1 - \frac{2}{\frac{1}{\frac{r_0}{r}} + \nu} \quad (55)$$

The values given by this equation are plotted in Figure 39 for several values of ν .

In some of the bellows applications which are of interest, it is desirable to use an elastic membrane with inextensible reinforcements in only the meridional direction. For this case,

$$q_2 = 0$$

and

$$\begin{aligned} q_1 &= \rho_1 P_i \\ &= (r - r_o) p_i \sec \alpha \end{aligned} \quad (56)$$

giving:

$$P = p_i \pi r^2 - 2 \pi r(r - r_o) p_i$$

or

$$\frac{P}{p_i \pi r^2} = \frac{2 r_o}{r} - 1 \quad (57)$$

This gives the same result as putting $\nu = 0$ in Equation (64). It is also the same as ignoring the curvature in the circumferential direction, and calculating the loads on the basis of two-dimensional theory, as was done in the case of metallic bellows.

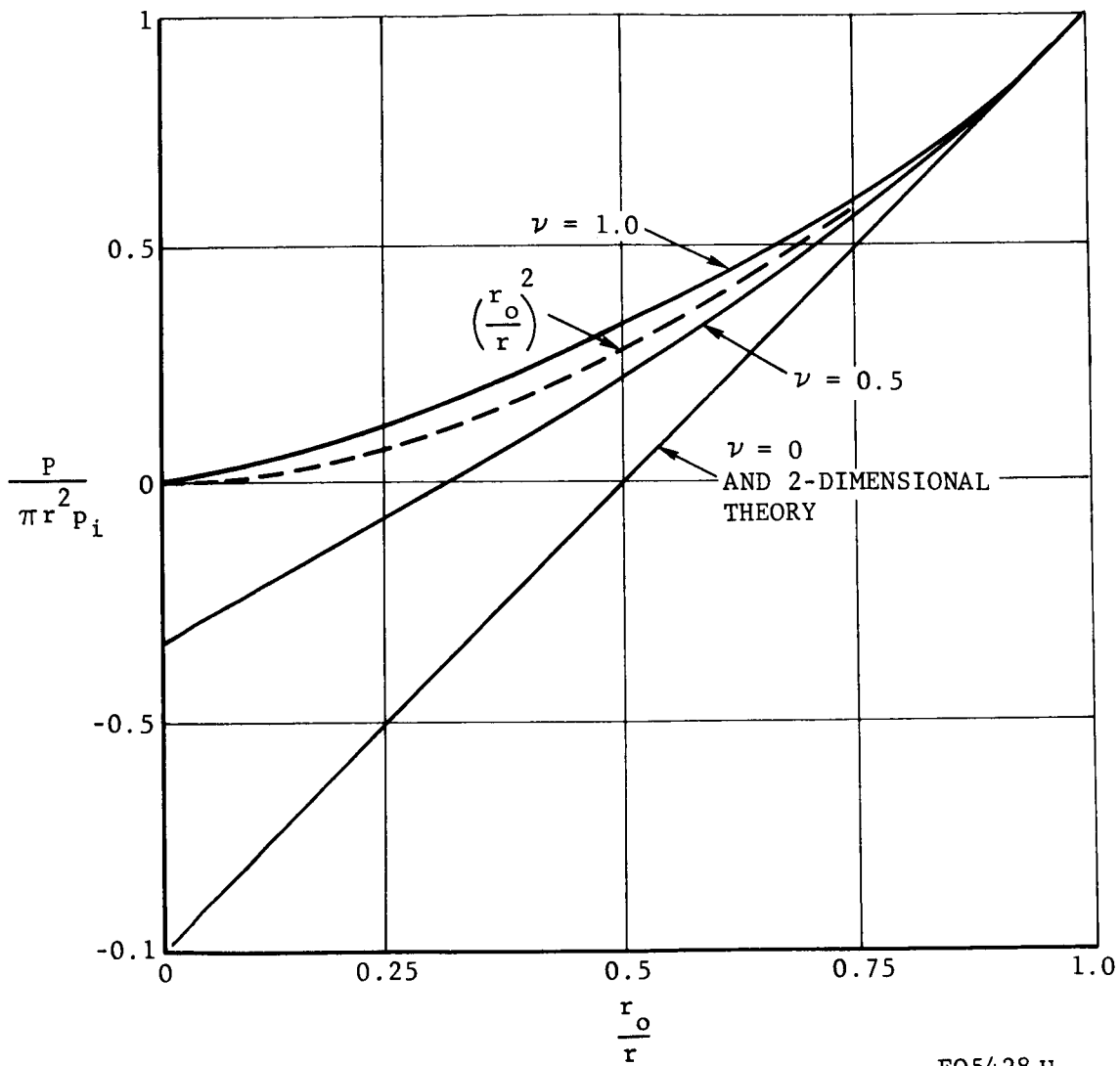
The above relations can be compared with the method usually used to predict the spring force in an air spring which is:

$$P = p_i \pi r_o^2$$

or

$$\frac{P}{p_i \pi r^2} = \left(\frac{r_o}{r} \right)^2 \quad (58)$$

This relation is also shown plotted in Figure 39. All of the expressions give substantially the same result in the range which is of most interest for the present study, that is, for values of r_o/r greater than about 0.75.



F05428 U

FIGURE 39. COMPARISON OF SPRING FORCE EXPRESSIONS

Of the various methods for calculating spring force, the two-dimensional method is simple, and gives reasonably accurate results. Since it can be used directly to give local forces, or integrated to give moments, it will be used in the subsequent work.

For use in design, it is desirable to convert the previous expressions which contain the unknown radius, r_0 , into forms which are in terms of known quantities. For the cases which are of most interest, the meridional length (l in Figure 38) can be assumed to be a known constant. For this case, simple expressions can be obtained for the resulting loads.

Using Equation (56), the longitudinal component of membrane tension loading per unit length around the ring is:

$$q = q_1 \cos \alpha = \rho_1 p_i \cos \alpha \quad (59)$$

From Figure 38,

$$l = 2 \alpha \rho_1 \quad (60)$$

Putting ρ_1 from Equation (60) into Equation (59) gives:

$$\frac{q}{l p_i} = \frac{\cos \alpha}{2 \alpha} \quad (61)$$

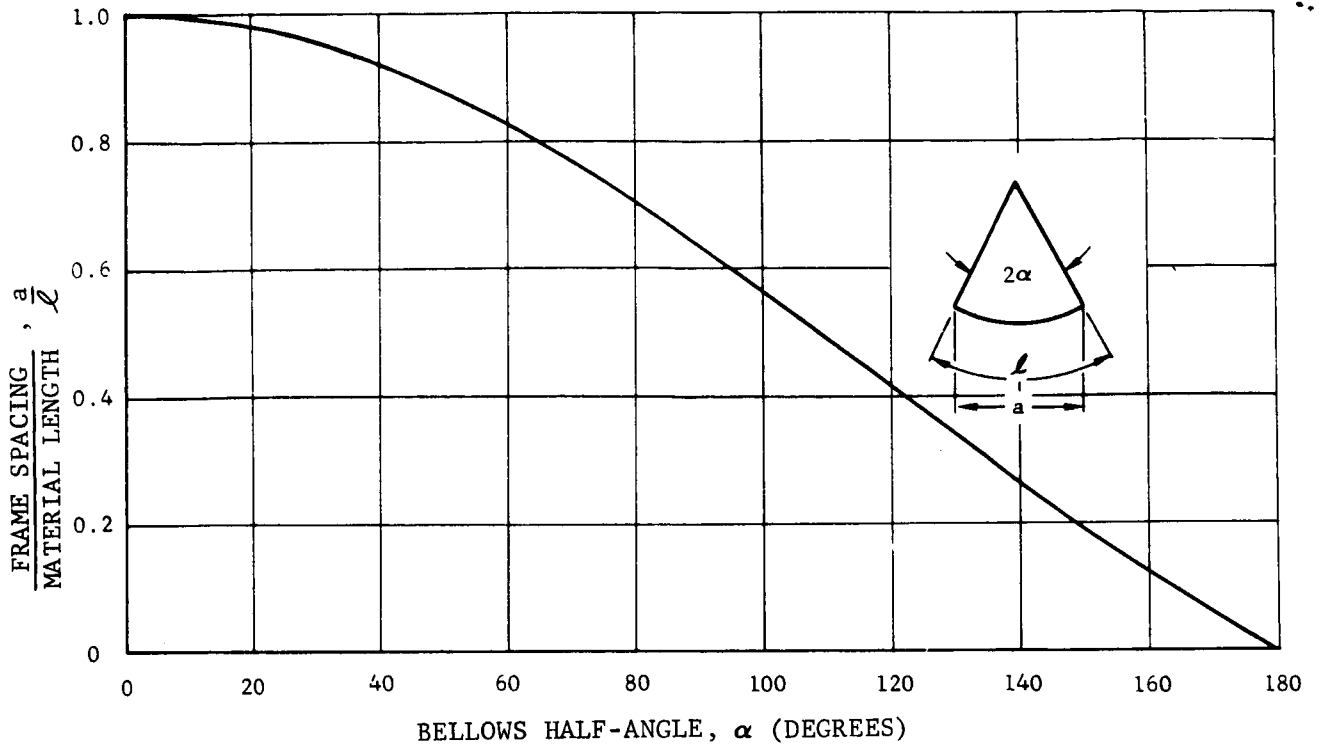
The value of α is obtained by noting in Figure 38 that

$$a = 2 \rho_1 \sin \alpha \quad (62)$$

Using Equation (60), this gives:

$$\frac{a}{l} = \frac{\sin \alpha}{\alpha} \quad (63)$$

This relationship is shown in Figure 40. By using this relationship, Equation (61) may be graphically transformed into a function of a/l , and the result is shown in Figure 41.



FO5429 U

FIGURE 40. BELLOWS GEOMETRY RELATIONSHIP

The spring rate can be obtained by differentiating Equations (61) and (63).

$$\begin{aligned} \frac{dq}{da} &= \frac{\frac{dq}{d\alpha}}{\frac{da}{d\alpha}} = \frac{\frac{l p_i}{2} \left(\frac{-\alpha \sin \alpha - \cos \alpha}{\alpha^2} \right)}{l \left(\frac{\cos \alpha - \sin \alpha}{\alpha^2} \right)} \\ &= \frac{p_i}{2} \cdot \frac{\sin \alpha + \frac{\cos \alpha}{\alpha}}{\frac{\sin \alpha}{\alpha} - \cos \alpha} \end{aligned} \quad (64)$$

This is shown as a function of a/l in Figure 42, the transformation being made by Equation (63). The force or spring rate per unit of circumference given in Figure 41 or 42 may be integrated around the ring to give total force

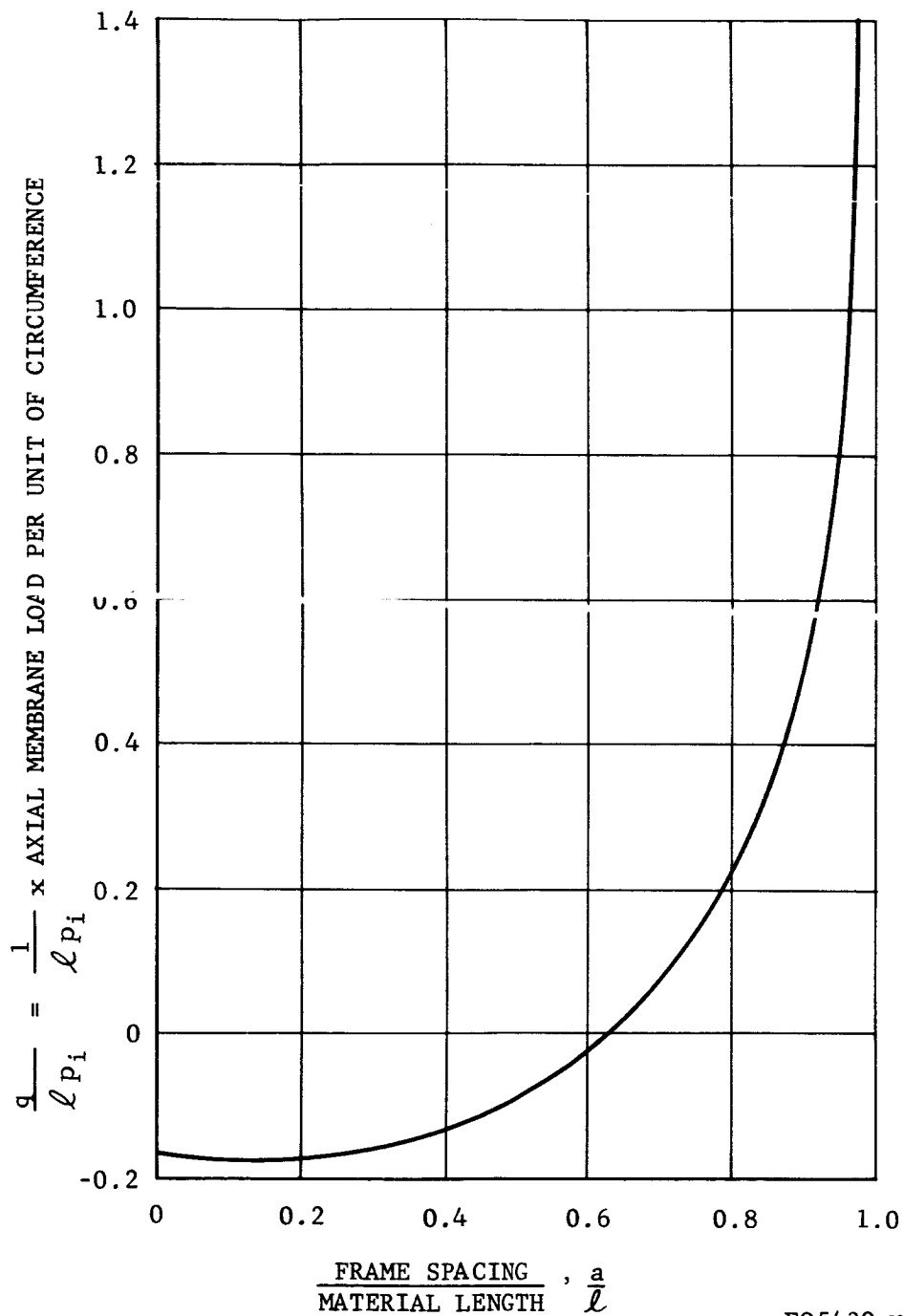


FIGURE 41. BELLOWS AXIAL MEMBRANE LOAD

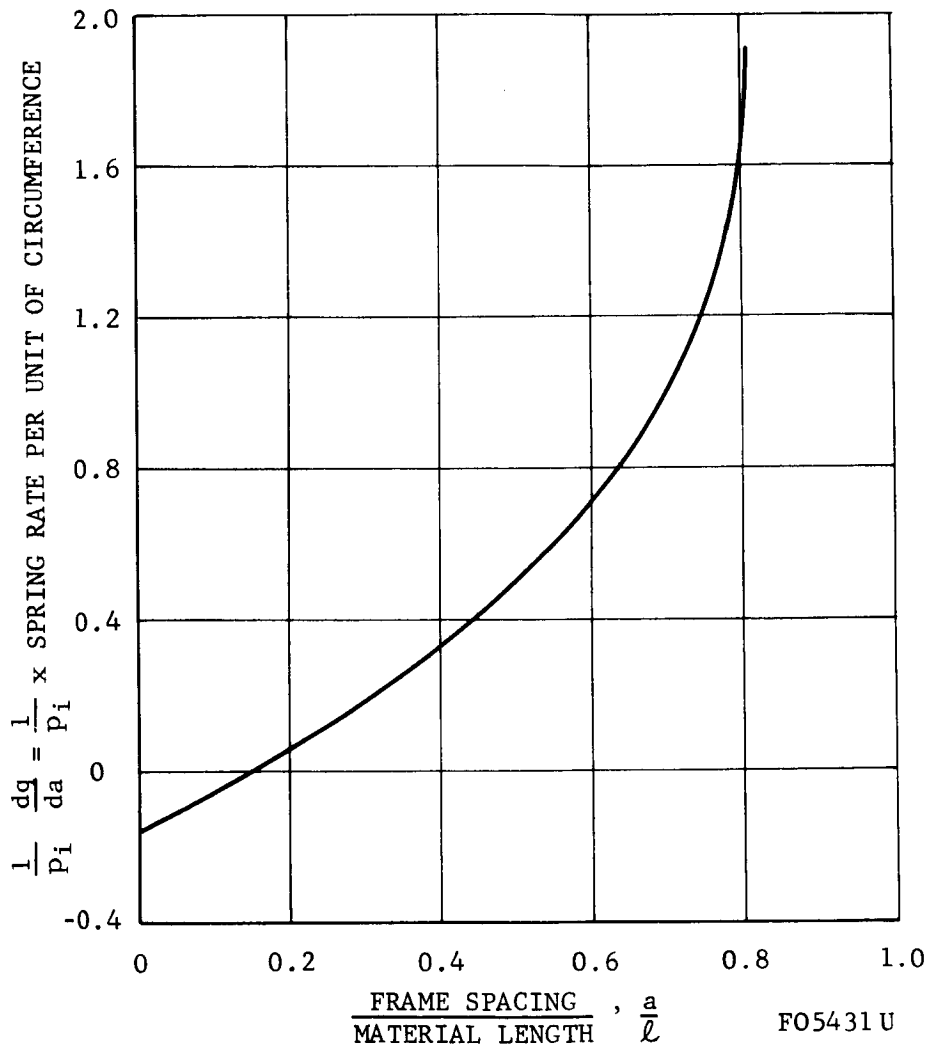


FIGURE 42. BELLOWS SPRING RATE

or moment. If the rings are circular and parallel, the net axial load and spring force become:

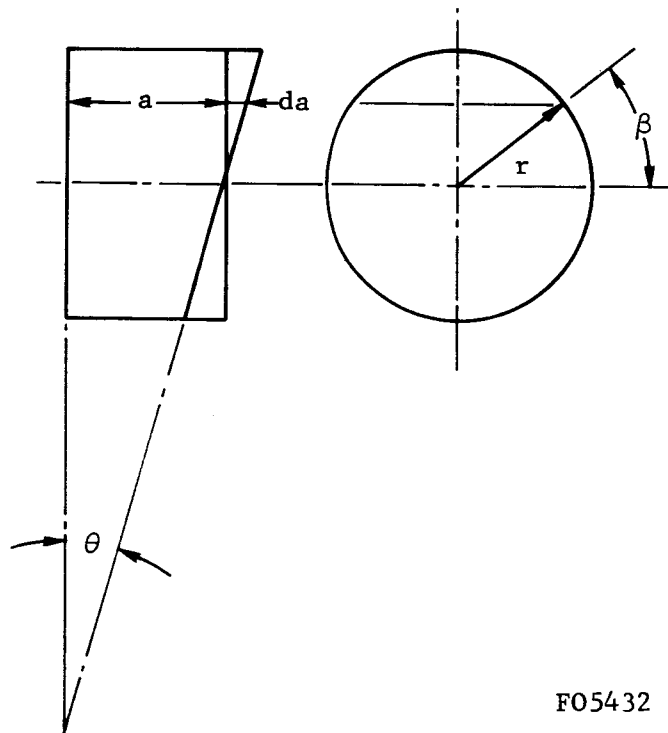
$$\begin{aligned}
 P &= \pi r^2 p_i - 2 \pi r q \\
 &= 2 \pi r \ell p_i \left[\frac{r}{2\ell} - \frac{q}{\ell p_i} \right]
 \end{aligned}
 \tag{65}$$

and

$$\frac{dP}{da} = 2 \pi r \cdot \frac{dq}{da} = 2 \pi r p_i \cdot \frac{1}{p_i} \frac{dq}{da}
 \tag{66}$$

where the functions $q/\ell p_i$ and $(1/p_i)(dq/da)$ can be read from the curves, and all other terms are known.

The bending stiffness can be obtained from Equation (66) by integrating around the circumference as shown in Figure 43.



F05432 U

FIGURE 43. GEOMETRY OF BELLOWS BENDING

For circular rings:

$$da = \theta \cdot r \sin \beta$$

$$\begin{aligned} M &= 2 \int_0^{\pi} r \sin \beta \cdot da \cdot \frac{dq}{da} \cdot r d\beta \\ &= 2 \theta r^3 \frac{dq}{da} \int_0^{\pi} \sin^2 \beta d\beta \\ &= \pi \theta r^3 \frac{dq}{da} \end{aligned}$$

This can be compared with the section stiffness of a beam

$$\begin{aligned} (EI)_{\text{eff}} &= \frac{Ma}{\theta} = \pi a r^3 \frac{P_i}{2} \cdot \frac{\sin \alpha + \frac{\cos \alpha}{\alpha}}{\frac{\sin \alpha}{\alpha} - \cos \alpha} \\ &= \frac{\pi}{2} \cdot r^3 P_i \ell \frac{\sin \alpha}{\alpha} \left[\frac{\sin \alpha + \frac{\cos \alpha}{\alpha}}{\frac{\sin \alpha}{\alpha} - \cos \alpha} \right] \end{aligned} \quad (67)$$

Buckling

All bellows have a tendency to buckle laterally when pressurized internally and restrained at the ends. The buckling load can be approximated by use of the Euler equation.

$$P = \frac{\pi^2 \cdot EI}{L^2} \quad (68)$$

In this equation, L is the column length between points of inflection, P can be replaced by its value from Equation (74) and EI by its value from Equation (67) giving,

$$\frac{r}{\ell} - \frac{\cos \alpha}{\alpha} = \frac{\pi^2 r^2}{2L^2} \cdot \frac{\sin \alpha}{\alpha} \left[\frac{\sin \alpha + \frac{\cos \alpha}{\alpha}}{\frac{\sin \alpha}{\alpha} - \cos \alpha} \right]$$

or

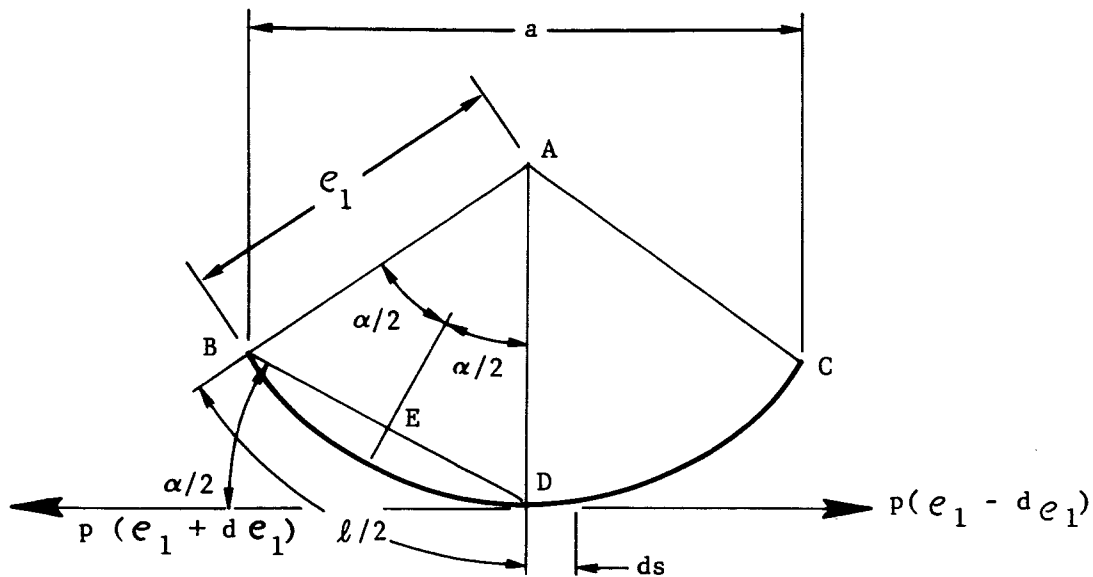
$$\left(\frac{L}{r}\right)^2 = \frac{\pi^2}{2} \frac{\sin \alpha}{\alpha} \left[\frac{\sin \alpha + \frac{\cos \alpha}{\alpha}}{\frac{\sin \alpha}{\alpha} - \cos \alpha} \right] \frac{1}{\frac{r}{l} - \frac{\cos \alpha}{\alpha}} \quad (69)$$

It is interesting to note that according to this equation, the column length is independent of pressure since the stiffness increases with pressure.

Shear Transfer to the Ground

In an application of a membrane bellows, it is proposed to use the convolutions as contact surfaces on the ground. For such an application, it is important to know how well the convolutions can transmit thrust to the surface, that is, what is the spring constant of a convolution in the horizontal direction. A simplified preliminary analysis of this characteristic is given in the following paragraphs.

In Figure 44, points B and C represent the attachment points for the flexible membrane BDC, which carries an internal pressure p_i and forms a cylindrical surface with radius, ρ_1 . The surface is assumed to contact the ground at D. The spring force will be taken as the unbalance in membrane tensile loads at D when this point is moved horizontally through a small displacement, ds .



F05433 U

FIGURE 44. GEOMETRY OF CONVOLUTION

The displacement of D to the right in Figure 44 causes the radius of the left-hand half of the cylinder to increase by $d\rho_1$ and that of the right-hand half to decrease by $d\rho_1$. The unbalance of force per unit length normal to the paper is then the internal pressure times the net difference in radii, or:

$$dP = p_i \cdot 2d\rho_1 \quad (70)$$

From the geometry of Figure 44, ds equals $1/(\cos \alpha/2)$ times the change in length of BED.

$$ds = \frac{d(\text{BED})}{\cos \frac{\alpha}{2}} \quad (71)$$

but:

$$(\text{BED}) = 2\rho_1 \sin \frac{\alpha}{2} = 2\rho_1 \sin \frac{l}{4\rho_1}$$

$$\left(\text{since } \frac{\alpha}{2} = \frac{l}{4\rho_1} \right).$$

$$\begin{aligned} \frac{d}{d\rho_1} (\text{BED}) &= 2\rho_1 - \frac{l}{4\rho_1^2} \cos \frac{l}{4\rho_1} + 2 \sin \frac{l}{4\rho_1} \\ &= 2 \sin \frac{\alpha}{2} - \alpha \cos \frac{\alpha}{2} \end{aligned} \quad (72)$$

Using Equations (70), (71), and (72), the spring constant becomes:

$$\begin{aligned} \frac{dP}{ds} &= \frac{2 p_i \cos \frac{\alpha}{2}}{\frac{d}{d\rho_1} (\text{BED})} \\ &= \frac{2 p_i \cos \frac{\alpha}{2}}{\left(2 \sin \frac{\alpha}{2} - \alpha \cos \frac{\alpha}{2} \right)} \end{aligned} \quad (73)$$

This result is shown in Figure 45 as a function of a/l , where again this transformation is made by the use of Equation (63). This demonstrates the importance of keeping a/l large (close to 1.0) if the bellows is to be stiff in transmitting shear to the ground.

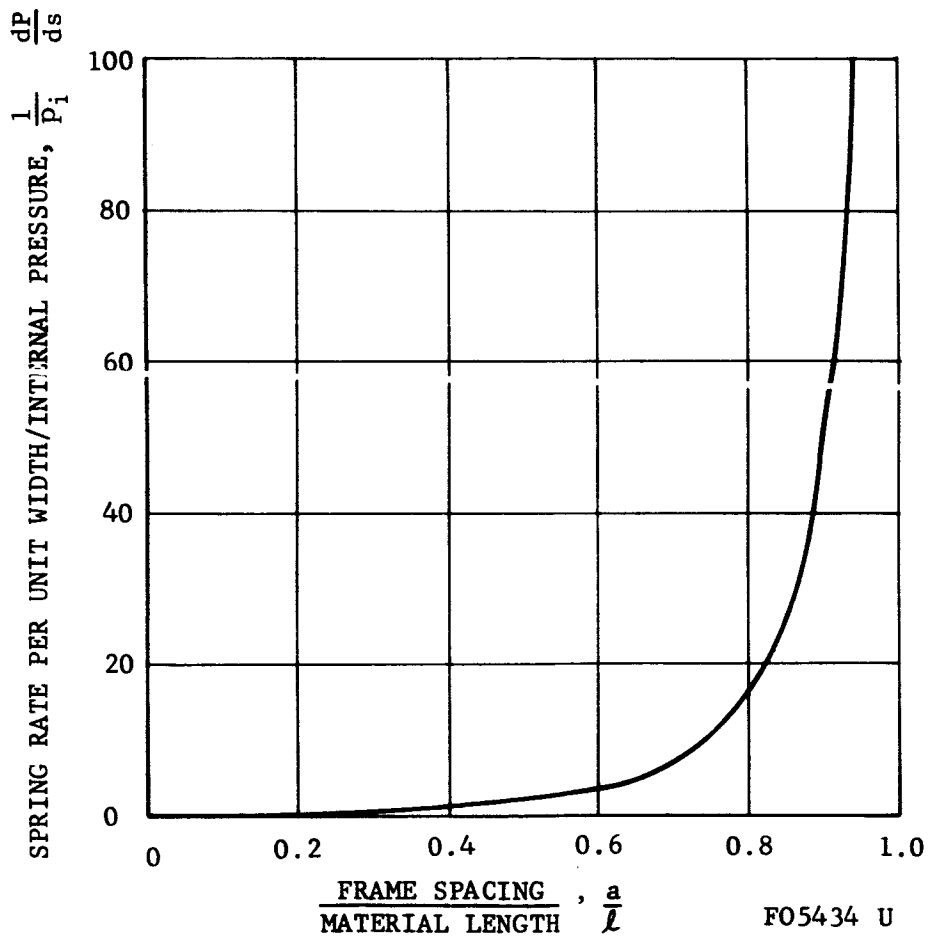


FIGURE 45. SHEAR STIFFNESS OF ONE CONVOLUTION

Consideration for Design Applications

The membrane bellows where loads are taken by tensile stresses in the skin provide a minimum weight structure to withstand a given pressure differential. Buckling is prevented primarily by change in geometry and is little affected by pressure differential. Load can be transferred to the lunar surface through the covering membrane by means of the internal pressure. The membrane tends to conform to the surface being traversed and a very uniform load distribution should result. Attention is required in designing the skin-frame-linkage system to avoid excessive lost motion in transfer of shear to the ground.

DESIGN STUDIES

SCOPE

Three preliminary studies have been made for the use of different bellows concepts as applied to several type missions in order to gain more insight regarding the desirability of using them in various practical situations. A different bellows concept has been studied for each of three type missions: lunar shelters which seldom have to be moved; a small unmanned vehicle used to explore a limited area; and a manned, extended range roving vehicle. The requirements of these missions encompass a broad range of mobility conditions, and, while the concept selected for study in each mission may not necessarily be the most optimum, it is considered sufficiently applicable to indicate the potential value of that particular concept.

The first study is for mobile shelters which would have the capability of moving from the landing site to the shelter site. Since ability to move is useful but not necessarily vital to the mission, the bellows concept used with shelters can have very low velocity, short range, low maneuverability, and a comparatively rough ride but weight of the mobility mechanism should be a small fraction of the overall shelter weight. The extension-contraction mode was selected as being appropriate for this study. The study is divided into two parts, one for a very large shelter and one for a small two-man shelter. Also briefly investigated is a novel concept of using the shelter as a very simple heat engine for propelling itself utilizing direct solar energy.

The second study is for a small unmanned vehicle suitable for exploratory purposes. The bellows concept suitable for such use can have low velocity, limited range, a moderate amount of maneuverability and the ride need not be soft. The rib-walking mode utilizing the double-acting bellows principle was selected as appropriate for this study. While several different type double-acting bellows structures were considered and are described, the study was arbitrarily limited to a metal bellows configuration with the bellows structure not in contact with the lunar surface.

The third study is for a manned, extended-range, roving vehicle. The bellows concept suitable for such use should have moderate velocity capability, good propulsive efficiency, good maneuverability, ability to cope with a wide range of surface roughness and soil strength, and a soft ride. The traveling wave mode utilizing a membrane bellows structure was selected as appropriate to meet these comparatively restrictive requirements.

All of the vehicles studied will require a steering and control system. The immediately following section describes such a system previously developed at Aeronutronic and considered applicable to control these vehicles in turning, climbing, and bridging.

STEERING AND CONTROL

The wormlike creatures in nature control the direction of their motion by bending their bodies. In many cases this control can be exerted in the vertical as well as the horizontal direction. An illustration of this is given in Figure 46, where a centipede is shown bridging across a gap in very rough simulated terrain.

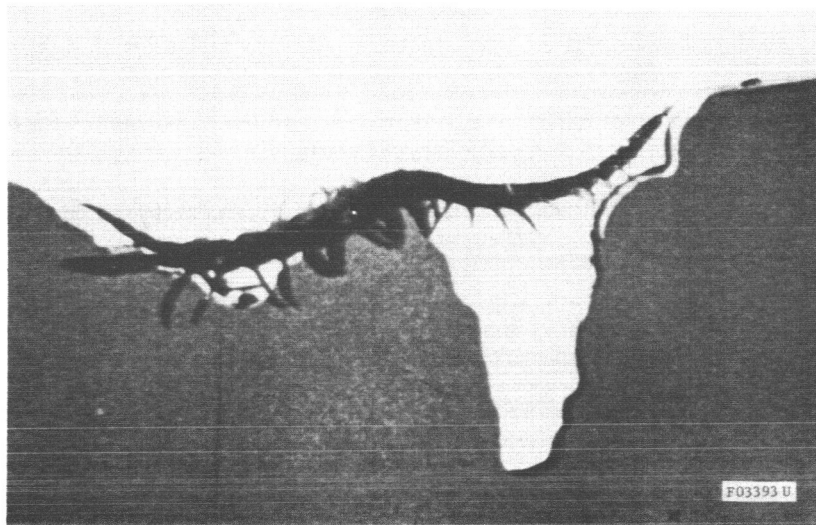
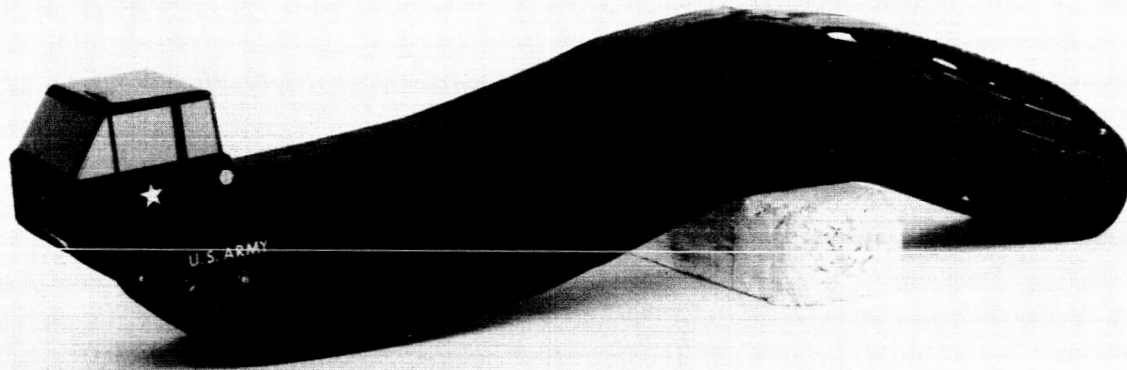


FIGURE 46. CENTIPEDE BRIDGING

The centipede bridges by anticipating the changes ahead and programming its path to smooth out all but those of longest wavelength. Analysis and analog studies show that this technique has the capability of reducing average accelerations on rough ground by an order of magnitude or more, for an average-sized vehicle.

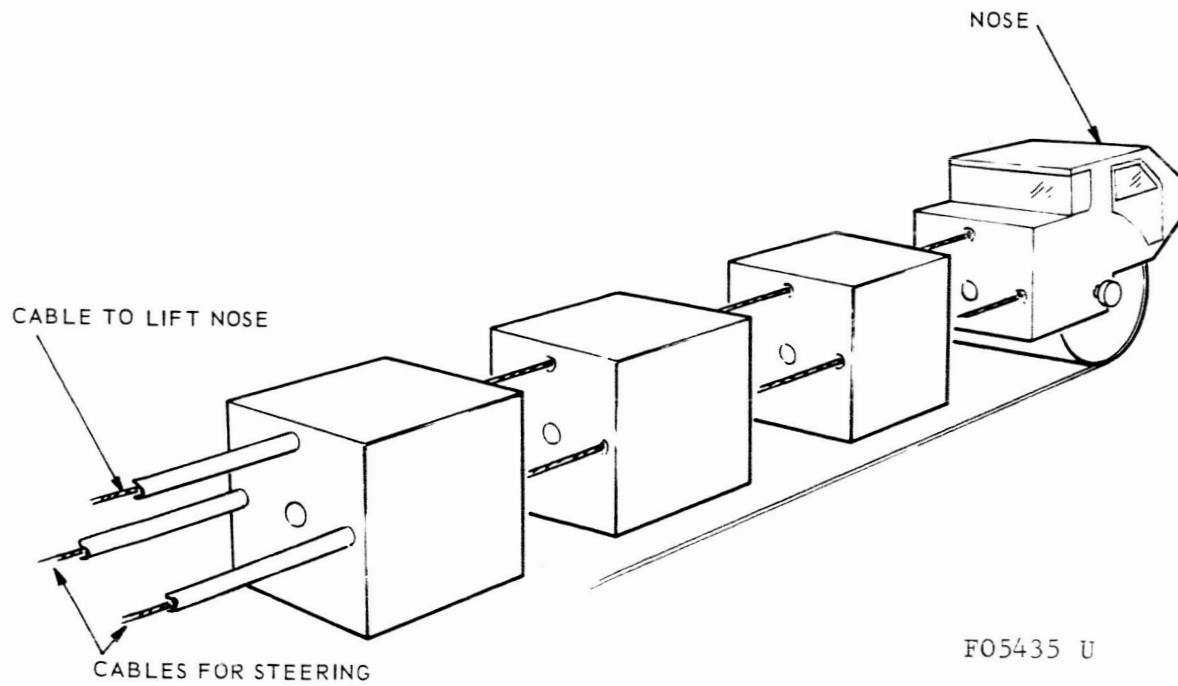
An attempt to mechanize some of these observed characteristics resulted in the Aeronutronic Bridging Off-Road Amphibian (BOA) concept. A powered model demonstrating this principle is shown in Figure 47. This vehicle uses a flexible, continuous track for propulsion, and is flexible and controllable both vertically and laterally. The vertical and lateral control is shown in Figure 48. The tension in the cables can be controlled remotely, thereby modifying the curvature of the vehicle. This is demonstrated in Figure 49 with the model turning, and in Figure 50 with the model bridging. This model was able to negotiate trenches up to one-third, and walls of one-sixth of its length. In addition, the smoothing effect of the length was very noticeable even though the model had no flexibility in its suspension.

The general method of steering and control which has been demonstrated with the Aeronutronic BOA model is applicable to the various configurations described in the following sections.



F03394 U

FIGURE 47. BOA MODEL



F05435 U

FIGURE 48. BOA STEERING MECHANISM

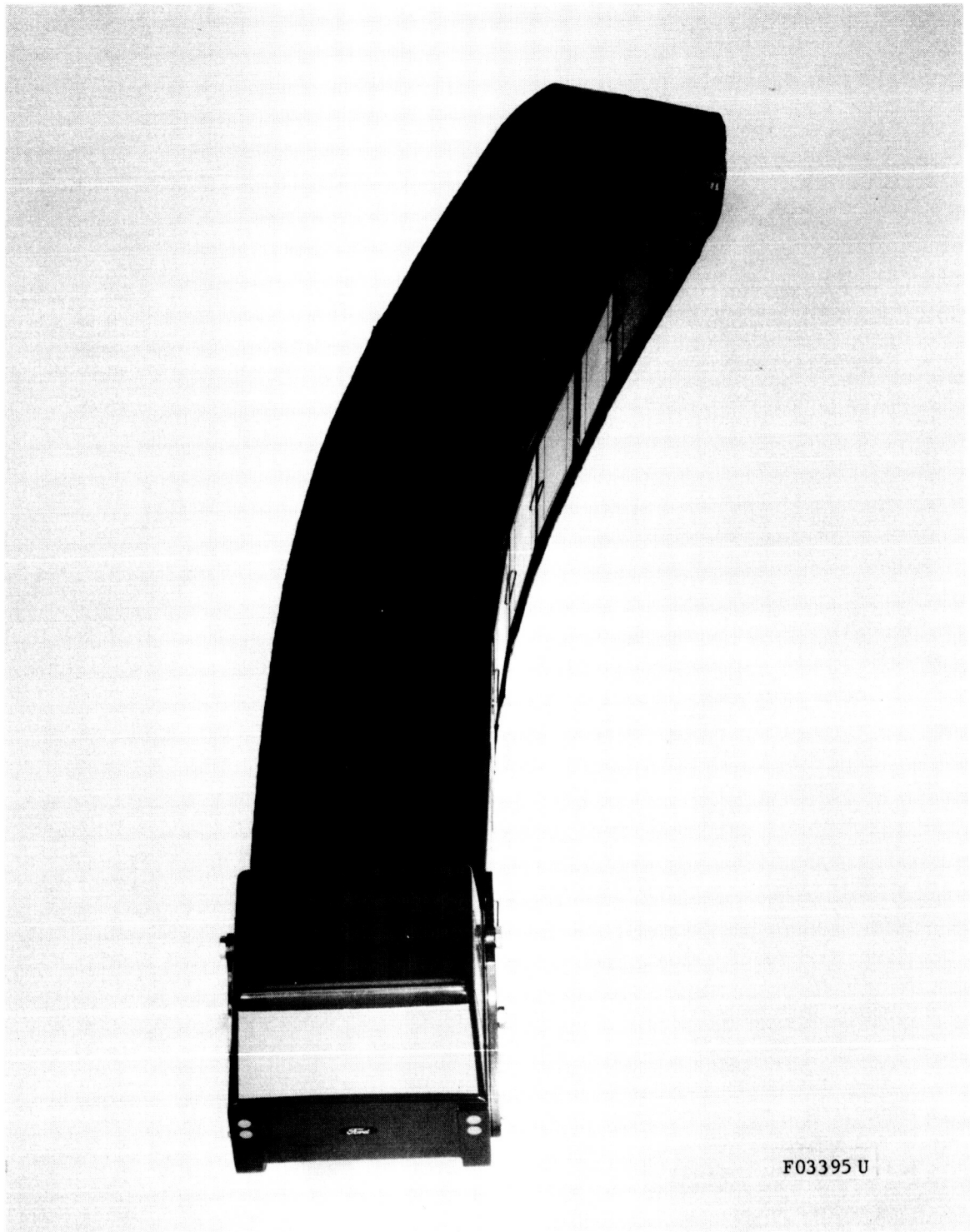


FIGURE 49. BOA MODEL TURNING

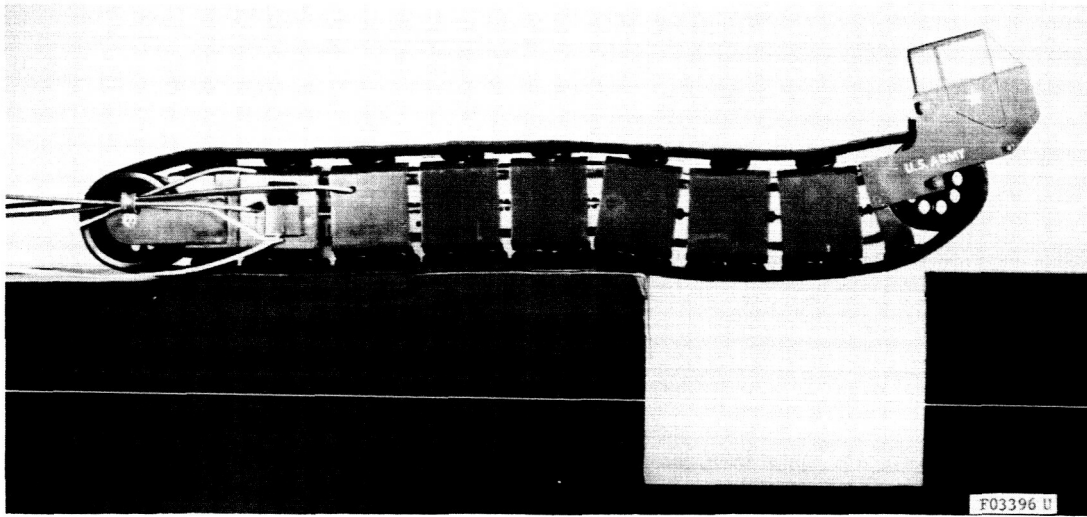


FIGURE 50. BOA BRIDGING

LUNAR SHELTER

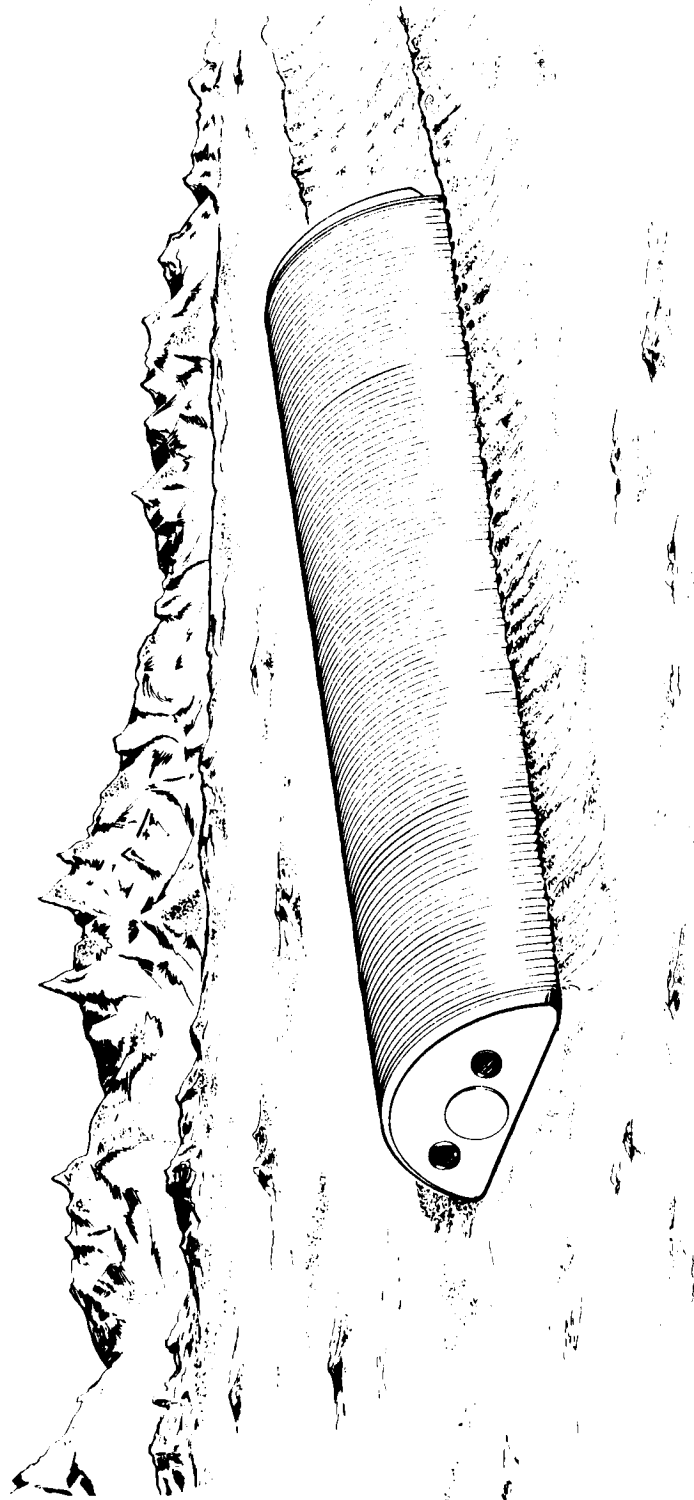
The lunar shelter would be used as living quarters by a group of astronauts for periods of up to one year. It would have limited mobility, that is, a range of a mile at a speed of 1/10 mile per hour. The sizes which are of interest range from a minimum two-man shelter up to the largest unit which could be carried as an Apollo payload (about 20 feet in diameter).

Large Lunar Shelter

Configuration requirements. - For this design, a large shelter which is normally stationary is desired. However, limited mobility - perhaps to change location once in its lifetime - is provided by the extension-contraction mode. An artist's sketch of the shelter is shown in Figure 51.

A welded metal type bellows will be assumed and the design principles and nomenclature discussed in the Bellows Analysis section will be used. The following characteristics are desired

Maximum width	20 feet
Maximum length	60 feet
Living pressure	7-1/2 psi
Maximum speed	0.1 mph



F05436 U

FIGURE 51. LARGE LUNAR SHELTER

Range

1 mile

Empty weight

minimum

A sketch of the shelter is shown in Figure 52. Three possible configurations for the corners are shown. A curved corner as in (a) avoids stress concentrations, and the analysis used applies without modification if the radius of curvature is large. The welded corners in (b) and (c) are used for convoluted bellows because of the difficulty of fabricating a curved corner. However, they involve unknown stress concentrations, and do not appear to have any advantage over (a) for welded bellows.

Bellows design. - Initially the following characteristics are assumed:

Semicircular cross section

Material Stainless steel

Fatigue limit 25,000 psi

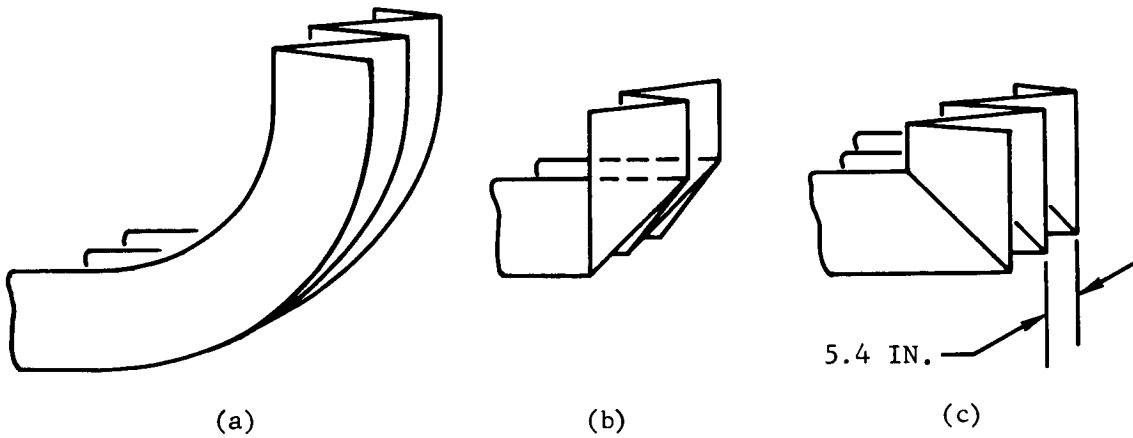
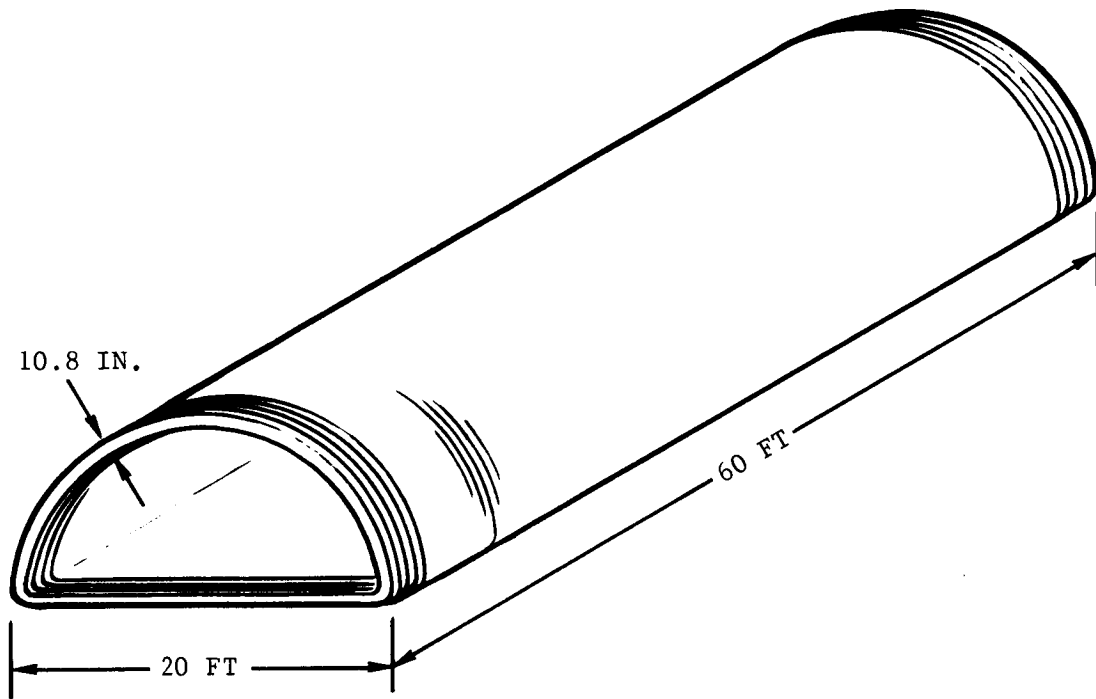
Young's modulus 28.5×10^6 psi

Mass density 0.283 lbm/in.³

Gravity factor, g_e/g 6

For minimum empty weight, the minimum working pressure and minimum d/b (bellows depth/vehicle width) are desired. To a first approximation, the working pressure can be one-fourth of the living pressure. This assumes that the "living" condition of the shelter is the unstrained position, and that while moving, it extends until pressure stresses are equal to bending stresses. This is the condition resulting from optimum geometry as discussed in the Bellows Analysis section. The allowable fatigue limit is assumed to be one-half of the allowable static stress. This is illustrated in Figure 53, where the stress is shown for one point on the surface of a bellows disc. The nominal length with working pressure is represented by A, and is seen to be one-half of the allowable fatigue stress. At this length, no stress due to extension exists, and the pressure may be raised a factor of four to point C, the allowable tensile stress of the material, if this pressure is not cyclic. Therefore, the design working stress must be greater than $7.5/4 = 1.87$ psi so the desired living pressure can be contained. A working pressure of 2 psi will be used for the design.

The design charts in Appendix F show that d/b (bellows depth to vehicle width ratio) of 0.04 will not contain a 2 psi internal pressure without exceeding the fatigue limit. A d/b of 0.045 will contain this pressure and leave an allowance to carry its own weight and some payload.



ALTERNATE CORNER CONFIGURATIONS

F05437 U

FIGURE 52. LARGE LUNAR SHELTER AND ALTERNATE CORNER CONFIGURATIONS

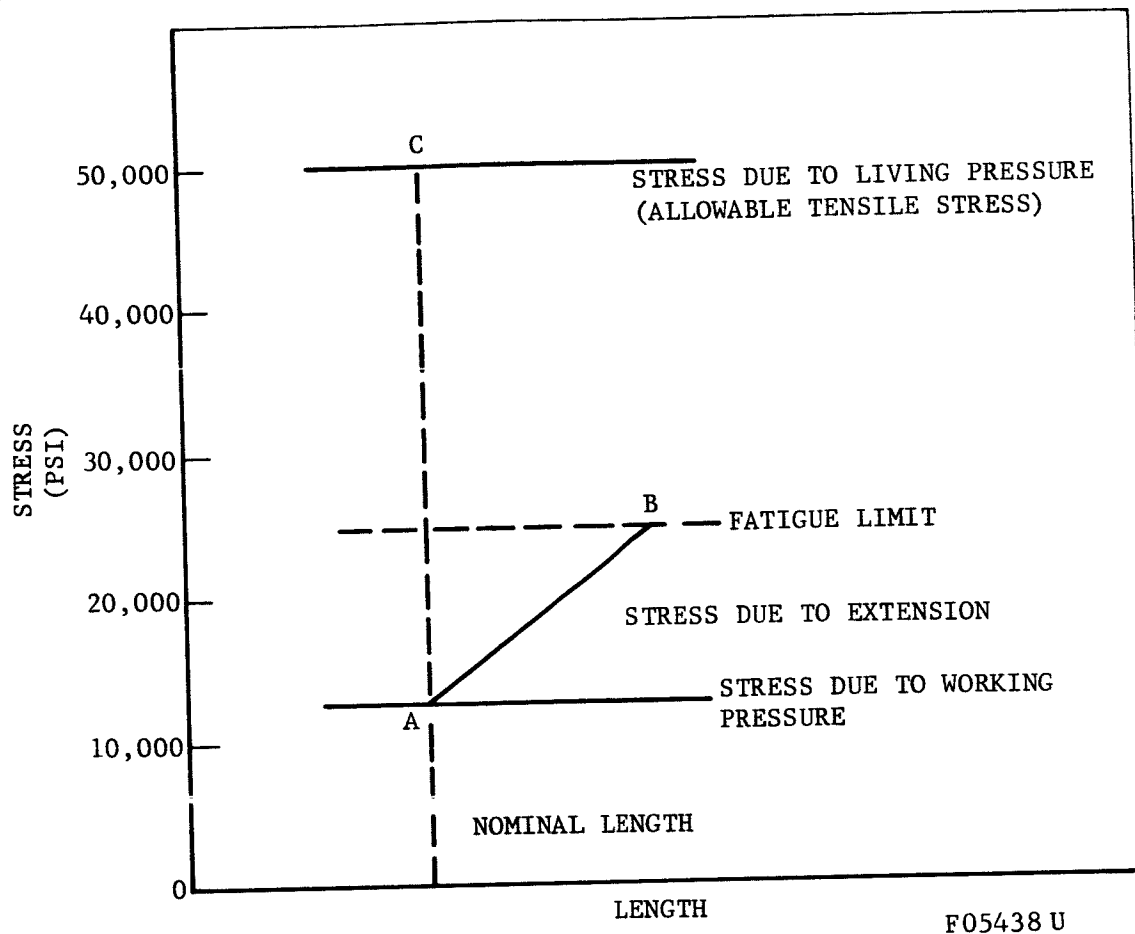


FIGURE 53. STRESS CONDITION OF BELLOWS

The bellows configuration is now fully specified by the optimum geometry considerations discussed previously. The calculation of the bellows parameters is given in Appendix F. The following is a summary of the assumed and calculated values from Appendix F.

Width, b	240 inches
Bellows depth, d	10.8 inches
d/b	0.045
Working pressure, p_i	2 psi
Maximum extended length, L_e	720 inches
Material thickness, t	0.0963 inch

Equivalent thickness, t_e	0.374 inch
Number of convolutions, N	128
Empty mass, M_e	47,000 lbm
Useful load (mass), M_u	334,000 lbm
Loading density, M_u/V	37.7 lbm/ft ³
Gross weight	381,000 lbm
Nominal extended length	675 inches
Closed length (theoretical flat plate)	24 inches
Maximum stroke	+45 inches
Maximum footprint pressure	0.42 psi
Maximum footprint when empty	0.052 psi
Maximum pressure force less bellows (spring) force	40,000 pounds

Bottom surface design. - If each convolution of the bellows has a foot (planing surface) it might take the form shown in Figure 54 at the maximum extended length.

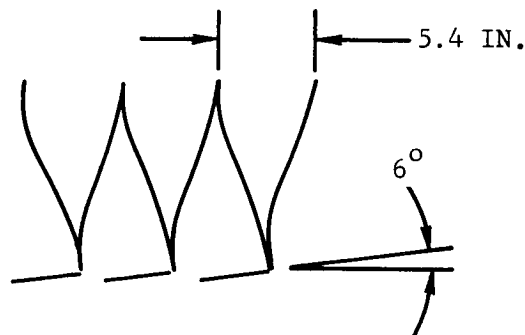


FIGURE 54. BELLOWS AND FEET IN EXTENDED POSITION

At maximum gross weight, the load per unit length on these feet is

$$\begin{aligned}
 m_p &= \frac{\text{Gross mass}}{N \cdot b} \cdot \frac{g}{g_e} \\
 &= \frac{381,000}{(128)(240)(6)} \\
 &= 2.07 \text{ lb/in. of vehicle width.}
 \end{aligned}$$

If this load is assumed to be concentrated at the center of the foot, it creates a moment of

$$M_b = 2.07 \left(\frac{5.4}{2} \right) = 5.6 \text{ in. -lb}$$

which is transferred to a unit of running length of two bellows sheets. This creates a stress in the bellows of

$$f = \frac{6M_b}{2t^2} = \frac{(6)(5.6)}{(2)(0.0963)^2} = 1810 \text{ psi}$$

which is small compared to the fatigue limit of 25,000 psi and may be absorbed in the conservatism of that number. If these feet are somewhat flexible, the friction coefficient differential may be increased since they will become flatter when moving forward and dig in when moving backward. Care must be taken in the design, however, to ensure that the cavities between discs empty of sand on the forward stroke.

Feet of this type may be initially stowed in the overlapped position as in Figure 55.

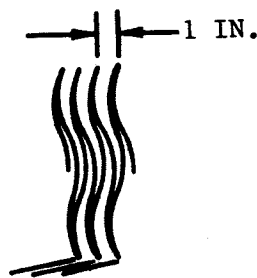


FIGURE 55. FEET AND BELLOWS IN CLOSED POSITION

Because of interference of the feet and their attachments, the bellows cannot fold to the flat-plate thickness of the bellows material. As shown in Figure 55, the vehicle closed length is

$$L_c = \frac{257}{2} \times 1 = 129 \text{ in.}$$

$$= 10.8 \text{ ft}$$

Mobility Analysis

In the Mobility section, it was shown that the allowable planform loading for planing is

$$P_{al} = \frac{\gamma_s l}{RJ} \frac{g}{g_e}$$

For typical parameters on the moon, this gives an allowable loading of $l/1000$. Calculating the desired foot length, l , using the loading of the present vehicles, gives

$$l \text{ (desired for planing)} = 420 \text{ inches (at maximum gross weight)}$$

$$= 52 \text{ inches (empty vehicle)}$$

On this basis, the feet shown above are small by a factor of 100 with the shelter loaded, and a factor of 10 with the shelter empty. Note, however, that this applies only to the "typical" soil (granular, $\gamma_s = 50 \text{ lbm/ft}^3$), and that even in the soil assumed, the planing concept has not been verified on this scale. The following analysis will be based on the assumption that the feet are properly designed to give the friction coefficient differential necessary for extension-contraction mobility.

As given in the Mobility section, the distance traveled in one cycle is

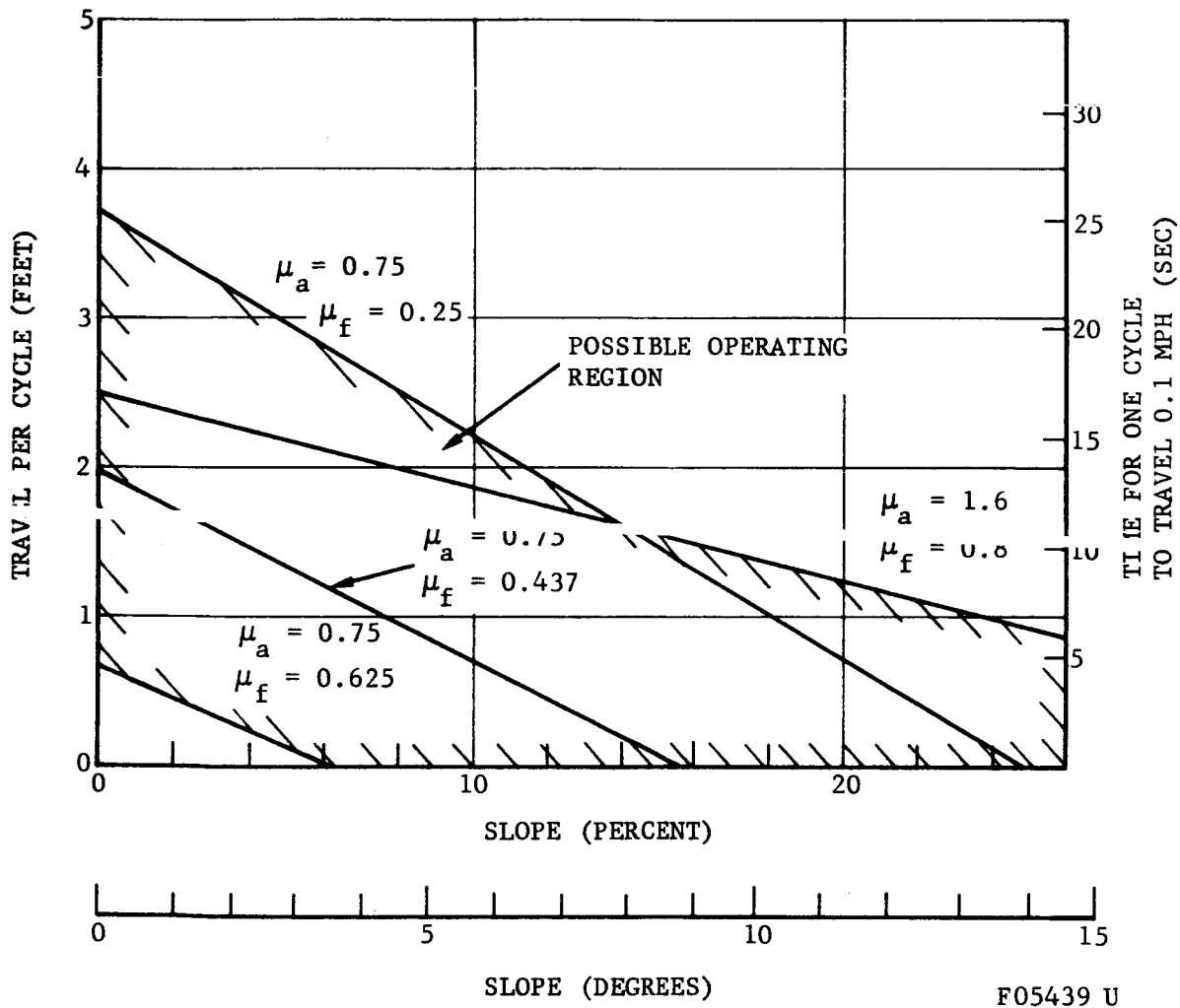
$$2s = 2L_e \delta_l \frac{k_a - k_f}{k_a + k_f} = 2L_e \delta_l \frac{\frac{k_a}{k_f} - 1}{\frac{k_a}{k_f} + 1}$$

where, on a slope

$$k_a = \mu_a - \tan \theta$$

$$k_f = \mu_f + \tan \theta$$

This is shown plotted on Figure 56 for several assumed friction coefficients. For the range of assumed friction coefficients, the travel per cycle is from 0.68 to 3.75 feet on level ground. This corresponds to 7800 to 1400 cycles to



F05439 U

FIGURE 56. MOVING SHELTER TRAVEL PER CYCLE

travel one mile. The time per cycle which will give the shelter a speed of 0.1 mph is

$$T = (\text{feet traveled per cycle})/0.147 \text{ second}$$

This is shown on the right hand scale in Figure 56.

The force required to extend the shelter against the soil frictional force on the maximum slope is

$$\begin{aligned} P_f &= \left(\frac{\mu_a + \mu_f}{4} \right) (\text{Gross mass}) \frac{g}{g_e} \\ &= (\mu_a + \mu_f)(0.25)(0.166)(381,000) \\ &= 15,900 (\mu_a + \mu_f) \end{aligned}$$

This force is then between 15,900 and 38,100 pounds for the soil friction conditions assumed. It was shown previously that 40,000 pounds of force was available at the working pressure of 2 psi.

The equivalent drag-to-weight ratio was shown in the Mobility section to be

$$\frac{D_e}{W} = \frac{k_a k_f}{k_a - k_f}$$

Since the vehicle weight is now given, this may be converted either to power to travel at a given speed or work required to travel a given distance. The power consumption is given by

$$\begin{aligned} P_t &= D_e v \\ &= \left(\frac{D_e}{W} \right) (M_e + M_u) L_e \frac{g}{g_e} v \\ &= \frac{1}{6} (381,000) v \left(\frac{D_e}{W} \right) \end{aligned}$$

At 0.1 mph (0.147 fps), this becomes

$$P_t = 9330 \left(\frac{D_e}{W} \right) \text{ ft-lb/sec}$$

or

$$HP = 17 \frac{k_a k_f}{k_a - k_f} \text{ horsepower}$$

This is shown in Figure 57.

Small Lunar Shelter

Configuration requirements. - The subject of this study is a minimum-size shelter for the protection of a two-man team during an eight- to thirty-day stay on the moon; and includes the requirement that the empty shelter shall be able to move under its own power at low speeds over distances up to about a mile.

The design procedure used in this study is similar to that used in the previous section for a large lunar shelter.

The nominal external dimensions for the shelter in a fully extended condition are given in Figure 58, and a sketch is shown in Figure 59. It is designed for a normal internal living pressure of 5 psi, and is made up of a main shelter 7 feet in diameter by 12-1/2 feet long and an airlock of the same diameter, 5 feet long.

As shown in Figure 58, the airlock and the shelter are of metallic bellows construction, and the entire assembly can be collapsed to a length of about 5 feet for transport.

Bellows design. - For a final living pressure of 5 psi, the working pressure will be 1.25 psi. For this analysis it will be assumed that the bellows shape is equivalent to one of 60-inch width. Reading from Figure F-1 of Appendix F, a d/b of about 0.037 will sustain a pressure of 1.25 psi so the bellows depth will be made.

$$d = 0.037 \times 60 = 2.23 \text{ inches}$$

Since the bellows will require welding, some of the material will be in the annealed condition, so an allowable stress of 25,000 psi will be used. This stress level, together with the working pressure, defines the optimum geometry given in the Mobility section.

$$\frac{d}{t} = \sqrt{\frac{F}{p_i}} = \sqrt{\frac{25,000}{1.25}} = 141$$

The optimum thickness would therefore be

$$t = \frac{2.23}{141} = 0.0158 \text{ inch}$$

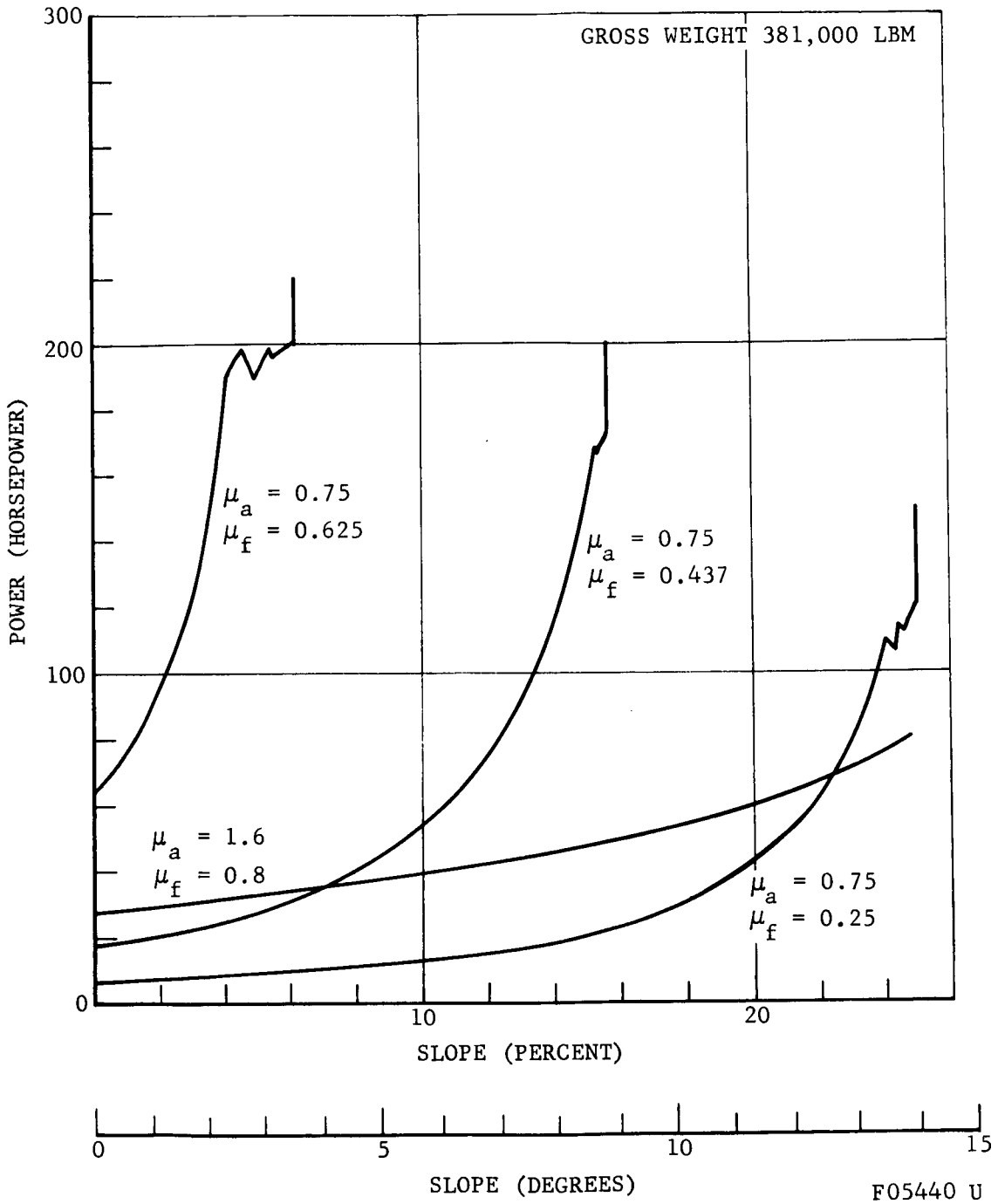
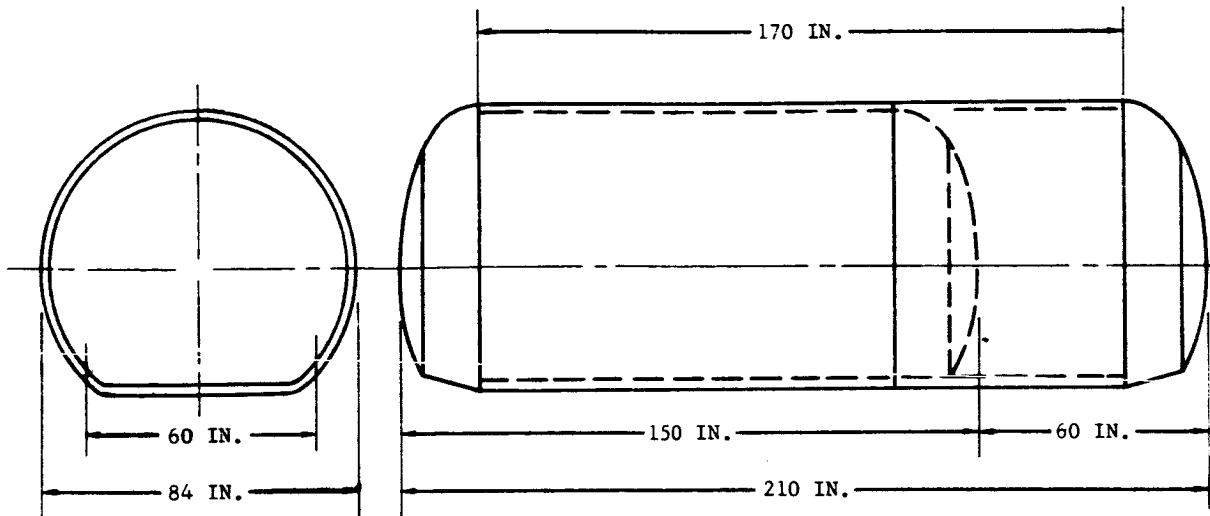


FIGURE 57. POWER TO MOVE LARGE LUNAR SHELTER 0.1 MPH



F05441 U

FIGURE 58. SMALL LUNAR SHELTER LAYOUT

In the subsequent work, the values of d and t will be rounded off to

$$d = 2.25 \text{ inches;}$$

$$t = 0.016 \text{ inch}$$

If the maximum extension per plate is held at 25 percent of the depth, the bellows maximum length per plate will be

$$0.016 + 0.25 \times 2.25 = 0.579$$

For the total active bellows length of 170 inches, the number of plates will be

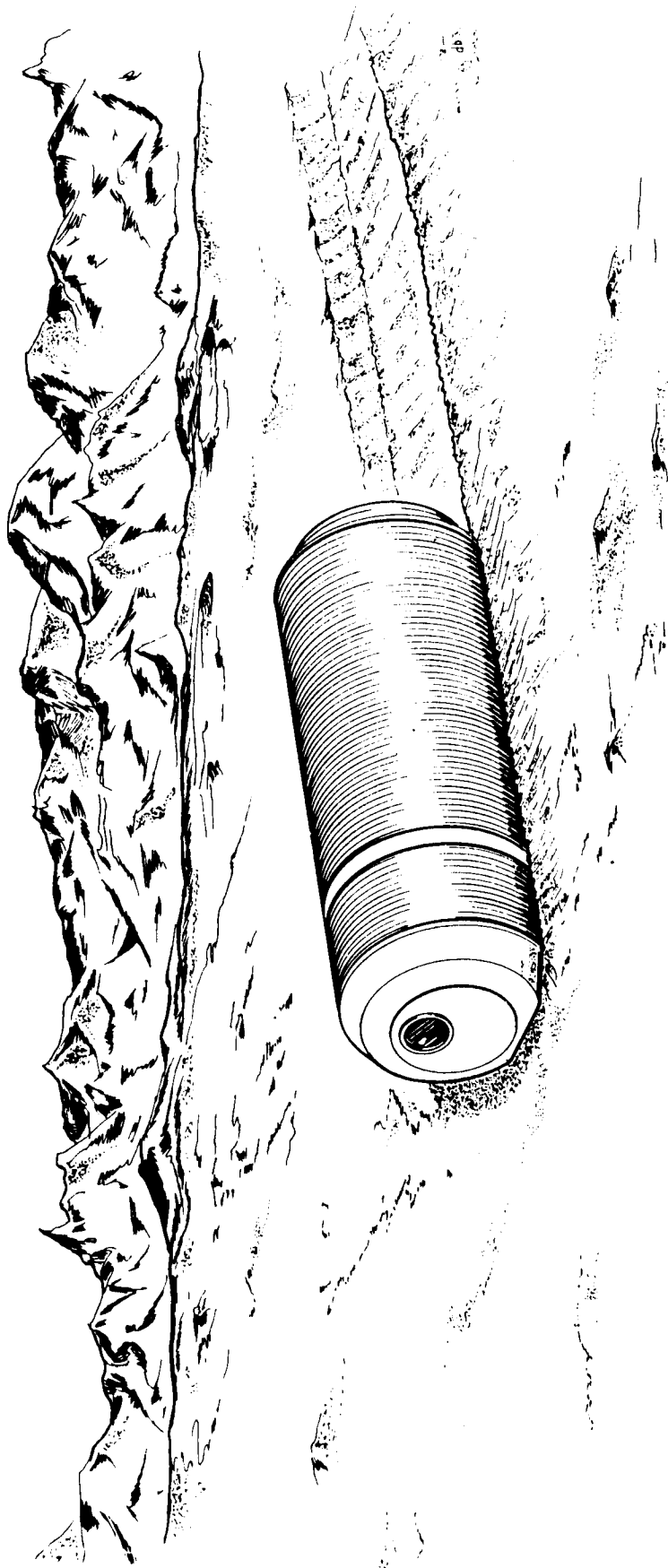
$$2N = \frac{170}{0.579} = 294$$

The theoretical minimum closed length will be

$$L_c = 294 \times 0.016 = 4.7 \text{ inches}$$

The ratio of maximum deflection to closed length is given by Equation (35) of the Bellows Analysis section

$$\frac{\delta}{t} = \frac{F^2}{3p_1 E} = \frac{(25,000)^2}{6 \times 1.25 \times 28.5 \times 10^6} = 2.92$$



F05442 U

FIGURE 59. SMALL LUNAR SHELTER

The total stroke will therefore be

$$L_s = \underline{+2.92} \times 4.7 = 20 \text{ inches}$$

This is 44.4 percent of the stroke calculated for the large lunar shelter, and the resulting travel per cycle is shown in Figure 60. This was obtained from Figure 56 by the required reduction of ordinate scale.

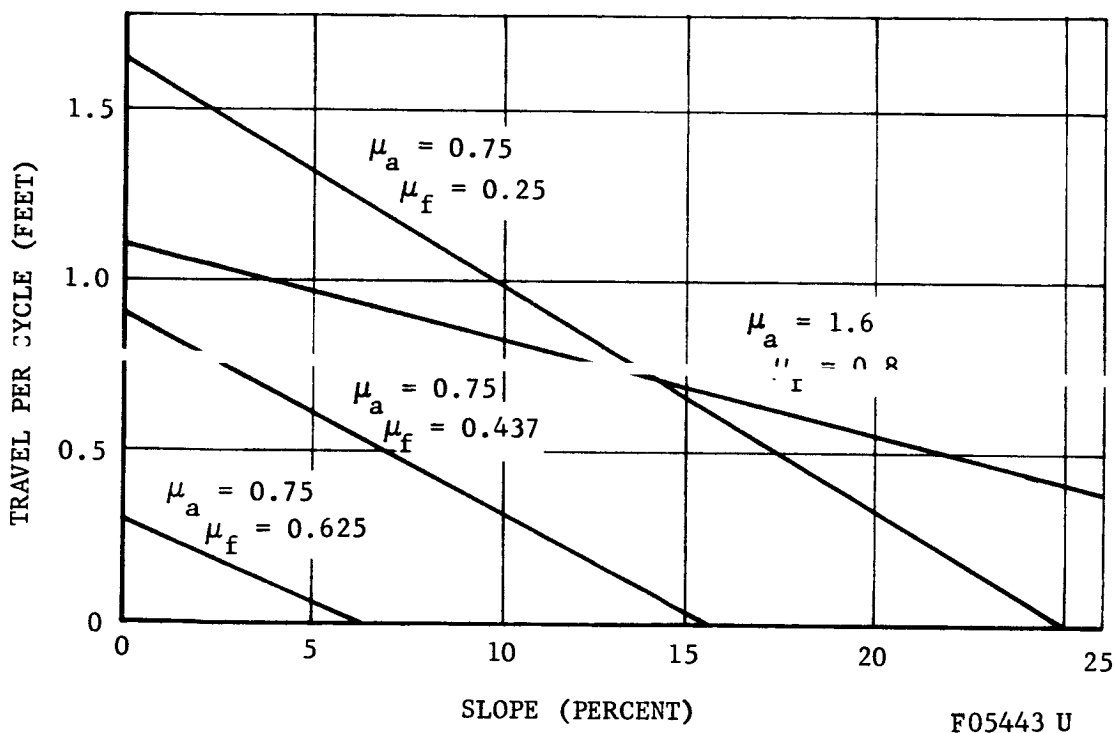


FIGURE 60. TRAVEL PER CYCLE

The mass of bellows material will be approximately

$$M_1 = \pi D L_c d \gamma = \pi \times 84 \times 4.7 \times 2.25 \times 0.283$$

$$= 790 \text{ lbm}$$

If the closing bulkheads are in the form of 2:1 ellipsoids of revolution, the maximum radius will be

$$r_m = \frac{42^2}{21} = 84 \text{ inches}$$

If the maximum bulkhead stress is to be held to 25,000 psi for an internal pressure of 5 psi, the bulkhead skin thickness must be

$$t = \frac{P_i r_m}{F} = \frac{5 \times 84}{2 \times 25,000} = 0.003 \text{ inch}$$

Since this is considerably less than would be suitable for handling loads, an effective thickness (based on projected area) of 0.016 will be used, giving a mass for three bulkheads of

$$M_2 = 3 \times 0.785 \times 84^2 \times 0.016 \times 0.283 = 75 \text{ lbm}$$

Doubling this mass to allow for reinforcing rings and attachment fittings, gives an order-of-magnitude estimate for the bare structural mass

$$M_3 = 150 + 790 = 940 \text{ lbm}$$

To obtain traction in the extension-contraction mode, some type of foot structure will be needed. To a first approximation, the total foot area will be equal to the footprint area in the extended position, which is

$$S = 60 \times 170 = 10,200 \text{ sq in.}$$

A lower limit for effective thickness for the feet would be about 0.020, giving a mass for the feet of

$$M_4 = 0.020 \times 10,200 \times 0.283 = 57.5 \text{ lbm}$$

Adding this to the structural weight of 940 lbm gives a figure of about 1000 lbm for the total structure.

At the extended length, the planform loading is

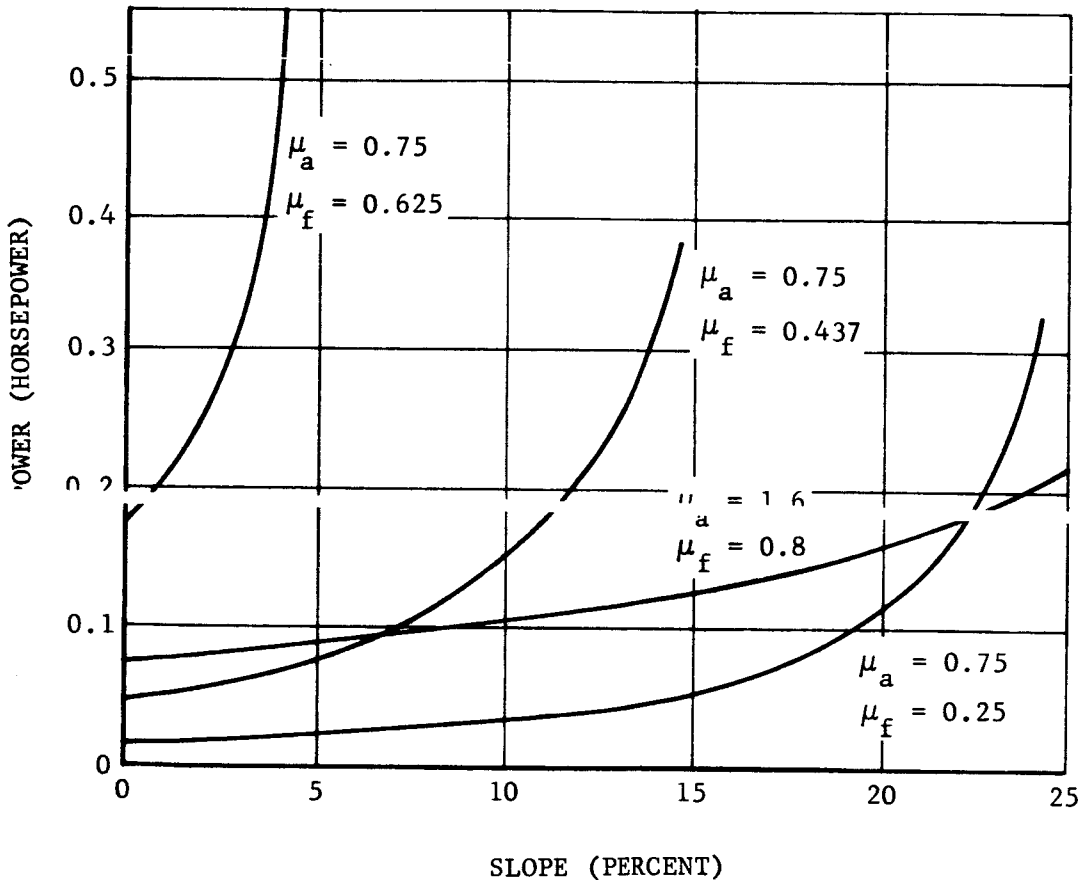
$$p_p = \frac{1000}{(6)(10,200)} = 0.016 \text{ lb/in.}^2$$

Then, according to the planing theory (see Equation (9)), for soil with density of 50 lbm/ft³, the minimum foot length for planing is

$$l_{\min} \sim 1000 p_p = 16 \text{ inches}$$

Building feet this large on this size vehicle appears to be a problem, but not necessarily an insurmountable one. In some types of soil, a foot on each bellows convolution would be adequate to produce a friction coefficient differential, and this could be accomplished quite easily.

Power analysis. - As in the case of travel per cycle, the power required to move the shelter can be obtained by reducing the values of Figure 57 in the ratio of masses, which is 1/381. The results are given in Figure 61 in terms of horsepower for a speed of 0.1 mile per hour for various slopes and friction coefficients.



F05444 U

FIGURE 61. POWER REQUIRED

As shown in Figure 61, the power required to move this shelter is quite low, but this power should be compared with that required to move it by other means. Since it is assumed that the shelter is empty and that some other method used to move its eventual contents, it is conceivable that the shelter could be dragged or rolled to its final destination. Assuming a friction coefficient of 0.625, the power required to drag a mass of 1000 pounds on the moon at 0.1 mile per hour would be

$$HP = \frac{1000}{6} \times 0.625 \times \frac{0.1}{375} = 0.028$$

If the shelter has a circular section and is rolled, the power requirement would be still less.

The tentative conclusion from this brief study is that the extension-contraction mode is not the most economical method for moving a small shelter if other vehicles are available.

Solar-Mechanical Energy Transfer System for Extension-Contraction Vehicle

A primary factor that makes the extension-contraction type of vehicle appear attractive is the possibility of utilizing the vehicle as a heat engine directly. This might be done if the vehicle can be made to selectively absorb or reject heat, resulting in a change in internal pressure due to a change in temperature of the gas inside. In a vacuum, the internal pressure can be used directly to extend the vehicle, but to contract the vehicle, some means such as a spring must be provided to supplement the low spring force of the bellows structure. Also, a mechanism is probably required to hold the vehicle contracted while it warms up, and hold it extended while it cools off.

The thermal property which is required is heat absorption when contracted and heat rejection when extended. Figure 62 shows the result of a preliminary thermal analysis of a configuration that has this property. The figure shows the equilibrium surface temperature as a function of the area ratio of two types of materials.

The thermal properties of the surfaces are:

Material	$\frac{\alpha}{\epsilon}$ (acceptance/emissivity)
White silicate paint	2.17
Hanovia gold	6.0

In the application of this concept it is expected that this area ratio is changed by the vehicle extension and contraction due to the change in geometry of the bellows. In this case, the two materials are Hanovia Gold 6518 paint (high temperature) and LMSC Silicate paint (low temperature). The assumptions made in the thermal analysis are:

- (1) Smooth cylinder
- (2) Longitudinal axis normal to the sun
- (3) The ends of the cylinder do not contribute to the heat transfer
- (4) An internal circulation system maintains a uniform temperature around the cylinder.

Heat sources considered include the sun, lunar albedo (reflected solar), and lunar infrared. Diffuse reflection was assumed for the lunar noon case, and no reflection was assumed for the sunset case. Probably the most significant factor omitted from this analysis is the effect of the shape of the bellows corrugations. This could probably most easily be evaluated by experiment, but is beyond the scope of the present work.

From Figure 62, under good conditions, maximum and minimum temperatures of 260°C and 90°C, respectively, are estimated. Regardless of

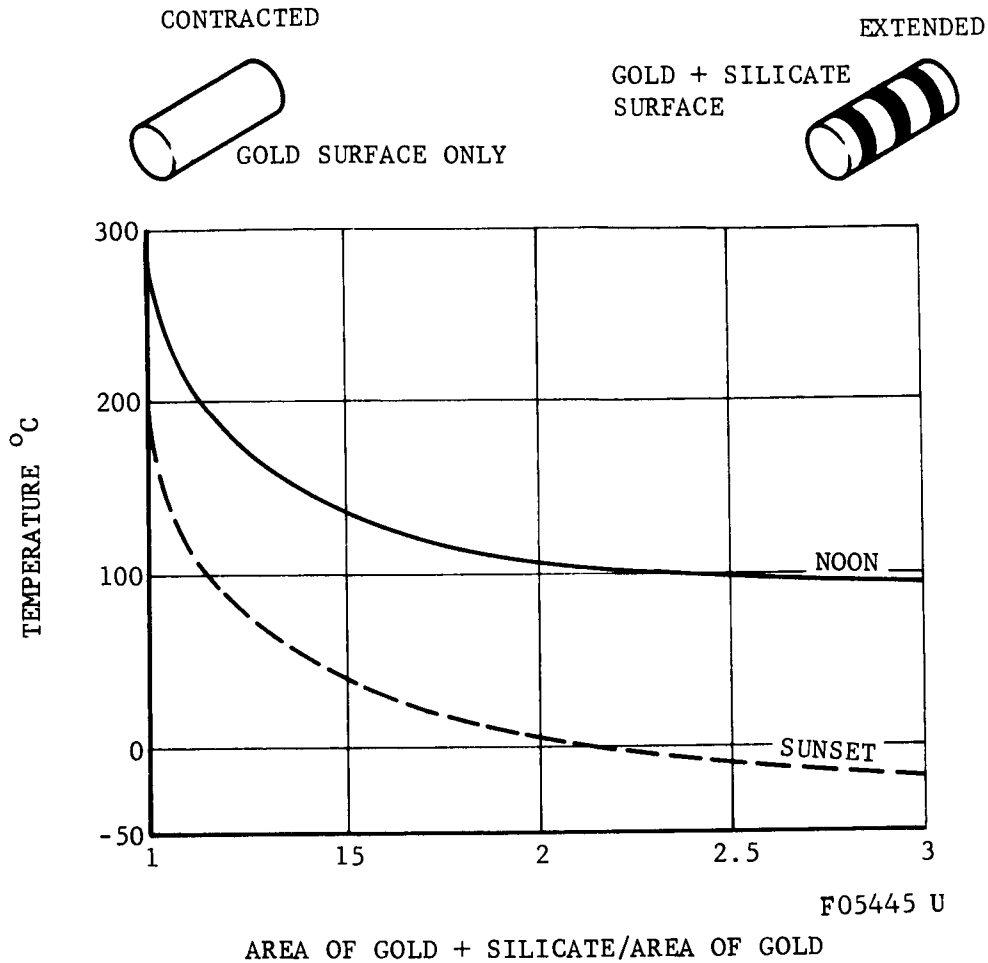


FIGURE 62. SURFACE TEMPERATURE OF SMOOTH CYLINDER WITH GOLD AND SILICATE SURFACES

the type of engine, its efficiency cannot exceed that of the Carnot cycle, which is

$$\eta_c = \frac{T_i - T_o}{T_i} = \frac{260 - 90}{260 + 273} = 0.313$$

For a solar constant of 442 Btu/ft² x hour the maximum possible power input per square foot of projected area would be

$$P_{in} = 0.313 \times 442$$

$$= 138 \text{ Btu/hr}$$

$$= 30 \text{ ft lb/sec}$$

If the sun is at or near the zenith the projected area is approximately equal to the footprint area, and the power required per unit area to move the vehicle at a speed v ft/sec becomes:

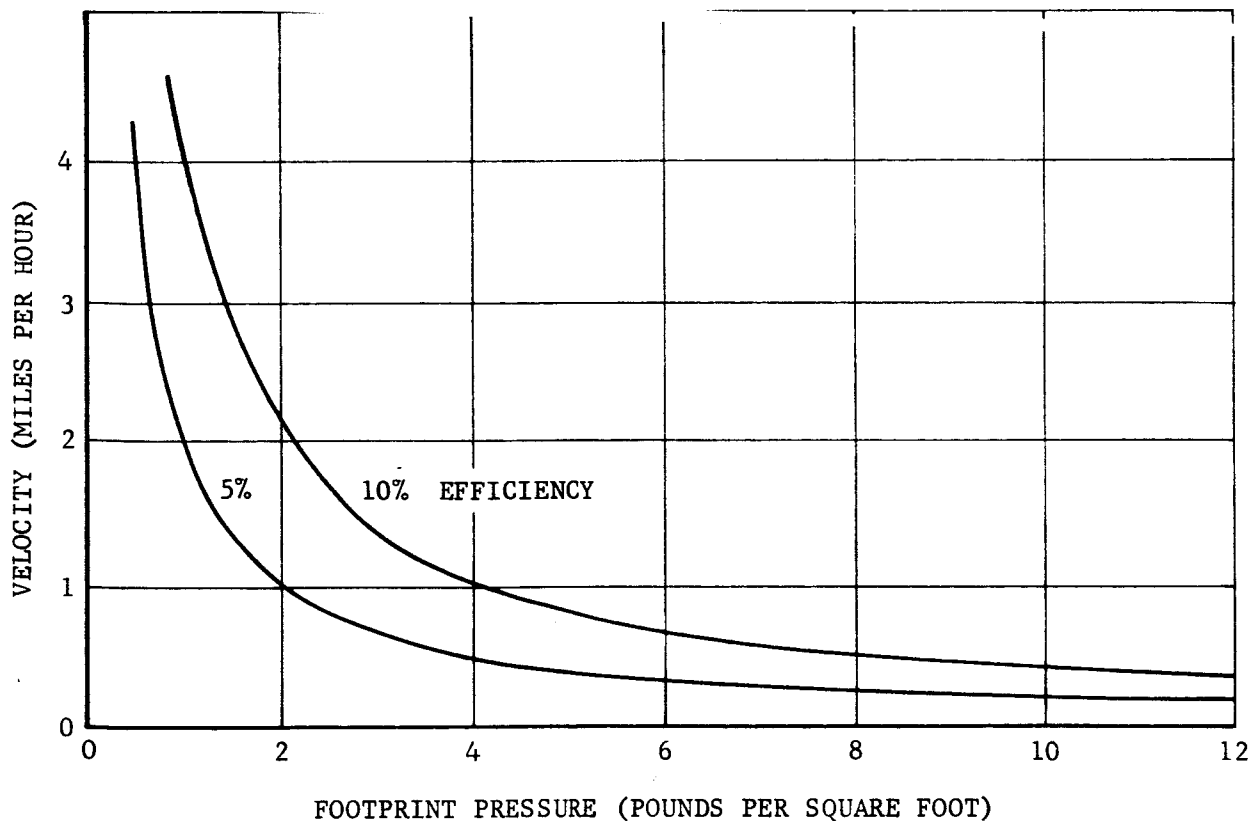
$$P_{\text{req}} = \frac{D_e}{W} \times p \times v \text{ ft lb/sec}$$

where p is the footprint pressure in pounds/square foot.

In an actual case, P_{in} will be reduced by a number of factors, such as the actual cycle efficiency, the ratio of projected area to footprint area, mechanical losses, etc. If all these are lumped together in a general efficiency factor η , the resulting velocity becomes

$$v = \frac{\eta \times 30}{\left(\frac{D_e}{W}\right) \times p} \text{ ft/sec}$$

Values of v , for different values of η and p and for an assumed value of (D_e/W) equal to 0.5 are plotted in Figure 63. The figure emphasizes the importance of low footprint pressure, and gives an idea of what overall efficiency must be achieved to give useful performance.



F05446 U

FIGURE 63. ESTIMATED PERFORMANCE OF EXTENSION-CONTRACTION BELLOWS VEHICLE UTILIZING SOLAR-MECHANICAL ENERGY TRANSFER SYSTEM

Design Evaluation

An all-metal bellows design for a lunar shelter does not appear to present any unusual problems regardless of shelter size. The shelter can be designed with footprint loading sufficiently low to allow planing for small size shelter but not for the large shelter by an estimated one order of magnitude. It is not clear however whether this is really the problem it seems, since the planing theory has not been confirmed, and the true soil properties are not known. The extension-contraction mode is not a particularly economical method for propulsion with regard to power consumption. The solar-mechanical energy transfer system however holds promise as a very inexpensive, lightweight means for supplying the mechanical energy for such operation.

SMALL UNMANNED VEHICLE

This section contains a preliminary design study of a small unmanned exploration vehicle utilizing the double-acting bellows concept, employing a circular convoluted stainless steel bellows.

Configuration Requirements

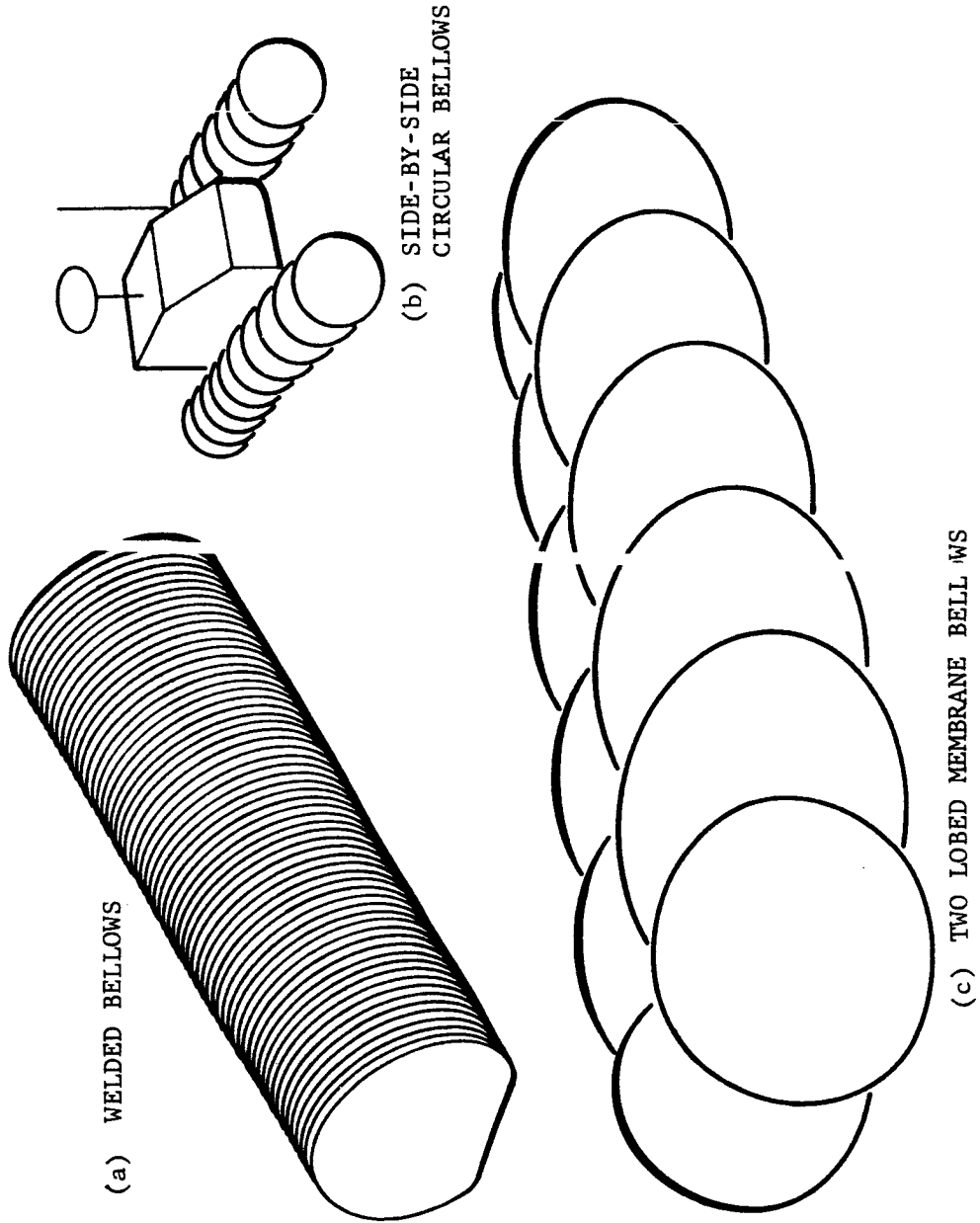
The following design requirements for the vehicle have been selected:

Useful load, including power plant	100 lbm
Average speed	1 mph
Total range	10 miles
Total life	15 days
Diameter	3 feet
Bellows working length	9 feet

Possible Configurations

The double-acting bellows principle selected for the small manned vehicle study can be utilized in a variety of configurations. Type of bellows structure and method of achieving roll stability are two variables. Several configurations are briefly described below.

Flat-bottom welded metal bellows. - Sketch (a) of Figure 64 shows a double-acting bellows of welded construction. Since the welded bellows, unlike the convoluted bellows, can be made with a noncircular section, it is possible to use a flat bottom and eliminate the feet necessary with a circular bellows and thus obtain roll stability. The bottom surface could be coated with an elastic, abrasion-resistant coating to prevent damage and wear.



F05447 U

FIGURE 64. DOUBLE-ACTING BELLOWS CONCEPTS

Practically the whole planform of the vehicle would be available as footprint area on soft surfaces. On hard surfaces, the contact area would be localized, thus minimizing slippage.

Side-by-side circular bellows. - Sketch (b) in Figure 64 shows another arrangement for achieving roll stability. Here, two circular bellows are used side-by-side. This is probably the simplest way to create a small vehicle, since standard components could be used. The lower surface of the bellows would require protection, and, because of the possibility of high local loads, the concept probably would be applicable only to small vehicles. Subject to this limitation, the concept appears to be quite practicable.

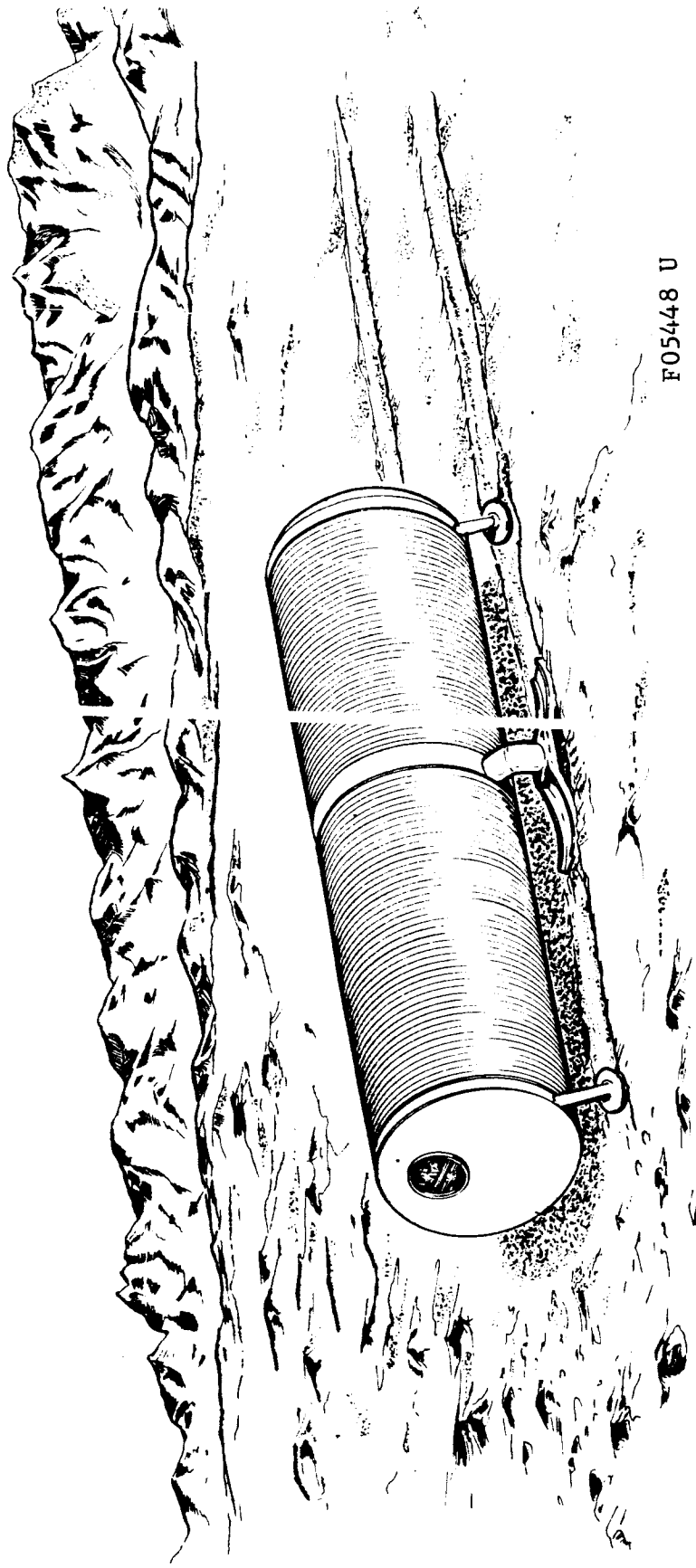
Two-lobed diaphragm bellows. - Sketch (c) in Figure 64 shows a possible application of the membrane bellows concept to the double-acting bellows configuration. Roll stability is achieved by the use of a two-lobed section, and since the entire structure is loaded entirely in tension, it should be very light. In a vehicle of this type there might be a problem in attachment of concentrated loads, so this configuration might be suitable for transporting bulk loads such as liquid or gas. Since the structural weight of this configuration approaches very closely the minimum possible weight for a pressure vessel, it has possibilities as a mobile storage container in very large sizes.

Circular bellows with feet. - Figure 65 shows an arrangement of circular metal bellows with roll stability obtained by the use of feet attached to the end bulkheads and to a non-bellows midsection. The arrangement, while probably not the lightest structure, offers no unusual problems beyond the state-of-the-art of bellows technology. The circular shape bellows are not subjected to abrasion or unusual eccentric loads caused by direct contact with the lunar surface such as would be experienced by the three previously considered arrangements. It was decided to limit to this arrangement the small unmanned vehicle study detailed in the following sections.

Bellows Design

The double-acting bellows utilizes a variation of the rib-walking motion, in which the path of travel of the feet is not necessarily circular. However, a preliminary choice of the stroke can be obtained from Figure 14 of the Mobility Studies section. This figure shows that in order to hold the effective drag-to-weight ratio in the "useful range" below 0.5 for a speed of 1.5 feet per second, the path radius should be at least 0.5 foot. Based on this, the crank radius will be set at 7 inches. With this radius, the maximum travel per crank rotation, assuming no slippage, would be 14 inches. Actually there will always be some slip, and in soft soil this can become quite large. Therefore, an average travel of 7 inches per cycle will be used for this study. This means that for the specified total range of 10 miles, close to 100,000 cycles will be required.

The chart in Figure 66 is based on test data and shows that for a life of 100,000 cycles, the completely reversed bending stress should not exceed 30,000 psi. Since the pressure in the bellows will be constant during



F05448 U

FIGURE 65. CIRCULAR BELLOWS WITH FEET

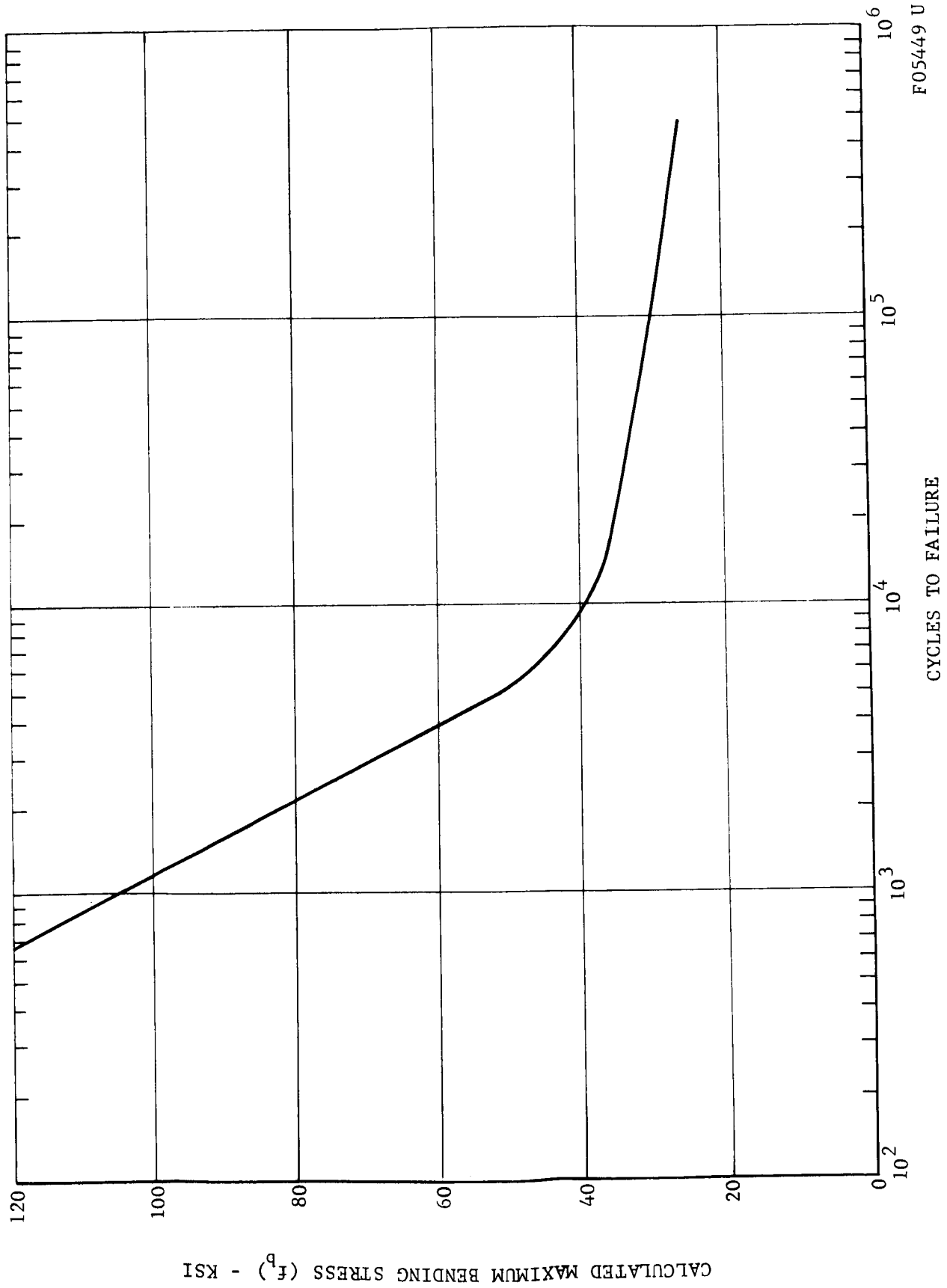


FIGURE 66. CYCLES TO FAILURE VERSUS MAXIMUM REVERSED BENDING STRESS FOR CRES 321 BELLAWS

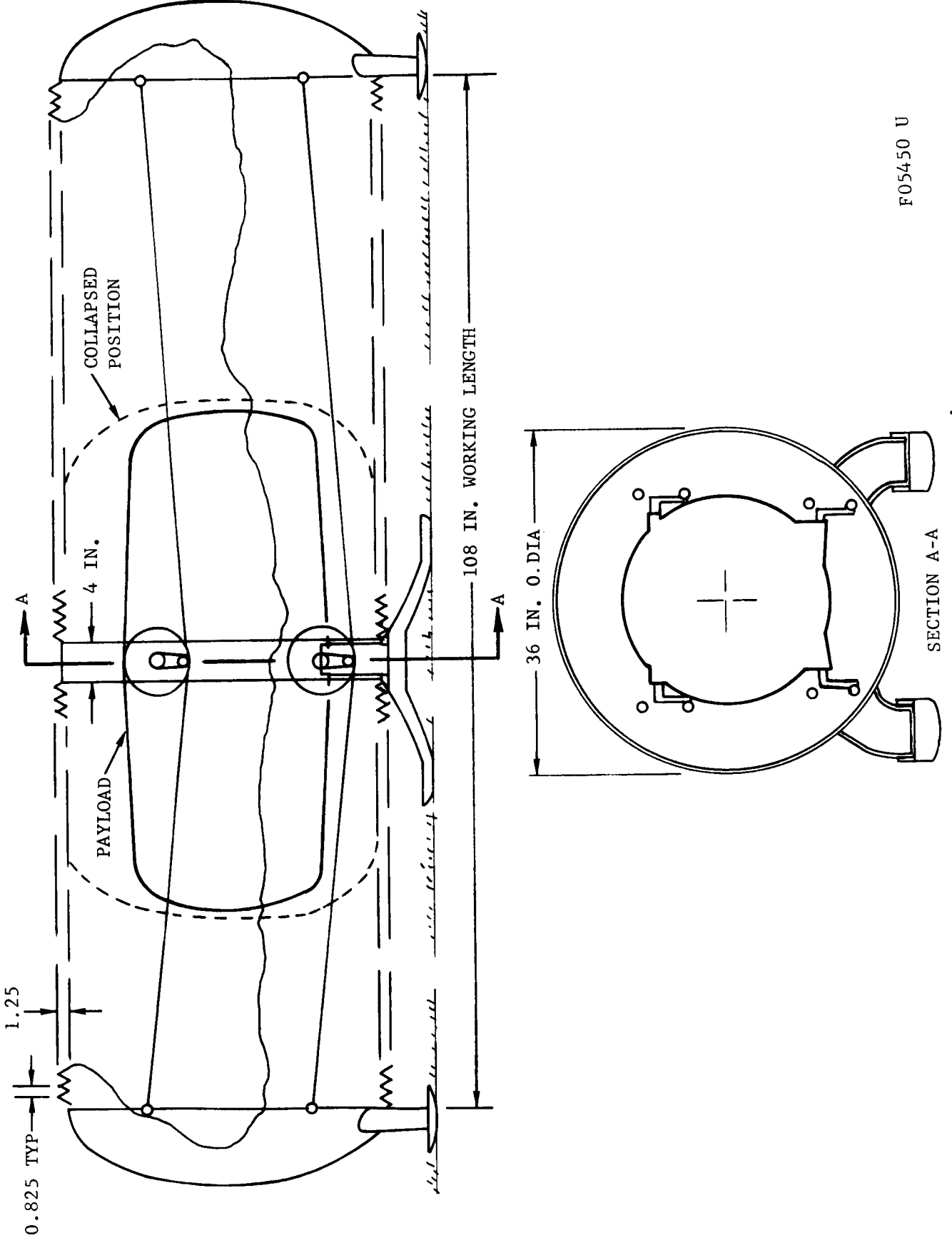
operation, the local bending stresses due to pressure will be ignored. Because the hoop stress due to pressure is negligible in this vehicle, it also will be ignored.

The configuration chosen for the design is shown in Figure 67. It is made of a short cylindrical center section which houses the payload, equipment, and power source, and two domed ends which are connected to the central section by lengths of circular bellows. Each of the three main components is supported by feet which rest on the ground. The center section supports two transverse shafts which have cranks of 7-inch radius on each end. The shafts are driven in such a manner that all four cranks are parallel at all times. The end bulkheads are connected to the cranks by four parallel cables which normally are equal in length so that while displacements normal to the vehicle centerline are possible, the three sections must remain parallel to each other at all times.

The motion of the vehicle is similar to that described under Double-Acting Bellows in the Mobility section, except that since four cables are used instead of two, the rotation of the end bulkheads is eliminated. This increases the efficiency, since sliding of the feet is reduced. The use of four cables also prevents instability since the additional cables force the bellows to buckle in a higher mode. This is illustrated in Figure 68, which shows the effect of various restraints on the buckling modes.

In Figure 68, the lowest buckling mode of a fixed-ended bellows is shown at (a). For this mode, the equivalent pin-ended column length, L (the distance between points of inflection), is one-half the distance between supports. If one of the ends is allowed to move laterally without rotation, as at (b), the equivalent column length is doubled and the bellows will buckle at one-fourth of the buckling load of (a). If, however, the median plane of the bellows is not allowed to rotate, as at (c), the equivalent column length again becomes one-half the overall distance between the end supports, and the buckling load is the same as at (a). This shows that when the three sections are held parallel, as at (c), Equation (33) for the critical buckling pressure is applicable.

The next consideration concerning the bellows is the amount of strain to be absorbed. The two critical conditions are shown in Figure 69 (a) and (b). In (a), the crank is horizontal and the average strain in the bellows is $2 A/L$.



F05450 U

FIGURE 67. DIMENSIONS OF UNMANNED VEHICLE

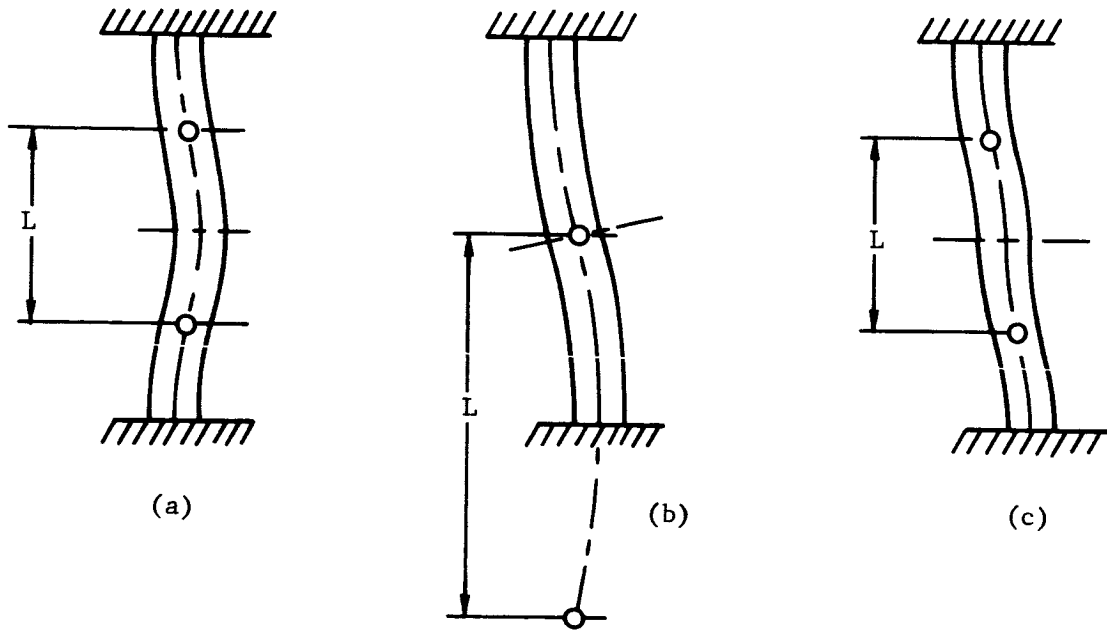


FIGURE 68. BELLOWS BUCKLING MODES

F05451 U

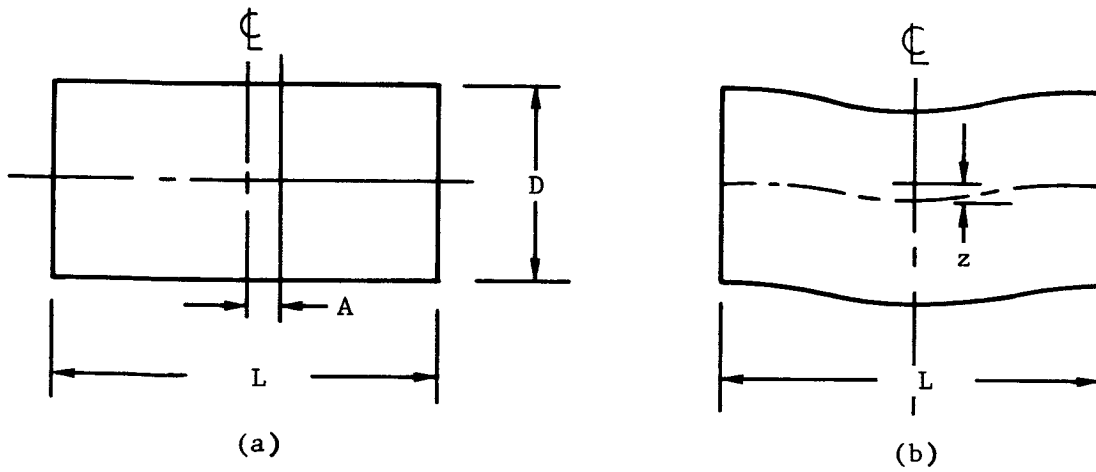


FIGURE 69. CRITICAL CONDITIONS FOR STRAIN

F05452 U

At (b) there is no longitudinal strain at the centerline, but the vertical deflection, z , at the center causes the bellows to bend to a radius which reaches a minimum value of $L^2/24 z$ at each end. This curvature produces maximum strains in the bellows of $12 Dz/L^2$. If the strain caused by bending is to be held to the same value as the longitudinal strain at the centerline, the vertical deflection must not exceed the value given by

$$\frac{12 Dz}{L^2} = \frac{2 A}{L}$$

or

$$\begin{aligned} z &= \frac{A L}{6 D} \\ &= \frac{7 \times 108}{6 \times 36} = 3.5 \text{ inches} \end{aligned}$$

That is, if the bellows fatigue life is not to be shortened, the vertical deflection should not exceed half the horizontal deflection. In addition, some parts of the bellows (the top and bottom portions at each end) may receive more than one stress reversal per crank cycle, with a possible lowering of fatigue life. Because of the many other unknowns in the study, it does not appear worthwhile to go into further detail on this point at present.

The minimum propulsive energy would be required if, on the forward stroke, the feet are slid along the ground, but with zero contact pressure; therefore the internal pressure and the crank location will be proportioned to accomplish this as nearly as possible.

Based on previous work, it will be assumed that the total bellows mass is 100 pounds, giving a gross mass of 200 pounds, of which 133 pounds is supported at the center and 33 pounds at each end. If the crank axis is displaced below the bellows centerline by a distance y , the condition at the extremes of vertical cable displacement are as shown at (a) and (b) in Figure 70.

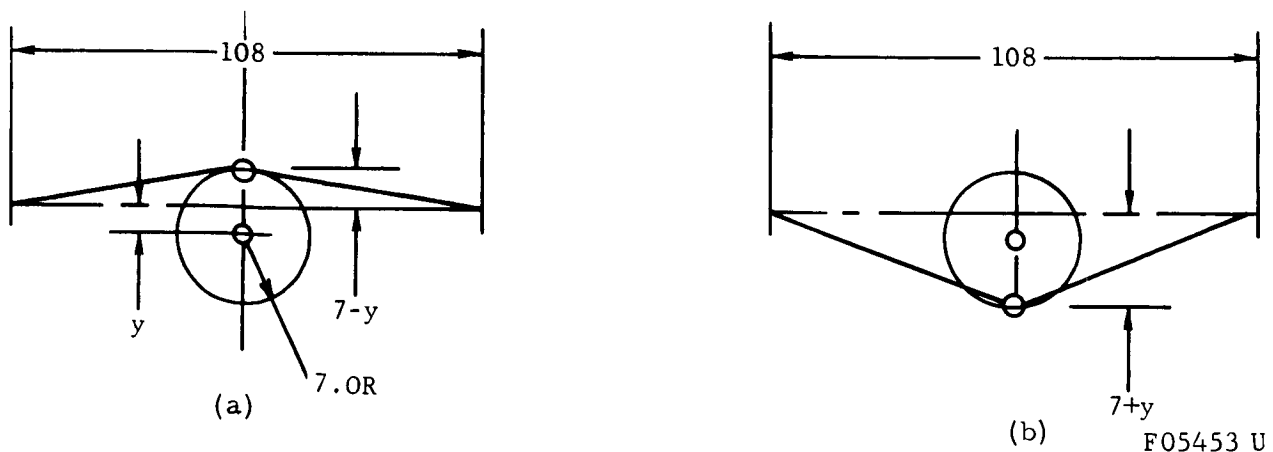


FIGURE 70. CABLE DISPLACEMENT

Assuming that the mean bellows diameter is 35 inches, the cable load will be

$$P = \frac{\pi}{4} \times 35^2 p_i = 960 p_i \text{ lb}$$

and the two conditions for Figure 70 are:

for (a):

$$960 p_i \times \frac{(7-y)}{54} = \frac{33}{6}$$

and for (b):

$$2 \times 960 p_i \times \frac{(7+y)}{54} = \frac{133}{6}$$

Solving these equations gives:

$$y = 2.33 \text{ inches}$$

$$p_i = 0.07 \text{ psi}$$

A pressure of 0.1 psi will be used in the remaining work.

The choice of the actual bellows convolution shape is based on two requirements: the required deflection, and the necessity of preventing column or "squirm" instability. The equivalent fixed-ended column has a length of 108 inches, and the required minimum total spring rate for the entire bellows is given by Equation (33).

$$P_{\text{buckle}} = \frac{2 \pi (R_s)}{L}$$

or

$$R_s = \frac{108 \times 0.1}{2} = 1.72 \text{ lb/in.}$$

This rate is so low that it would be exceeded by any useful bellows, so the only condition remaining is the required deflection. A bellows depth of 1.25 inches is within the range of good practice for a bellows of this diameter. The other bellows parameters are: the inside radius of the convolution to be 5 times the skin thickness, and the slope of the bellows walls to be 15 degrees. A sketch of the resulting shape for a skin thickness of 0.008 inch is given in Figure 71.

From Figure 72, based on computer calculations, the maximum allowable deflection per convolution for the bellows of Figure 71 is

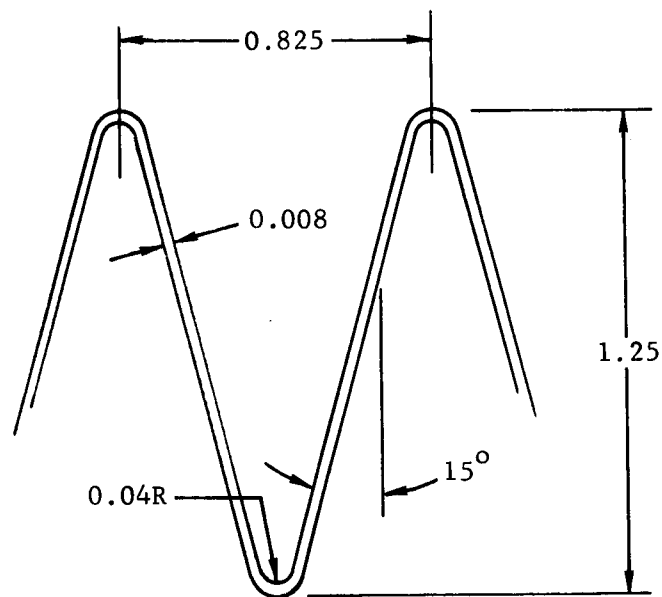
$$\delta = 0.13 \text{ inch}$$

Since the bellows length per convolution is 0.825 inch, the number of convolutions for each bellows section, assuming a convoluted length of 50 inches, is:

$$N = \frac{50}{0.825} \approx 60$$

and the allowable strain is

$$N\delta = 60 \times 0.13 = 7.8 \text{ inches}$$

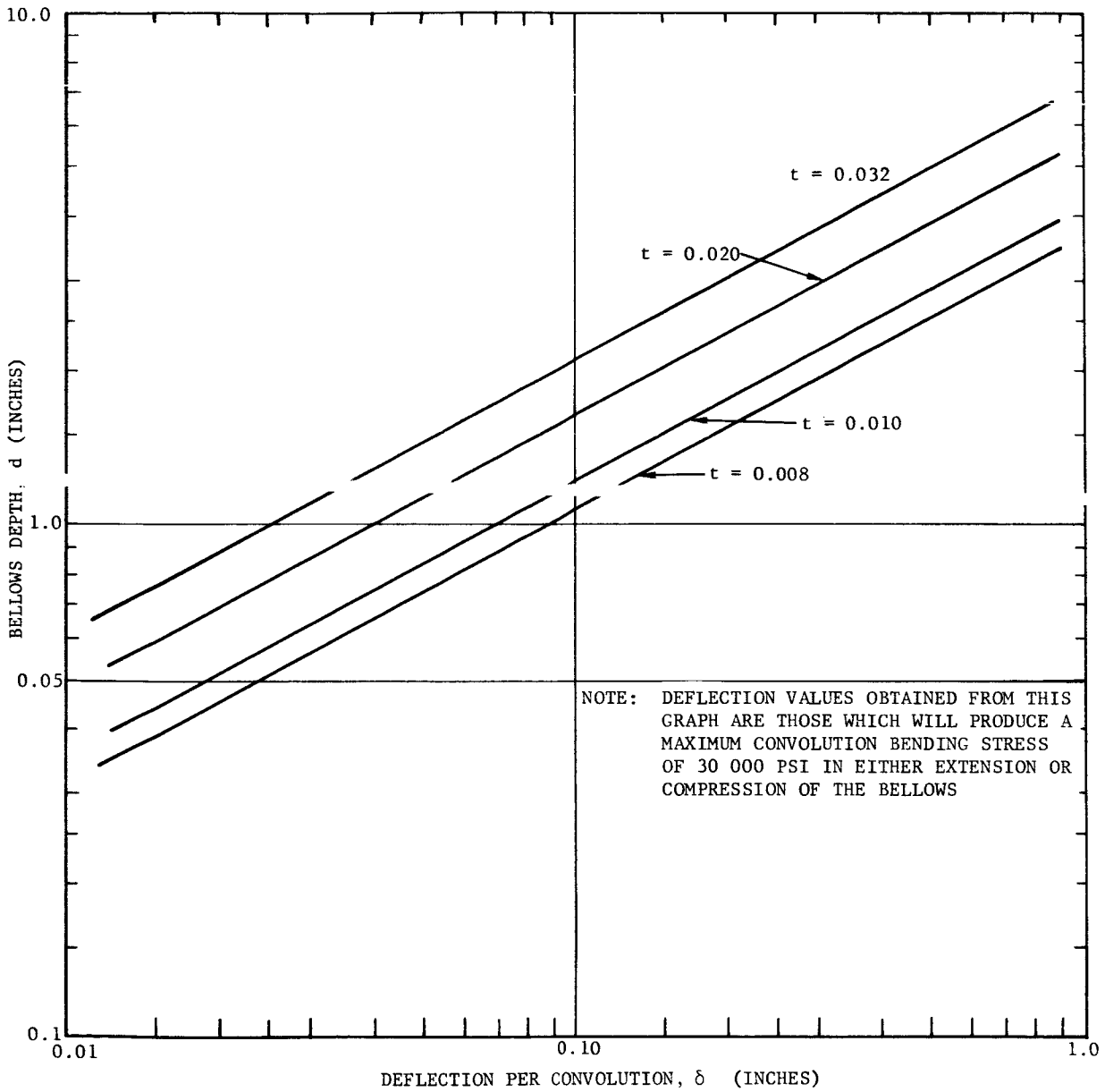


F05454 U

FIGURE 71. BELLOWS CONVOLUTION SHAPE

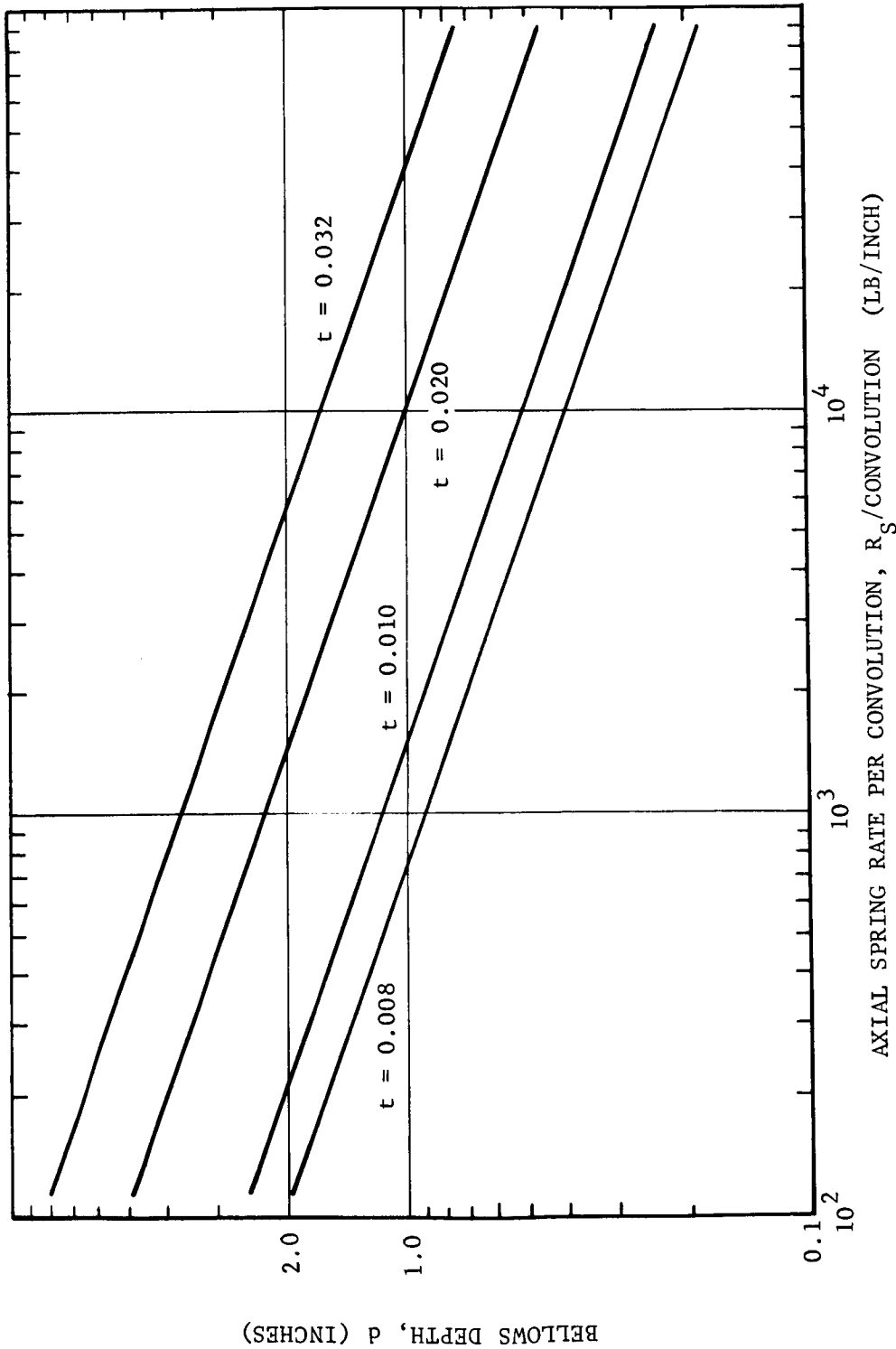
From Figure 73, the spring rate per convolution is 400 lb/in. giving a resultant linear strain rate for the whole bellows of

$$R_s = \frac{400}{120} = 3.33 \text{ lb/in.}$$



F05455 U

FIGURE 72. MAXIMUM DEFLECTION PER CONVOLUTION VERSUS BELLOWS DEPTH



F05456 U

FIGURE 73. AXIAL SPRING RATE PER CONVOLUTION VERSUS BELLOWS DEPTH

This indicates that the 0.008 inch skin thickness could be reduced to

$$t = 0.008 \sqrt{\frac{1.72}{3.33}} = 0.0058$$

without instability occurring.

The bellows mass per convolution for a wall thickness of 0.008 inch, from Figure 74, is 0.067 pound, giving a total mass for both bellows sections of:

$$M_{\text{bellows}} = 0.067 \times 120 = 80.5 \text{ lbm}$$

This appears to be consistent with the original estimate of 100 lbm for structural weight, especially when it is considered that the skin thickness could be reduced considerably without incurring instability.

The collapsed length of one convolution is about 0.12 inch, giving a total collapsed length per bellows of

$$L_c = 60 \times 0.12 = 7.2 \text{ inches}$$

Since this is probably much less than half the length of the payload section, the latter will govern the collapsed length of the vehicle.

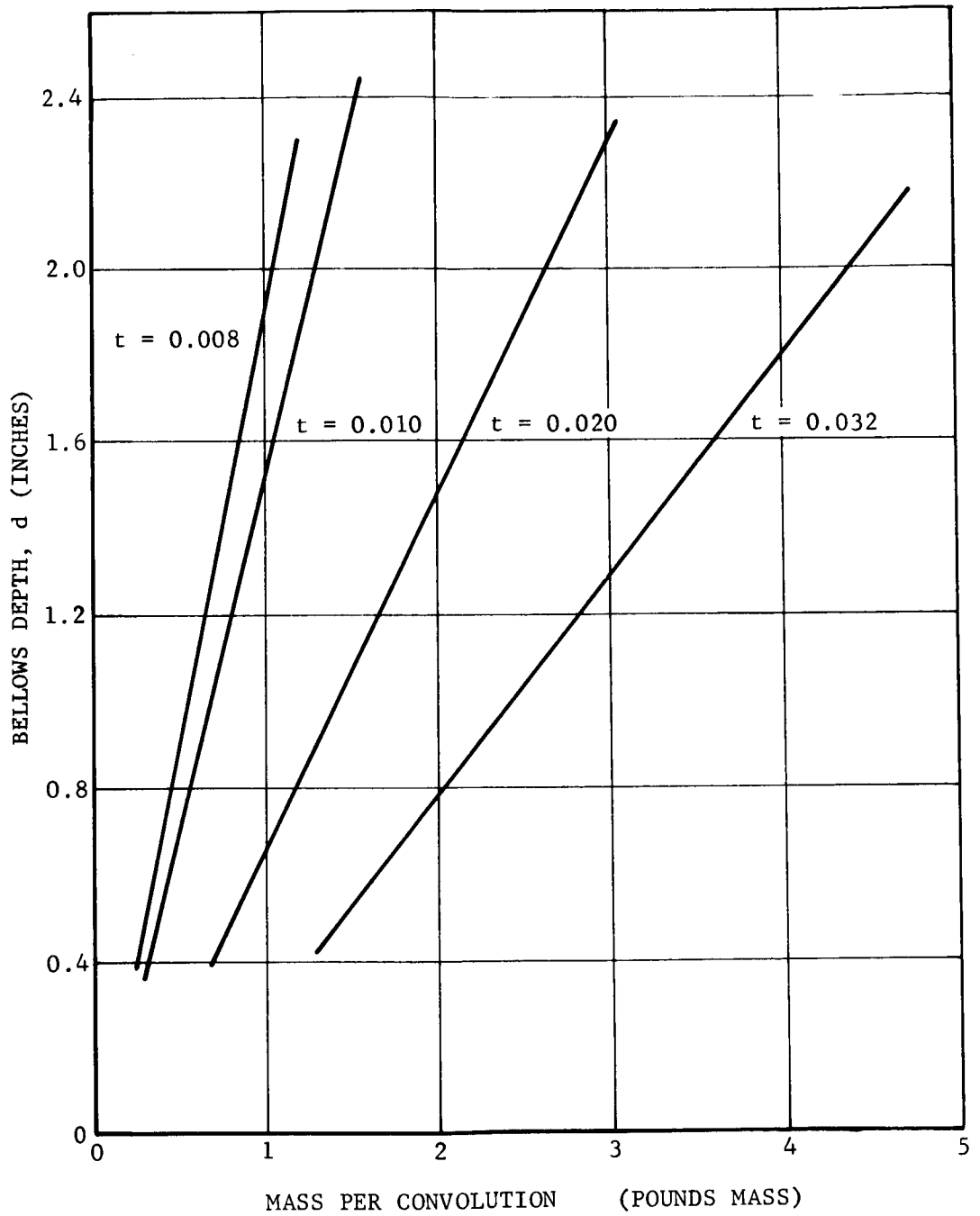
The vehicle, shown in Figure 67, has a loaded mass of 200 lbm, giving it a footprint pressure on the moon of about 4.2 pounds per square foot when all feet are on the ground. The power requirement will depend on the surface over which it travels, but at the target value of $D_e/W = 0.5$, the power consumed by the propulsive system at 1 mile/hour would be

$$P = \frac{200}{6} \times \frac{0.5 \times 1.47}{550} = 0.0445 \text{ HP} \\ = 33 \text{ watts}$$

Steering of this vehicle would be done by differential adjustment of the longitudinal cables. The vehicle has the capability of moving backward as well as forward, and can be collapsed at any time to about one-third of its normal length.

Design Evaluation

The double-acting bellows configuration which was studied is considered to be quite suitable for meeting the specified mission objectives. Structural weight and power requirements are considered reasonable. The only problem apparent at this time is not in the bellows structure but in the design of the feet, which undoubtedly will require more study to derive a configuration suitable for use on the surfaces expected to be encountered. Because of its simplicity, absence of external mechanism, and ease of deployment, the configuration should be quite suitable for many unmanned missions.



F05457 U

FIGURE 74. BELLOWS DEPTH VERSUS MASS PER CONVOLUTION

MANNED EXTENDED-RANGE ROVING VEHICLE

Configuration Requirements

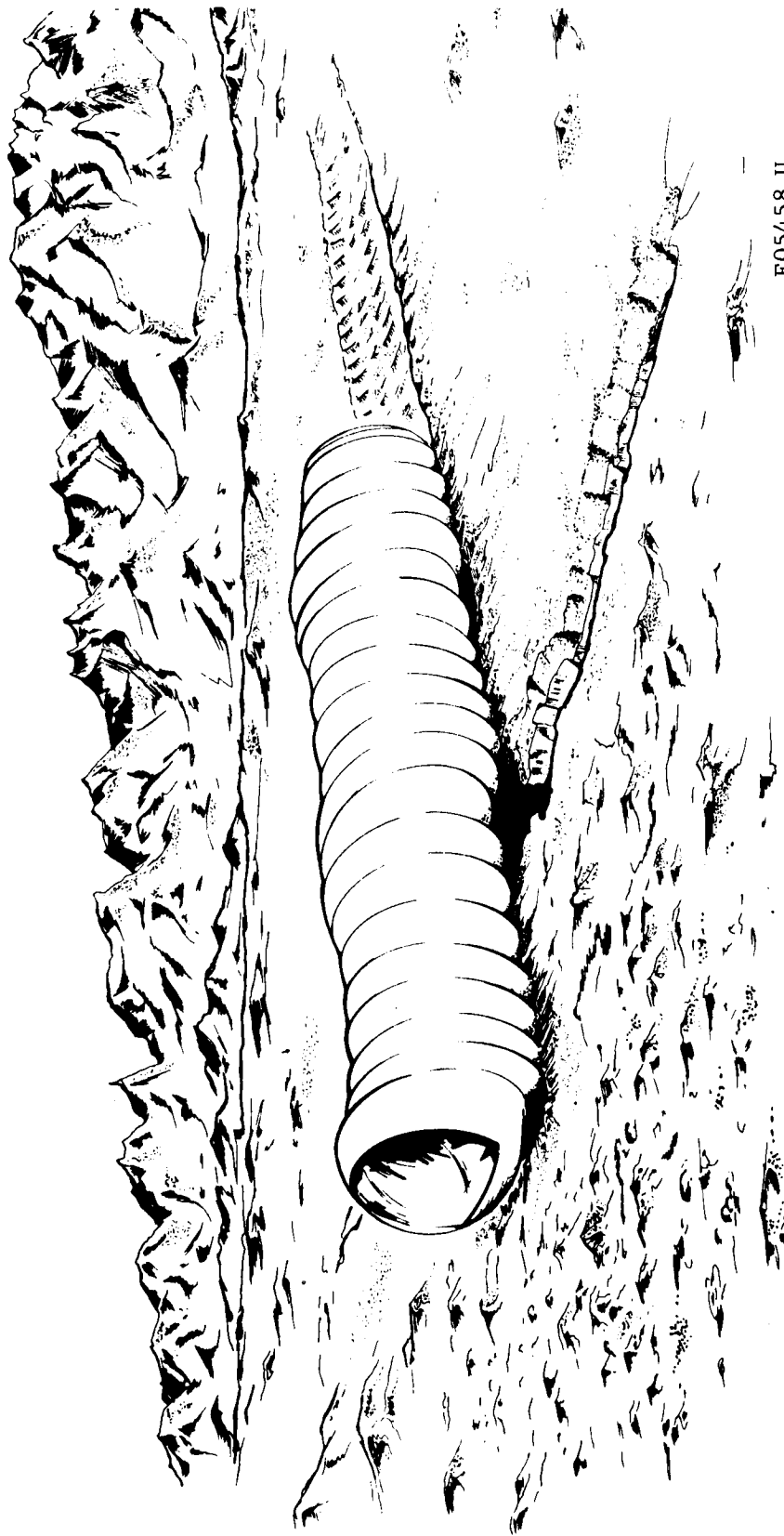
This section contains a preliminary design study of an extended range roving vehicle suitable for use by two men to carry out traverses of the lunar surface or perhaps to transport supplies. It utilizes the traveling wave mode with a membrane bellows structure. An artist's concept of this vehicle is shown in Figure 75. The vehicle is flexible and steerable both horizontally and vertically and can be collapsed for shipment or storage. It produces a smooth, constant-velocity motion, and appears capable of high speed. The configuration requirements selected for it are as follows:

Useful load	1000 lbm
Average speed	5 mph
Minimum range	100 miles
Minimum life	6 months
Diameter of crew cabin	6 to 10 feet
Length of crew cabin	10 feet

Bellows Design

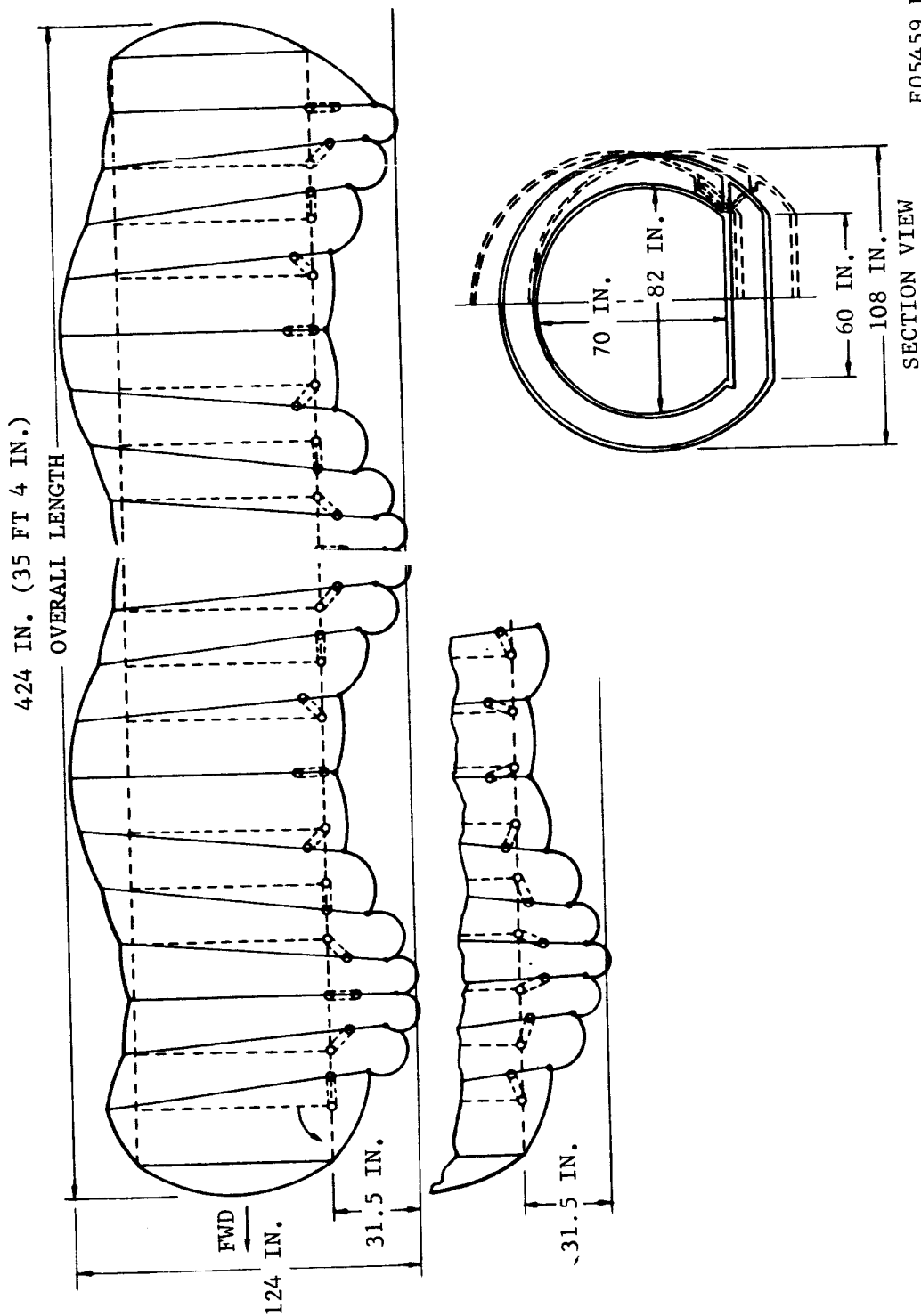
The details of this vehicle are shown in Figure 76. It is made up of two coaxial bellows of which the inner one is pressurized to a living atmosphere, such as 5 psi, and forms the main structure of the vehicle. This inner bellows is reinforced by frames which determine its shape and support the payload and equipment. Also, each frame carries a transverse shaft with a crank on each end. These cranks are driven in synchronism and fixed phase relationship by a power transmission system, and each crank carries with it an outer frame to which is attached the outer bellows.

The outer bellows is of flexible material and is pressurized to a comparatively low pressure. The movement of the outer frames causes this bellows to deform in a manner which supports and propels the vehicle. Since the main structural member is a bellows, it has some flexibility and can be warped horizontally or vertically by cables running along the sides as in the Aeronutronic BOA model.



F05458 U

FIGURE 75. LUNAR SUPPLY VEHICLE



F05459 U

FIGURE 76. LUNAR SUPPLY VEHICLE - RELIMINARY SKETCH

Referring again to the vehicle configuration sketch in Figure 76 it can be seen that the shape of the lower surface is not the sine wave which might have been expected. Rather, it is a curtate cycloid with the lower portion more sharply curved than the upper portion. In addition, the lower portion of the skin is compressed while the upper portion is expanded. This is not the result of the particular linkage which is used, but is a fundamental characteristic of this type of wave motion.

In the configuration which is being studied at present, the skin of the outer bellows is being used to transfer the loads to the ground by means of the internal pressure of the bellows and the resulting membrane stresses. Since the skin is compressed longitudinally at the feet, it can billow outward at these points forming soft cushions to support and propel the vehicle. However, one problem which arises here is that these pillows are quite flexible in shear, and this causes some lost motion. The shear stiffness of the pillows is investigated in a preliminary way in the section on membrane bellows which indicates the nature of this problem.

From the studies made on the traveling wave concept, it appears that the larger the number of cranks or the equivalent that are used per wavelength, the smoother and more efficient the resulting motion will be. In the proposed design, eight cranks are used per wavelength. At the present time it cannot be said with certainty that this is the optimum number.

For an assumed effective drag-to-weight ratio of 0.25, which should be quite feasible with such a vehicle, the propulsive power required on the moon would be:

$$P = \frac{3000}{6} \times 0.25 \times \frac{5}{375} = 1.65 \text{ HP}$$
$$= 1.23 \text{ kw}$$

This power seems quite low and could be supplied by any one of a number of power sources.

The footprint pressure of a vehicle of this type adjusts itself to the surface over which it is traveling. On hard ground the footprint pressure equals the pressure in the outer bellows, which in the configuration shown is about 0.35 pound per square inch. On soft soil the entire lower surface of the vehicle can rest on the surface, and the average pressure would drop to about 0.02 pound per square inch or about 3 pounds per square foot. As shown in the section on Mobility, the vehicle would still be able to make progress under these conditions, but the speed would be reduced by about 50 percent for the same power input.

Design Evaluation

A traveling wave bellows design concept utilizing membrane construction appears quite attractive for a manned extended-range roving vehicle. Both structural weight and power requirements are considered quite low. The vehicle tends to mold itself to the terrain with a very low footprint pressure which should permit travel: (1) over a spiny type surface (such as a bed of nails), (2) over and through very soft soils, and (3) over rough terrain without vehicle lift-off and bounce under low gravity conditions. Its feasibility is dependent upon the availability of a suitable membrane covering material. This cover must withstand the lunar environment while still remaining flexible and abrasion resistant. The concept produces a smooth, constant-velocity motion and appears capable of moderate to high speed and efficiency as well as great versatility.

OVERALL EVALUATION

With any technical concept, the ultimate measure of practicability of the concept lies in its ability to perform some mission better than any other concept. The result depends upon the mission definition and its specific requirements as well as the measures of performance that are used to evaluate and compare the systems. A detailed evaluation is beyond the scope of this study since the input data are not sufficiently well defined. However, a few observations will be made here and an attempt will be made to put the lunar worm vehicles into perspective with respect to more conventional vehicles.

COMPARISON WITH OTHER VEHICLES

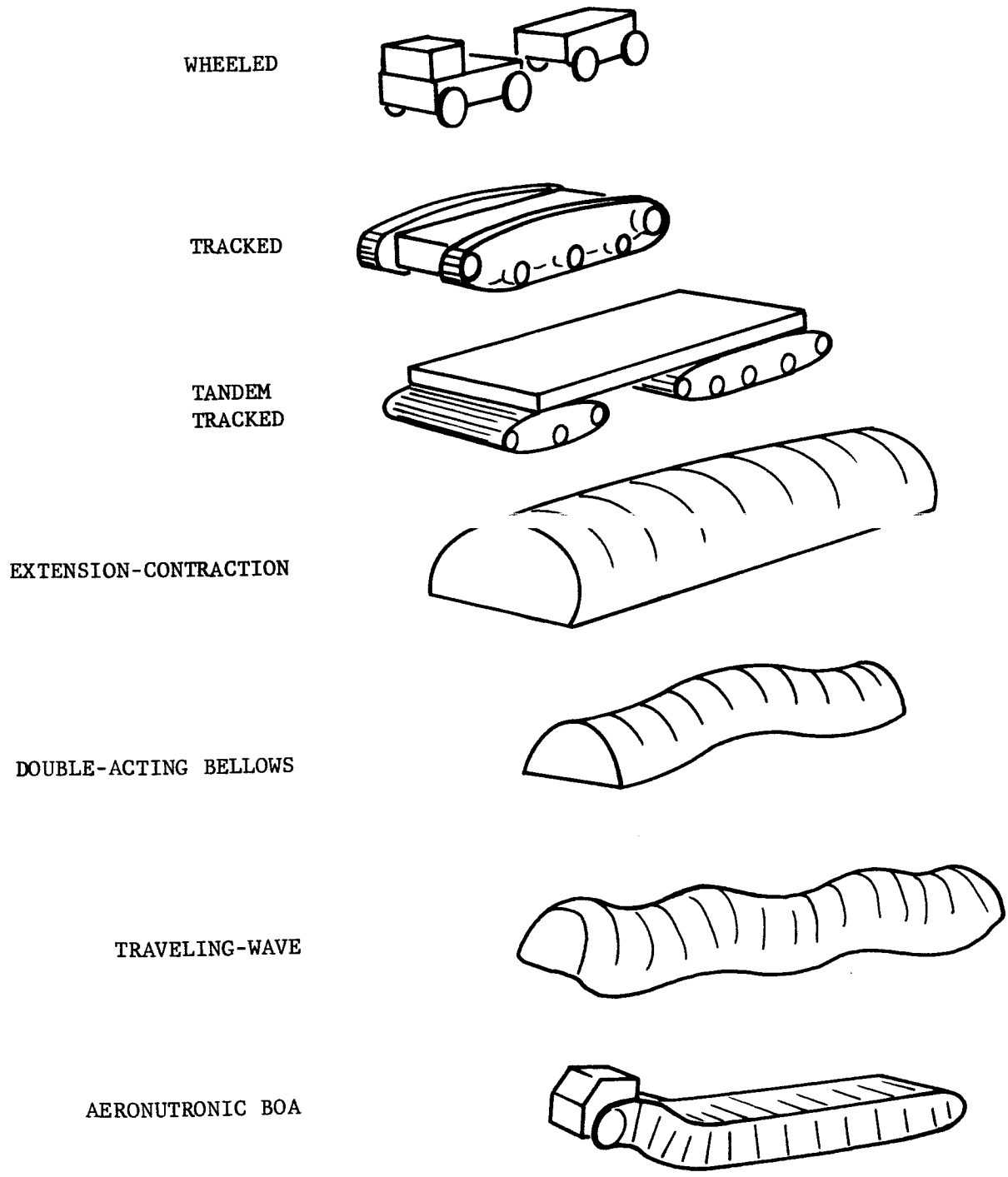
Vehicle Types

To realistically evaluate the new concepts which have been presented in this study, parametric comparisons will be made between those concepts and more conventional vehicle types. These types are listed and illustrated by diagrammatic sketches in Figure 77.

Vehicle Parameters

Vehicle reliability is of prime importance in a lunar vehicle. The degree of reliability of a vehicle mechanism is not as much of a characteristic of vehicle type as it is of the amount of detail design and development effort which have been expended on it. Reliability in the sense of probability of completing a mobility mission, however, is related to some of the basic capabilities of the vehicle.

Since there is a good possibility that allowable soil bearing pressures may be low on the moon, it seems logical to classify vehicle types with regard to the degree to which their weight is distributed over the total planform envelope of the vehicle. In general, on soft or fluid surfaces it is necessary to spread the weight over as large an area as possible, and this is facilitated by the fact that such surfaces are usually reasonably smooth and level. With increasing roughness of the surface, the portion of the vehicle in contact with the surface necessarily decreases, but it still is an advantage to have a large contact area because of the averaging effects of widely spaced contact points. If the surface is rough but comparatively weak structurally, a distinct possibility on the moon, many of the higher projections will be flattened down by the vehicle, particularly if the contact surface on the vehicle is unyielding. Although this process tends to smooth the ride it is undesirable since it consumes considerable power; therefore, in this it is also beneficial to increase the contact surface area. Only in the case of a hard smooth surface is it desirable to use small contact areas and the accompanying high footprint pressures.



F05460 U

FIGURE 77. VEHICLE SYSTEMS FOR COMPARISON

Based on the above reasoning, the ratio of footprint area to planform envelope is considered a basic parameter for comparison of vehicles. For any unprepared surface, it is desirable to have the footprint area as large as possible.

In order to be able to travel over any type of surface on the moon, a parameter of major importance in a vehicle is the size of obstacle it can clear. Since obstacle clearance usually requires climbing, the vehicle automatically will be able to climb a slope equal to the obstacle height/vehicle length; therefore, this latter ratio will be used to characterize the vehicle maneuverability. The various vehicle systems can be classified generally with respect to footprint area and obstacle clearance as shown in Figure 78, where each type of vehicle is shown occupying a shaded area on the chart. The values for the conventional vehicles are typical values from references such as the OTAC Tracked Versus Wheeled Vehicle report.⁶ The values for the worm type vehicles are estimated on the basis of the analysis and design studies in this report. The values obtained from Figure 78, together with the fineness ratios (length-to-width ratio) of the vehicles are listed in the following table and from design studies of proposed lunar wheeled vehicles, References 8 and 9.

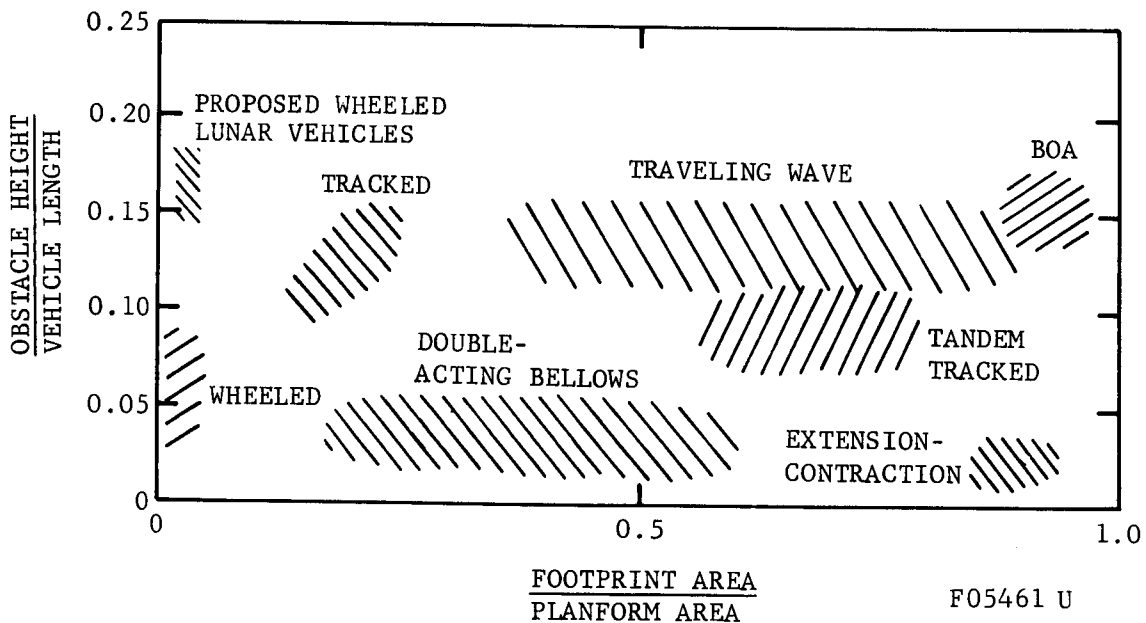


FIGURE 78. VEHICLE OBSTACLE CLEARANCE CAPABILITY

Vehicle Type	Obstacle height Vehicle length $\frac{h_o}{L}$	Footprint area Platform area $\frac{S}{Lb}$	Length Width $\frac{L}{b}$
Wheeled	0.03 - 0.08	0.005 - 0.013	3
Tracked	0.1 - 0.15	0.15 - 0.25	2
Tandem Tracked	0.07 - 0.12	0.6 - 0.8	4
Extension-Contraction	0.01 - 0.04	0.8 - 0.9	6
Traveling Wave	0.13 - 0.17	0.4 - 0.9	6
Double-Acting Bellows	0.02 - 0.06	0.4 - 0.6	6
Aeronutronic BOA	0.13 - 0.17	0.85 - 0.95	6
Proposed Lunar Wheeled Vehicles	0.15 - 0.18	0.02 - 0.04	2

By using the parameters given in the table, and assuming a vehicle density, γ , nondimensionalized obstacle clearance and footprint pressure can be converted to absolute values as a function of vehicle size. Using the nomenclature h, b, and L for vehicle height, width, and length, this can be done as follows. The height is assumed equal to the width.

$$M = \gamma b^3 \left(\frac{L}{b} \right) \tag{74}$$

$$S = Lb \left(\frac{S}{Lb} \right) \tag{75}$$

$$\begin{aligned}
 p &= \frac{M}{S} \cdot \frac{g}{g_e} \\
 &= \frac{g}{g_e} \gamma^{\frac{2}{3}} \frac{M^{\frac{1}{3}}}{\left(\frac{L}{b} \right)^{\frac{1}{3}} \left(\frac{S}{Lb} \right)} \tag{76}
 \end{aligned}$$

This result is shown in Figure 79 for an assumed density of 10 lbm/ft³. Typical vehicle densities are shown by Bekker⁵, and 10 lbm/ft³ is typical of small lightweight vehicles. Larger vehicles, especially typical military vehicles tend to be heavier than this. The result on Figure 79 can be ratioed by $\gamma^{2/3}$ to give results for other densities.

The obstacle clearance capability, h_o , is given by

$$\begin{aligned} h_o &= \left(\frac{L}{b}\right) \left(\frac{h_o}{L}\right) b \\ &= \left(\frac{M}{\gamma}\right)^{\frac{1}{3}} \left(\frac{h_o}{L}\right) \left(\frac{L}{b}\right)^{\frac{2}{3}} \end{aligned} \quad (77)$$

This is shown in Figure 80.

An interesting presentation of power requirements of mobility systems, originally pointed out by Gabrielli and Von Kármán, is derived from the work of Bekker and shown in Figure 81. The figure shows equivalent drag-to-weight ratio (sometimes called specific power) as a function of speed. The Gabrielli - Von Kármán line, defined by $D_e/W = v/1720$ in ft-lb-sec units, has been considered to be a limiting condition imposed by technology. Figure 82 shows the worm type of vehicles plotted to the same scale. It is seen that the estimated performance of the extension-contraction and rib-walking vehicles is in the area traditionally occupied by animals. The traveling wave is generally in the region of present cross-country vehicles. Although it is not anticipated that the traveling wave can match conventional vehicles (wheels) on a hard surface, it is anticipated that the range of soils in which it is useful will be much greater.

MISSION SUITABILITY

Mission Requirements

The proper performance measures for a vehicle are strongly dependent upon the detailed requirements of the mission. Cost, the conventional all-encompassing measure of a transportation system, does not appear as a primary parameter in the evaluation of lunar vehicles. Parameters which might be considered are weight, size, reliability, power requirements and speed. Speed is not considered a primary requirement in the present spectrum of missions, but will most certainly become more important in the future. Reliability is often the most important requirement of all. This may take at least two forms in the type of vehicles being considered here: reliability as a shelter, and reliability as a transportation system. This distinction allows a tentative classification of the concepts into mission categories.

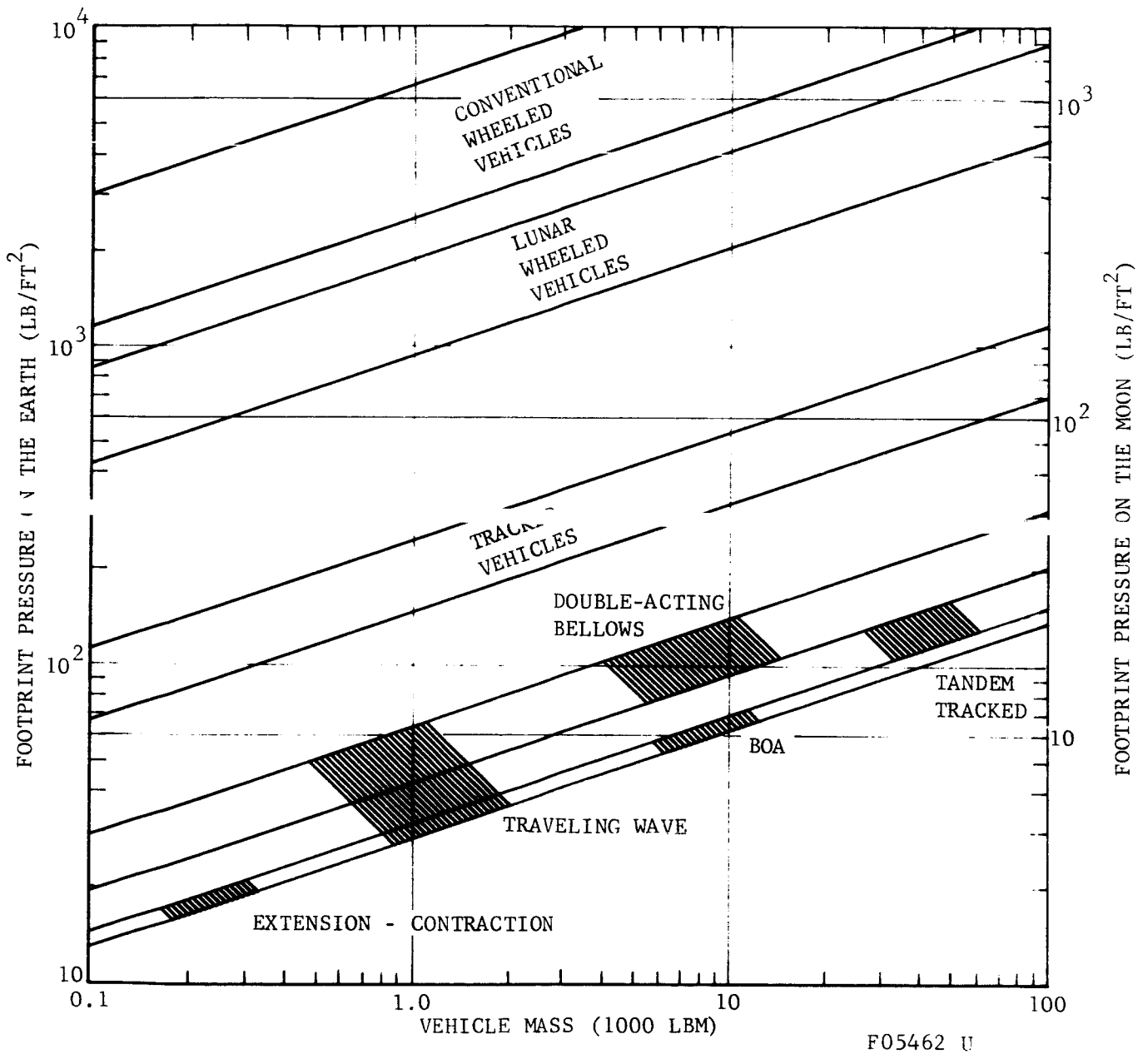


FIGURE 79. VEHICLE FOOTPRINT PRESSURES

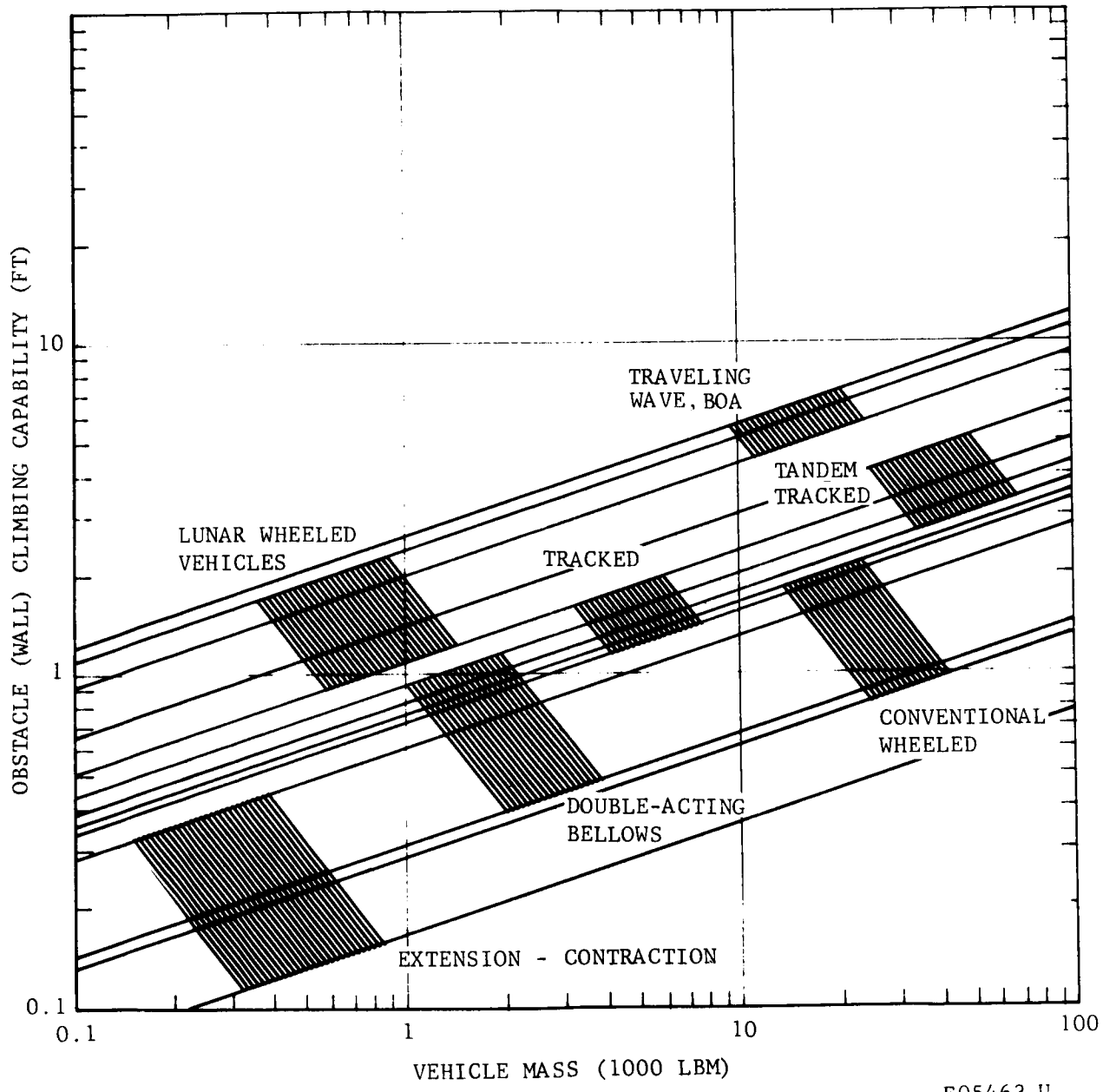


FIGURE 80. VEHICLE OBSTACLE CLIMBING CAPABILITY

F05463 U

Power requirements are generally an important consideration only in that they usually directly affect the size and weight because of the requirement for batteries or other energy storage or collection devices. Size and weight while operating are unimportant, but during the trip to the moon are very important. On larger vehicles some kind of folded, collapsed, or disassembled mode is required to meet the size constraint.

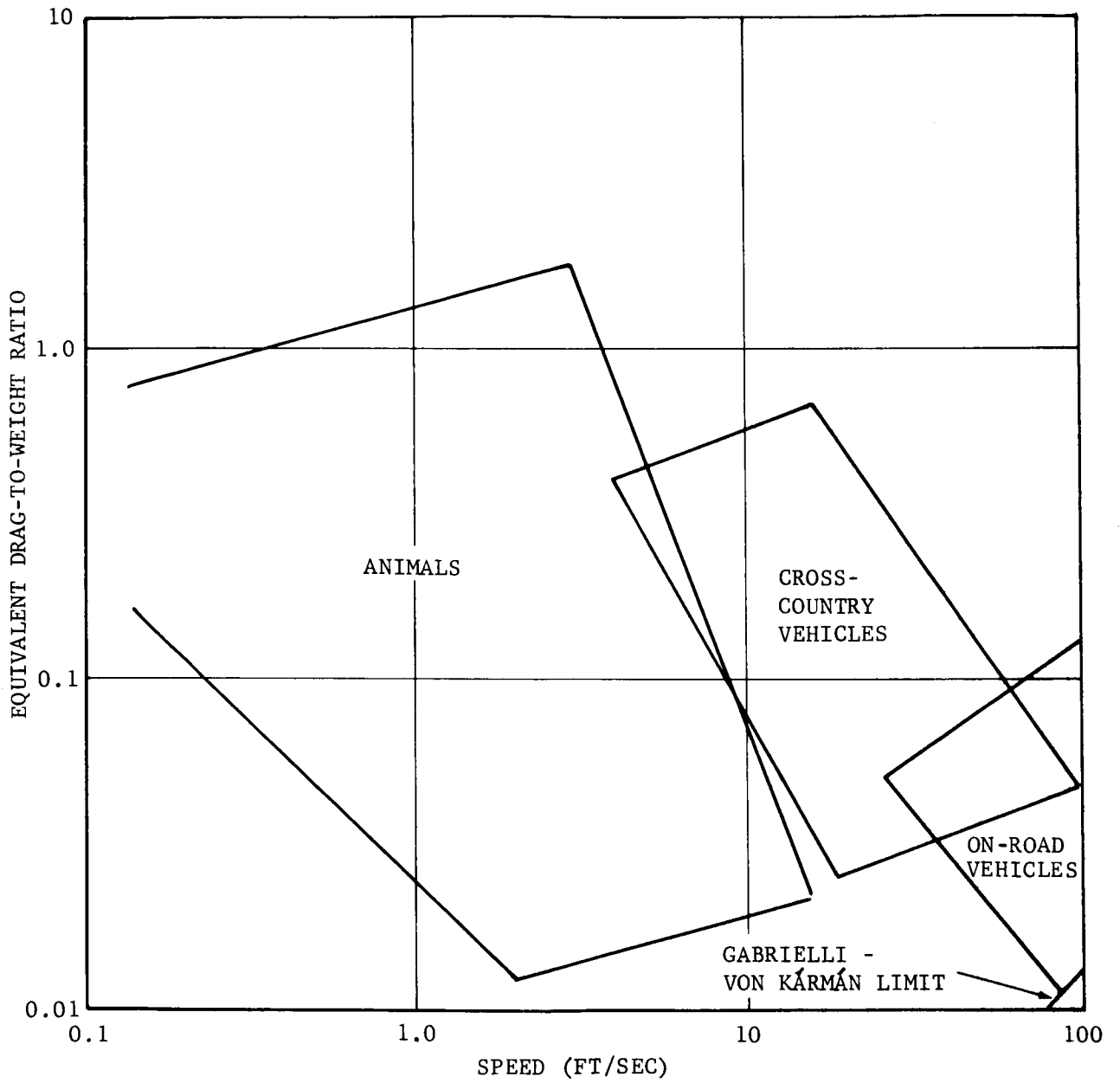
The vehicle performance parameters must specifically consider the ability of the device to perform satisfactorily in the lunar mission environment. Conditions that potentially pose design and operational constraints on a vehicle are high vacuum, temperature extremes, solar radiation, abrasive surface material, and meteorite bombardment.

Ability to Fulfill Mission Requirements

The design studies in this report demonstrate some of the possible mission applications of these mobility concepts. The mobile shelters may be thought of first as a shelter, and must have high reliability of functioning as such. The ability to move, on the other hand, may be useful, but not vital in the performance of the mission. This reasoning tends to favor the extension-contraction device, which requires a minimum of mechanisms, moving parts, and appendages to the basic shelter structure to provide mobility. The reliability of this method of propulsion is no better than the confidence that the soil characteristics are as predicted and are fairly uniform and reasonably smooth. Generally, this device cannot back out of a corner, nor can it move at all in a soil for which it was not designed. The extension-contraction vehicle requires special consideration in this respect, since it has been proposed that solar energy might be used directly for propulsion, thereby avoiding the usual weight penalty for power consumption. Conversely, the lunar supply vehicle mission may require high reliability as a transportation device to avoid leaving the occupants stranded in a remote area, while its function as a shelter may or may not be important. This concept favors the traveling wave vehicle which claims, as its primary attribute, the ability to move on an extremely wide range of soil types. It also has the ability to bridge crevices having widths approaching one-third its length. The unmanned missions generally require mobility somewhere in between these two, and are possible applications of the double-acting bellows and rib-walking concepts.

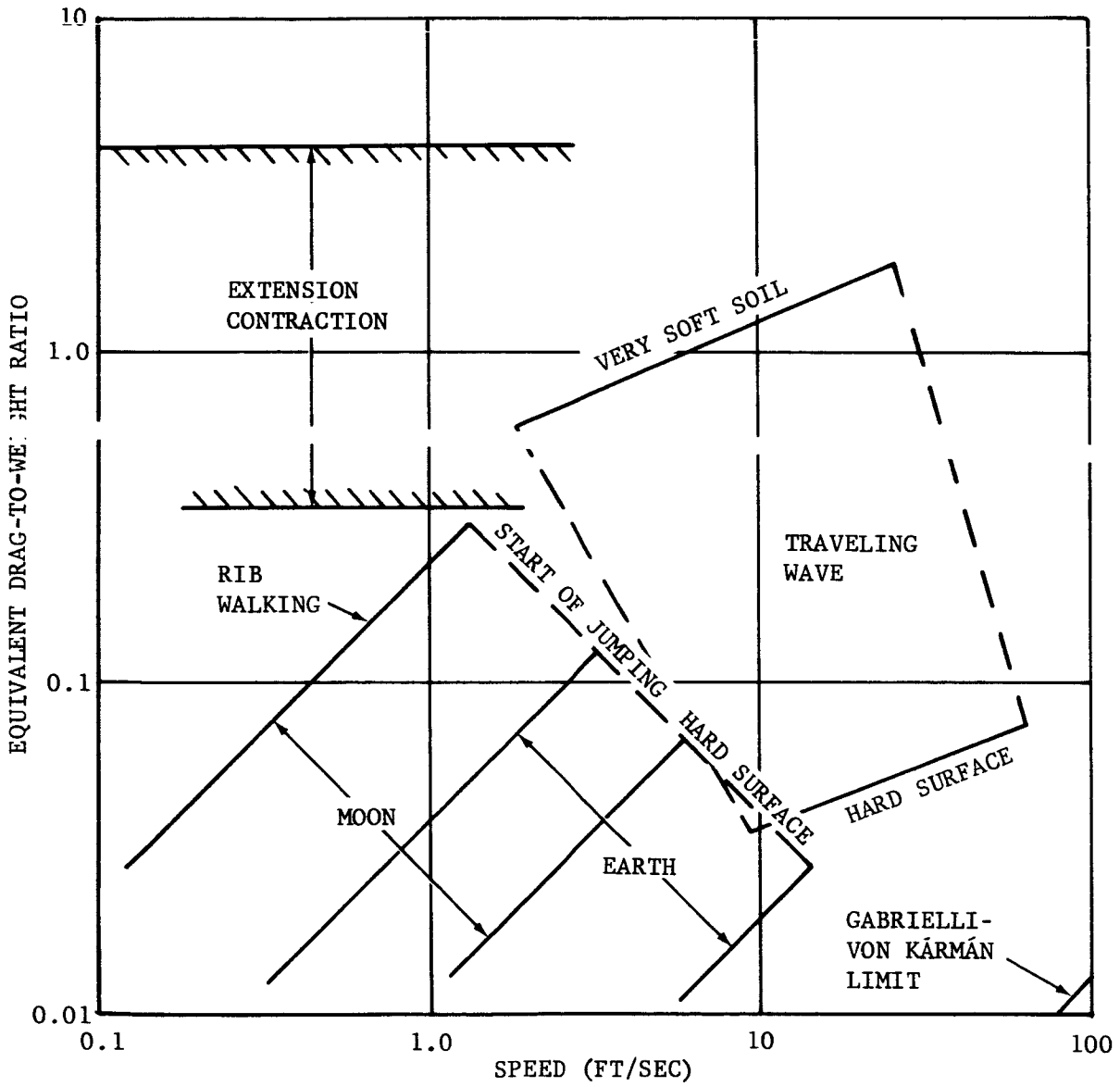
All bellows concepts studied can have all moving parts internally located in a protected pressurized environment to protect rubbing or sliding surfaces from cold welding in the extreme vacuum environment of the moon.

All concepts are suitable for delivery in an undeployed length generally less than one-third their nominal length. A possibility exists of using bellows contraction as an emergency measure to provide additional protection from radiation during solar flares. If the bellows were made of metal and were sufficiently contracted, the effective thickness for shielding would be substantially increased. The degree of such protection which could be obtained was not established in the present study but some observations can be



F05464 U

FIGURE 81. EQUIVALENT DRAG-TO-WEIGHT RATIO OF PRESENT SYSTEMS



F05465 U

FIGURE 82. EQUIVALENT DRAG-TO-WEIGHT RATIO OF WORM-TYPE VEHICLES

made regarding the degree of contraction possible with metal bellows. If a welded bellows cross section is employed, such as shown in Figures 54 and 55 for the lunar shelter, the bellows can contract nearly to their flat plate thickness and will be limited by other structural elements such as cleats or internal linkage systems. In the case of the large shelter it was estimated the shelter could be retracted to nearly one-sixth its maximum length. If a formed corrugated metal bellows cross-section is employed, however, which has sizable radii instead of cusps at the inner and outer edges of the convolutions, the length can be changed only about ten percent without exceeding the fatigue limit of the material.

Versatility Versus Complexity

Of the mobility modes discussed here, the traveling wave mode is potentially the most versatile and efficient but probably will require the most complex actuating mechanism. The extension-contraction mode is the least versatile and efficient, but the simplest. Its low efficiency may be partially compensated for by its potential ability to directly convert solar energy to power for propulsion, although the practicability of this concept has yet to be established. The versatility of the double-acting bellows version of the rib-walking mode lies somewhere between the traveling wave mode and the extension-contraction mode. While it will require a relatively simple mechanism, it is limited in obstacle climbing ability and by roughness of ride.

CONCLUDING SECTION

CONCLUDING REMARKS

An analytical study has been carried out concerning the feasibility of the bellows vehicle concept for use on the moon. Since most of the work is based on motions which have been successfully used by animals, many of the results have application to mobility in general and are therefore of interest in connection with other programs.

Of the several modes of bellows motion studied the traveling wave mode appears to be potentially the most versatile since, with the proper phasing of adjacent bellows segments, it is capable of moderate to high speeds over rough terrain with a smooth ride and good maneuverability. Compared with current cross-country vehicles it has good propulsive efficiency, better obstacle climbing ability, and better ability to bridge crevices. It can be designed with a very low footprint loading suitable for use over a wide variety of surfaces including spiny rock, low bearing strength materials, and even fluid-like soils through which it is capable of swimming partially or completely submerged. It is adaptable for a pressurized membrane-type construction which not only reduces weight but also allows the vehicle lower surface to mold itself to the terrain and thus minimize vehicle bounce and lift-off under low gravity conditions. Its feasibility is dependent upon the availability of a suitable membrane cover material which will remain flexible and abrasion resistant in the lunar environment.

The rib-walking bellows motion where adjacent ribs contacting the ground are 180 degrees out of phase requires a large path radius motion to yield acceptable drag-to-weight ratios. A double-acting bellows concept was developed to provide such motion with only a moderately rough ride. This concept, when used in a brief design study of a small unmanned vehicle of modest range appeared quite suitable with regard to simplicity, ease of deployment, weight, and power requirements but was somewhat limited in ability to clear obstacles. In this study, feet were utilized to provide roll stability and to prevent contact of the metal bellows surface with the ground, thus keeping the structural design within the present state-of-the-art of bellows technology. Other possible configurations include side-by-side bellows and double-lobed membrane bellows.

The extension-contraction bellows motion would appear to have limited use because of the high drag-to-weight ratio resulting from the sliding action of the lower surface over the terrain even with the use of a low-friction type coating and a variable geometry profile such as flexible cleats which retract during the forward stroke. The extension-contraction bellows configuration is, however, uniquely suited for incorporation of a novel solar-mechanical energy transfer system which from exploratory calculations holds promise as a lightweight, inexpensive means for supplying the mechanical energy for propulsion. A brief design study of using the extension-contraction bellows concept to propel a lunar shelter restricted to forward motion at very low speed over a short distance did not reveal any unusual problems regardless of shelter size.

All bellows concepts studied can have all moving parts internally located in a protected pressurized environment. All concepts are suitable for delivery in an undeployed length generally less than one-third their nominal length.

In carrying out the present study fundamental analytical treatment was given: to a stepped surface planing over soil; to wave motions which might be used by a variety of vehicles and which included traveling waves in soft soil with no hysteresis; and to membrane bellows structural properties and shear transfer. It was also necessary to establish a lunar soil model more realistic than the ELMS model for studies involving short stroke and cyclic motion.

RECOMMENDATIONS FOR FUTURE WORK

For all the vehicle concepts discussed in this report, the principal problem area is the interface between vehicle and soil. The predicted performance of the various propulsion mechanisms should be checked by carefully planned tests supported by additional analysis and evaluation.

The traveling-wave configuration which has been presented requires the development of an abrasion-resistant elastomer which will not deteriorate in the lunar environment. Further study should be undertaken to determine whether such a material can be produced.

The performance of the various systems over rough ground has not been investigated. This performance, particularly in the case of the traveling wave, is strongly dependent on the degree of flexibility and control built into the body. Dynamic studies and tests are needed to obtain quantitative design information on these relationships.

In order to obtain an overall evaluation of these concepts, mission-oriented trade-off studies should be performed, and resulting vehicle designs compared with other proposed vehicle designs.

APPENDIX A

UNITS AND CONVERSION FACTORS

In most cases, the text and equations of this report use standard English units. The inch is used widely as the unit of length since the ELMS model was given in this form, and since inches are traditionally used in structural work. The only unusual unit used is pounds mass as the unit of mass. A pound mass is defined as the mass which weighs one pound on earth. In this system, a body's mass and weight are numerically equal on earth.

The conversion factors to convert English units to the International System of Units are given below. The International System is abbreviated SI for *Système International* and is based upon the meter, kilogram, and second. These units are described and the conversion factors quoted here are given in Reference 7 and elsewhere. The first two digits of each conversion factor represent a power of 10 multiplier. For example, in the first conversion below, +03 1.06 means multiply by 1.06×10^3 .

<u>TO CONVERT</u>	<u>TO</u>	<u>MULTIPLY BY</u>	
British thermal unit	joule	+03	1.06
foot	meter	-01	3.048
horsepower	watt	+02	7.457
inch	meter	-02	2.54
pound (pound force)	newton	+00	4.448
pound mass (lbm)	kilogram	-01	4.536
mile (U. S. statute)	meter	+03	1.609
ton (short, 2000 lb)	kilogram	+02	9.072
ACCELERATION			
foot/second ²	meter/second ²	-01	3.048
free fall, standard	meter/second ²	+00	9.807
AREA			
foot ²	meter ²	-02	9.290
inch ²	meter ²	-04	6.452
DENSITY			
lbm/inch ³	kilogram/meter ³	+04	2.768
lbm/foot ³	kilogram/meter ³	+01	1.602

<u>TO CONVERT</u>	<u>TO</u>	<u>MULTIPLY BY</u>	
ENERGY			
British thermal unit	joule	+03	1.06
foot pound	joule	+00	1.356
POWER			
foot pound/second	watt	+00	1.356
horsepower	watt	+02	7.457
PRESSURE			
pound/foot ²	newton/meter ²	+01	4.788
pound/inch ²	newton/meter ²	+03	6.895
SPEED			
foot/second	meter/second	-01	3.048
mile/hour (U. S. statute)	meter/second	-01	4.470
VOLUME			
foot ³	meter ³	-02	2.832
inch ³	meter ³	-05	1.639

APPENDIX B

THE ENGINEERING LUNAR MODEL SURFACE (ELMS)

The ELMS document, ¹ is an attempt to present a uniform model of the lunar surface, in order to make the mobility studies of various contractors consistent with one another. It defines the mathematical form of the description of soil properties, and specifies the range of soil property parameters that should be considered, as well as giving typical lunar surface profiles. The soil description portion is based largely upon the work of Bekker, ^{2,3} and, since it is pertinent to the present study, a summary is given here.

The relationship between footprint pressure, σ , and soil penetration depth, z , is given by

$$\sigma = \left(\frac{K_c}{b} + K_\phi \right) z^n$$

where b is the width of the print, and K_c , K_ϕ , and n are soil parameters whose significance is described elsewhere in the List of Symbols. For the lunar surface, K_c is taken as zero, and the values for K_ϕ and n are given in Table B.1, together with a corresponding description of the soil and the expected description on the lunar surface.

TABLE B. 1

LUNAR SURFACE PENETRATION

Slope Angle	Percent of Traverse		Soil Constants		Soil Description
	Maria	Uplands	n	K_ϕ	
Degrees	Percent	Percent	$\frac{Lb}{\text{In.}^{n+2}}$	(No Dimensions)	
0-4	84.0	57.1	1.0	0.05	Extreme soil
5-7.5	10.5	23.4	0.5	0.5	Loose, fluffy, dust
10-20	5.0	18.3	0.75	1.0	
22-25	0.3	1.0	1.0	3.0	Loose, dry, sand
30-35	0.2	0.2	1.25	6.0	Hard, compacted, sand
			-	-	Hard surface

The "extreme soil" has been predicted by some theorists, but no speculation as to its distribution is made. The result of Equation (B. 1) with the range of parameters given in Table B. 1 is plotted in Figure 2 of this report.

The shear stress, τ , is given in its general form by

$$\tau = (c + \sigma \tan \phi) f(j) \quad (\text{B. 2})$$

$$f(j) = \frac{y}{y_{\max}} \quad (\text{B. 3})$$

$$y = \exp \left[\left(-K_2 + \sqrt{K_2^2 - 1} \right) K_1 j \right] - \exp \left[\left(-K_2 - \sqrt{K_2^2 - 1} \right) K_1 j \right] \quad (\text{B. 4})$$

The function $f(j)$ gives the variation of tractive force with j , the displacement of the soil from its initial location, and has a maximum value of 1.0. The shape of this curve is determined by soil parameters K_1 and K_2 . The level of the maximum friction coefficient is given by the coefficient of cohesion, c , and the angle of friction of the soil grains, ϕ . The lunar surface is assumed to be a noncohesive material and c is therefore taken as zero. The friction angle, ϕ , is assumed to be 32 degrees which corresponds approximately to dry sand, except for the "extreme soil" which is assumed to have a coefficient of $\phi = 20$ degrees. Slippage factors, K_1 and K_2 , are conservatively chosen, low values reflecting a pessimistic prediction of vehicle performance. K_1 generally ranges from 0.3 (average soil) to 1.0 (coherent soil), and K_2 from 1.0 (coherent soil) to 3.0 (loose sand). NASA analyses are based on $K_1 = 0.2$ and $K_2 = 1.25$, thus yielding a conservative vehicle performance estimate.

Using these values, Equation (A. 2) becomes

$$\tau = \frac{\tan \phi}{0.472} \left(e^{-0.1j} - e^{-0.4j} \right) \quad (\text{B. 5})$$

This relationship is plotted in Figure 1 of the report.

APPENDIX C

MOBILITY OF EXTENSION-CONTRACTION TYPE OF VEHICLE

As discussed in the body of the report, three soil models are considered as follows:

Case I - $\frac{\tau}{\sigma}$ constant

$$\frac{\tau}{\sigma} \text{ (aft direction)} = k_a$$

$$\frac{\tau}{\sigma} \text{ (forward direction)} = k_f$$

$$\text{Nominal values: } k_a = 1.2 \quad k_f = 0.75$$

$$k_f = 0.625$$

Case II - $\frac{\tau}{\sigma}$ proportional to displacement

$$\frac{\tau}{\sigma} \text{ (aft direction)} = k_a j$$

$$\frac{\tau}{\sigma} \text{ (forward direction)} = k_f j$$

$$\text{Nominal values: } k_a = 0.475 \text{ in.}^{-1}$$

$$k_f = 0.396 \text{ in.}^{-1}$$

Case III - ELMS Model

$$\frac{\tau}{\sigma} = C \left(e^{-0.1j} - e^{-0.4j} \right)$$

$$\text{Nominal values: } \text{Aft } C_a = 1.58$$

$$\text{Forward } C_f = 1.32$$

The nominal constants given make the τ/σ for Case I equal to the peak value of the ELMS model, and the slope for Case II equal to the slope at the origin of the ELMS model.

The vehicle length is taken at any time as $L(1 + e)$, where L is the minimum length during an operating cycle, and e is the vehicle strain. The length of the stroke is the Le . Since the constants given for the ELMS model are given for inches as the unit of length, inches will be used throughout this section. The motion of the vehicle will be referred to the midpoint, and since the vehicle is considered to have a uniform density, this will also be the center of gravity (cg). The point on the vehicle which is instantaneously at rest with respect to the ground will be labeled p . The vehicle weight, the tractive force, and the portion of the minimum length, L , on either side of p will be subscripted a and f for aft and forward of this point. At this time no external or inertial forces are considered.

Analysis of Case I

The geometry for this case is shown in Figure C-1. The following relationships apply

$$H = k\sigma S \quad (C.1)$$

$$\sigma = \frac{W}{L(1 + e)} \quad (C.2)$$

$$W_a = W \frac{L_a}{L} \quad (C.3)$$

$$W_f = W \frac{L_f}{L} \quad (C.4)$$

$$W = W_a + W_f \quad (C.5)$$

$$L = L_a + L_f \quad (C.6)$$

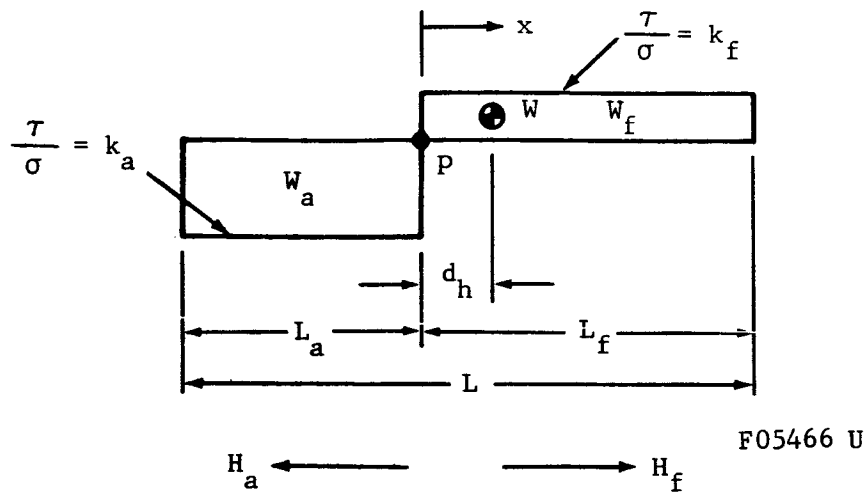


FIGURE C-1. CASE I τ/σ CONSTANT

Since no external forces are considered, the location of the stationary point, p, is given by setting the thrust equal to drag ($H_a = H_f$), and by substitution of Equations (C. 1) through (C. 6) gives

$$k_a L_a = k_f L_f \quad (C. 7)$$

$$L_a = L \frac{k_f}{k_a + k_f} \quad (C. 8)$$

$$L_f = L \frac{k_a}{k_a + k_f} \quad (C. 9)$$

The point p remains fixed throughout one extension or contraction stroke. The location of the cg with respect to p is

$$d_h = 1/2 L (1 + e) \frac{k_a - k_f}{k_a + k_f} \quad (C. 10)$$

and the cg travel during a half cycle is

$$s = d_h - h_{ho} = 1/2 L e \frac{k_a - k_f}{k_a + k_f} \quad (C. 11)$$

The work required to move this distance may be found as follows (where only the aft end of the vehicle is considered):

$$dH_a = k_a W_a \frac{dx}{L_a (1+e)} \text{ on element } dx$$

$$ds = \frac{x}{L_a (1+e)} d(Le) \text{ for an incremental expansion } d(Le)$$

$$\begin{aligned} \text{Work})_a &= \int_0^{L_a e} \int_0^{L_a (1+e)} dH_a ds \\ &= 1/2 k_a W_a L_a e \end{aligned} \tag{C.12}$$

Writing a similar expression for the forward end of the vehicle, and substituting from Equations (C.3) to (C.6) gives the work for the whole vehicle

$$\text{Work})_{\text{tot}} = 1/2 WLe \frac{k_a k_f}{k_a + k_f} \tag{C.13}$$

Then, using Equations (C.11) and (C.13), the equivalent drag-to-weight ratio for the vehicle is

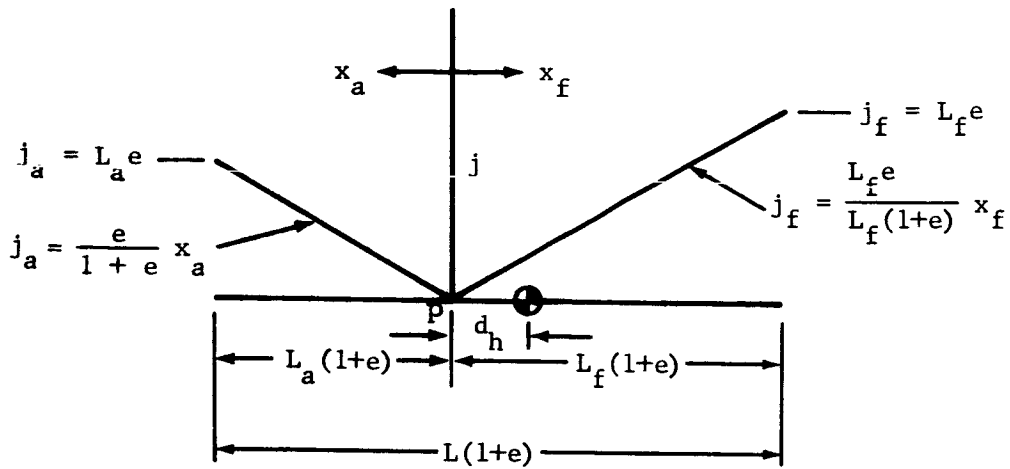
$$\frac{D_e}{W} = \frac{\text{Work})_{\text{tot}}}{Ws} = \frac{k_a k_f}{k_a - k_f} \tag{C.14}$$

Analysis of Case II

Case II is illustrated in Figure C-2. Equations (C.2) through (C.6) apply to this case, but the tractive force is given by

$$\begin{aligned} H_a &= \int_0^{L_a (1+e)} \tau_a dS \\ &= \frac{W}{bL (1+e)} \int_0^{L_a (1+e)} b k_a \frac{e}{1+e} dx \\ &= 1/2 W k_a L_a e \frac{L_a}{L} \end{aligned} \tag{C.15}$$

$$H_f = 1/2 W k_f e \frac{L_f^2}{L} \quad (C. 16)$$



F05467 U

FIGURE C-2. CASE II τ/σ PROPORTIONAL TO DISPLACEMENT

Proceeding as for Case II, the following relationships result:

$$H_a = H_f$$

$$k_a L_a^2 = k_f L_f^2 \quad (C. 17)$$

$$L_a = \frac{\sqrt{k_f}}{\sqrt{k_a} + \sqrt{k_f}} L \quad (C. 18)$$

$$L_f = \frac{\sqrt{k_a}}{\sqrt{k_a} + \sqrt{k_f}} L \quad (C. 19)$$

$$s = 1/2 L e \frac{\sqrt{k_a} - \sqrt{k_f}}{\sqrt{k_a} + \sqrt{k_f}} \quad (C. 20)$$

$$dH_a = \frac{W}{bL_a (1 + e)} k_a \frac{e}{1 + e} x b dx$$

$$ds = \frac{x}{L_a (1 + e)} d(L_a e)$$

$$\text{Work})_a = 1/6 W_a k_a L_a^2 e^2 \quad (\text{C. 21})$$

$$\text{Work})_{\text{tot}} = 1/6 W(Le)^2 \frac{k_f k_a}{\left(\sqrt{k_a} + \sqrt{k_f}\right)^2} \quad (\text{C. 22})$$

$$\frac{D_e}{W} = 1/3 L e \frac{k_a k_f}{k_a - k_f} \quad (\text{C. 23})$$

Analysis of Case III (ELMS Model)

For this case, the point p is at rest only momentarily, and its location changes continuously. The variation of the location of this point has not been solved. However, it is known that at the beginning of a stroke the location of p is given by Case II, and it has been shown graphically that its departure from this location is not great up to a stroke length of about ten inches. Therefore, an approximate solution may be obtained by assuming the p remains fixed as given by Case II, and computing the resulting power consumption.

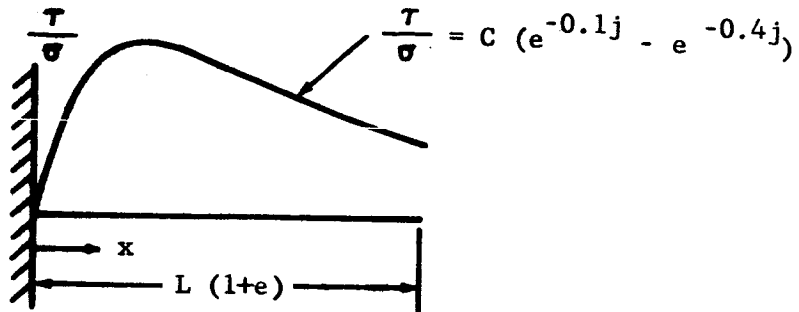
The forces on a vehicle segment with one end fixed are shown in Figure C-3. The tractive force on the vehicle may be found as follows:

$$\left(\frac{\tau}{\sigma}\right)_{\text{ave}} = \frac{1}{Le} \int_0^{Le} \frac{\tau}{\sigma}(j) dj \quad (\text{C. 24})$$

$$H = W \frac{\tau}{\sigma}_{\text{ave}}$$

$$= \frac{W}{Le} \int_0^{Le} C \left(e^{-0.1j} - e^{-0.4j} \right) dj$$

$$H = C \frac{W}{Le} \left(7.5 - 10 e^{-0.1 Le} + 2.5 e^{-0.4 Le} \right) \quad (\text{C. 25})$$



F05468 U

FIGURE C-3. CASE III ELMS MODEL - VEHICLE FIXED AT ONE END

The work consumed during a half cycle is given by

$$\text{Work} = \int_0^{Le} \int_0^{L(1+e)} dH da \quad (\text{C. 26})$$

where

$$dH = \frac{W}{bL(1+e)} \frac{\tau}{\sigma}(x) b dx \quad (\text{C. 27})$$

$$da = \frac{x}{L(1+e)} d(Le) \quad (\text{C. 28})$$

Making the substitutions, and performing the first integration gives

$$\text{Work} = W F_1(Le)$$

where the function $F_1(Le)$ is given by

$$F_1(Le) = \int_0^{Le} \frac{C}{(Le)^2} \left[-10^2 \left(\frac{Le}{10} + 1 \right) e^{-0.1 Le} + 2.5^2 \left(\frac{Le}{2.5} + 1 \right) e^{-0.4 Le} + 93.75 \right] d(Le) \quad (C. 30)$$

This function may be evaluated numerically, and the result is shown in Figure 9.

For a complete vehicle which is free to move, the location of p is assumed to be the same as given for Case II, and the distance traveled per stroke is given by Equation (C. 20). The work is found by applying Equation (C. 29) to each end of the vehicle.

$$\text{Work}_{\text{tot}} = \frac{L_a}{L} W F_1(L_a e) + \frac{L_f}{L} W F_1(L_f e) \quad (C. 31)$$

where the function, F_1 is defined by Equation (C. 30). Then, by using Equations (C. 20) and (C. 31), the equivalent drag-to-weight ratio is given by

$$\frac{D_e}{W} = \frac{\text{Work}}{Ws} = \frac{2}{Le} \frac{\sqrt{C_a}}{\sqrt{C_a} - \sqrt{C_f}} \left[\sqrt{\frac{C_a}{C_f}} F_1(L_a e) + F_1(L_f e) \right] \quad (C. 32)$$

where L_a and L_f are given by Equations (C. 18) and (C. 19). It can be shown that performing a first order approximation for small Le to this expression gives the same result as Equation (C. 23), the solution for Case II.

Results

The results of the analysis are shown and discussed in the body of the report. The work required to extend a vehicle which is fixed at one end is shown in Figure 9, and is obtained from Equations (C. 12), (C. 21), and (C. 29). This much of the solution is exact within the limitations of the assumptions made. The equivalent drag-to-weight ratio is given by Equations (C. 14), (C. 23), and (C. 32), and is shown in Figure 10. Here, the additional assumption is made that the point p remains fixed at the location given by Case II, an assumption which is not valid for large stroke lengths.

APPENDIX D

MATHEMATICAL MODEL OF WAVE MOTIONS

The following is a mathematical description of motion which might be used by various types of vehicles. It is hoped that this model might prove useful in future studies of the mobility and dynamics of vehicles using these principles. The general type of motion which is to be considered consists of traveling waves along the lower surface of an elongated body, as shown in Figure D-1.

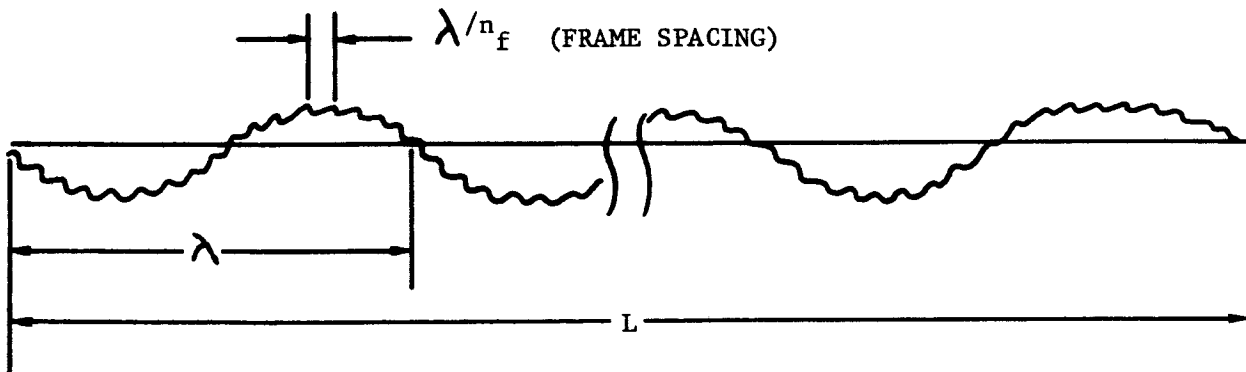


FIGURE D-1. VEHICLE CONFIGURATION

If it is assumed that the vehicle length L contains N similar waves, the fundamental wavelength will be

$$\lambda = L/N_w \quad (D.1)$$

The vertical and horizontal components of the motion will be taken as sinusoidal. This does not mean, however, that the wave shape is sinusoidal. In fact, the typical traveling wave vehicle mechanized by a series of cranks as discussed in this report is conspicuously nonsinusoidal in shape and actually is a curtate cycloid.

The coordinate system will be chosen as shown in Figure D-2 (fixed in vehicle). The ground plane will be represented by $Z = 0$.

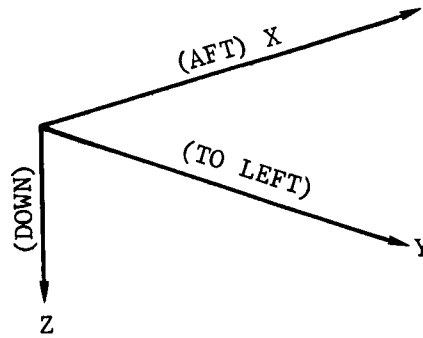


FIGURE D-2. COORDINATE SYSTEM

All points will be assumed to move in planes parallel to the XZ plane. If X is the distance in feet from the nose, and v_w is the wave velocity in the aft direction in feet per second, the components of displacement of a point (x, y, z) with respect to the point (X, Y, Z) will be:

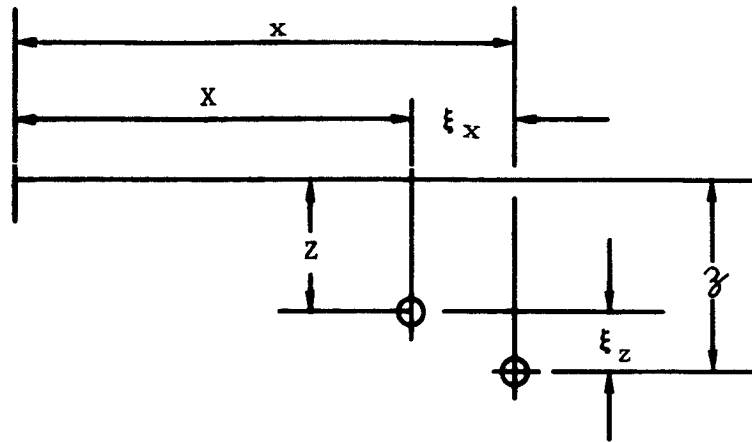
Longitudinal Displacement:

$$\xi_x = A_x \cos \frac{2\pi}{\lambda} (X - v_w t) \quad (D.2)$$

Transverse (vertical) Displacement:

$$\xi_z = A_z \cos \frac{2\pi}{\lambda} (X - v_w t + X_0) \quad (D.3)$$

In these equations, A_x and A_z are shown as constants, although they might vary with Y or Z for certain more complicated types of motion. In order for useful thrust to be produced, X_0 will normally be close to $\lambda/4$, thus producing circular or elliptical local displacements. Values $0 < X_0 < \pi$ give propulsion in the forward direction. If X_0 is outside this range, propulsion in the opposite direction results. The displacements are shown in Figure D-3.



F05470 U

FIGURE D-3. DISPLACEMENTS

One additional parameter is the number of frames or bulkheads per wavelength. This will be called n_f .

From Equation (D.2), the longitudinal displacement velocity of a point x is

$$\dot{x} = \dot{\xi}_x = A_x \frac{2\pi v_w}{\lambda} \sin \frac{2\pi}{\lambda} (X - v_w t) \quad (D.4)$$

which has a maximum value

$$v_{tm} = 2\pi A_x \frac{v_w}{\lambda} = 2\pi f A_x$$

This is the velocity with which the vehicle would move under ideal conditions on hard ground with no slip. Under these conditions, the speed of the wave relative to the ground (in the aft direction) is:

$$v = v_{tm} - v = \left(v \frac{2\pi A_x}{\lambda} - 1 \right) \quad (D.5)$$

That is, for $A_x = \lambda/2\pi$, the wave is stationary with respect to the ground (the centipede case).

Special Cases:

The extension-contraction motion discussed in this report is a standing wave obtained from Equations (D.2) and (D.3) by setting $A_z = 0 \equiv \xi_z$ and

$$\begin{aligned}\xi_x &= \frac{A_x}{2} \left[\cos \frac{2\pi}{\lambda} (X - v_w t) \quad \cos \frac{2\pi}{\lambda} (X + v_w t) \right] \\ &= A_x \left(\cos \frac{2\pi X}{\lambda} \cdot \cos 2\pi f t \right).\end{aligned}\tag{D.6}$$

Putting $X = \frac{\lambda}{4} + \delta$, where $\delta \ll \lambda$ gives:

$$\begin{aligned}\xi_x &= -A_x \sin \frac{2\pi\delta}{\lambda} \cdot \cos 2\pi f t \\ &\approx -\delta \cdot \frac{2\pi A_x}{\lambda} \cdot \cos 2\pi f t.\end{aligned}\tag{D.7}$$

(where f = frequency in cycles/sec)

The rib-walking motion is approximated by setting

$$X_0 = \lambda/4; n_f = 2$$

This gives for successive ribs, $X = r \cdot \frac{\lambda}{2}$ ($r = 0, 1, 2$, etc.)

$$\begin{aligned}\xi_x &= A_x \cos \frac{2\pi}{\lambda} \left(r \frac{\lambda}{2} - v_w t \right) \\ &= A_x \cos (r\pi - 2\pi f t) \\ &= -A_x \cos 2\pi f t \quad (r \text{ odd}) \\ \text{or} \quad &+ A_x \cos 2\pi f t \quad (r \text{ even})\end{aligned}\tag{D.8}$$

and

$$\begin{aligned}\xi_z &= A_z \sin (r\pi - 2\pi f t) \\ &= -A_z \sin 2\pi f t \quad (r \text{ odd}) \\ \text{or} \quad &= + A_z \sin 2\pi f t \quad (r \text{ even})\end{aligned}\tag{D.9}$$

That is, successive ribs describe ellipses, 180 degrees out of phase with each other.

The traveling wave motion may be represented by setting

$$\lambda = 2L, \quad A_x = A_z = A, \quad X_0 = \lambda/4$$

giving:

$$\xi_x = A \cos \frac{\pi}{L} (X - v_w t) \quad (\text{D.10})$$

$$\xi_z = A \sin \frac{\pi}{L} (X - v_w t) \quad (\text{D.11})$$

APPENDIX E

MOBILITY OF A TRAVELING WAVE IN SOFT SOIL WITH NO HYSTERESIS*

Introduction

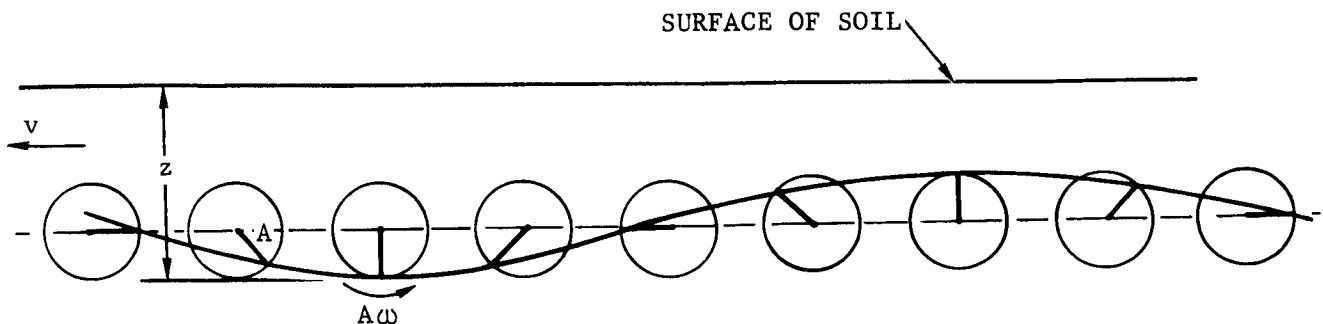
An analysis of the mobility of a traveling wave in soft soil with one set of assumptions regarding geometry and soil behavior has been completed. A wave made up of rotating cranks as shown in Figure E-1 is considered. However, the crank radius is assumed small compared to the wave length, resulting in a sinusoidal shape and certain other simplifications in the analysis. Many cranks are assumed, giving approximately a continuous wave. The soil normal force is assumed to depend only upon the depth below the original surface of the soil, and to be directly proportional to that depth. The soil friction is assumed to be directly proportional to the normal force, i. e., the classical friction coefficient.

The principal results of the analysis are shown in Figures 22, 24 and 25 in the report. Figure 22 shows the ratio of the vehicle forward velocity, V , to the crank velocity, $A\omega$. Figure 25 shows the depth that a wave will penetrate into the soil as a function of the planform loading. Figure 24 gives the equivalent drag-to-weight ratio, which is actually a measure of vehicle power consumption under the specified conditions.

Analysis - Entire Wave Below Soil Surface

Assume a traveling wave on the lower surface of a vehicle, which may be made up of many cranks as shown in Figure E-1. Each crank has radius A , and is rotating counter-clockwise with angular velocity ω , and the wave is moving from left to right.

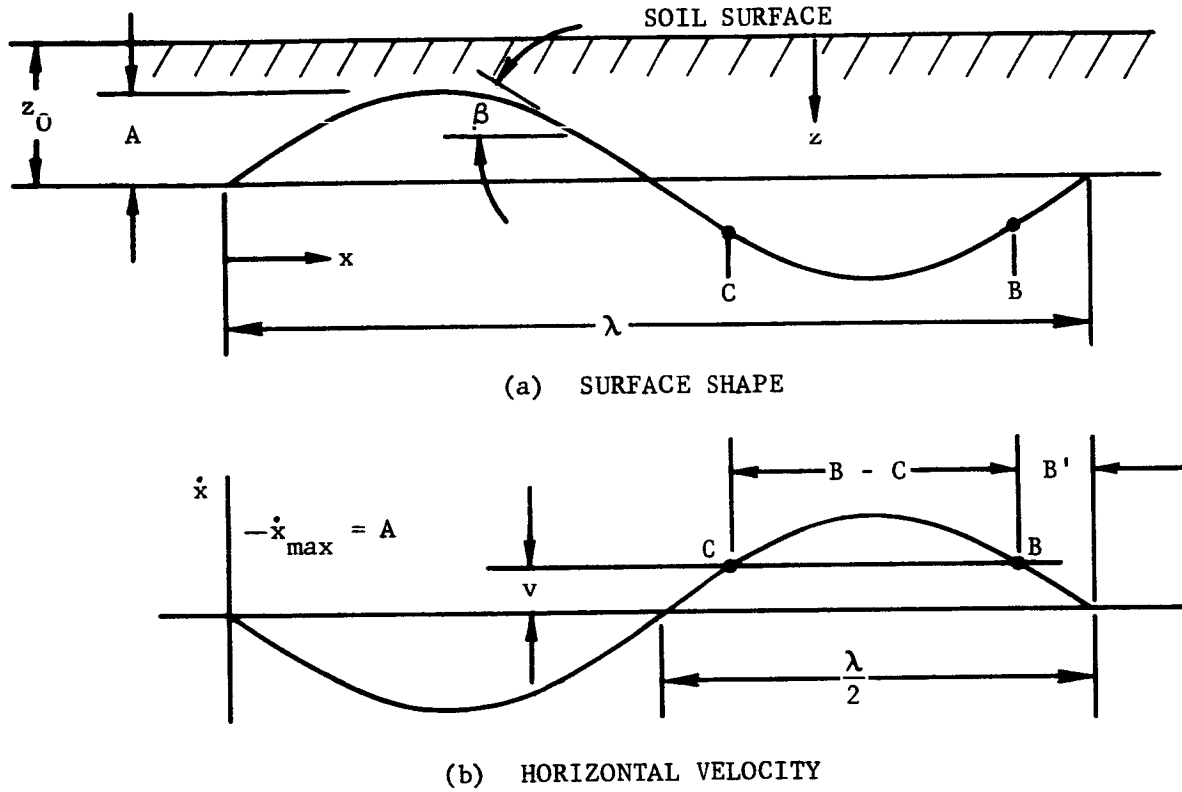
* See footnote on page 1.



F05471 U

FIGURE E-1. TRAVELING WAVE MADE UP OF CRANKS

If there are many cranks, and the radius is small compared to the wave length, then this will approximately represent a smooth, continuous, sinusoidal curve as shown in Figure E-2(a).



F05473 U

FIGURE E-2. CONTINUOUS WAVE SURFACE

The coordinate system of the traveling wave is fixed in the vehicle. For this case the entire wave will be assumed below the ground surface.

The soil is assumed to have a linear relationship between sinkage depth and footprint pressure

$$\sigma = K_{\phi} z \quad (E.1)$$

and this relationship is assumed to hold even though the surface of the wave may be receding from the soil. The depth of the wave in the soil as shown in Figure E-2(a) is:

$$z = z_0 - A \sin 2\pi \frac{x}{\lambda} \quad (E.2)$$

The horizontal velocity of each point of the wave is:

$$\dot{x} = -A\omega \sin 2\pi \frac{x}{\lambda} \quad (\text{E.2a})$$

as in Figure E-2(b), where positive velocities are to the right. With respect to the vehicle, the ground is moving to the right with velocity V. Therefore, in Figure E-2(a), the portions of the surface between C and B are moving to the right faster than the ground, and are providing propulsion. All other points are contributing drag.

The footprint pressure at any point is, from Equations (E.1) and (E.2):

$$\sigma = K_{\phi} z_0 - K_{\phi} A \sin 2\pi \frac{x}{\lambda} \quad (\text{E.3})$$

A constant friction coefficient is assumed so that

$$\tau = \mu \sigma \quad (\text{E.4})$$

which is independent of velocity. Therefore, the propulsive thrust per unit of vehicle width for one wave length

$$\begin{aligned} H_p &= \int_L \tau \, dS \\ &= \mu K_{\phi} z_0 \int_C^B \left(1 - \frac{A}{z_0} \sin 2\pi \frac{x}{\lambda} \right) dx \quad (\text{E.4a}) \end{aligned}$$

The horizontal component of the force parallel to the surface is taken here by using the area of the surface which is projected on the horizontal plane; i. e., $dS = dx$. Similarly the drag force on the wave surface is given by:

$$\begin{aligned} H_d &= \int_0^{\frac{\lambda}{2}} \tau \, dS + \int_{\frac{\lambda}{2}}^C \tau \, dS + \int_B^{\lambda} \tau \, dS \\ &= \int_0^{\frac{\lambda}{2}} \tau \, d\xi \times 2 + \int_B^{\lambda} \tau \, dS \quad (\text{E.5}) \end{aligned}$$

The net propulsive thrust on the wave is $H_p - H_d$, and from Equations (E. 4a) and (E. 5),

$$H_{\text{net}} = \int_C^B \tau dS - \int_0^C \tau dS - \int_B^{\lambda} \tau dS \quad (\text{E. 6})$$

$$= 2\left(B - C \frac{\lambda}{2}\right) + \frac{A}{z_0} \frac{\lambda}{2\pi} 2\left(\cos 2\pi \frac{B}{\lambda} - \cos 2\pi \frac{C}{\lambda}\right) \quad (\text{E. 7})$$

However, from inspection of Figure E-2, it may be seen that:

$$B - C - \frac{\lambda}{2} = -2(\lambda - B)$$

$$-\cos 2\pi \frac{B}{\lambda} = \cos 2\pi \frac{C}{\lambda}$$

and Equation (E. 7) may then be written as:

$$\frac{H_{\text{net}}}{\mu K_{\phi} z_0} = -4(\lambda - B) + \frac{A}{z_0} \frac{\lambda}{2\pi} \cdot 4 \cos 2\pi \frac{B}{\lambda} \quad (\text{E. 8})$$

If there are other forces acting on the vehicle which total D per unit of vehicle width for each wave length, then:

$$H_p - H_d = D \quad (\text{E. 9})$$

Equation (E. 8) can then be written as:

$$\frac{D}{\mu K_{\phi} z_0} + 4(\lambda - B) = 4 \frac{A}{z_0} \frac{\lambda}{2\pi} \cos 2\pi \frac{B}{\lambda} \quad (\text{E. 9a})$$

This may be written as:

$$\frac{U}{4} + \frac{B'}{\lambda} = \frac{1}{2\pi} \frac{A}{z_0} \cos 2\pi \frac{B'}{\lambda} \quad (\text{E. 10})$$

where the following terms are defined:

$$U = \frac{D}{\mu K_{\phi} z_0 \lambda} \quad (\text{E. 11})$$

$$B' = \lambda - B \quad (\text{E. 12})$$

and where

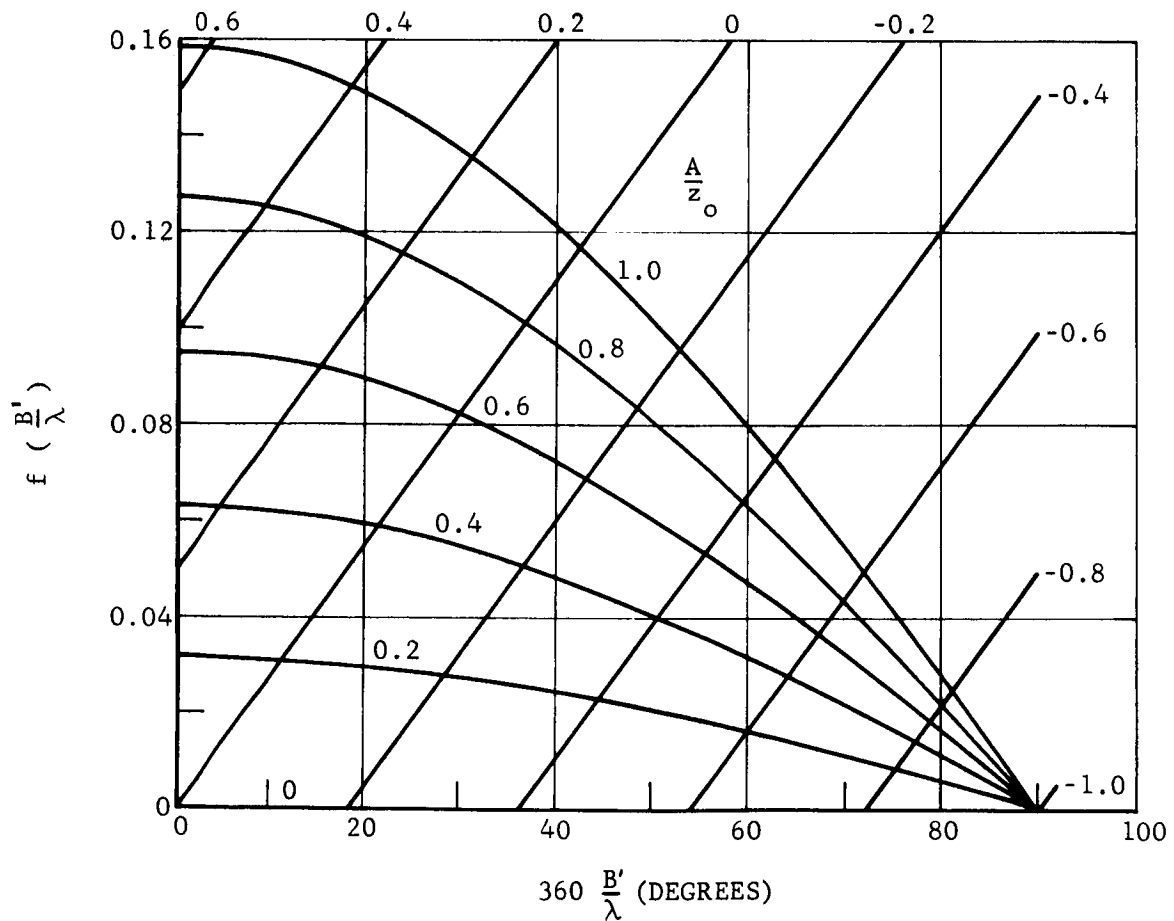
$$\cos 2\pi \frac{B}{\lambda} = \cos 2\pi \frac{B'}{\lambda} \quad (\text{E. 13})$$

A graphical solution to Equation (E. 13) is given in Figure E-3. The intersection of the two families of curves on Figure E-3 is the solution of the equation for B'/λ for that set of parameters.

From Figure E-2(b), the ground velocity is:

$$v = A\omega \sin \frac{B'}{\lambda} \cdot 2\pi \quad (\text{E. 14})$$

$$U = \frac{D}{\mu K_{\phi} z_0 \lambda}$$



F05472 U

FIGURE E-3. TRAVELING WAVE POINT OF ZERO VELOCITY

This result is plotted in Figure 22, by using the solution for B'/λ given by Figure E-3. In this figure, U is designated by the terminology which will be given by Equation (E. 17) and (E. 19) below. For clarity of presentation, the depth parameter is converted to z_m , the maximum depth of the wave below the surface (rather than mean depth, z_0). This is given by:

$$z_m = z_0 + A$$

$$\frac{z_m}{A} = \frac{z_0}{A} + 1 \quad (\text{E. 15})$$

Therefore, in Figure E-3, the curves for z_m/A from 2.0 to infinity represent the present case of a fully submerged wave. The curves for z_m/A less than 2.0 are for a wave partially above the surface; this case is discussed later.

The vehicle weight (one wave length one unit wide) is, from Equation (E. 3),

$$W_1 = \int_0^\lambda \sigma \, dA$$

$$= \int_0^\lambda \left(K_\phi z_0 - K_\phi A \sin 2\pi \frac{x}{\lambda} \right) dx$$

$$= K_\phi z_0 \lambda \quad (\text{E. 16})$$

This is the same weight that would result if the vehicle had a flat bottom, at depth z_0 below the ground surface. From Equation (E. 16), the term U given by Equation (E. 11) may be written as:

$$U = \frac{1}{\mu} \cdot \frac{D}{W_1} = \frac{1}{\mu} \cdot \frac{\text{External Drag}}{\text{Weight}} \quad (\text{E. 17})$$

If the drag, D , is the gravity force when the vehicle is on a slope of angle ϕ ,

$$D = W_1 \tan \theta \quad (\text{E. 18})$$

and Equation (E. 17) becomes:

$$U = \frac{1}{\mu} \tan \theta \quad (\text{on a slope}) \quad (\text{E. 19})$$

The power consumed by one wave length of the wave one unit wide is:

$$\text{Power} = \text{Force} \times \text{Velocity} \quad (\text{E. 20})$$

The power to drive the cranks as shown in Figure E-1 is due to forces parallel to the wave and forces normal to the wave. We have assumed, however, that the pressure, σ , is acting normal to the surface, and is the same when

the wave is receding from the soil as when it is advancing toward the soil. Therefore, the power used in overcoming the normal force component is recovered in another part of the cycle, and only the frictional component need be considered.

From Equations (E. 3) and (E. 4), the frictional force on an element of the surface in Figure E-2(a) is:

$$\begin{aligned} dP_f &= \tau dA \\ &= \mu K_\phi z_0 \left(1 - \frac{A}{z_0} \sin 2\pi \frac{x}{\lambda} \right) dS \end{aligned} \quad (E.21)$$

The required area increment is the actual area along the wave surface and is given by:

$$dS = \frac{dx}{\cos \beta} \quad (E.22)$$

where β is the angle shown in Figure E-2(a), and $\tan \beta$ is the slope of the wave at location x . The slope is given by

$$\begin{aligned} \tan \beta &= \frac{d}{dx} A \sin 2\pi \frac{x}{\lambda} \\ &= A \frac{2\pi}{\lambda} \cos 2\pi \frac{x}{\lambda} \end{aligned} \quad (E.23)$$

Therefore,

$$\begin{aligned} \cos^2 \beta &= \frac{1}{1 + \tan^2 \beta} \\ \cos \beta &= \left[1 + \left(A \frac{2\pi}{\lambda} \cos 2\pi \frac{x}{\lambda} \right)^2 \right]^{-1/2} \end{aligned} \quad (E.24)$$

The velocity required for Equation (E. 20) is the tangential velocity of the surface relative to the vehicle, and from Equation (E. 2a),

$$v_t = \frac{\dot{x}}{\cos \beta} = \frac{-A\omega}{\cos \beta} \sin 2\pi \frac{x}{\lambda} \quad (E.25)$$

If the vehicle has no forward motion, the friction force defined by Equation (E.21) is always opposing the direction of the motion given by Equation (E. 25). The following discussion leading to Equation (E. 29) is restricted to this case. The more general case with forward motion is treated as a correction to the zero-velocity case and is illustrated in Figure E-5.

The power may now be written as

$$P_1 = - \int_0^{\frac{\lambda}{2}} v_t \tau \, dS \int_{\frac{\lambda}{2}}^{\lambda} v_t \tau \, dS \quad (\text{E.26})$$

Note that τ is always a positive number, but that v_t is negative in the first interval, and positive in the second interval of Equation (E.26). The division of the integral with the sign shown in this equation then makes the power positive, and additive over the whole surface.

Adopting the nomenclature

$$- \int_0^{\frac{\lambda}{2}} f(x) dx + \int_{\frac{\lambda}{2}}^{\lambda} f(x) dx \triangleq - \int_L f(x) dx, \quad (\text{E.27})$$

the power may be written by using Equations (E.22), (E.25), (E.24), and (E.26) as,

$$P_1 = \mu K_{\phi} z_0 A \omega \int_L \sin 2\pi \frac{x}{\lambda} \left(1 - \frac{A}{z_0} \sin 2\pi \frac{x}{\lambda} \right) \times \left[1 + \left(A \frac{2\pi}{\lambda} \cos 2\pi \frac{x}{\lambda} \right)^2 \right] dx$$

Performing the integration and combining terms gives:

$$P_1 = 4\mu K_{\phi} z_0 A \omega \frac{\lambda}{2\pi} \left[1 + \frac{1}{3} \left(2\pi \frac{A}{\lambda} \right)^2 \right] \quad (\text{E.28})$$

If the wave is relatively flat compared to the wave length, the second term of Equation (E.28) becomes small, and the power may be written as

$$P_1 = \frac{2}{\pi} \mu K_{\phi} z_0 \lambda A \omega \quad (\text{E.29})$$

The power given by Equation (E.29) is the power to move the wave surface when the vehicle is not moving, and power is being put into the wave internally at all points. Figure E-4 shows the frictional force on a wave which is on a vehicle with forward motion. The cranks as in Figure E-1 are rotating counter-clockwise. The plane A-A represents the level on the surface at which the wave velocity is equal to the vehicle velocity. The arrows below the wave represent the direction of the frictional force on the wave due to relative velocity between the wave and the soil. The arrows above the wave represent the direction of the velocity of the wave with respect to the vehicle. Over most of the wave surface, the friction force is opposing the motion, and the friction is, therefore, extracting power from the vehicle. However, from

$\lambda/2$ to C, and from B to λ , the reverse is true and the frictional force is putting power into the vehicle mechanism if that mechanism is reversible. The power represented by Equation (E.29) represents vehicle power consumption only for $B = \lambda$ ($B' = 0$). For $B' \neq 0$, the power given by Equation (E.29) is too large by two times the power represented by the wave in the increments $\lambda/2$ to C and B to λ , or four times the power represented by the increment of wave from B to λ , if the mechanism is reversible. The power that the vehicle can extract from the portion of the wave from B to λ is, from Equation (E.26),

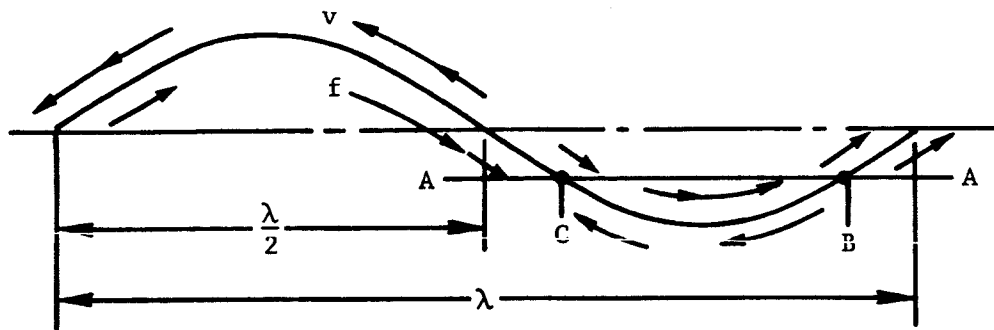
$$\Delta P = \int_B^\lambda v_t \tau ds \quad (\text{E.30})$$

and the true power consumption for a reversible mechanism is

$$P = P_1 - 4 \Delta P \quad (\text{E.31})$$

From the step preceding Equation (E.28), Equation (E.30) becomes

$$\begin{aligned} \frac{\Delta P}{\mu K_\phi z_0 A \omega} = & \left[- \frac{\lambda}{2\pi} \cos 2\pi \frac{x}{\lambda} \right. \\ & - \frac{1}{3} \left(2\pi \frac{A}{\lambda} \right)^2 \frac{\lambda}{2\pi} \cos^3 2\pi \frac{x}{\lambda} \\ & - \frac{A}{z_0} \left(\frac{x}{2} - \frac{1}{4} \frac{\lambda}{2\pi} \sin 2 \cdot 2\pi \frac{x}{\lambda} \right) \\ & - \frac{1}{2} \frac{A}{z_0} \left(2\pi \frac{A}{\lambda} \right)^2 \\ & \left. \left(\frac{x}{2} - \frac{1}{4} \frac{\lambda}{4\pi} \sin 4 \cdot 2\pi \frac{x}{\lambda} \right) \right]_{x=0}^{-B'} \end{aligned}$$



F05474 U

FIGURE E-4. FRICTIONAL FORCES ON A WAVE

Dropping terms containing $(A/\lambda)^2$ gives the approximate solution

$$\frac{\Delta P}{\mu K_{\varphi} z_0 A \omega} \approx \frac{\lambda}{2\pi} \left[1 - \cos 2\pi \frac{B'}{\lambda} + \frac{1}{2} \frac{A}{z_0} \left(2\pi \frac{B'}{\lambda} - \frac{1}{2} \sin 2\pi \frac{B'}{\lambda} \right) \right] \quad (\text{E. 32})$$

Then, combining (E. 29) with (E. 31) and (E. 32) gives

$$P = \frac{2}{\pi} \mu K_{\varphi} z_0 \lambda (A \omega) f_2 \left(\frac{B'}{\lambda}, \frac{A}{z_0} \right) \quad (\text{E. 33})$$

where the function f_2 is defined as

$$f_2 \left(\frac{B'}{\lambda}, \frac{A}{z_0} \right) = \cos 2\pi \frac{B'}{\lambda} - \frac{1}{2} \frac{A}{z_0} \left(2\pi \frac{B'}{\lambda} - \frac{1}{2} \sin 2\pi \frac{B'}{\lambda} \right) \quad (\text{E. 34})$$

Using the power given by Equation (E. 33), the weight given by Equation (E. 16), and the velocity given by Equation (E. 14), the equivalent drag-to-weight ratio may be found by:

$$\frac{D_e}{W} = \frac{P}{vW_1} = \frac{2}{\pi} \cdot \frac{\mu}{\sin 2\pi \frac{B'}{\lambda}} f_2 \left(\frac{B'}{\lambda}, \frac{A}{z_0} \right) \quad (\text{E. 35})$$

The function f_2 is defined by Equation (E. 34), and B'/λ is given in Figure 22 of the report. The result of Equation (E. 35) is shown on Figure 24 in the report. This equation applies only to the fully submerged case which corresponds to z_m/A from 2.0 to infinity. The penetration depth, z_m , is defined by Equation (E. 15).

Part of Wave Above Soil Surface

A case of a wave which is partially above the soil surface is illustrated in Figure E-5.

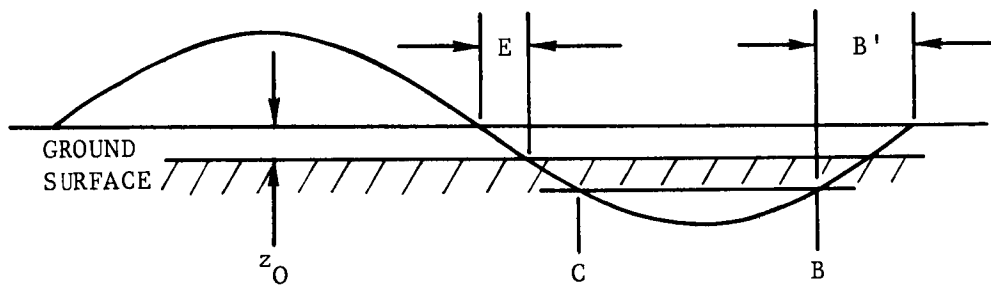


FIGURE E-5. PARTIALLY SUBMERGED WAVE

The location of the intersection of the wave with the ground surface is defined as E and is given by

$$\sin 2\pi \frac{E}{\lambda} = \frac{-z_0}{A}$$

$$E = \frac{\lambda}{2\pi} \sin^{-1} \frac{-z_0}{A} \quad (\text{E. 36})$$

Proceeding as for Equation (E. 6) through (E. 10), the net thrust is given by:

$$H_{\text{net}} = \int_{B'}^{\frac{\lambda}{2} - B'} \mu K_{\phi} \left(A \sin 2\pi \frac{x}{\lambda} + z_0 \right) dx - 2 \int_E^{B'} \mu K_{\phi} \left(A \sin 2\pi \frac{x}{\lambda} + z_0 \right) dx$$

$$\frac{H_{\text{net}}}{\mu K_{\phi} A} = -\frac{\lambda}{2\pi} \left(-2 \cos 2\pi \frac{B'}{\lambda} - 2 \cos 2\pi \frac{B'}{\lambda} + 2 \cos 2\pi \frac{E}{\lambda} \right)$$

$$+ \frac{z_0}{A} \left(\frac{\lambda}{2} - 2B' - 2B' + 2E \right)$$

Setting this equal to external drag, gives

$$\frac{1}{2\pi} \cdot \frac{A}{z_0} \cos 2\pi \frac{B'}{\lambda} = \frac{D}{4\mu K_{\phi} z_0} + \frac{B'}{\lambda} + \frac{1}{4\pi} \frac{A}{z_0} \cos 2\pi \frac{E}{\lambda}$$

$$- \frac{1}{2} \frac{E}{\lambda} - \frac{1}{8} \quad (\text{E. 37})$$

The vehicle weight is given by

$$W_1 = K_{\phi} \left\{ \int_0^{\frac{\lambda}{2}} \left(A \sin 2\pi \frac{x}{\lambda} + z_0 \right) dx - 2 \int_0^E \left(A \sin 2\pi \frac{x}{\lambda} + z_0 \right) dx \right\}$$

$$W_1 = K_{\phi} A \lambda \left\{ \frac{1}{\pi} \cos 2\pi \frac{E}{\lambda} + \frac{z_0}{A} \left(\frac{1}{2} - 2 \frac{E}{\lambda} \right) \right\} \quad (\text{E. 38})$$

Combining Equations (E. 37) and (E. 38) gives

$$\frac{1}{2\pi} \cdot \frac{A}{z_0} \cos 2\pi \frac{B'}{\lambda} = \frac{D}{4\mu W_1} \left[\frac{1}{\pi} \cdot \frac{A}{z_0} \cos 2\pi \frac{E}{\lambda} - 2 \frac{E}{\lambda} + \frac{1}{2} \right] + \frac{B'}{\lambda}$$

$$+ \frac{1}{4\pi} \frac{A}{z_0} \cos 2\pi \frac{E}{\lambda} - \frac{1}{2} \frac{E}{\lambda} - \frac{1}{8} \quad (\text{E. 39})$$

For $z_0/A = 0$, this becomes

$$\cos 2\pi \frac{B'}{\lambda} = \frac{1}{2} \left(\frac{D}{\mu W_1} + 1 \right) \quad (\text{E. 40})$$

which gives a closed form solution for the half-submerged case.

Equation (E. 39) can be solved graphically in the same manner as was done for Equation (E. 10) in Figure E-3. If the equation is first multiplied through by z_0/A , Figure E-3 can be used to obtain the solution, since the left-hand side of the resulting equation is represented by the cosine curve for $A/z_0 = 1.0$ on Figure E-3. The right-hand side of the equation is a straight line for any combination of z_0/A and $D/\mu W_1$ and may easily be sketched on Figure E-3. The solution is the intersection of the two lines. The equation is valid for z_0/A from -1.0 to $+1.0$. The result in terms of penetration depth defined by Equation (E. 15) is given on Figure 22. The curves for d/A less than 2.0 are from Equation (E. 39); curves for d/A greater than 2.0 are from Equation (E. 10).

The power for the special case of a wave half submerged ($z_0 = 0$, or $d/A = 1.0$) may be easily obtained. In this case, the portion of the wave from $\lambda/2$ to C and from B to λ is absorbing power from the soil, and the portion from C to B requires a power input from the vehicle as shown in Figure E-4. Then, using the form of Equation (E. 26),

$$P = \int_C^B v_t \tau \, dS - 2 \int_{\frac{\lambda}{2}}^C v_t \tau \, dS \quad (\text{E. 41})$$

For this case, $z_0 = 0$, and Equation (E. 41) can be multiplied through by z_0/A , and the terms containing a z_0 are dropped before making the evaluation.

Using the relationships

$$B' = \lambda - B = C - \frac{\lambda}{2} \quad (\text{E. 42})$$

$$\sin 2\pi \frac{2C}{\lambda} = - \sin 2\pi \frac{2B}{\lambda} \quad (\text{E. 43})$$

$$\sin 2\pi \frac{4C}{\lambda} = - \sin 2\pi \frac{4C}{\lambda} \quad (\text{E. 44})$$

and dropping terms containing $(A/\lambda)^2$ gives

$$\frac{P}{\mu K_{\phi} A(A\omega)} = \frac{\lambda}{4} \left[1 - \frac{4}{\pi} f_1 \left(\frac{B'}{\lambda} \right) \right] \quad (\text{E. 45})$$

where,

$$f_1 \left(\frac{B'}{\lambda} \right) \triangleq 2\pi \frac{B'}{\lambda} - \frac{1}{2} \sin 2\pi \frac{2B'}{\lambda} \quad (\text{E. 46})$$

By using the power from Equation (E. 45), the weight from Equation (E. 38), and the velocity from Equation (E. 14), the equivalent drag-to-weight ratio becomes,

$$\frac{D_e}{W} = \frac{P}{vW} = \mu \frac{\pi}{4} \frac{1 - \frac{4}{\pi} f_1 \left(\frac{B'}{\lambda} \right)}{\sin 2\pi \frac{B'}{\lambda}} \quad (\text{E. 47})$$

This is shown on Figure 23 as the line for $z_m/A = 1.0$.

Results

If the amplitude of the wave is small compared to the wave length, the significant geometry parameter is seen to be the ratio of maximum soil penetration to wave amplitude, z_m/A (or alternately z_0/A as given by Equation (E. 15)). The relationship of z_m/A to the vehicle platform loading is given by Equations (E. 16) and (E. 38) and is plotted in Figure 25. The velocity ratio is given in Figure 22, and the equivalent drag-to-weight ratio in Figure 24. These are given as a function of a parameter which may be interpreted either as a slope, or as the ratio of some external drag force to the vehicle weight, divided by the friction coefficient of the soil.

In Figure 22, the maximum slope capability is determined by the point at which the velocity ratio goes to zero. This is plotted as a function of z_m/A on Figure 23. It may be seen that a vehicle that is less than half submerged ($z_m/A < 1.0$) can climb a slope equal to the soil friction angle.

APPENDIX F

CORRUGATED BELLOWS METHODS

Design Charts

To define the limitations of the welded metal type of bellows, and to aid in vehicle preliminary design, a number of graphs are shown which are based upon the equations in the report. Two materials were assumed. Unless otherwise noted, the material is stainless steel with a fatigue limit of 25,000 psi, Young's modulus of 28.5×10^6 psi, and mass density of 0.283 lbm/in.³. In a few cases, results are shown for fiberglass with a 20,000 psi fatigue limit, Young's modulus of 3×10^6 , and density of 0.065 lbm/in.³. The difference between these materials is most noticeable in its effect on allowable deflection, since the largest difference in the materials is in Young's modulus. The gravity factor g/g_e is taken as 1/6.

Equation (47) in the report body is plotted on Figure F-1 for stainless steel. The ordinate of the graph is $f(d/b)$, but this parameter is not required except for computation and the scale is omitted. This graph may be read as in the following example. Enter with the desired d/b at point A, follow the dashed line to the desired working pressure at B, and to the desired width, b , at C. The useful weight to gross weight ratio is read at D. For a discussion of the dashed crossing lines, see Equation (F. 7) below.

Figure F-2 is the same thing for fiberglass for two pressures. The change in material affects the curve on the right only by the change in stress level; the curves on the left are affected only by the change in density.

The vehicle footprint pressure is defined as the gross weight in the local gravity divided by the projected area at the bottom surface. This is given by

$$p = \frac{g}{g_e} \left(\frac{M_u}{b} + \frac{M_e}{b} \right) \quad (\text{F. 1})$$

From Equations (44), (45), and (39) of the report body, this becomes

$$p = \frac{g}{g_e} \left\{ \frac{g_e}{g} \left[\frac{4}{3} \cdot F \left(\frac{d}{b} \right)^2 \frac{1}{1 + \frac{1}{4} \sqrt{\frac{F}{p_i}}} - p_i \right] + \frac{2 \gamma d}{1 + \frac{1}{4} \sqrt{\frac{F}{p_i}}} \right\}$$

$$= \frac{g}{g_e} \cdot \frac{\frac{d}{b}}{1 + \frac{1}{4} \sqrt{\frac{F}{p_i}}} \left[f\left(\frac{d}{b}\right) + 2 \gamma b \right] \quad (\text{F. 2})$$

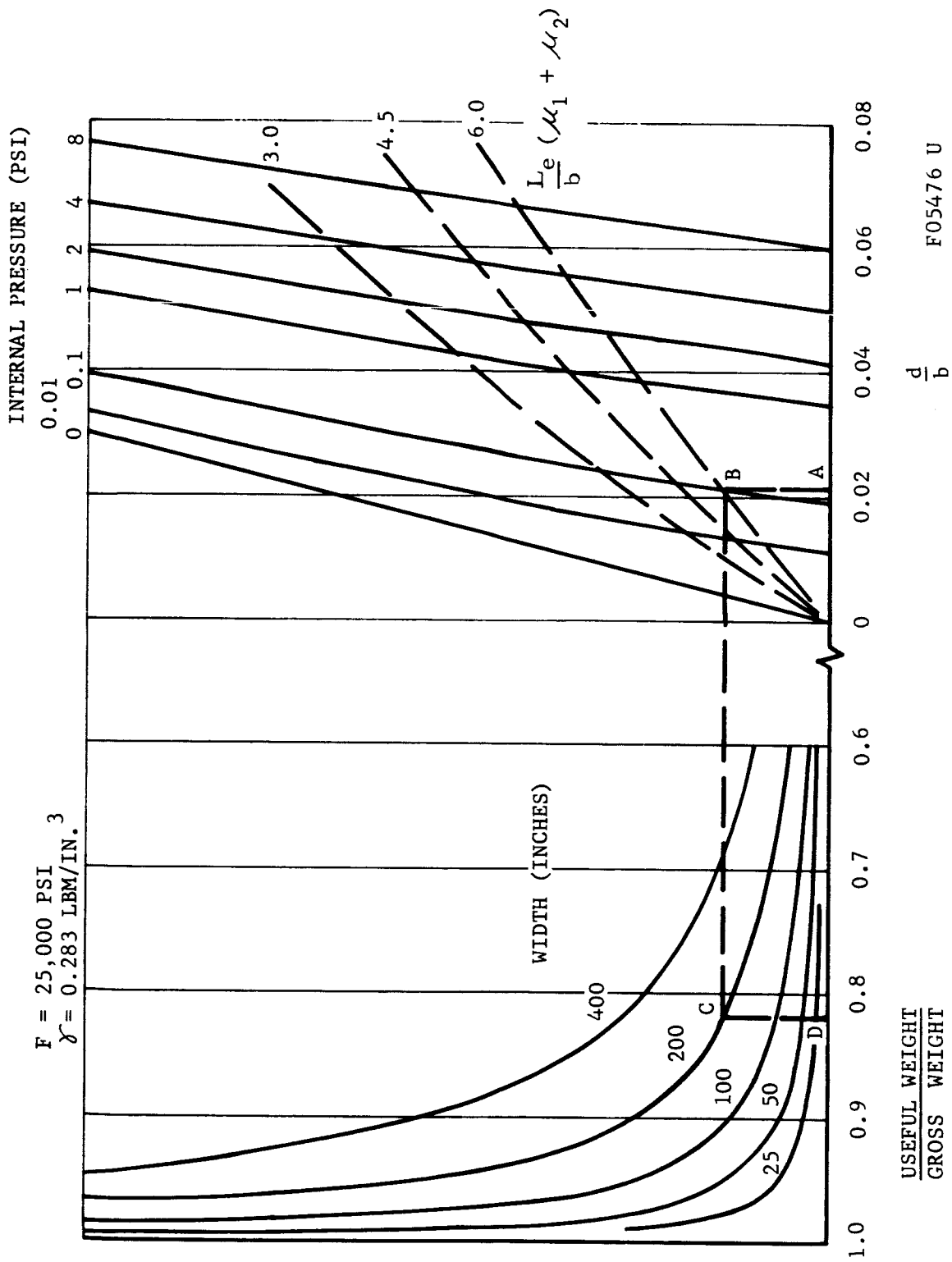


FIGURE F-1. PAYLOAD TO GROSS WEIGHT RATIO FOR STAINLESS STEEL BELLOWES

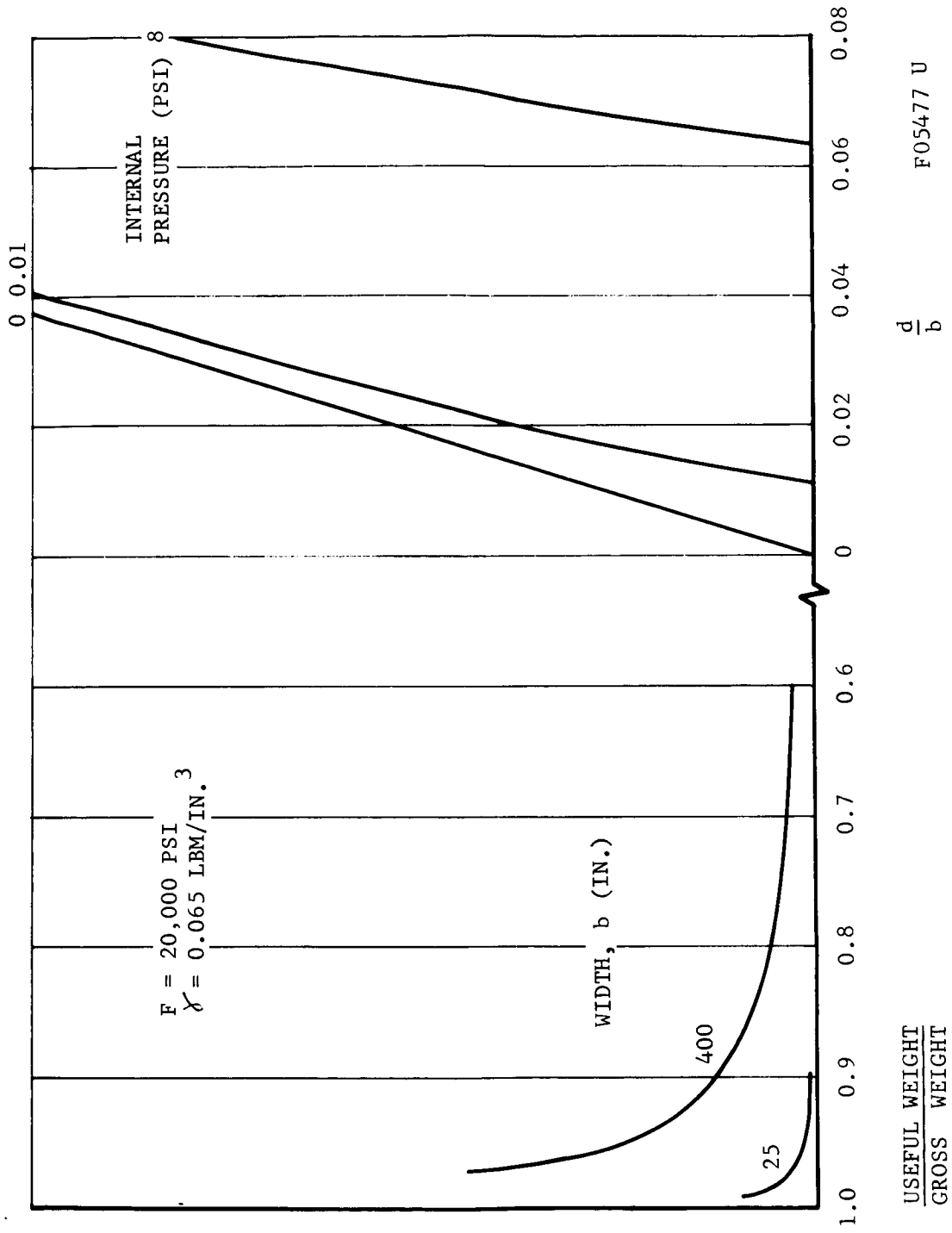


FIGURE F-2. USEFUL LOAD TO GROSS WEIGHT RATIO FOR FIBERGLASS BELLOWS

where $f(x)$ is defined in Equation (48). This is shown for stainless steel in Figures F-3 and F-4. The footprint pressure is low for small pressures because the bellows material becomes light and cannot support much payload. At high internal pressures, the payload becomes small because bending stress in the bottom surface is used in supporting the internal pressure. The effect of width is seen to be small.

Assuming that the vehicle cross-sectional area is equivalent to a semi-circle of diameter, b , the force exerted on the ends by the internal pressure is

$$P_i = \frac{\pi}{8} b^2 p_i \quad (\text{F. 3})$$

The maximum bellows spring force is, from Equation (36) modified for a section with circumference equal to b ,

$$P_{s \text{ max}} = \frac{1}{2} b d p_i = \frac{1}{2} b^2 \frac{d}{b} p_i \quad (\text{F. 4})$$

From the Mobility section, the maximum force required to overcome ground friction is (incremental extension)

$$P_f = \frac{1}{4} (\mu_a + \mu_f) \frac{g}{g_e} (M_u + M_e) L_e \quad (\text{F. 5})$$

where $(M_u + M_e)L_e$ is the vehicle gross weight fully loaded. The requirement that the internal pressure at least be able to overcome bellows spring force plus ground friction may be stated as

$$P_i \geq P_{s \text{ max}} + P_f$$

Substituting in the above relationships, this becomes

$$\frac{\pi}{8} b^2 p_i \geq \frac{1}{2} b^2 \frac{d}{b} p_i + \frac{1}{4} (\mu_a + \mu_f) \frac{g}{g_e} (M_u + M_e) L_e$$

If this is made an equality and solved for p_i , the result is the design pressure, p_{crit} , which will just overcome spring force and ground friction in the vehicle which is designed to that pressure as a structural criterion.

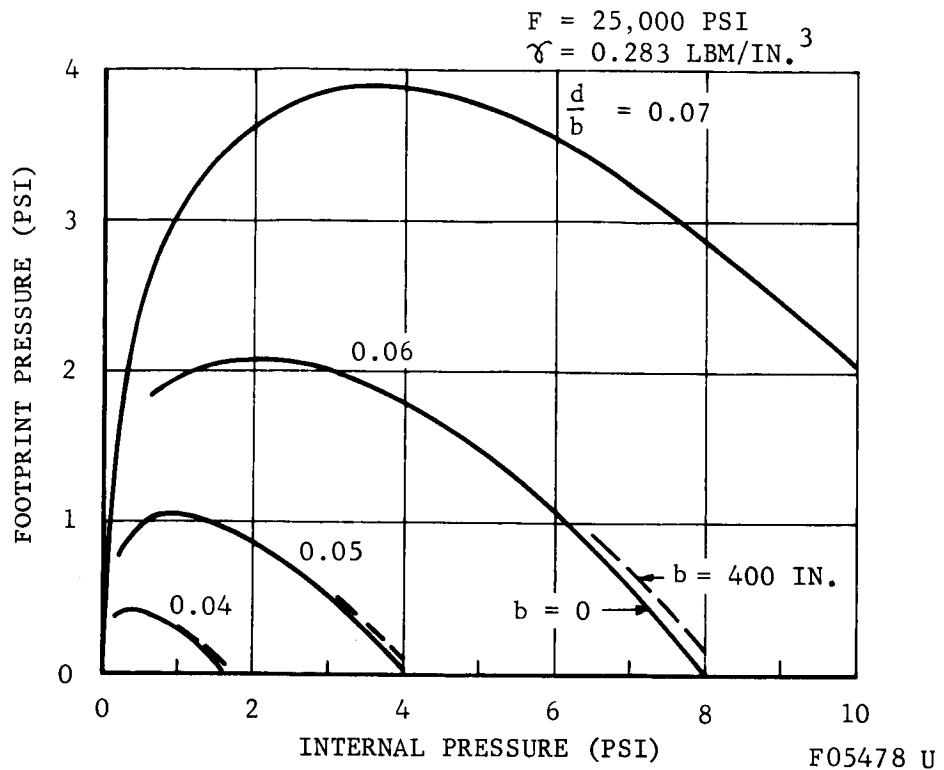


FIGURE F-3. VEHICLE FOOTPRINT PRESSURE

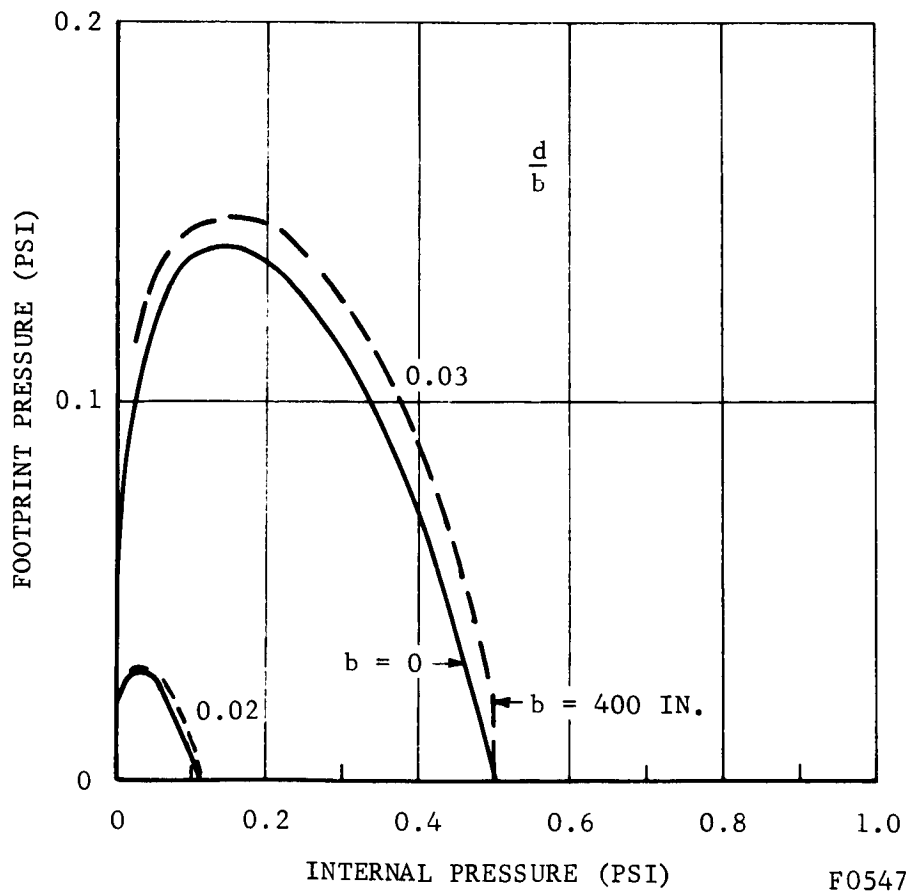


FIGURE F-4. VEHICLE FOOTPRINT PRESSURE FOR SMALL d/b

$$\begin{aligned}
P_{\text{crit}} &= \frac{1}{2} \cdot \frac{g}{g_e} \frac{(\mu_a + \mu_f)(M_u + M_e)L_e}{b^2 \left(\frac{\pi}{4} - \frac{d}{b} \right)} \\
&= \frac{1}{2} \cdot \frac{g}{g_e} \cdot \frac{L_e}{b} \left(\frac{M_u}{b} + \frac{M_e}{b} \right) \frac{\mu_a + \mu_f}{\frac{\pi}{4} - \frac{d}{b}} \quad (\text{F. 6})
\end{aligned}$$

Substituting the footprint pressure from Equation (F. 1) gives

$$P_{\text{crit}} = \frac{1}{2} \frac{L_e}{b} (\mu_a + \mu_f) \frac{p}{\frac{\pi}{4} - \frac{d}{b}} \quad (\text{F. 7})$$

where p is given by Equation (F. 2). Note that footprint pressure, p , is a function of pressure, so that P_{crit} now appears on both sides of Equation (F. 7). Ignoring the small effect of W in Figure F-3, P_{crit} is a function only of d/b and the parameter $L_e/b (\mu_a + \mu_f)$, and may be solved graphically.

The result (for stainless steel) is shown in Figure F-5. This may be interpreted as the minimum design pressure for given parameters, d/b and $L_e/b (\mu_a + \mu_f)$, which will result in a vehicle which can extend itself to maximum allowable length by internal pressure alone. This same result is also shown on Figure F-1 as the dashed crossing lines.

Equation (38) may be solved for the number of convolutions, N

$$N = \frac{L_e}{2d \left(\frac{1}{4} + \sqrt{\frac{P_i}{F}} \right)} \quad (\text{F. 8})$$

From Equations (34) and (35):

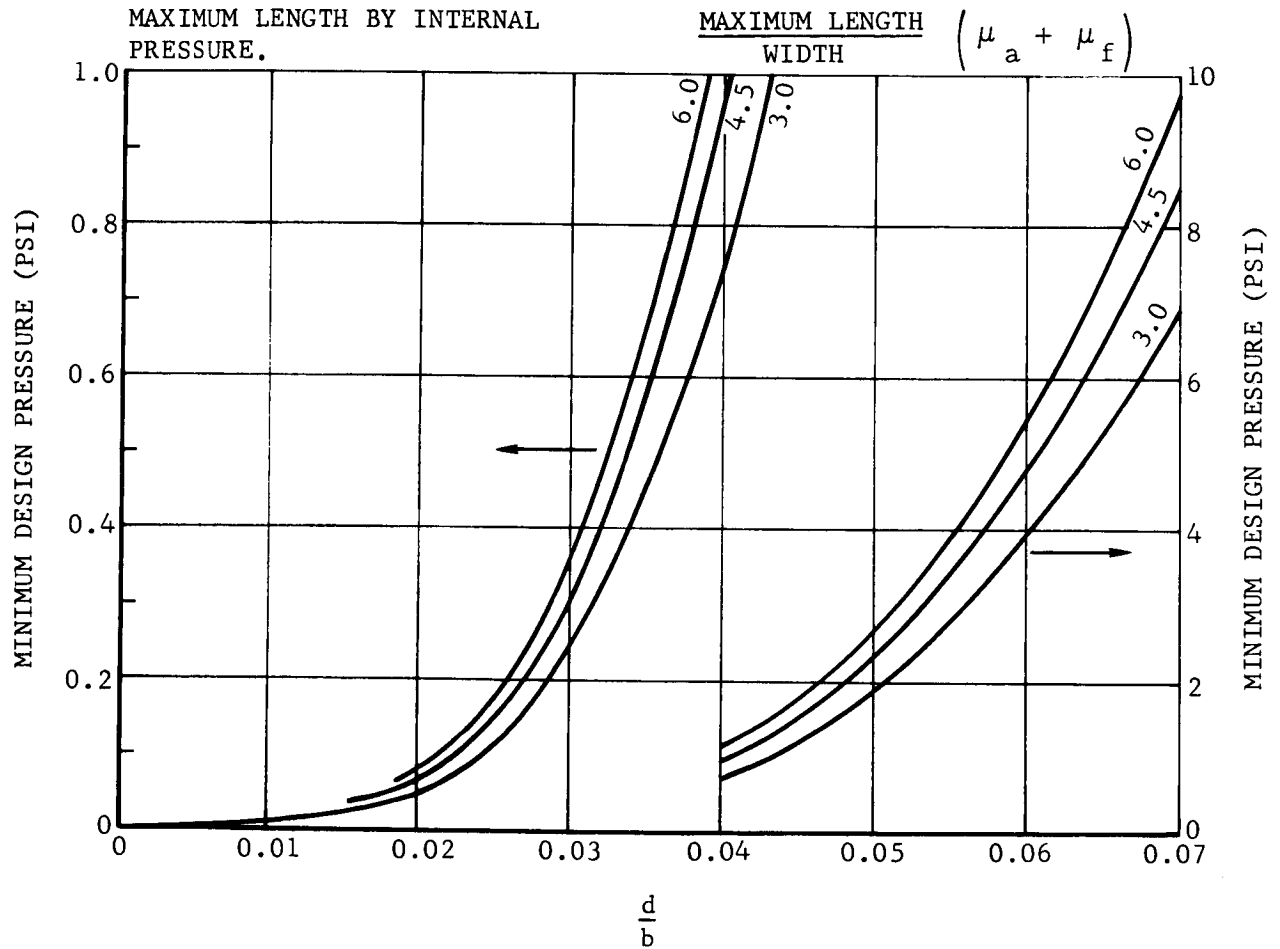
$$\delta_{\text{max}} = \frac{F^2 t}{3 p_i E} = \frac{F^2 d}{3 p_i E} \sqrt{\frac{P_i}{F}} \quad (\text{F. 9})$$

The deflection of the vehicle is given by $N\delta$ and by using Equations (F. 8) and (F. 9):

$$\frac{N\delta}{L_e} = \frac{1}{6 E} \cdot \frac{F^2}{p_i \left(1 + \frac{1}{4} \sqrt{\frac{F}{P_i}} \right)} \quad (\text{F. 10})$$

which is the maximum vehicle strain referred to the maximum extended length. Note that this is a function of only the material properties and the pressure.

A VEHICLE DESIGNED TO A LOWER PRESSURE THAN GIVEN CANNOT EXTEND ITSELF TO MAXIMUM LENGTH BY INTERNAL PRESSURE.



F05480 U

FIGURE F-5. MINIMUM ALLOWABLE DESIGN PRESSURE

Equation (F. 10) is plotted on Figure 30 for both stainless steel and fiberglass. For the large strains that result with fiberglass, the two dimensional Equations (28) through (31) no longer apply and the result is not valid. However, the large difference between steel and fiberglass in allowable deflection is evident and is valid within reasonable limits.

The bellows spring force at this maximum deflection is:

$$P_{s \max} = \frac{1}{2} b^2 \frac{d}{b} P_i \quad (\text{F. 11})$$

This is plotted on Figure F-6, and is seen to be independent of the material.

Combining Equations (45) and (39) gives the vehicle empty mass:

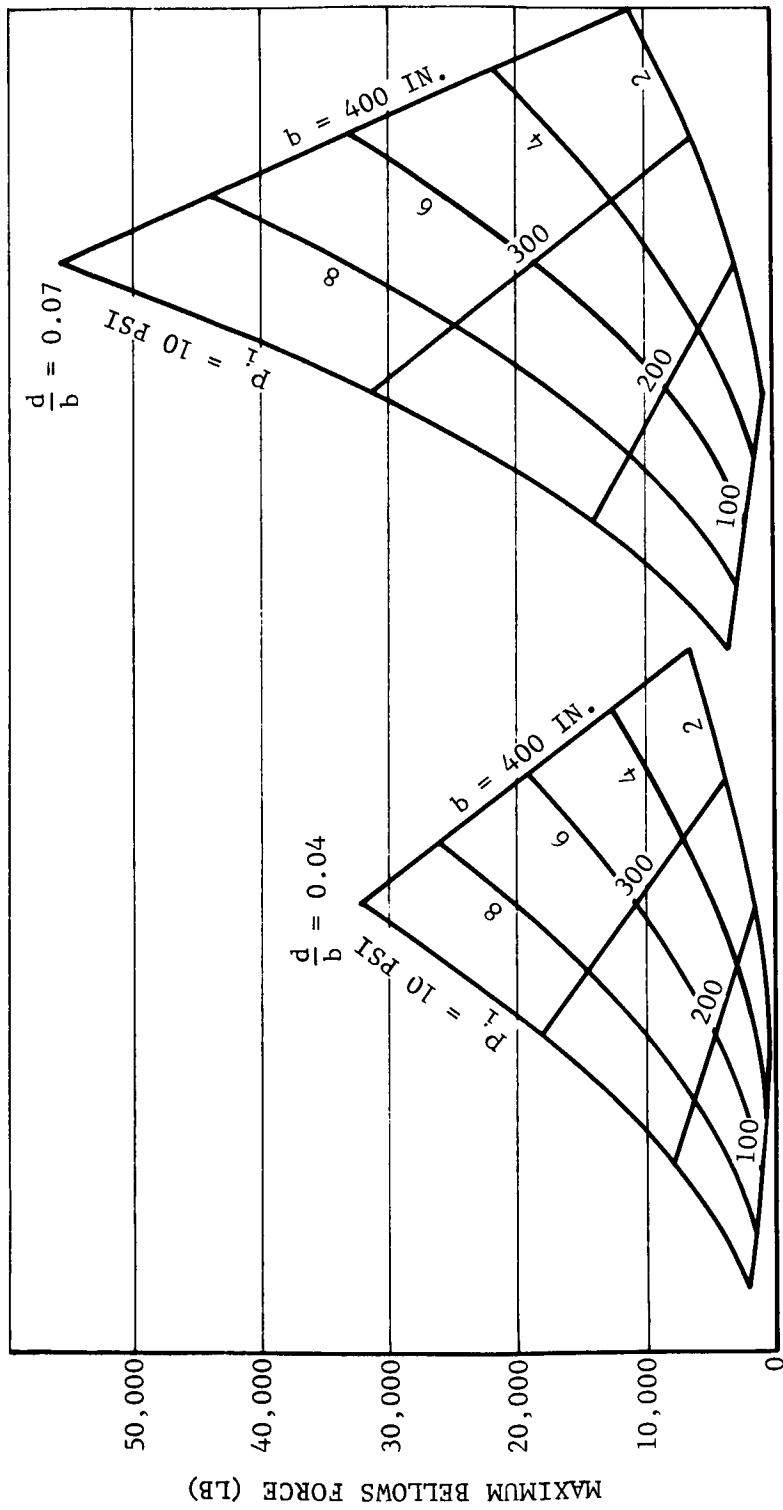
$$M_e = 3 \gamma b^2 \frac{d}{b} \cdot \frac{1}{1 + \frac{1}{4} \sqrt{\frac{F}{P_i}}} \quad (\text{F. 12})$$

This is plotted on Figure F-7 for stainless steel. This quantity may be critical in a design because of the requirement for transport to the moon. A minimum value of empty mass which defines the limit of what can be achieved by using the design principles assumed here. This is obtained by using d/b at each pressure which will result in the allowable stress being caused by beam loading of the bottom due to internal pressure only. This design can carry no payload; nor can it withstand the bending stress due to its own structural weight. This relationship is the solution of Equation (43) for M_u and γ equal to zero, giving

$$\left(\frac{d}{b}\right)^2 = \frac{3 P_i}{4 F} \frac{1}{1 + \frac{1}{4} \sqrt{\frac{F}{P_i}}} \quad (\text{F. 13})$$

This gives the value of d/b at which the curves on the right in Figure F-1 intersect the abscissa, and is also plotted in Figure 31. This will be referred to as the minimum weight design.

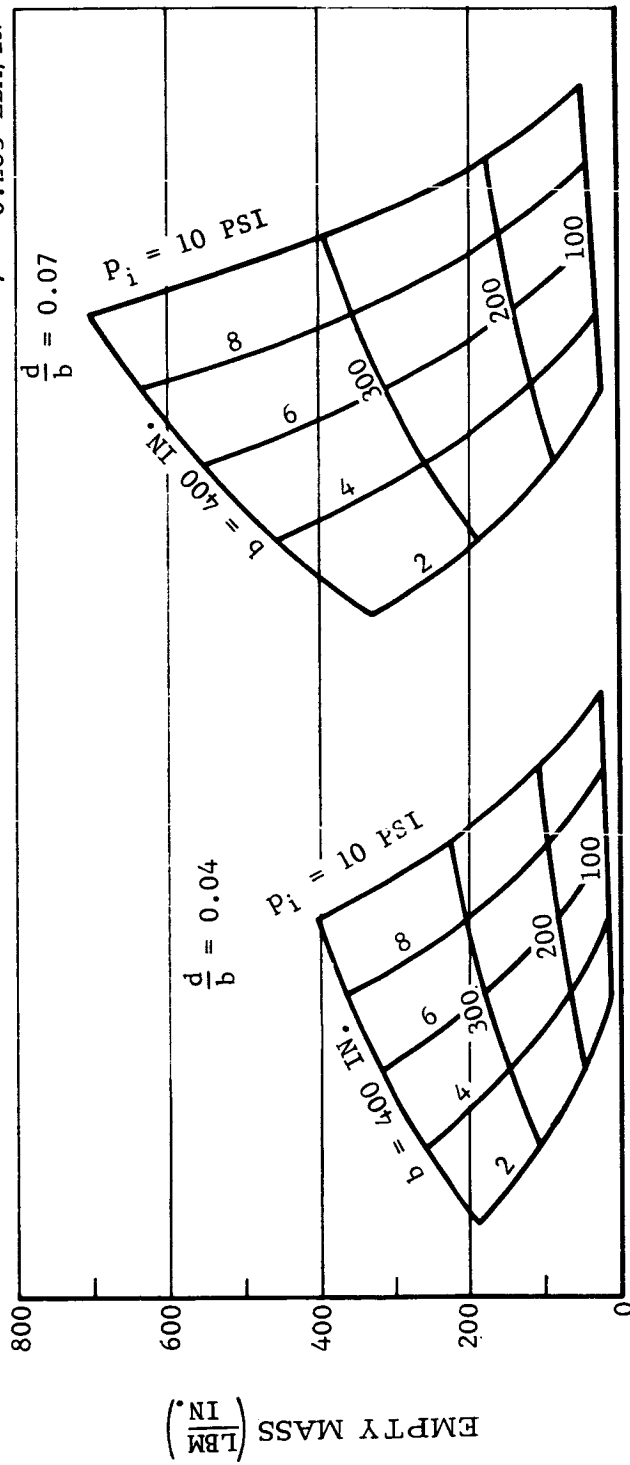
Using the value of d/b given by Equation (F. 13) in Equation (F. 12) gives the empty mass of the minimum weight vehicle. This is plotted in Figure 32.



F05481 U

FIGURE F-6. BELLOWS FORCE AT MAXIMUM DEFLECTION

$F = 25,000 \text{ PSI}$
 $\gamma = 0.283 \text{ LBM/IN}^3$



F05482 U

FIGURE F-7 VEHICLE EMPTY MASS

If the vehicle is operated empty, the footprint pressure is the empty weight per unit length divided by the width. From Equation (F.12) this gives

$$p_e = 3 \frac{g}{g_e} \gamma b \left(\frac{d}{b} \right) \frac{1}{1 + \frac{1}{4} \sqrt{\frac{F}{p_i}}} \quad (\text{F. 14})$$

Using the d/b for the minimum weight vehicle in this expression gives the empty footprint pressure of the minimum weight vehicle. This is shown on Figure 33. The thickness of the bellows material required for this minimum weight design may be found from Equation (34) and is shown in Figure 34.

For a vehicle of unit length, the enclosed volume is equal to the cross-sectional area which is given by

$$V = \frac{\pi}{8} b^2 \quad (\text{F. 15})$$

as for Equation (F.10). Using the empty mass from Equation (45), and equivalent thickness from Equation (39), then gives the empty mass to enclosed volume ratio

$$\frac{M_e}{V} = \frac{24}{\pi} \gamma \frac{d}{b} \frac{1}{1 + \frac{1}{4} \sqrt{\frac{F}{p_i}}} \quad (\text{F. 16})$$

This is shown on Figure 35. For comparison, the ratio is also shown for a cylinder and a sphere designed to contain the same pressure. These latter structures are much more efficient than the bellows vehicles, since all stresses are taken in tension.

The Mobility section discusses the concept of a foot planing on a granular type of soil and gives an expression for the maximum allowable footprint pressure if this planing is to take place. This may be written as

$$p_{al} = \frac{g}{g_e} \frac{\gamma_s}{RJ} \ell \quad (\text{F. 17})$$

where l is the length of a planing foot in the direction of motion, γ_s is the soil mass density, and R and J are functions of the soil friction and the angle of attack of the foot. If it is assumed that each corrugation of the bellows has a foot, the maximum effective length of each foot is given as for Equation (38) as

$$\begin{aligned} l_{\max} &= 2 d \left(\sqrt{\frac{p_i}{F}} + \frac{1}{4} \right) \\ &= 2 \left(\frac{d}{b} \right) b \sqrt{\frac{p_i}{F}} \left(1 + \frac{1}{4} \sqrt{\frac{F}{p_i}} \right) \end{aligned} \quad (\text{F. 18})$$

when the vehicle is at maximum length. Then from Equation (F. 17), the maximum footprint loading for planing is

$$p_{al} = 2 \frac{g}{g_e} \frac{\gamma_s}{RJ} b \left(\frac{d}{b} \right) \sqrt{\frac{p_i}{F}} \left(1 + \frac{1}{4} \sqrt{\frac{F}{p_i}} \right) \quad (\text{F. 19})$$

Setting this equal to the empty vehicle footprint pressure given by Equation (F. 14) defines the conditions for a vehicle design which will just plane. This gives

$$\sqrt{\frac{p_i}{F}} \left(1 + \frac{1}{4} \sqrt{\frac{F}{p_i}} \right)^2 = \frac{3}{2} \frac{\gamma}{\gamma_s} RJ$$

where γ is the density of the bellows material and γ_s is the density of the soil. Solving this for p_i gives

$$\sqrt{\frac{1}{p_i}} = \frac{4}{\sqrt{F}} \left[3 \frac{\gamma}{\gamma_s} JR - 1 + \sqrt{\left(3 \frac{\gamma}{\gamma_s} JR - 1 \right)^2 - 1} \right] \quad (\text{F. 20})$$

For $\frac{\gamma}{\gamma_s} JR$ large, this becomes approximately

$$\sqrt{\frac{1}{p_i}} \approx \frac{8}{\sqrt{F}} \left(3 \frac{\gamma}{\gamma_s} JR - 1 \right) \quad (\text{F. 21})$$

This relationship is shown in Figure 36. The pressure p_i given is the maximum design pressure which may be used if the feet are to plane under the stated conditions.

Calculation of Bellows Parameters for Large Lunar Shelter

The following calculations are based upon both the preceding equations and the vehicle characteristics given in the Design section of the report. Alternately, most of the values could be read from the design charts.

In the nomenclature used for the bellows analysis, the assumed values are as follows:

$$\begin{aligned}b &= 240 \text{ inches} \\ \frac{d}{b} &= 0.045 \\ d &= (240)(0.045) = 10.8 \text{ inches} \\ p_i &= 2 \text{ psi} \\ L_e &= (60)(12) = 720 \text{ inches} \\ F &= 25,000 \text{ psi} \\ \gamma &= 0.283 \text{ lbm/in}^3\end{aligned}$$

The material thickness is

$$\begin{aligned}t &= d\sqrt{\frac{p_i}{F}} \\ &= 10.8\sqrt{\frac{2}{25,000}} = \frac{10.8}{112} = 0.0963\end{aligned}$$

The equivalent thickness at the maximum extended length is

$$\begin{aligned}t_e &= \frac{d}{1 + \frac{1}{4}\sqrt{\frac{F}{p_i}}} \\ &= \frac{10.8}{1 + (0.25)(112)} = \frac{10.8}{28.9} = 0.374\end{aligned}$$

The vehicle empty mass is

$$\begin{aligned} L_e M_e &= \left(1 + \frac{\pi}{2}\right) b \gamma t_e L_e \\ &= (2.57)(240)(0.283)(0.374)(720) \\ &= 47,000 \text{ lbm} \end{aligned}$$

The useful load is the weight which can be loaded into the vehicle floor without exceeding the allowable stress when the floor is supported as a simple beam supported at the ends. This is given by

$$\begin{aligned} L_e M_u &= L_e b \left[\left(\frac{4}{3} \cdot \frac{F d t_e}{b^2} - p_i \right) \frac{g_e}{g} - t_e \gamma \right] \\ &= (720)(240) \left[\left(\frac{4}{3} \cdot \frac{(25,000)(10.8)(0.374)}{(240)^2} - 2 \right) 6 - (0.374)(0.283) \right] \\ &= 1.73 \times 10^5 \left[(2.34 - 2)(6) - 0.106 \right] \\ &= (1.73)(10)^5 (2.04 - 0.11) \\ &= 334,000 \text{ lbm} \end{aligned}$$

The maximum gross weight is $334,000 + 47,000 = 381,000$ lbm and the useful load to gross weight ratio is

$$\frac{334,000}{381,000} = 0.877$$

At maximum length, the footprint pressure on the moon is

$$P_{\min} = \frac{381,000}{(720)(240)} \cdot \frac{1}{6} = 0.368 \text{ psi}$$

The maximum deflection of the bellows from the neutral position is

$$\begin{aligned} \frac{\delta}{2} &= \frac{F^2 t}{6 p_i E} = \frac{(25,000)^2 (0.0963)}{(6)(2)(28.5 \times 10^6)} \\ &= 0.176 \text{ in. /disc} \end{aligned}$$

The number of discs may be solved from the given maximum extended length which is based on an assumed 1:4 slope of the discs

$$2 N = \frac{L_e}{d \left(\frac{1}{4} + \sqrt{\frac{P_i}{F}} \right)}$$

$$= \frac{720}{(10.8)(0.25 + 0.0089)} = 257 \text{ discs}$$

Then the maximum vehicle deflection is

$$\delta N = (0.176)(257) = 45.2 \text{ inches}$$

The vehicle neutral length (nonstressed position)

$$L_e = 720 - 45 = 675 \text{ inches}$$

and it operates with a stroke of +45 inches about this point. The minimum length is

$$720 - 90 = 630 \text{ inches}$$

and the maximum footprint pressure is

$$p = \frac{381,000}{(630)(240)(6)} = 0.42 \text{ psi}$$

The spring force developed by the bellows at the maximum deflection is

$$P_s = \frac{1}{6} (2.57) b d p_i$$

$$= \frac{1}{6} (2.57)(240)(10.8)(2)$$

$$= 2220 \text{ pounds}$$

The cross sectional area of the vehicle is

$$S_c = \frac{1}{2} \frac{\pi b^2}{4} = \frac{1}{2} \cdot \frac{\pi (240)^2}{4} = 22,600 \text{ in.}^2$$

The force exerted on the ends by the internal pressure is

$$P_i = (2)(22,600) = 42,000 \text{ pounds}$$

At the maximum deflection this leaves $P_i - P_s = 40,000$ pounds of force to overcome friction while moving.

The shelter volume at its nominal length is

$$\begin{aligned} V &= L_e S_c \\ &= (22,600)(675) \\ &= 15.3 \times 10^6 \text{ in.}^3 \end{aligned}$$

and the empty mass to volume ratio is

$$\frac{47 \times 10^6}{15.3 \times 10^6} = 3.07 \times 10^{-3} \frac{\text{lbm}}{\text{in.}^3}$$

The closed length is

$$\begin{aligned} L_c &= 2Nt \\ &= (257)(0.0963) = 24.8 \text{ inches} \end{aligned}$$

The density of cargo which would fill the vehicle with its maximum useful load (loading density) is

$$\frac{334,000}{(15.3 \times 10^6)} (1728) = 37.7 \frac{\text{lbm}}{\text{ft}^3}$$

REFERENCES

1. Mason, R. L., McCombs, W. M., and Cramblit, D. C.: Engineering Lunar Model Surface (ELMS). NASA TR-83-D, 1964.
2. Bekker, M. G.: Theory of Land Locomotion. University of Michigan Press, c. 1956.
3. Bekker, M. G.: Off-the-Road Locomotion. University of Michigan Press, Ann Arbor, c. 1960.
4. Jumikis, A. R.: Soil Mechanics. Van Nostrand, 1962.
5. Feely, F. J., Jr., and Goryl, W. M.: Stress Studies on Piping Expansion Bellows. J Appl Mech, June 1950, pp 135-141.
6. Lucas, Harold : A Method for Comparative Evaluation of Tracked Versus Wheeled Vehicles. Report No. RR-33-2, Research and Engineering Directorate, U.S. Army OTAC, Detroit, Michigan, 1961 (Available from ASTIA as 280495L).
7. Mechtley, E. A.: The International System of Units of 1960, Physical Constants and Conversion Factors. NASA SP-7012, 1964.
8. Anon: Apollo Logistics Support Systems Payloads Design Study, Final Report, Volume II, Book 2, Bendix Corporation, June 1965, (Contract NAS 8-11287).
9. Anon: Apollo Logistics Support Systems Payloads Design Study, Final Presentation, Volume I, D2-36072-3, The Boeing Company, April 1965 (Contract NAS 8-11411).
10. Anon: Mechanics of Soil-Vehicle Systems. Proceedings of the First International Conference on the Mechanics of Soil-Vehicle Systems. Torino-Saint Vincent, 1961.

ABSTRACT

A feasibility study has been carried out of various concepts of using a bellows to provide cross country mobility, particularly on the moon. Effort was directed toward analytical treatment of bellows mobility and of bellows structure including both corrugated and membrane bellows, and applying the results to several brief design studies of typical missions. All concepts studied can have relatively low footprint loading, can have all moving parts internally located in a protected, pressurized environment and can be considerably foreshortened during delivery.

The concept wherein the bottom surface of the vehicle moves in the form of a traveling wave similar to the motion used by snakes and centipedes appears to be potentially the most versatile and is shown to have performance superior to conventional off-road vehicles. The double-acting bellows concept, which is a variation of rib-walking, has good performance suitable for unmanned vehicles but does have some restrictions. The extension-contraction bellows concept, wherein propulsion is derived from asymmetry built into the lower surface is limited in performance but is uniquely suited for incorporation of a simple solar-mechanical energy transfer system which appears promising.

Also included in fundamental analytical treatment of a stepped surface planing over soil, of wave motions which might be used by a variety of vehicles, and of the structure of membrane bellows. A lunar soil model suitable for short stroke and cyclic motion studies was developed.